THE LUMINESCENT SOLAR CONCENTRATOR

Thesis by

John Samuel Batchelder

In Partial Fulfillment of the Requirements

for the degree

of

Doctor of Philosophy

California Institute of Technology

Pasadena, California

1982

(Submitted August 4, 1981)

Dedicated to my parents,

Joyce and John Batchelder

ACKNOWLEDGMENTS

I wish to express my gratitude to Professor Ahmed H. Zewail for his invaluable support and guidance in this work.

I have also greatly profited from useful discussions with Dr. Terry Cole, Dr. James McCaldin, Dr. John Lambe, and Dr. Amitava Gupta. I wish to thank Dr. Krishna Koliwad, Dr. James Liu, Bob Mueller, Taher Daud, Sandy Hyland, and co-workers at JPL for their generous assistance in prototype testing. I am thankful to Stuart Vincent for his help in casting plates and in the degradation experiments, and to Prakash Kasiraj for his meticulously written software. I am grateful to my compatriots Bill Lambert, Dave Millar, Dean Neikirk, Joe Perry, and Duane Smith for their help and comradeship. I have appreciated the assistance of many of the staff at the Institute, particularly Tom Dunn, Linda Dozsa, Fran Bennett, Charlie Beebe, Delmer Dill, and Jim Olson. I especially thank Tina Wood for her care and effort in typing this thesis.

I appreciate the financial support that I have received from the California Institute of Technology and from the Department of Energy Solar Energy Research Institute.

ABSTRACT

The Luminescent Solar Concentrator (LSC) allows sunlight to be concentrated through the use of light pipe trapping of luminescence. Such concentrators do not require tracking, and they can reduce the cost of solar energy conversion by reducing the required area of photovoltaic cells. We have conducted the following experimental and theoretical investigations in order to optimize the LSC's performance.

The spectral characteristics of 18 organic laser dyes are studied for their applicability as luminescing centers. The spectral homogeneity and self-absorption characteristics of representative dyes are examined in detail. The relative spectral homogeneity of such dyes is shown to depend upon the surrounding material using narrow band laser excitation. We develop three independent techniques for measuring self-absorption rates; these are time-resolved emission, steady state polarization anisotropy, and spectral convolution. Prototype devices are tested for performance, and the componant dyes are tested for stability to solar exposure.

A model is developed which predicts the efficiency and gain of and LSC from the spectroscopic characteristics of its components. A critical optical density (CODE) is assigned to the dyes surveyed which predicts the self-absorption limited performance for a particular dye. The maximum efficiency of an LSC is found using a simple model and the experimentally measured Stokes shift required to minimize self-

absorption.

We find that the performance of LSCs which achieve high light concentration is primarily limited by self-absorption and by photodegradation. The maximum efficiency possible is about 9% in such systems, and present devices can achieve about 3%. A typical lifetime for an LSC using organic laser dyes due to photodegradation is on the order of a month.

TABLE OF CONTENTS

CHAPTER 1

I. INTRODUCTION

Electricity generated from solar energy is an appealing alternative energy source. It has the acclaimed advantages of being non-polluting, renewable, widely distributed, and of delivering peak power at the times of peak load. The use of photovoltaic energy today is restricted primarily to satellites and other specialized applications due to tis high cost. The motivation for this study of Luminescent Solar Concentrators (LSCs) is to explore a potential technique for reducing the cost of photovoltaic power generation. Since the cells which perform the conversion from light to electricity are typically the most expensive componant of such systems, it is advantageous to reduce the required acreage of cells for a given power output by concentrating the sunlight prior to illuminating the cells (Hovel, 1978). LSCs offer a unique advantage with respect to other types of concentrators such as mirrors and lenses. We have demonstrated LSCs which concentrate sunlight by factors of five, and which should be capable of factors greater than twenty with some modification, without requiring hourly or seasonal tracking. We also show that the penalty paid for obtaining such light concentration without tracking is that the upper limit on the overall efficiency of the converter is about 9%.

II. LSC CONCEPTS

There are three principal processes which are combined in an LSC. These processes are light concentration, light pipe trapping, and luminescence. Since the solar cells are in general the most

expensive part of the converter, we wish to span the area directed at the sun with a concentrator which directs the incident light towards a smaller area of cells. This idea imitates nature's use of chlorophyll as an antenna for absorbing sunlight and transmitting the resulting excitation to a center for chemical reaction. The typical LSC is a plate of transparent material, such as glass or plastic, which contains luminescing centers that adsorb and then emit light, such as phosphorus or organic laser dyes. Sunlight enters the upper face of the plate and is partially absorbed by these centers. A fraction of the resulting luminescence is trapped by total internal reflection. Successive reflections transport the luminescence to edge-mounted solar cells, which in turn generate electricity. Figure 1 depicts an example of the operation of an LSC.

Suppose that the surface of the LSC plate which faces the sun has an area A_{face}, and that the edge on which the solar cells are mounted has an area A_{edge}. We will refer to the ratio of the area of the face to the area of the edge as the geometric gain of the plates: $G_{geom} = A_{face}/A_{edge}$. This geometric gain is roughly analogous to the concentrating power of a mirror or lens. For example, if an LSC is completely efficient, such that all of the sunlight which can be converted by the edge-mounted cells is absorbed by the plate and transmitted without any losses to the cells, then the cells would absorb a flux that was denser than the incident sunlight by a factor equal to the geometric gain. Our task to determine the performance of an LSC is, therefore, to quantify these loss mechanisms.

Figure 1. Operation of an LSC. Sunlight enters from above, passes through the plate, through an air gap to a mirror, and back through the plate. Part of this light is absorbed by luminescing material, which then emits into the plate. About 70% of this emission is trapped by total internal reflection. This light propagates in the plate until it is absorbed by the edge-mounted cells.

OPERATION OF A LUMINESCENT SOLAR CONCENTRATOR (LSC)

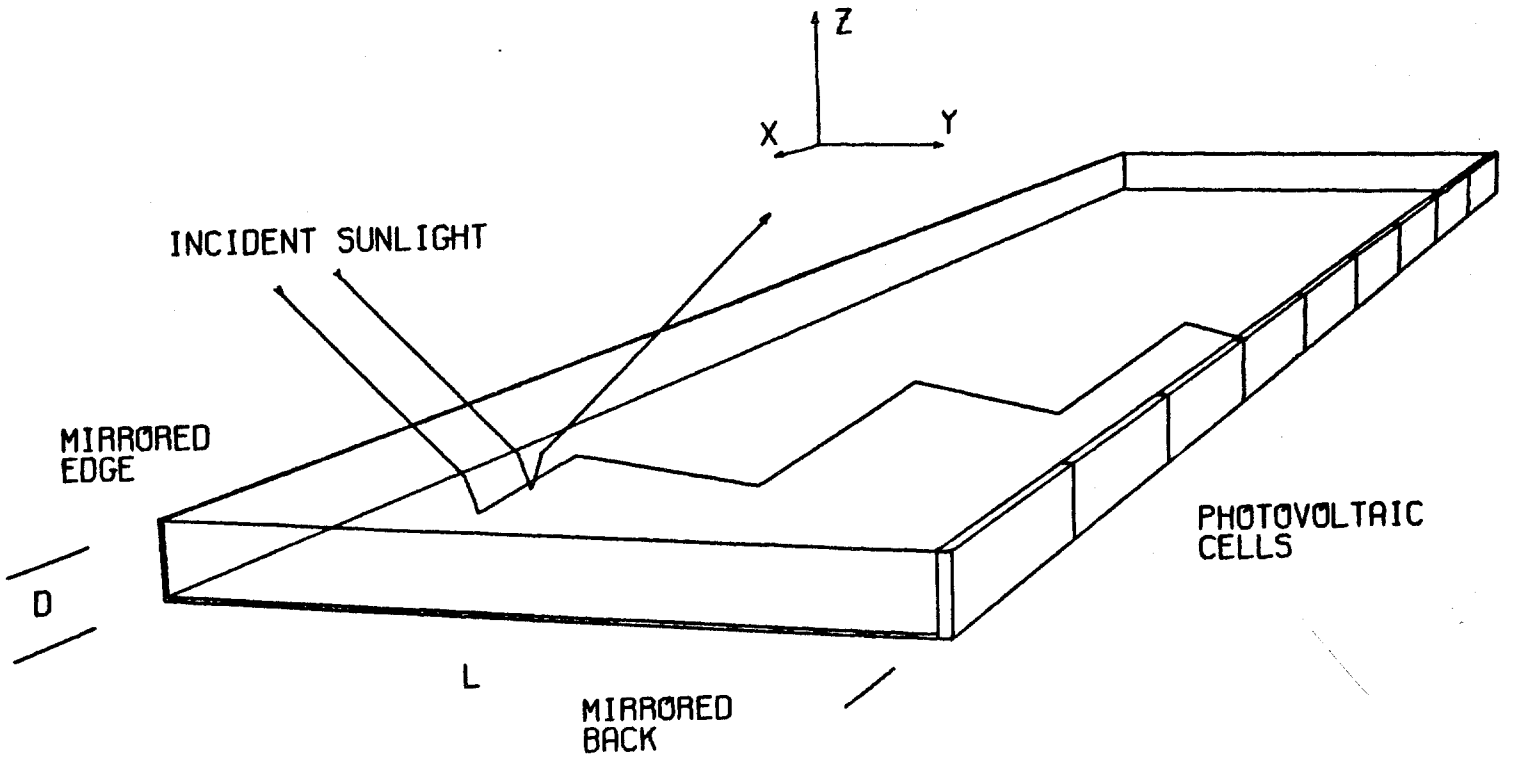

III. HISTORICAL DEVELOPMENT

A number of precursors to the LSC developed independently over the last twenty years. Lerner at MIT had built a solar collecting device embodying this principle, consisting of a solution of laser dye contained between two sheets of glass. This was described in a 1973 NSF grant proposal. In 1975 D. P. Weilmenster, working under Lerner's direction at MIT, submitted a senior thesis on this device. A similar device for radiance amplification in scintillation counters was proposed by Shurcliff (Shurcliff and Jones, 1949, and Shurcliff, 1951). Garwin discussed some thermodynamic aspects of trapped radiation converters (Garwin, 1960). Kiel published results of experiments on plastic radiation converters for scintillation counters (Keil, 1969). More recently, quantum counters for scintillation detection analogous to LSCs have been explored (Mandal, Pearson, and Demas, 1980).

The first actual use of an LSC was probably not for solar energy at all. The LSC concept was employed for (unpublished) astronomical observations by Weekes. She used sheets of dye-doped plastic, which were edge-coupled to photomultiplier tubes, in an attempt to observe Cerenkov radiation from cosmic ray showers in the upper atmosphere (Lerner, 1979).

Weber and Lambe, working at Ford Research, initially suggested both the concept of luminescence trapping for solar concentrators, and the name of luminescent greenhouse collector (Weber and Lambe, 1976). The term greenhouse was suggested because of the similarity between

the LSC's absorption of sunlight in the visible followed by emission in the red, and the well-known atmospheric greenhouse effect. The first prototype devices were made at Ford by Levitt and Weber from ED2 neodymium glass and from rhodamine-590 doped polymethyl methacrylate (PMMA) (Levitt and Weber, 1977). (The PMMA plate was a commonly available red-colored drafting triangle).

Photon Sorting

Since the luminescing material selectively absorbs radiation in a certain energy window, then a number of different luminescing materials, each in separate LSC plates, can separate light into its spectral components. It is thus possible to un-mix broadband sunlight in a manner similar to a dispersive prism. Goetzberger, Greubel and Baur in Germany proposed this use of a multi-layered LSC structure to further increase the overall efficiency (Goetzberger and Greubel, 1977, and Baur and Greubel, 1977). This technique is analogous to the splitting of concentrated sunlight by a dichroic mirror so that higher energy flux is converted by gallium arsenide cells and lower energy flux is converted by silicon cells.

Dye Cascade

The selective absorption of luminescing material is advantageous for sorting light by its energy, but it is problematic when one LSC plate is suppose to utilize the largest possible portion of the solar spectrum. A possible solution is to include a variety of properly chosen luminescing materials in a single plate (Swartz, Cole and Zewail, 1977). The materials are chosen such that their absorption bands form a sequence from highest to lowest energy, such that the

absorption of one material overlaps strongly with the emission band of the next material. Light absorbed by one material will be emitted and then absorbed by the next material until it is emitted by the last material. The result is an LSC which appears to have a very broad absorption band across the solar spectrum.

Dye Orientation

Organic laser dye molecules usually have absorption and emission radiation patterns similar to that of a simple dipole antenna. We observed that if these molecules could be oriented in the plate such that these emission dipoles were principally normal to the plane of the plate, then the emission from these dipoles would be more likely to be trapped by total internal reflection (Batchelder, Zewail, and Cole, 1979). For example, an isotropically absorbing and emitting source in a PMMA plate will have about 74% of its emission trapped in the plate, while a dipole emission source in the plate oriented perpendicular to the plate will have about 91% of its emission trapped in the plate.

Glass Systems

Organic dyes tend to undergo photodegradation in sunlight. Some materials are considerably hardier, however, and these are being explored for applicability to LSCs. Work on LSCs based on inorganic ion luminescence in glasses, such as uranium glass, has been done by Andrews and Lempicki at GTE and by Offenhartz and Micheels at EIC Corporation (Lempicki et al., 1980, and Offenhartz and Micheels, 1980).

Thin Films

Owens-Illinois is developing LSC plates which incorporate organic laser dyes which reside in thin plastic films, which are then attached to clear substrates (Friedman, 1980). Relatively exotic plastic hosts can be used, and dyes which would otherwise react with each other can be isolated in separate film layers. Finally, if the dyes degrade due to solar exposure, the films can be removed and replaced.

Geometry

Hexagonal LSCs appear to give the best compromise between uniform illumination of the cells, close packing of the concentrator plates, and moderate light pathlengths in the concentrators. The amount of light trapped in the plate can be increased by curving the upper surface of the plate (Batchelder, Zewail, and Cole, 1979). The geometric gain of a plate can be somewhat increased by forming the edge of the plate into a mirrored surface that focusses the output light onto the edge (Goetzburger and Schirmer, 1979). For example, this technique can increase the concentration by about 30% in a PMMA plate.

IV. OUTLINE OF THE THESIS

Chapter 2 contains experimental procedures and data. We surveyed the spectroscopic characteristics of component LSC materials. Preliminary degradation studies were made on organic laser dyes under solar exposure in a variety of conditions. The relative homogeneity of the absorption and emission spectra of rhodamine-575 was

measured in three different hosts, and its self-absorption rates were measured using spectral convolution, emission polarization, and transient lifetime techniques. Finally, prototype devices were made and tested.

In Chapter 3 we present a model for predicting the performance of an LSC. We start with a flow chart for the various energy flow channels. The necessary device parameters, such as solar absorption, trapping probability, and self-absorption probability, are defined or derived. These are computed for a specific device geometry.

Chapter 4 further elaborates on self-absorption models. We derive relations for the performance of a purely scattering plate, which is a limiting case of a highly self-absorbing system. A technique is developed which calculates the output emission spectrum from an LSC rod, with the contribution of higher order generations of self-absorbed excitations taken into account. We develop models to distill self-absorption rates from emission polarization and transient lifetime measurements. Two approximate techniques are developed to include self-absorption effects. The first is the characteristic pathlength approximation, in which the self-absorption probability is found by assuming an average pathlength for emission propagation in the plate. The second is the critical optical density calculation, (CODE), which assigns to each dye a number which specifies the largest plate in which the dye can be efficiently incorporated without significant self-absorption losses.

In Chapter 5 we analyze the data from Chapter 2 using the techniques developed in Chapters 3 and 4. We find that the literature

values for the quantum efficiency for photodegradation (molecules destroyed per absorbed photon) for typical laser dyes in general are comparable to those that we have measured. We find that dye spectra are relatively homogeneous in solution and in diffused plastic, and are predominantly inhomogeneously broadened in cast plastic. The self-absorption model for the emission spectrum from an LSC rod compares favorably with experimental spectra. We find very good agreement between the three techniques for measuring the self-absorption rate of rhodamine-575. We perform a calculation of the efficiency of a single dye LSC as a function of size and concentration, and find that it compares well with prototype results. Finally, the CODEs for the dyes surveyed are calculated and tabulated.

In Chapter 6 we analyze the performance of an LSC from a thermodynamic point of view. We show that the light amplifying characteristics can be calculated by substituting black body absorbers for the edge-mounted solar cells, and by balancing the input and output energy to this absorber. We compare the generalized brightness theorem result of Yablonovitch as a function of the positions of the absorption and emission bands of the dyes to the CODE calculations for the gain of an LSC, and we find that the Yablonovitch result is useful only for dyes with the smallest energy difference between their absorption and emission bands. Finally, a simple model similar to that used to calculate the optimal efficiency of an ideal solar cell as a function of its bandgap energy shows that the optimal efficiency of a high gain LSC is about 9%.

Chapter 7 summarizes the important results. We find that dye degradation rates are typically two orders of magnitude higher than what would be required for a 20 year useful life. We have experimentally determined that peak position Stokes shifts of about 0. 7 ev (6,000 cm^{-1}) are necessary to reduce self-absorption to a negligible level. We have demonstrated performance of concentration ratios (flux gains) of 5. 1 and efficiencies of 1. 9% (not by the same device). The highest efficiency reported to date is 3. 2%. The maximum performance predicted by the thermodynamic model is an efficiency of about 9% for a flux gain of about 100.

A series of appendices are included which give background material to topics relevant to this thesis. Appendix I develops a simple economic model for LSCs. Appendix II describes the process of absorption and emission in molecules. Appendix III describes the LSC as a waveguide. Appendix IV describes some characteristics of a photon gas which are used in Chapter 6. Appendix V is a discussion of solar cell efficiency approximations used in the text. Appendix VI gives a description of the brightness theorem from geometric optics.

V. SUMMARY

1. The conceptual operation of an LSC is as follows: Sunlight enters the face of a transparent plate of material containing a luminescent specie. Part of this light is absorbed and re-emitted. Part of this emission is trapped by total internal reflection, so that it propagates in the plate until it reaches the edge-mounted solar cells, where it is converted into electricity.

2. The primary motivation for developing LSCs is economic. We wish to reduce the area of the most expensive component, which is usually the solar cells, by concentrating the sunlight onto a smaller area of cells. LSCs have an advantage over other types of concentrators in that they can achieve moderately high concentrations without hourly or seasonal tracking. Their disadvantage is that they are less efficient than most lens and mirror systems.

3. We define the geometric gain, G_{geom}, of an LSC to be the area of the face exposed to the sun divided by the area of the edge which is covered by solar cells. If an LSC were completely efficient, such that all of the sunlight which can be converted by the solar cells is absorbed by the plate and transmitted losslessly to the cells at an energy which can be converted by the cells, then the light output would be concentrated by a factor equal to the geometric gain.

CHAPTER 2

I. SURVEY OF COMPONENT MATERIALS

There are three functionally distinct components in an LSC: these are the plate or matrix material, the luminescing specie(s), and the photovoltaic converter. Our aim was to develop an optimal combination of these by cataloging their relevant individual characteristics, and by using these data to make a priori prototype designs.

All possible candidate systems could not be examined. We omitted inorganic ion-glass systems because of their usually unacceptably low quantum efficiency of luminescence at room temperature (typically less than 50%). Color- or F-center materials were omitted for the same reason. Nonlinear optical techniques usually require electric field strengths of about four orders of magnitude greater than that available from unconcentrated sunlight (100,000 volts/cm vs 10 volts/cm; see Bloembergen, 1965).

The luminescent material of choice was the organic laser dyes. A variety of such dyes have been developed in response to demand from the tunable dye laser industry. They typically have high quantum efficiencies, and offer a choice of absorption peaks from the ultraviolet to the near infrared. They can be utilized in liquids or in suitable solid matrices in which the dyes are soluable.

Matrix Materials

The important characteristics of the matrix or solvent material is its index of refraction and its absorption spectrum. We needed to know the absorption and emission spectra for the dyes in their appropriate media, as well as their quantum efficiency of luminescence.

Finally, we needed to know the spectral response of the photovoltaic cells used, their AM1 efficiency, and their change in efficiency with light concentration. We measured only some of these quantities.

We did not measure the index of refraction or the absorption coefficients for the various matrix materials. Our standard matrix material was polymethyl methacrylate (PMMA, trade name Plexiglass), which has an index of refraction of 1.49. The absorption spectrum for optical fiber made from PMMA by du Pont was measured by du Pont, and this spectrum is shown in Figure 2. Typical attenuation in PMMA is less than 10% per meter from 5,000Å to 7,000Å, which is the most likely spectral band for emission from an LSC. The primary alternative plastic is polycarbonate (Lytle, Wilkerson, and Jaramillo, 1979).

Dye Sample Preparation

The source of the organic laser dyes used was Exciton Chemical. Dyes were used as received without further purification. Liquid samples were made at known concentrations by dissolving quantities of dye weighed on a Cahn-25 electrobalance in reagent grade methanol. These samples were stored in soda-lime glass bottles and kept in darkness at room temperature. The concentrations of the samples for absorption measurements were chosen such that the peak optical density of a one centimeter pathlength of the solution was between 0.5 and 1.5 in the range between 10,000 and 30,000 cm^{-1}.

Dye spectra were also taken in a variety of other hosts. The principal solid matrix material was PMMA, which usually contained

Figure 2. Optical density per centimeter of polymethylmethacrylate (PMMA) optical fiber. This has been adopted from data published by du Pont on transmission of commercial fiber (Friedman, 1980).

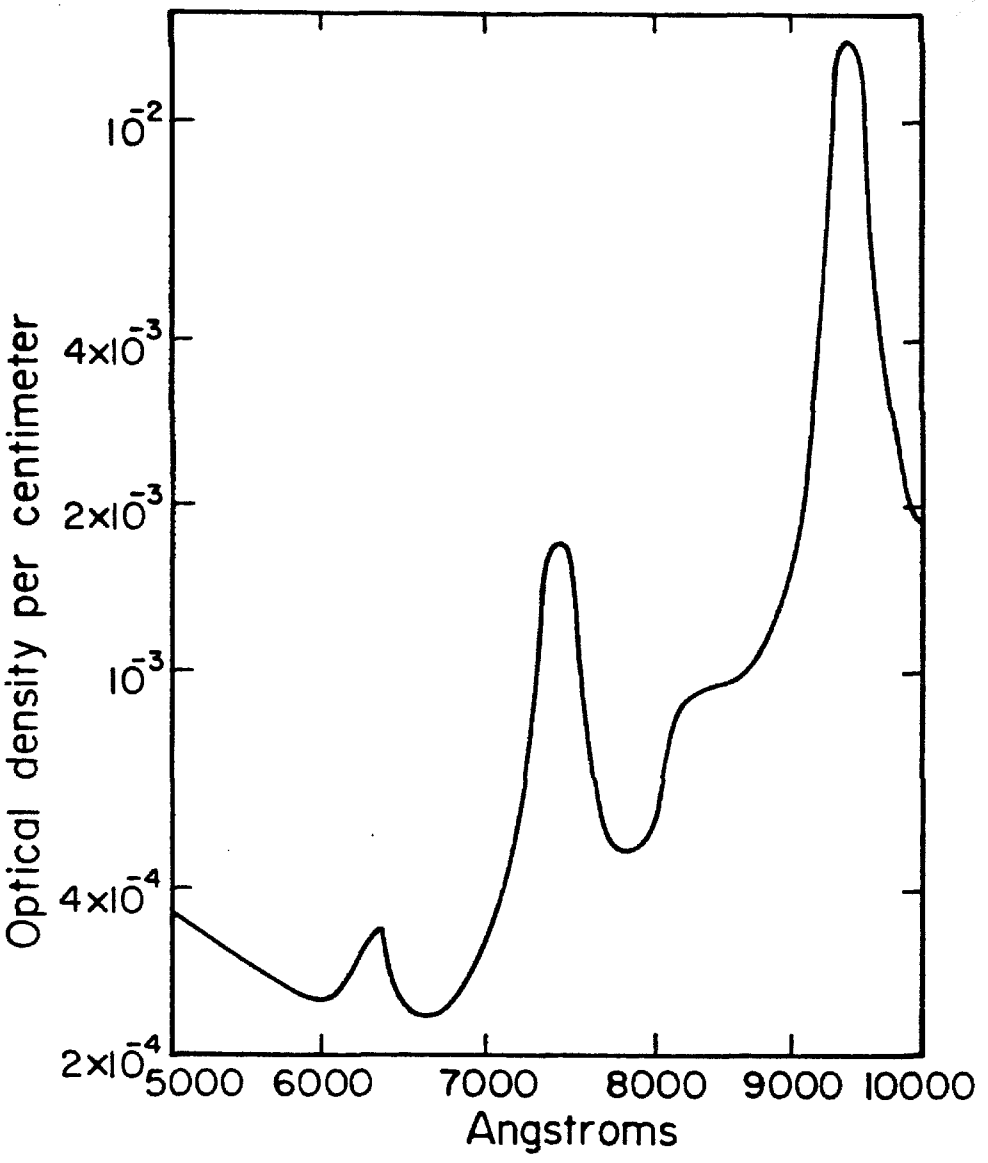

Absorption of DuPont PMMA Optical Fiber

5% hydroxy ethyl methacrylate (HEMMA) by weight to increase the solubility of the more polar dyes. Large PMMA plates were made to our specifications by Acrilex, Inc. Smaller test samples were fabricated in the following manner. Aldrich monomer, containing hydroquinone monomethyl ether as an inhibitor, was purified by fractional distillation in a nitrogen atmosphere using a vacuum-jacketed vigreaux column. This distilled monomer was combined with technical grade HEMMA, and the desired dyes were dissolved therein. Small amounts (less than 2% by volume) of methanol and/or acetic acid were added to the solution to increase the dye solubility if rhodamine dyes were to be used. Some samples were prepared by adding the concentrated dye-monomer solution to prepolymerized PMMA and continuing the polymerization. However, best results were usually obtained by polymerizing just the monomer-dye solution. Two percent by weight of azobisisobutyronitrile was added as initiator, and the mixture was poured into a mold formed by two glass plates. The plates were separated by polyethylene tubing, and by aluminum spacers around the periphery to maintain a constant plate thickness. A very thin coat of silicon vacuum grease on the glass plates acted as mold release agent. These molds were then immersed in a water bath and placed in a convection oven. Polymerization was initiated at about 85° C, when a noticeable increase in viscosity occured, at which time the temperature was lowered to 55° C for 48 hours. The molds were removed from the bath for a final one hour 95° C cure. Typically, significant fractions of the dye did not go into solution, so that the dye concentration

in the final plates were assayed by measuring the peak optical density of the plate and assuming that the peak extinction coefficient was that of the methanol solutions. (A possible problem with this technique is that the peak extinction coefficient of the dyes in PMMA might be different from that of the dyes in methanol. We have observed factors of two differences in the peak extinction coefficient of DCM in various solvents.) We found that dye concentrations in excess of 10 micromolar caused significant amounts of monomer to remain unpolymerized in the cured plates in the case of the rhodamine and oxazine dyes, and that this monomer could be slowly driven out by vacuum degassing at 50° C. After curing, the plates were removed from the molds and were scribed and broken to size. The edges were polished with a sequence of grits. The final buffing compound was a cerium oxide rouge.

We developed an alternative technique for making PMMA samples. If commercial transparent PMMA plate or rod material is immersed in a methanol solution containing the dye of interest, the dye will infuse into the plate along with the methanol. This technique has the great advantage of not requiring distillation, casting, or curing. A solution of 9% dichloromethane by volume in methanol was found to be the best compromise between speed of infusion and maintaining a good surface finish on the plate. The time required to achieve useful dye concentrations in the plastic for an eigth-inch rod was about 15 minutes, and for a sixteenth-inch thick plate the time was about 12 hours. The infusion was at room temperature in both cases. Coumarin-540 infused faster than rhodamine-640, possibly due to the difference in molecular weight.

It appeared to the eye that the dyes typically resided in a film between 0.1 and 1.0 mm from the surface of the plate, depending on the temperature and the soak time, so that the infusion technique does not yield a uniform dye concentration across the thickness of the plate. It is unlikely that the dye concentration in the film would be greater than that of the soaking solution, so that the solution concentration yields an upper bound on the local dye concentration. Measuring the peak optical density and assuming a uniform dye dispersion in the plate gives the average concentration in the plate.

Dye Spectra

Absorption spectra of all samples were made using either a Cary-14 or Cary-17 dual beam spectrophotometer. These produced strip-chart paper output, which was digitized using a Houston Instruments Hipad digitizer. Absorption spectra were usually taken from 12,500 cm^{-1} (8,000Å) to 30,000 cm^{-1} (3,333Å). Baseline corrections were always required over such a broad range, so that a base line spectrum was recorded, digitized, and subtracted from each absorption spectrum. The spectra were manipulated and stored on diskettes using a Terak-packaged PDP 11-03/2. The digitization accuracy was five-hundreths of an inch, which is finer than the pen line of the chart recorder output. The base line noise in the spectra was typically 1,000 liters per mole per cm, or in other words, the signal to noise was on the order of 100.

Emission and excitation spectra of the dyes were made at micromolar concentrations using the computer-controlled apparatus as shown

in Figure 3. The excitation source was either a 200 watt Oriel 6323 tungsten lamp or a 200 watt Oriel 6137 high pressure mercury lamp. The light was collimated with quartz optics, chopped by a PAR 191 chopper, and monochromated by a Jarrell-Ash (model 82-410, f-3.5, 0.25 meter) monochrometer with either a 6,000Å blased grating (1180 grooves/mm), or with a 3,000Å blazed grating, (2365 grooves/mm). In order that phase sensitive detection produce accurate excitation and emission spectra when the excitation source is chopped, it is important that the lifetimes of the dyes must be short compared to the chopping period. The chopping period in these experiments was 2.5 msec, which is several orders of magnitude longer than the lifetimes of the dyes measured. The excitation linewidth was fixed at 90Å across the tuning range.

The emission 90 degrees from the excitation was analyzed by a similar Jarrell-Ash monochromator. Adjustable slits allowed the resolution to vary between 2 and 90Å. The output light was detected by a 928 Hamamatsu photomultiplier tube (PMT) biased at 900 volts. The PMT output was terminated into 100k ohms in parallel with a PAR-HRB lock-in amplifier. The analog output of the lock-in was digitized and recorded by the PDP 11-03/2. Care was taken to keep the PMT current at a level less than 20% below its rated output current of 100 microamps. The RC time constant of the lock-in was kept at least as short as the time between digital sampling of the emission. These samples were taken typically every 10Å. Both monochromators were driven by a Slo-Syn SP151 Driver such that one or both monochromators could scan under the control of the PDP 11-03/2. This allowed spectra to be

Figure 3. Apparatus for emission and excitation measurements. A regulated mercury or tungsten source was focussed, chopped, and monochromated prior to illuminating the sample. The resulting emission was monochromated and detected by a PMT, and the resulting signal was amplified by phase-sensitive detection. A remote computer controlled both monochromators and recorded the spectra.

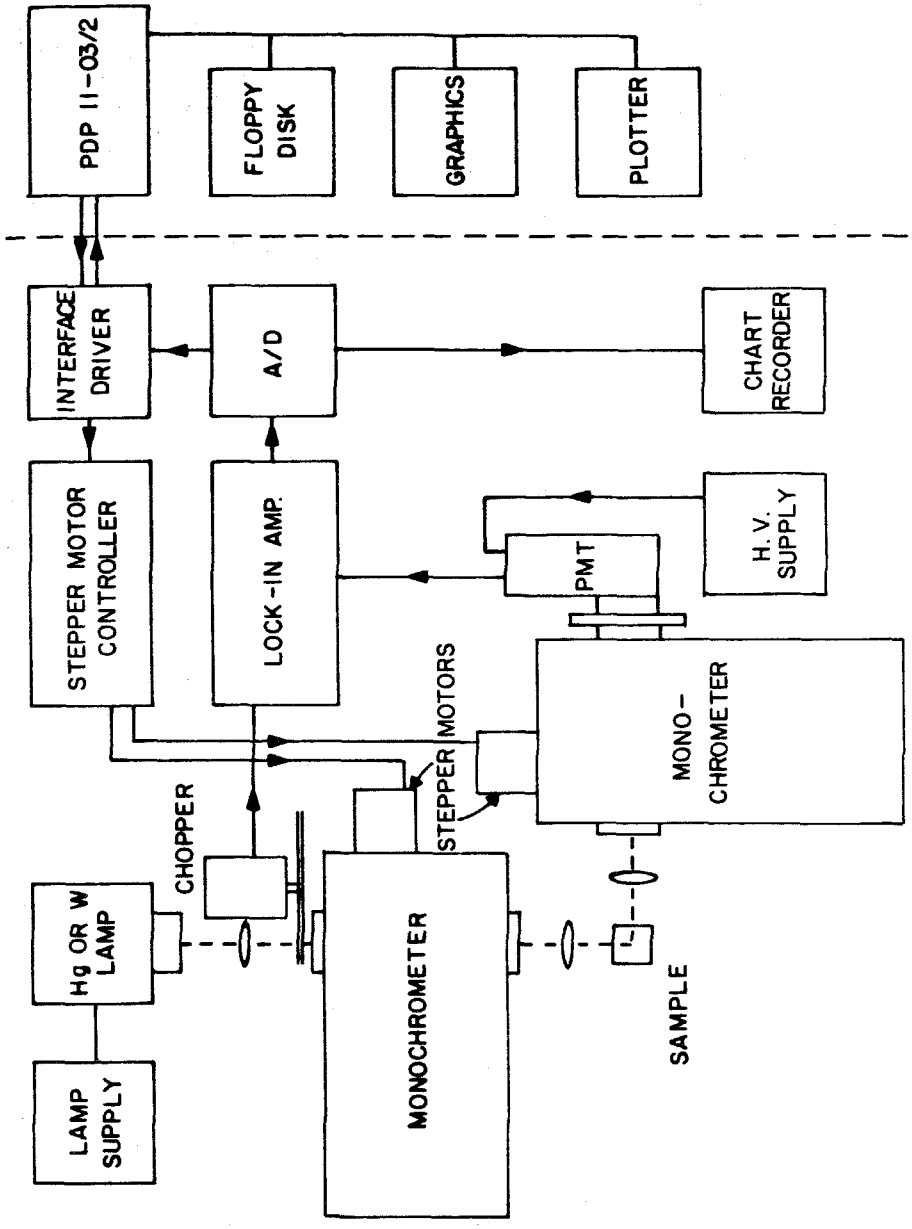
PDP 11-03/2
FLOPPY DISK
GRAPHICS
PLOTTER
INTERFACE DRIVER
A/D
CHART RECORDER
STEPPER MOTOR CONTROLLER
LOCK-IN AMP.
PMT
H.V. SUPPLY
STEPPER MOTORS
MONO-CHROMETER
CHOPPER
Hg OR W LAMP
MONOCHROMETER
LAMP SUPPLY
SAMPLE

acquired in cm^{-1} even though the monochromators had wavelength drives. Computer control also provided backlash correction.

Frequency calibration of the monochromators was done with the 5,451Å line from a mercury germicidal lamp. The system response was measured using an Eppley Laboratory calibrated EPI-1669 quartz halogen (tungsten) lamp in a custom housing. Calibration data provided with the lamp showed that the spectral response of the lamp could be accurately approximated by that of a 3,074° K black body for a lamp current of 7.9 amps. We used the black body spectrum to extrapolate the lamp response between the commercially calibrated data points. The system response function is given in Figure 4. The roll-off in the blue is due to the grating response, and the roll-off in the red is primarily due to the PMT.

Emission spectra were corrected by dividing out this system response, and were normalized so that the luminescence integrated over all wavenumbers equals one. The peak position of the emission for the dyes tested is given in Table 1. Correcting the excitation spectra for the response of the system requires a calibrated detector as well as a calibrated source. Using both it is possible to determine the response of the monochromator that is scanning the excitation. We were not successful in obtaining such a response using a Laser Precision Rk-3440 pyrometer detector. Instead we made the approximation that the PMT response was flat over the region of interest. In this approximation the variation of the scanning excitation intensity is assumed to be the measured response to the tungsten lamp. Excitation spectra were corrected by dividing out this measured response.

Figure 4. System response of the detection monochromator and PMT.

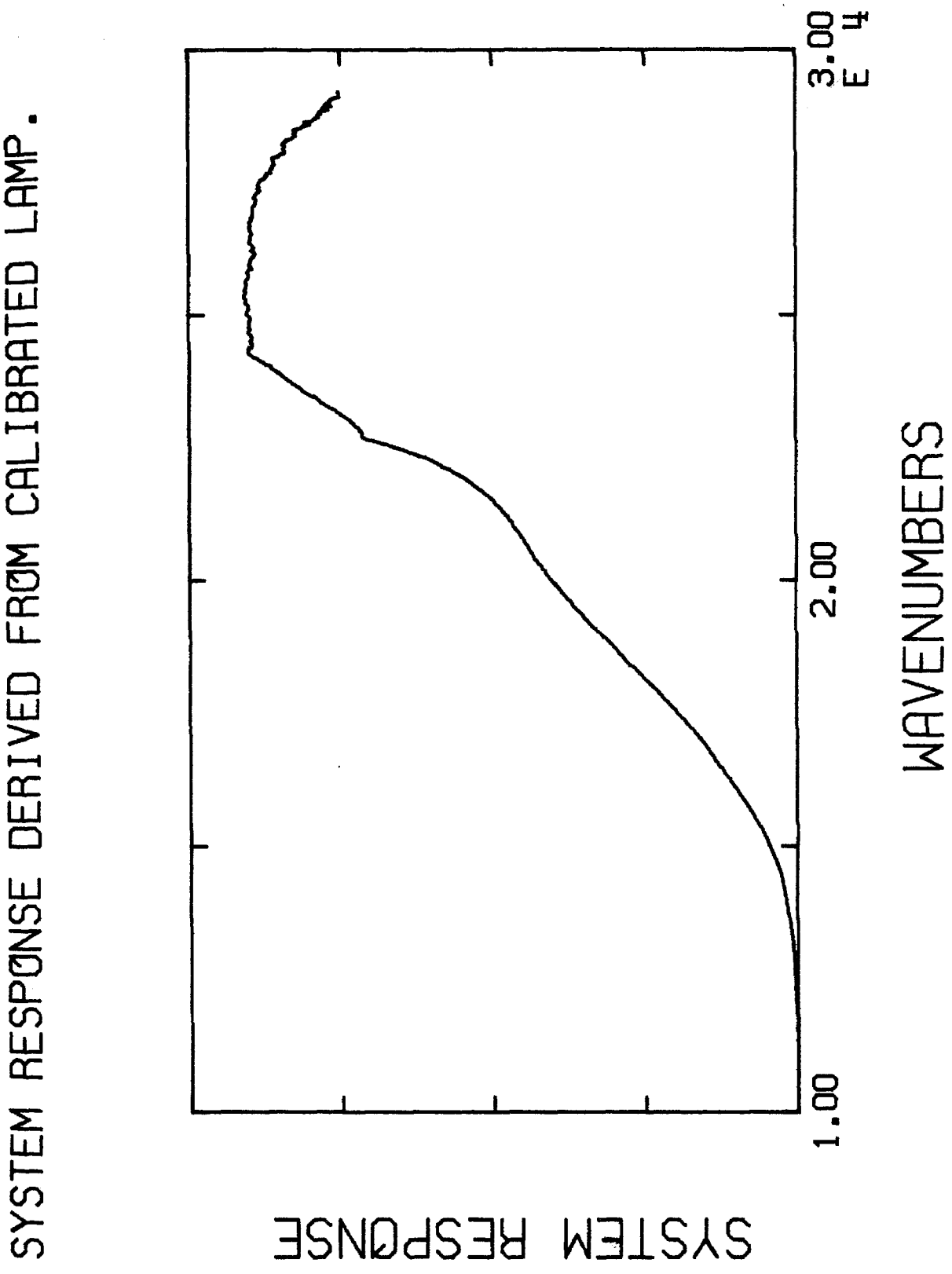
SYSTEM RESPONSE DERIVED FROM CALIBRATED LAMP.
SYSTEM RESPONSE
1.00
2.00
3.00
E 4
WAVENUMBERS

Table 1. Spectroscopic parameters for 18 organic laser dyes. The name of the dye given is the name used by Exciton. The number following the name is the approximate wavelength in nanometers of the dye's peak lasing power. All extinction coefficients were measured in methanol. The emission spectra were similarly methanol solutions. Literature values are given for the quantum efficiency of luminescence in various solvents. The critical optical density (CODE) is described on page 195 and following.

Table 1.

Exciton Dye (Kodak name)	ϵ_{max} (mole/cm/liter in methanol)	$\bar{\nu}(\epsilon_{max})$ cm^{-1}	$\lambda(\epsilon_{max})$ Å	$\bar{\nu}(f_{max})$ cm^{-1}	$\lambda(f_{max})$ Å	Stoke Shift $\nu(\epsilon_{max}) - \nu(f_{max})$ cm^{-1}	η Solvent	CODE ± 30%
Coumarin-480 (Coumarin-102)	22,000	25,730	3,890	21,200	4,720	4,560	0.58[a] ethanol	110.
Coumarin-500	19,900	25,660	3,900	20,200	4.950	5,440	0.53[a] ethanol	140.
Coumarin-535 (Coumarin-7)	52,200	23,120	4,320	20,400	4,900	2,720		90.
Coumarin-540 (Coumarin-6)	52,200	21,860	4,580	19,700	5,070	2,130	0.78[a] ethanol	80.
DCM	28,900	21,500	4,650	15,700	6,360	5,760	0.71[b] DMSO	240.
Rhodamine-560 (Rhodamine-110)	82,000	20,120	4,970	19,000	5,250	1,080	0.85[c] ethanol	25.
Rhodamine-575	93,800	19,330	5,170	18,300	5,460	1,010		35.
Rhodamine-590 (Rhodamine-6G)	107,000	18,940	5,280	18,000	5,550	900	0.98[d] methanol	25.
Rhodamine-610 (Rhodamine-B)	114,000	18,380	5,440	17,500	5,710	870	0.5[e] ethanol	36.
Kiton red-620 (Sulforhodamine-B)	111,000	17,990	5,560	17,300	5,800	740	0.83[g] ethanol	16.
Rhodamine-640 (Rhodamine-101)	106,000	17,670	5,660	16,800	5,940	830	1.[c] ethanol	17.
Sulforhodamine-640 (Sulforhodamine-101)	120,000	17,360	5,760	16,700	6,000	690	1.[h] ethanol	17.
Cresyl Violet-670 (Oxazine-9)	57,900	16,880	5,920	16,100	6,220	810	0.54[f] methanol	17.
Oxazine-720 (Oxazine-170)	81,800	16,170	6,190	15,600	6,420	600		17.
Oxazine-750	90,600	15,140	6,600	14,500	6,920	680		25.
DODCI	238,000	17,160	5,830	16,500	6,050	630		11.
DOTCI	236,000	14,770	6,770	14,000	7,140	770		8.
IR-144	153,000	13,560	7,370	12,000	8,340	1,560		16.

[a] G. A. Reynolds, K. H. Drexhage, Optics Comm., 13, No. 3, 222 (1975).

[b] P. R. Hammond, Optics Comm., 29, No. 3, 331 (1979).

[c] K. H. Drexhage, "Structure and Properties of Laser Dyes," ed. F. P. Schafer, Topics in Dye Lasers, Applied Physics I (Springer-Verlag, New York, 1977) p. 144.

[d] A. Baczynski, T. Marszalek, H. Walerys, B. Zietek, Acta Phys. Polo., A44, No. 6, 805 (1973).

[e] T. Karstens, K. Kobs, J. Phys. Chem., 84, No. 14, 1871 (1980).

[f] D. Magde, J. H. Brannon, T. L. Cremers, J. Olmsted III, J. Phys. Chem., 83, No. 6, 696 (1979).

[g] J. M. Drake, R. T. Morse, R. N. Steppl, D. Young, Chem. Phys. Lett., 35, No. 2, 181 (1975).

[h] C. F. Rapp et al., Final Report of Owens Illinois, Sand77-7005, p. 40.

The inadequacy of this correction procedure is evidenced by the mismatch between the excitation spectra corrected in this manner and the corresponding absorption spectra for most dyes whose absorption peaks were on the sloped regions of the system response.

Both the emission and excitation spectra of these dyes were taken only at micromolar dye concentrations in order to minimize the red-shifting effect of self-absorption. The optical density of the sample in the region where the absorption and emission overlap must be sufficiently low so that the blue tail of the emission spectrum is not artificially filtered out. The excitation samples must be dilute for a second reason. Away from the peak of the absorption, where the absorption per unit length is small, the exciting beam intensity does not vary greatly along the beam path in the sample. However, as the excitation is scanned across the peak of the absorption, most of the exciting light is absorbed in a thin surface layer in the sample if the concentration is too high. This effect changes the spatial distribution of the emission, and thus can alter the observed excitation spectrum.

The results of these dye spectra measurements are given in Figures 5 through 27. The dyes are ordered by decreasing energy of the absorption peaks. All dyes are in methanol solutions except for three additional DCM spectra in chloroform, DMSO, and PMMA. The solar flux given on each spectrum is an idealized 5800K black body spectrum. The three titles in small letters in the upper right hand corner of the plots are the diskette file names of the absorption, emission, and excitation spectra. The peak positions of the absorption and emission spectra of these dyes, as well as the peak extinction

Figures 5 - 25. Survey of laser dye spectra. The extinction coefficient in liters per mole centimeter (solid lines); the normalized emission spectrum in arbitrary units (long dashed line); and the excitation spectrum in arbitrary units (short dashed line), are presented for 18 common organic laser dyes. The dotted line is the flux spectrum from a 5800°K black body. The small titles in the upper right corner refer to diskette file names. The figures are organized as follows:

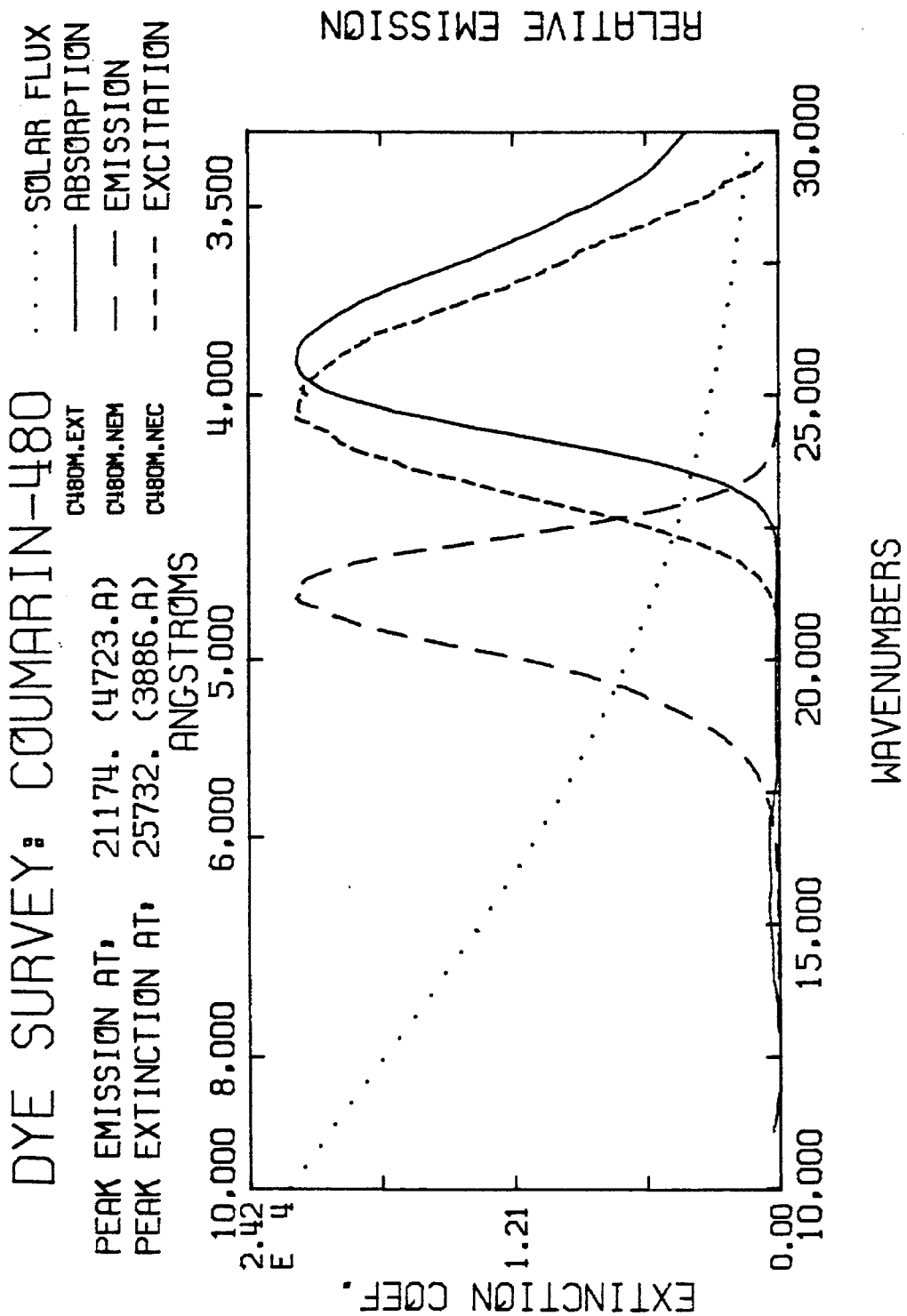
DYE SURVEY: COUMARIN-480
C480M.EXT
C480M.NEM
C480M.NEC
SOLAR FLUX
ABSORPTION
EMISSION
EXCITATION
PEAK EMISSION AT, 21174. (4723.A)
PEAK EXTINCTION AT, 25732. (3886.A)
ANGSTROMS
10,000 8,000 6,000 5,000 4,000 3,500
30,000 25,000 20,000 15,000 10,000
WAVENUMBERS
2.42 E 4
1.21
0.00
EXTINCTION COEF.
RELATIVE EMISSION

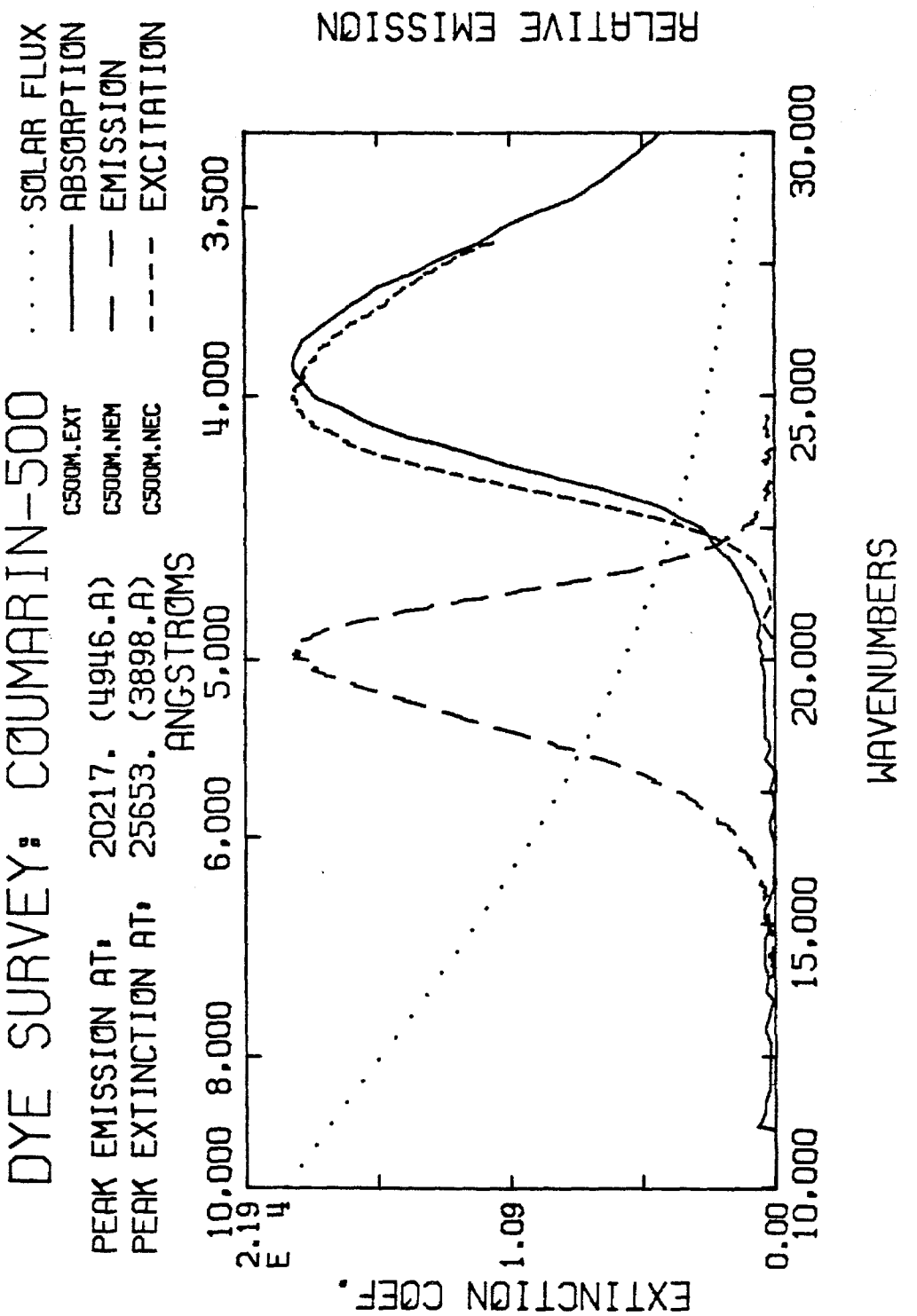
DYE SURVEY: COUMARIN-500
C500M.EXT
C500M.NEM
C500M.NEC
SOLAR FLUX
ABSORPTION
EMISSION
EXCITATION
PEAK EMISSION AT: 20217. (4946.A)
PEAK EXTINCTION AT: 25653. (3898.A)
ANGSTROMS
10,000 8,000 6,000 5,000 4,000 3,500
2.19 E 4
1.09
0.00
10,000 15,000 20,000 25,000 30,000
WAVENUMBERS
EXTINCTION COEF.
RELATIVE EMISSION

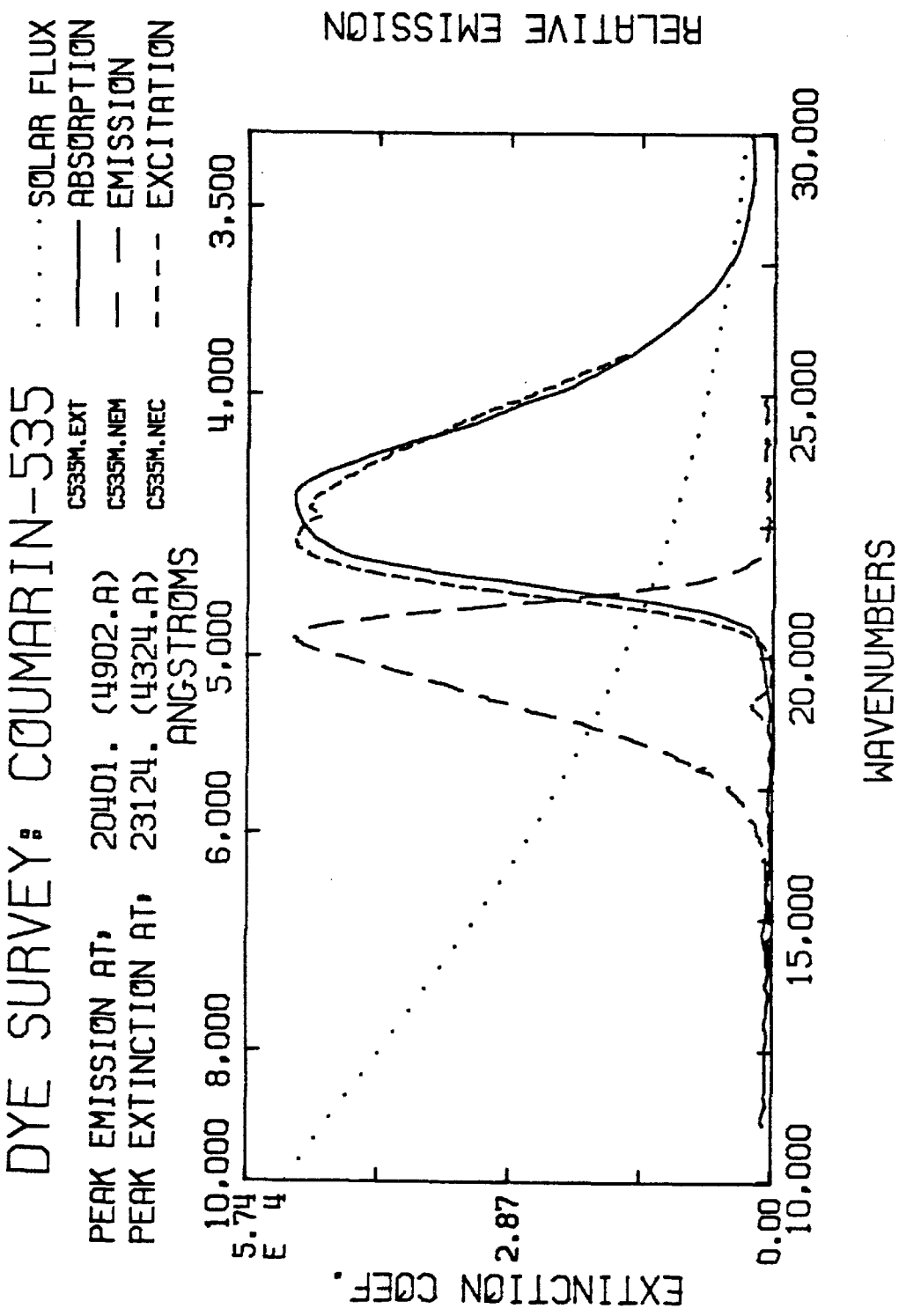
DYE SURVEY: COUMARIN-535
C535M.EXT
C535M.NEM
C535M.NEC
SOLAR FLUX
ABSORPTION
EMISSION
EXCITATION
PEAK EMISSION AT, 20401. (4902.A)
PEAK EXTINCTION AT, 23124. (4324.A)
ANGSTROMS
10,000 8,000 6,000 5,000 4,000 3,500
30,000 25,000 20,000 15,000 10,000
WAVENUMBERS
RELATIVE EMISSION
EXTINCTION COEF.
5.74 E 4
2.87
0.00

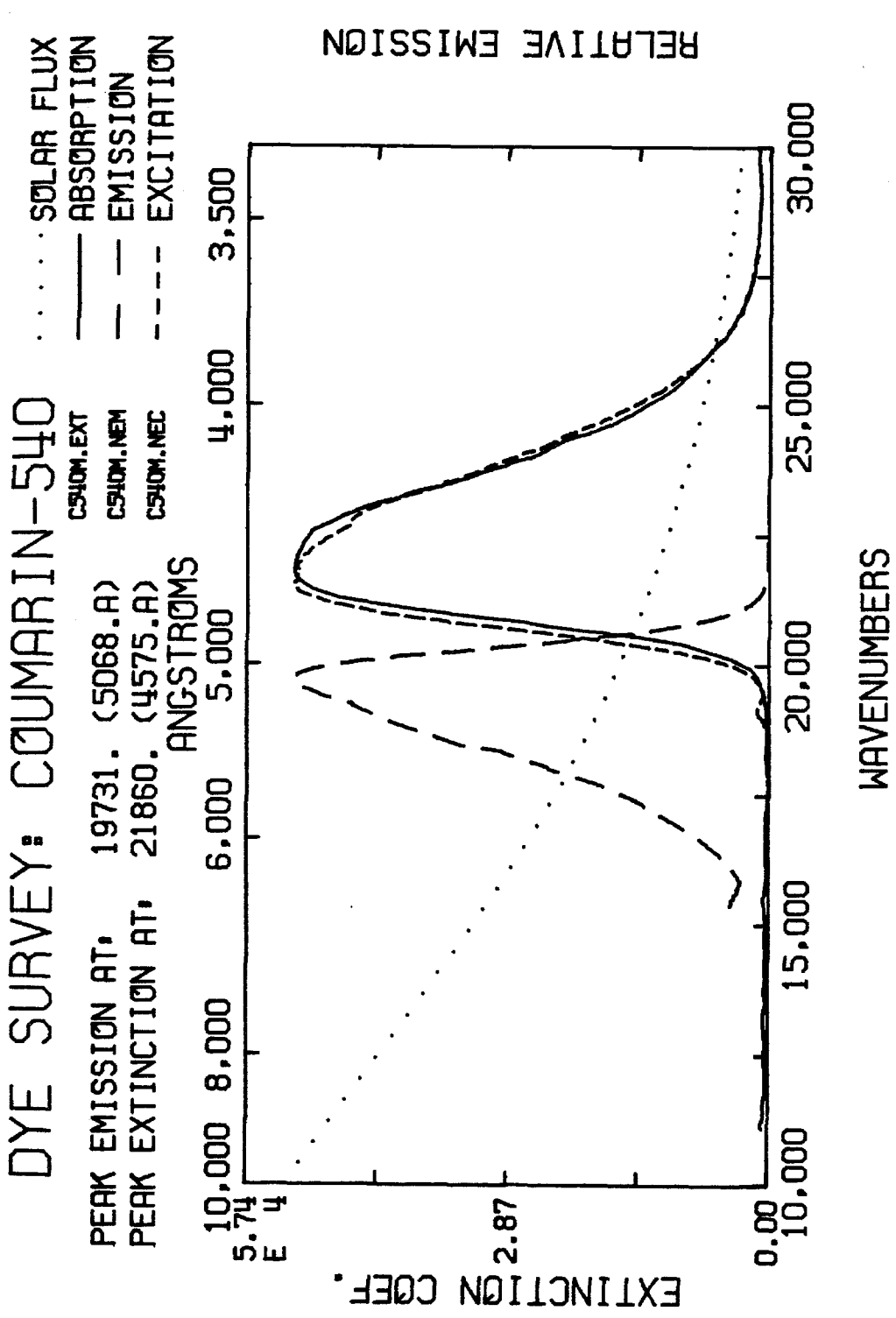
DYE SURVEY: COUMARIN-540
C540M.EXT
C540M.NEM
C540M.NEC
SOLAR FLUX
ABSORPTION
EMISSION
EXCITATION
PEAK EMISSION AT: 19731. (5068.A)
PEAK EXTINCTION AT: 21860. (4575.A)
ANGSTROMS
10,000
8,000
6,000
5,000
4,000
3,500
30,000
25,000
20,000
15,000
10,000
5.74 E 4
2.87
0.00
EXTINCTION COEF.
RELATIVE EMISSION
WAVENUMBERS

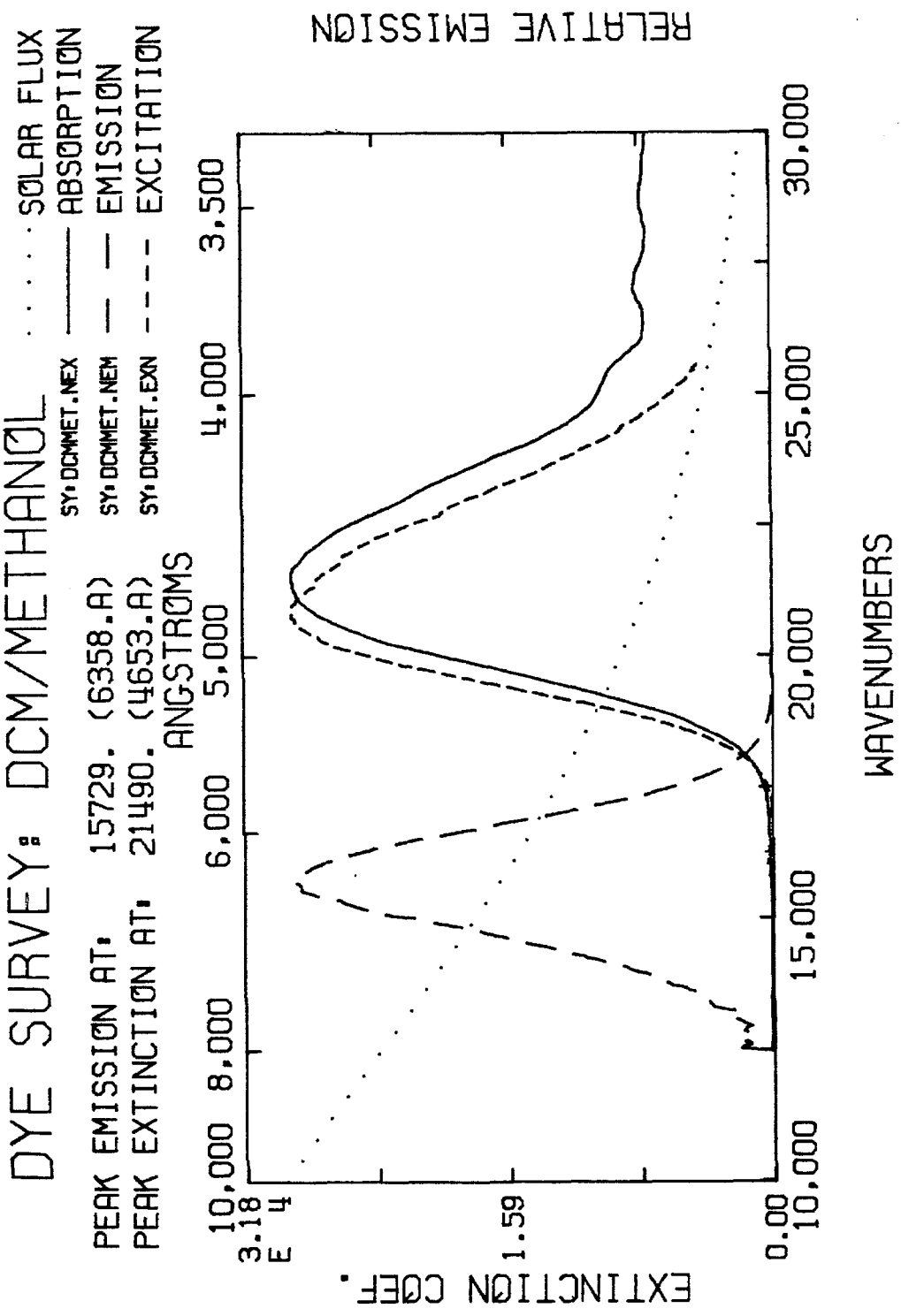
DYE SURVEY: DCM/METHANOL
SOLAR FLUX
ABSORPTION
EMISSION
EXCITATION
SY:DCMMET.NEX
SY:DCMMET.NEM
SY:DCMMET.EXN
PEAK EMISSION AT: 15729. (6358.A)
PEAK EXTINCTION AT: 21490. (4653.A)
ANGSTROMS
10,000 8,000 6,000 5,000 4,000 3,500
30,000 25,000 20,000 15,000 10,000
WAVENUMBERS
RELATIVE EMISSION
EXTINCTION COEF.
3.18 E 4
1.59
0.00

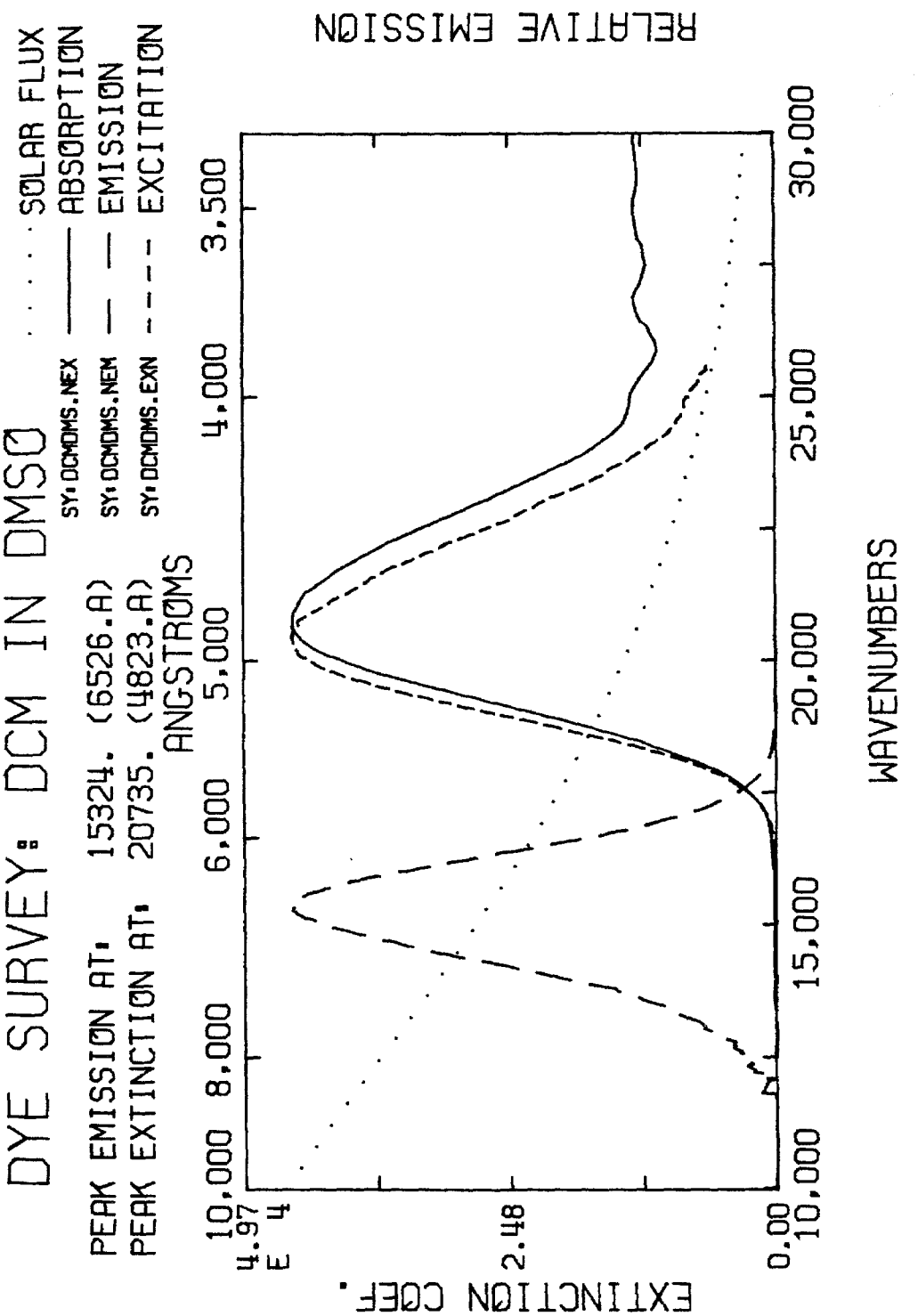
DYE SURVEY: DCM IN DMSO
PEAK EMISSION AT: 15324. (6526.A)
PEAK EXTINCTION AT: 20735. (4823.A)
SY:DCMDMS.NEX
SY:DCMDMS.NEM
SY:DCMDMS.EXN
SOLAR FLUX
ABSORPTION
EMISSION
EXCITATION
RELATIVE EMISSION
EXTINCTION COEF.
4.97 E 4
2.48
0.00
10,000
15,000
20,000
25,000
30,000
3,500
4,000
5,000
6,000
8,000
10,000
ANGSTROMS
WAVENUMBERS

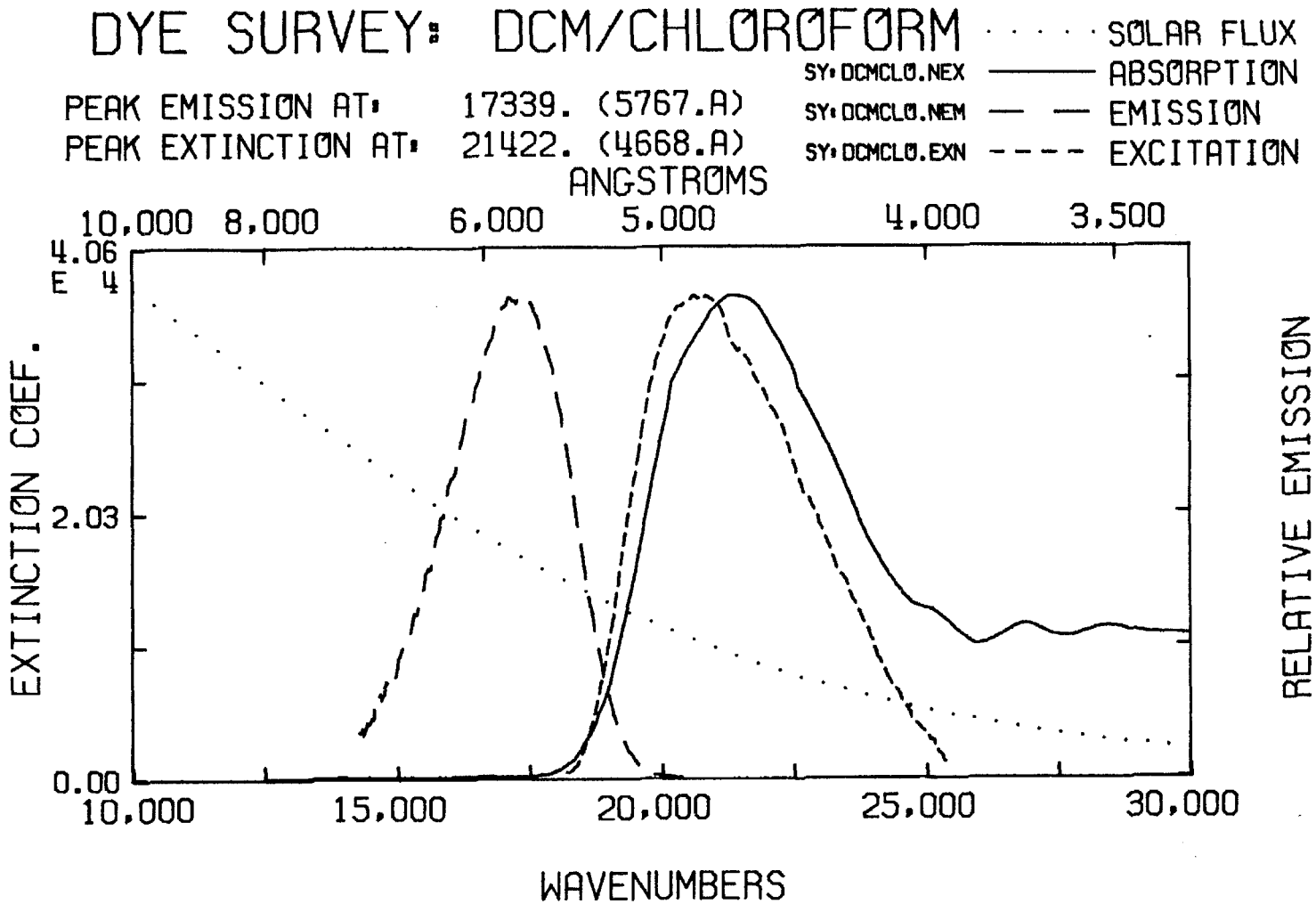
DYE SURVEY: DCM/CHLOROFORM
SOLAR FLUX
SY:DCMCLO.NEX ABSORPTION
SY:DCMCLO.NEM EMISSION
SY:DCMCLO.EXN EXCITATION
PEAK EMISSION AT: 17339. (5767.A)
PEAK EXTINCTION AT: 21422. (4668.A)
ANGSTROMS
10,000 8,000 6,000 5,000 4,000 3,500
4.06
E 4
2.03
0.00
EXTINCTION COEF.
RELATIVE EMISSION
10,000 15,000 20,000 25,000 30,000
WAVENUMBERS

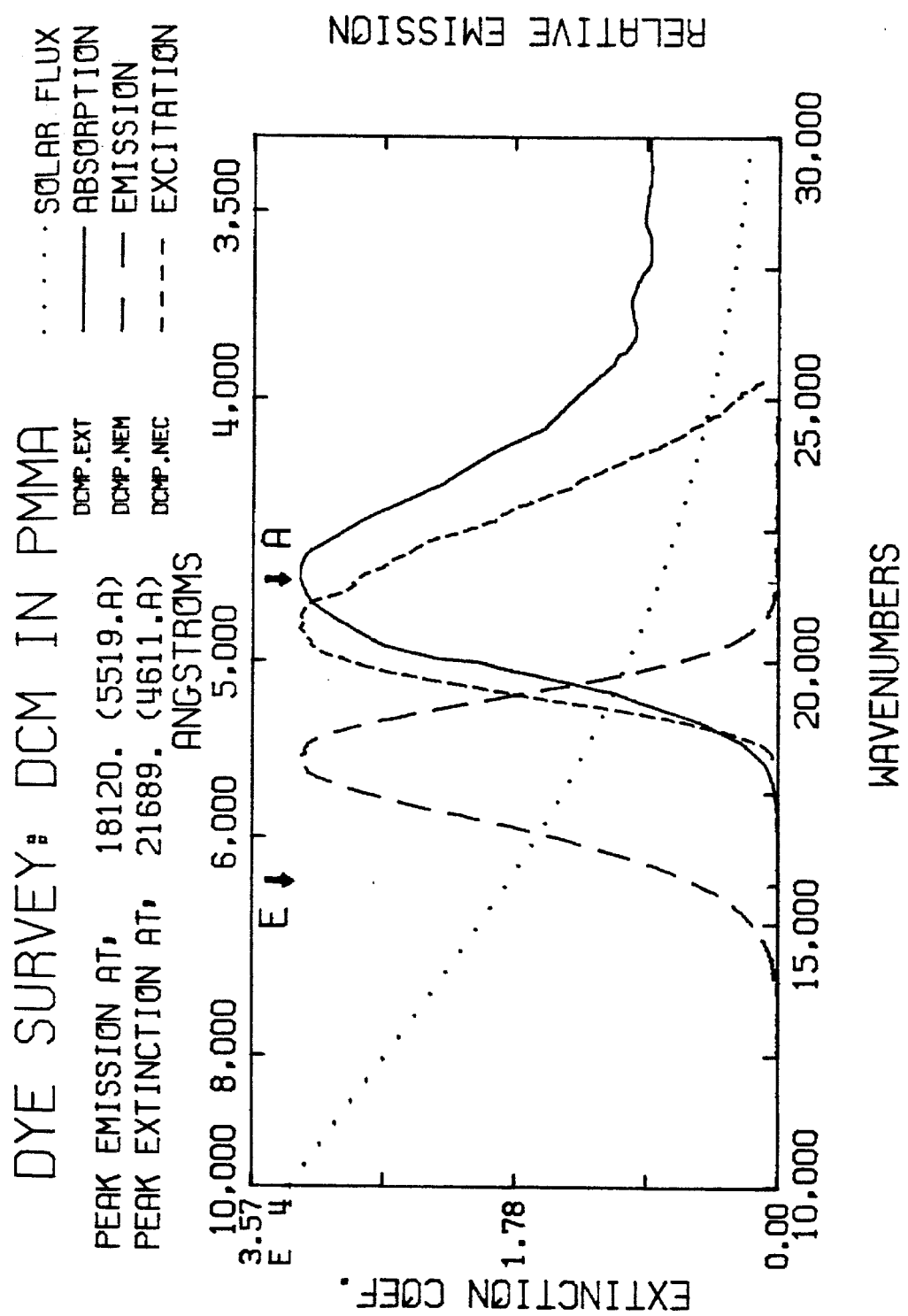
DYE SURVEY: DCM IN PMMA
PEAK EMISSION AT, 18120. (5519.A)
PEAK EXTINCTION AT, 21689. (4611.A)
DCMP.EXT
DCMP.NEM
DCMP.NEC
SOLAR FLUX
ABSORPTION
EMISSION
EXCITATION
RELATIVE EMISSION
EXTINCTION COEF.
3.57
E 4
1.78
0.00
10,000
8,000
6,000
5,000
4,000
3,500
ANGSTROMS
E
A
10,000
15,000
20,000
25,000
30,000
WAVENUMBERS

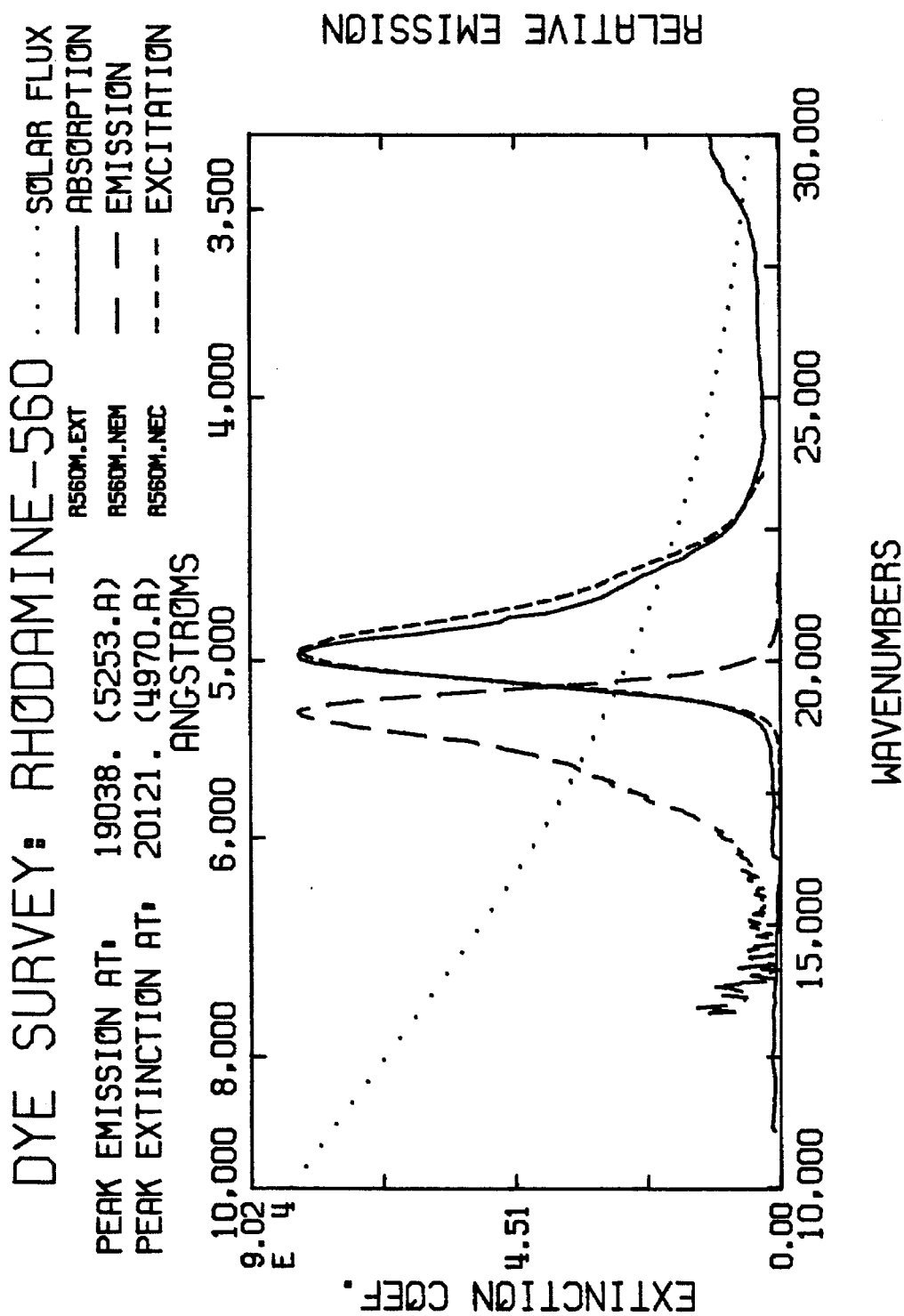
DYE SURVEY: RHODAMINE-560
SOLAR FLUX
ABSORPTION
EMISSION
EXCITATION
R560M.EXT
R560M.NEM
R560M.NEC
PEAK EMISSION AT: 19038. (5253.A)
PEAK EXTINCTION AT: 20121. (4970.A)
ANGSTROMS
10,000 8,000 6,000 5,000 4,000 3,500
9.02 E 4
4.51
0.00
10,000 15,000 20,000 25,000 30,000
EXTINCTION COEF.
RELATIVE EMISSION
WAVENUMBERS

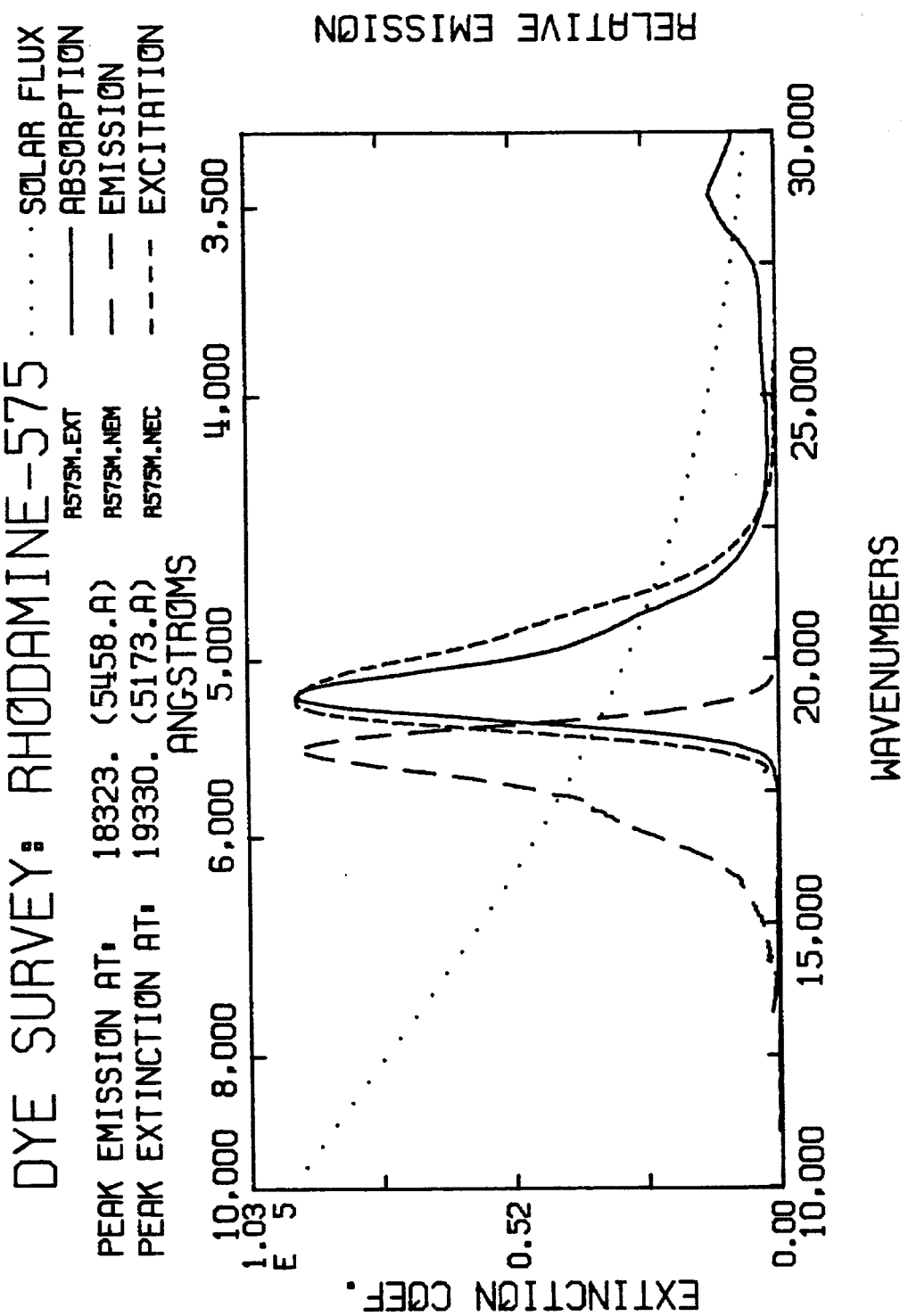
DYE SURVEY: RHODAMINE-575
PEAK EMISSION AT: 18323. (5458.A)
PEAK EXTINCTION AT: 19330. (5173.A)
R575M.EXT
R575M.NEM
R575M.NEC
SOLAR FLUX
ABSORPTION
EMISSION
EXCITATION
ANGSTROMS
10,000
8,000
6,000
5,000
4,000
3,500
30,000
25,000
20,000
15,000
10,000
WAVENUMBERS
RELATIVE EMISSION
EXTINCTION COEF.
1.03 E 5
0.52
0.00

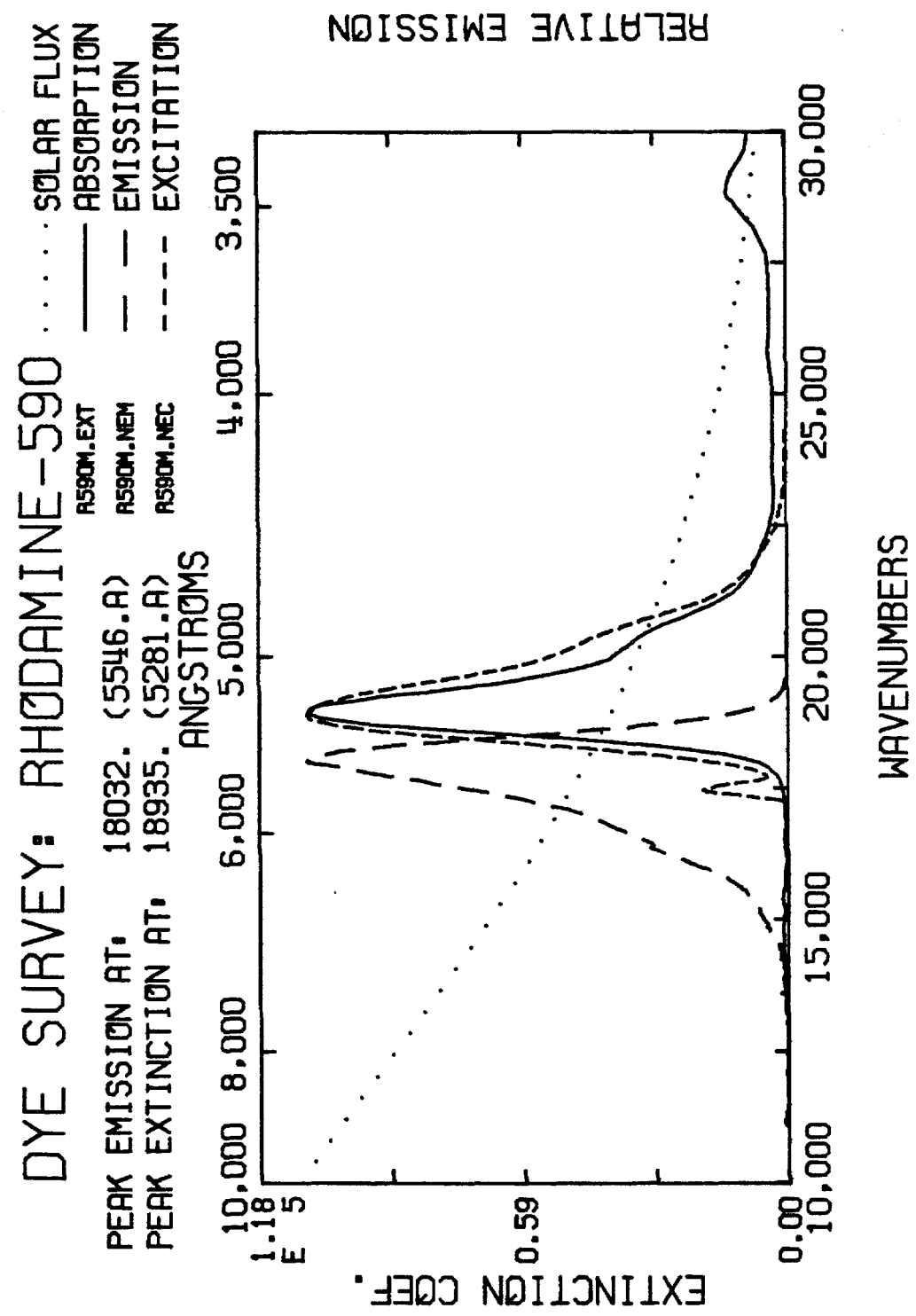
DYE SURVEY: RHODAMINE-590
PEAK EMISSION AT: 18032. (5546.A)
PEAK EXTINCTION AT: 18935. (5281.A)
R590M.EXT
R590M.NEM
R590M.NEC
SOLAR FLUX
ABSORPTION
EMISSION
EXCITATION
ANGSTROMS
10,000 8,000 6,000 5,000 4,000 3,500
30,000 25,000 20,000 15,000 10,000
WAVENUMBERS
EXTINCTION COEF.
1.18 E 5
0.59
0.00
RELATIVE EMISSION

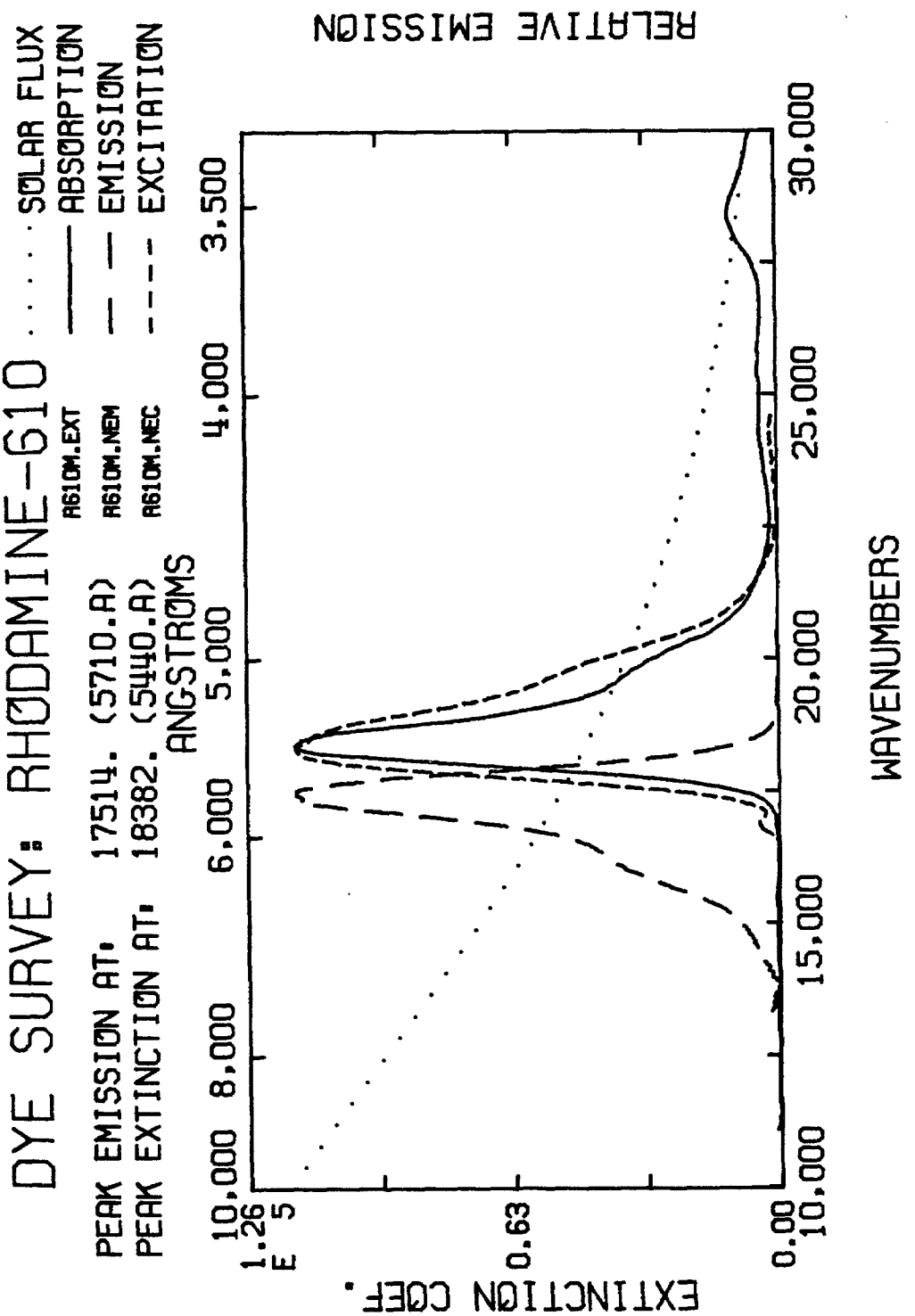
DYE SURVEY: RHODAMINE-610
PEAK EMISSION AT: 17514. (5710.A)
PEAK EXTINCTION AT: 18382. (5440.A)
R610M.EXT
R610M.NEM
R610M.NEC
SOLAR FLUX
ABSORPTION
EMISSION
EXCITATION
RELATIVE EMISSION
EXTINCTION COEF.
1.26 E 5
0.63
0.00
10,000
8,000
6,000
5,000
4,000
3,500
ANGSTROMS
10,000
15,000
20,000
25,000
30,000
WAVENUMBERS

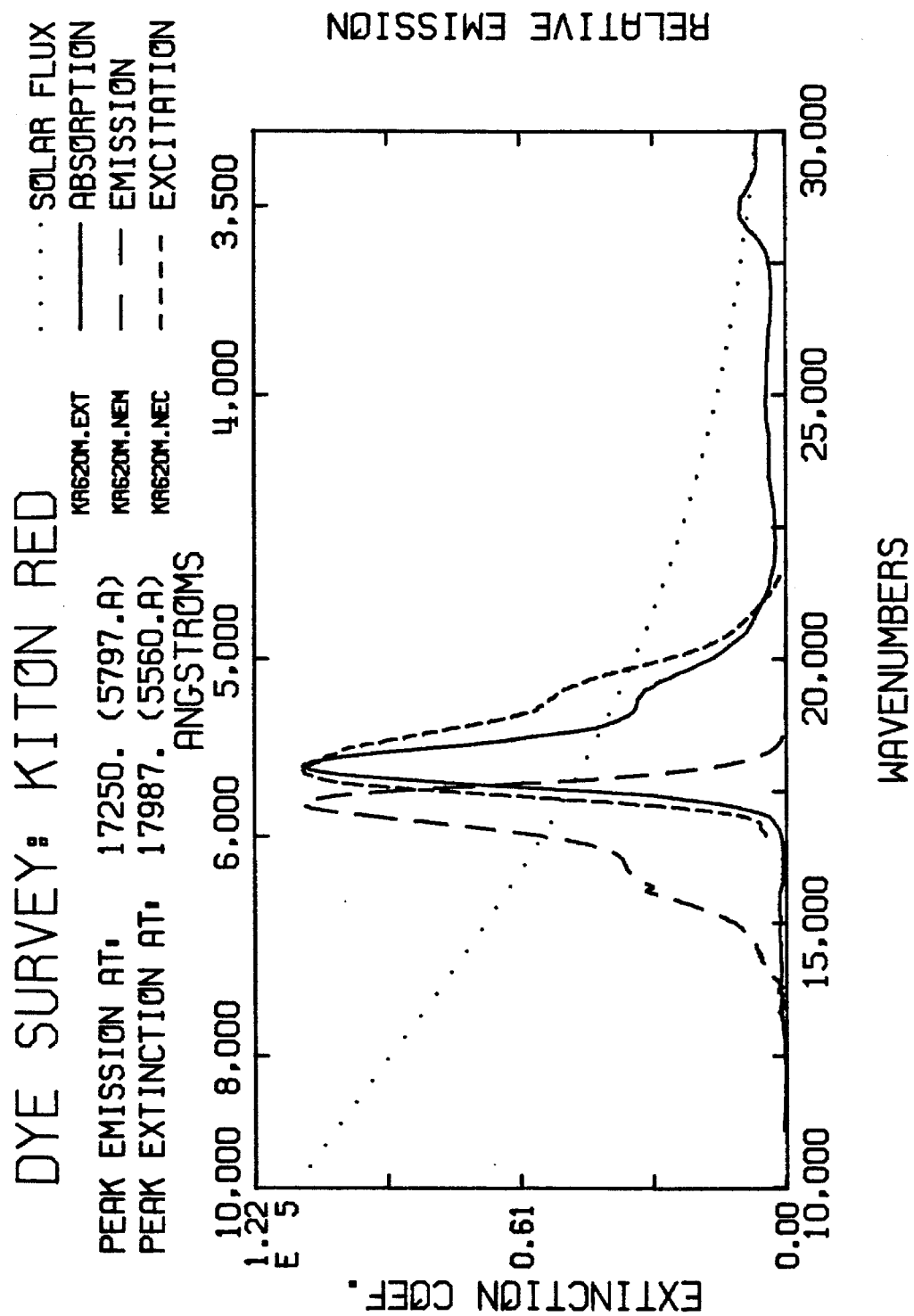
DYE SURVEY: KITON RED
PEAK EMISSION AT: 17250. (5797.A)
PEAK EXTINCTION AT: 17987. (5560.A)
KR620M.EXT
KR620M.NEM
KR620M.NEC
SOLAR FLUX
ABSORPTION
EMISSION
EXCITATION
ANGSTROMS
10,000
8,000
6,000
5,000
4,000
3,500
WAVENUMBERS
10,000
15,000
20,000
25,000
30,000
EXTINCTION COEF.
1.22 E 5
0.61
0.00
RELATIVE EMISSION

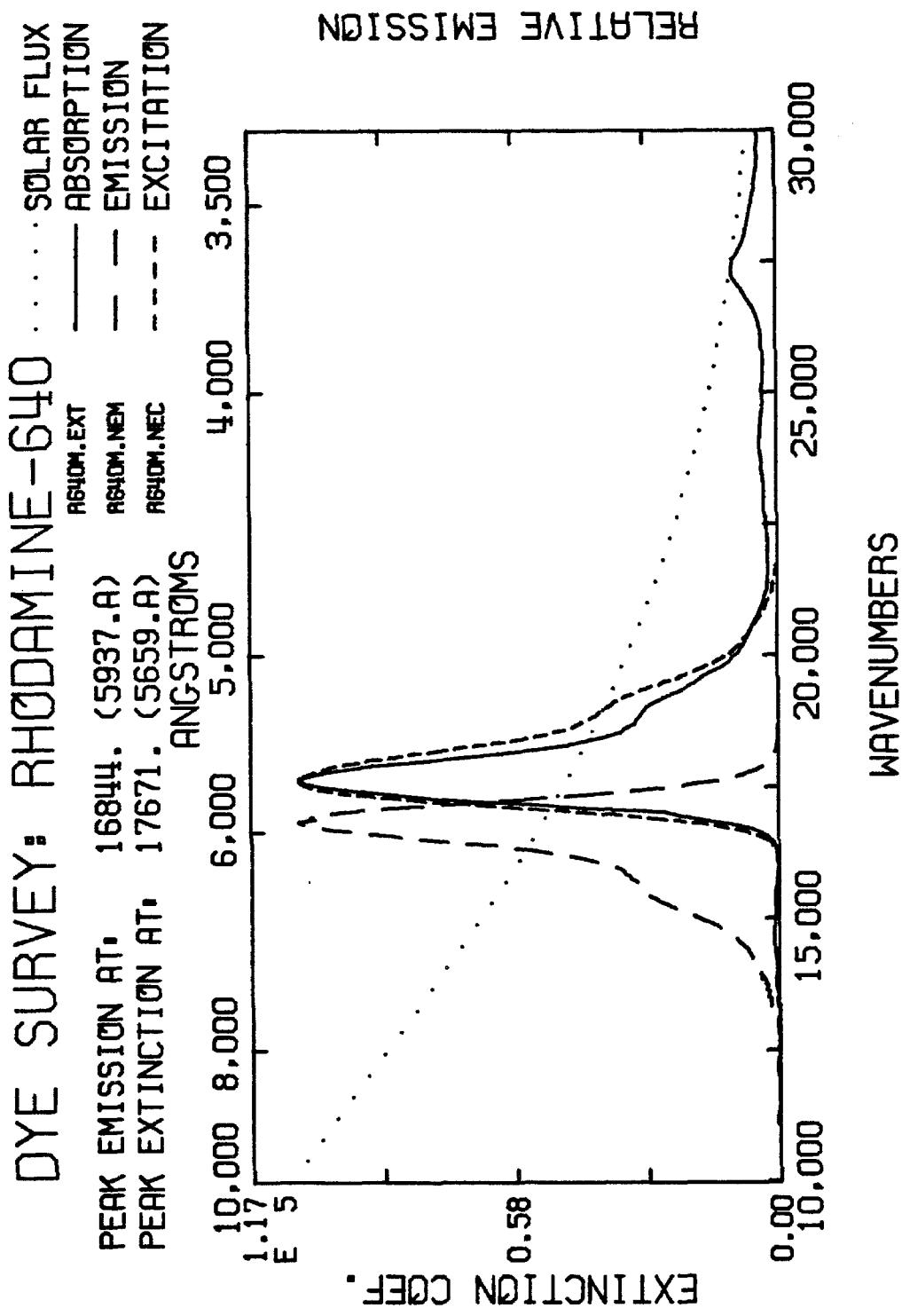
DYE SURVEY: RHODAMINE-640
PEAK EMISSION AT: 16844. (5937.A)
PEAK EXTINCTION AT: 17671. (5659.A)
R640M.EXT
R640M.NEM
R640M.NEC
SOLAR FLUX
ABSORPTION
EMISSION
EXCITATION
ANGSTROMS
10,000 8,000 6,000 5,000 4,000 3,500
30,000 25,000 20,000 15,000 10,000
WAVENUMBERS
EXTINCTION COEF.
1.17 E 5
0.58
0.00
RELATIVE EMISSION

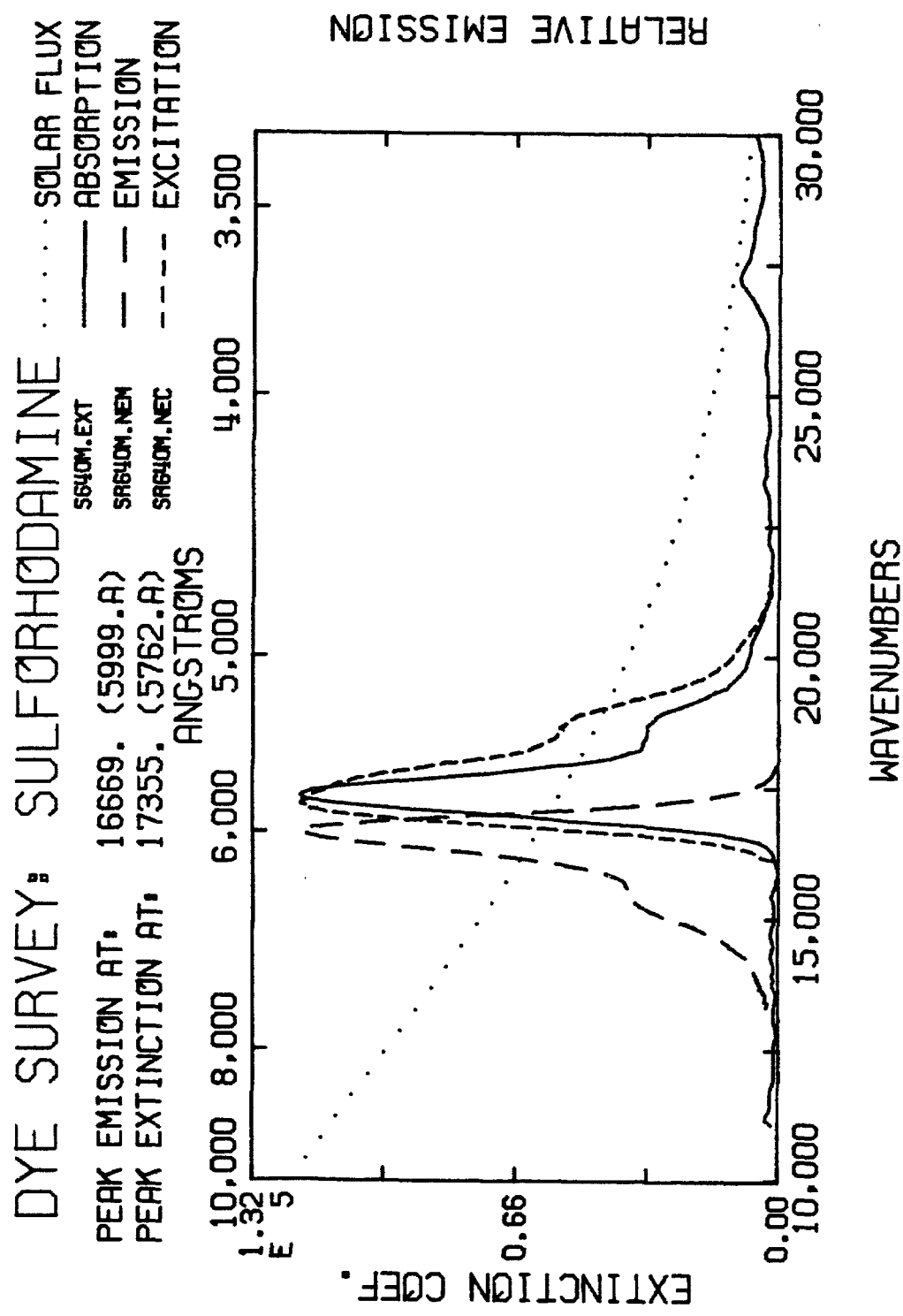
DYE SURVEY: SULFORHODAMINE
PEAK EMISSION AT: 16669. (5999.A)
PEAK EXTINCTION AT: 17355. (5762.A)
SBWDM.EXT
SRBWDM.NEW
SRBWDM.NEC
SOLAR FLUX
ABSORPTION
EMISSION
EXCITATION
ANGSTROMS
10,000
8,000
6,000
5,000
4,000
3,500
RELATIVE EMISSION
EXTINCTION COEF.
1.32 E 5
0.66
0.00
10,000
15,000
20,000
25,000
30,000
WAVENUMBERS

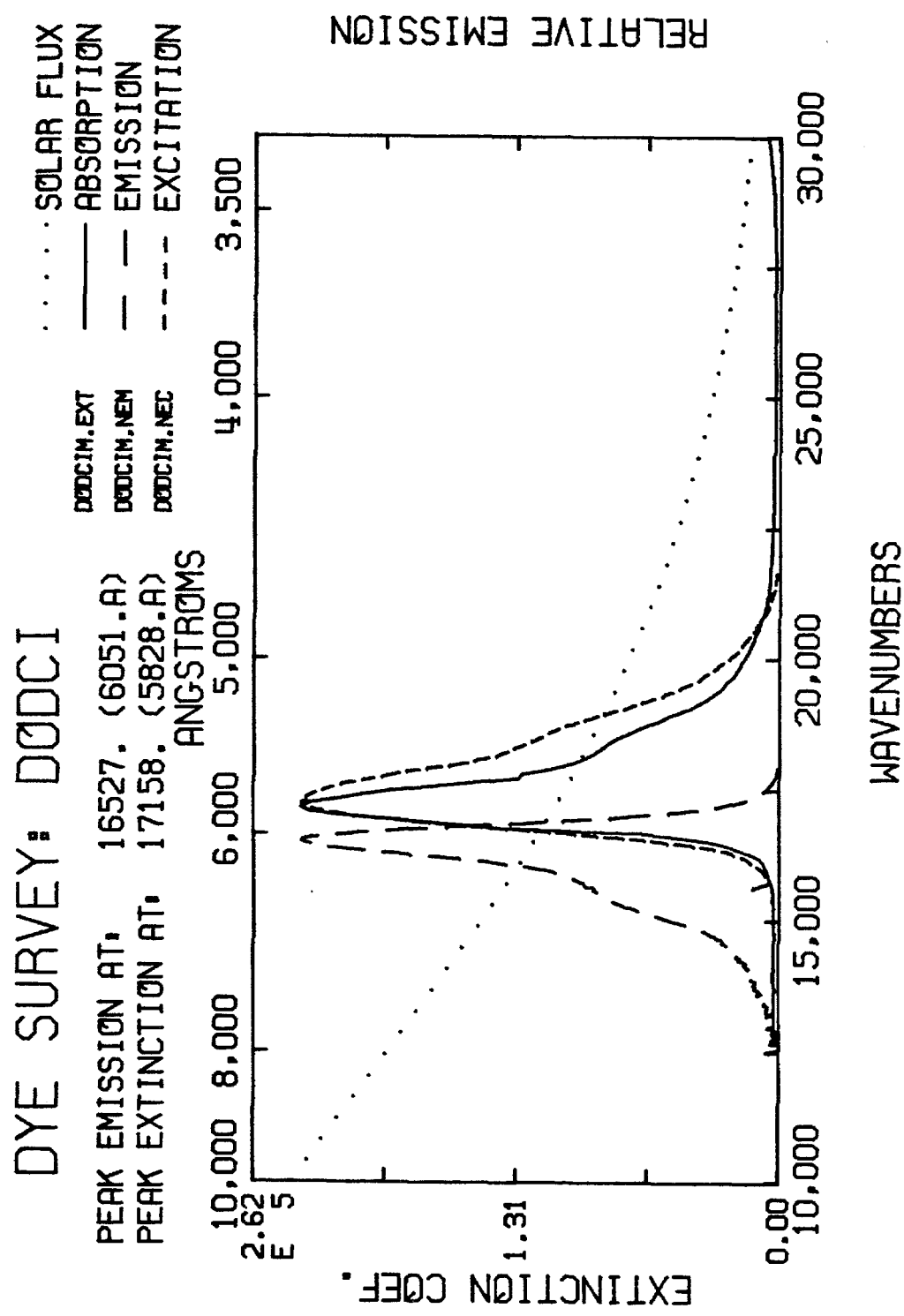
DYE SURVEY: DODCI
PEAK EMISSION AT: 16527. (6051.A)
PEAK EXTINCTION AT: 17158. (5828.A)
DODCIM.EXT
DODCIM.MEM
DODCIM.MEC
SOLAR FLUX
ABSORPTION
EMISSION
EXCITATION
RELATIVE EMISSION
EXTINCTION COEF.
2.62 E 5
1.31
0.00
10,000
15,000
20,000
25,000
30,000
WAVENUMBERS
10,000
8,000
6,000
5,000
4,000
3,500
ANGSTROMS

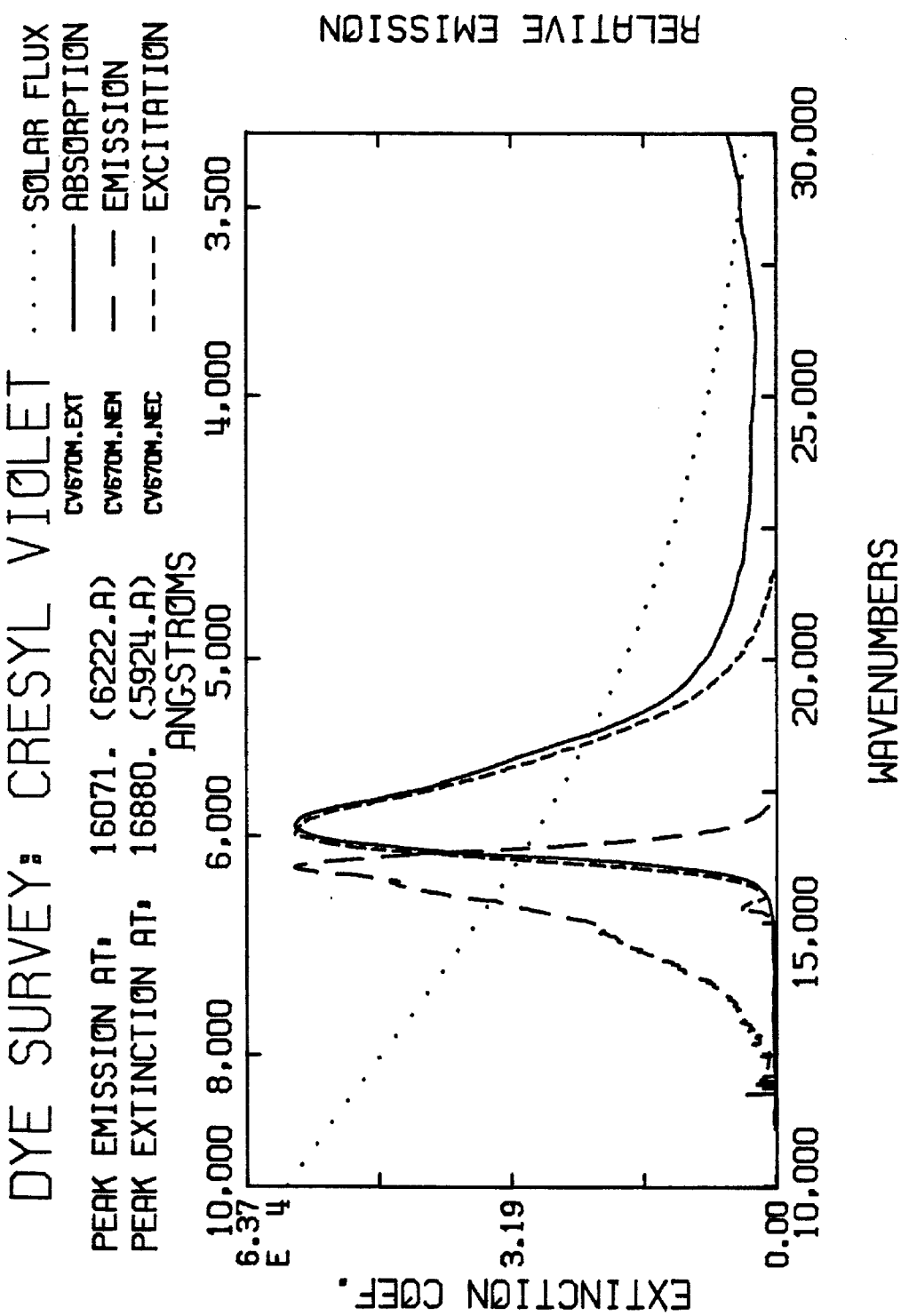
DYE SURVEY: CRESYL VIOLET
CV670M.EXT
CV670M.NEM
CV670M.NEC
SOLAR FLUX
ABSORPTION
EMISSION
EXCITATION
PEAK EMISSION AT: 16071. (6222.A)
PEAK EXTINCTION AT: 16880. (5924.A)
ANGSTROMS
10,000
8,000
6,000
5,000
4,000
3,500
30,000
25,000
20,000
15,000
10,000
WAVENUMBERS
6.37
E 4
3.19
0.00
EXTINCTION COEF.
RELATIVE EMISSION

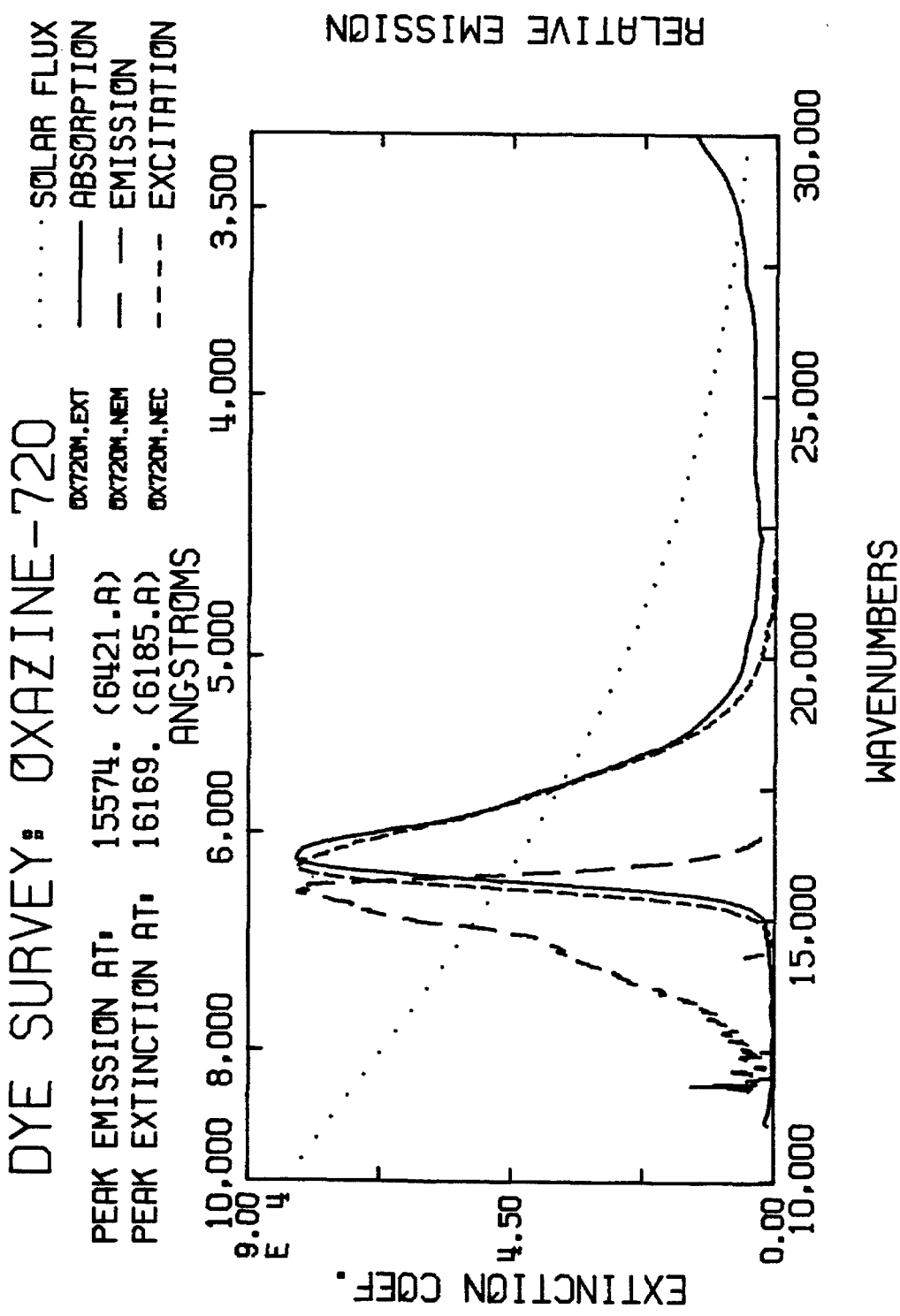
DYE SURVEY: OXAZINE-720
PEAK EMISSION AT: 15574. (6421.A)
PEAK EXTINCTION AT: 16169. (6185.A)
OX720M.EXT
OX720M.MEM
OX720M.MEC
SOLAR FLUX
ABSORPTION
EMISSION
EXCITATION
RELATIVE EMISSION
EXTINCTION COEF.
E 4
9.00
4.50
0.00
10,000
8,000
6,000
5,000
4,000
3,500
ANGSTROMS
10,000
15,000
20,000
25,000
30,000
WAVENUMBERS

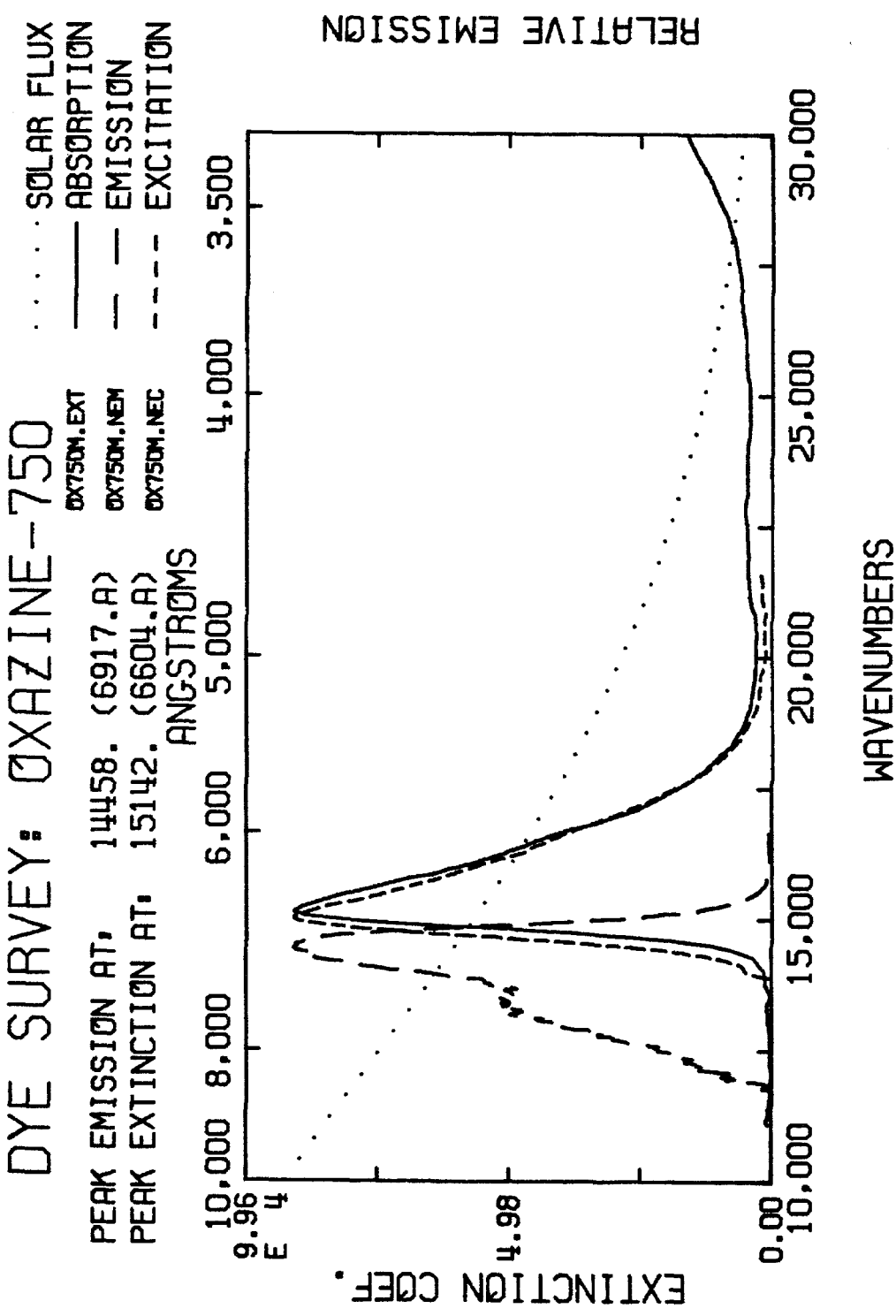
DYE SURVEY: OXAZINE-750
PEAK EMISSION AT: 14458. (6917.A)
PEAK EXTINCTION AT: 15142. (6604.A)
OX750M.EXT
OX750M.NEM
OX750M.NEC
SOLAR FLUX
ABSORPTION
EMISSION
EXCITATION
ANGSTROMS
10,000
8,000
6,000
5,000
4,000
3,500
EXTINCTION COEF.
9.96 E 4
4.98
0.00
10,000
15,000
20,000
25,000
30,000
WAVENUMBERS
RELATIVE EMISSION

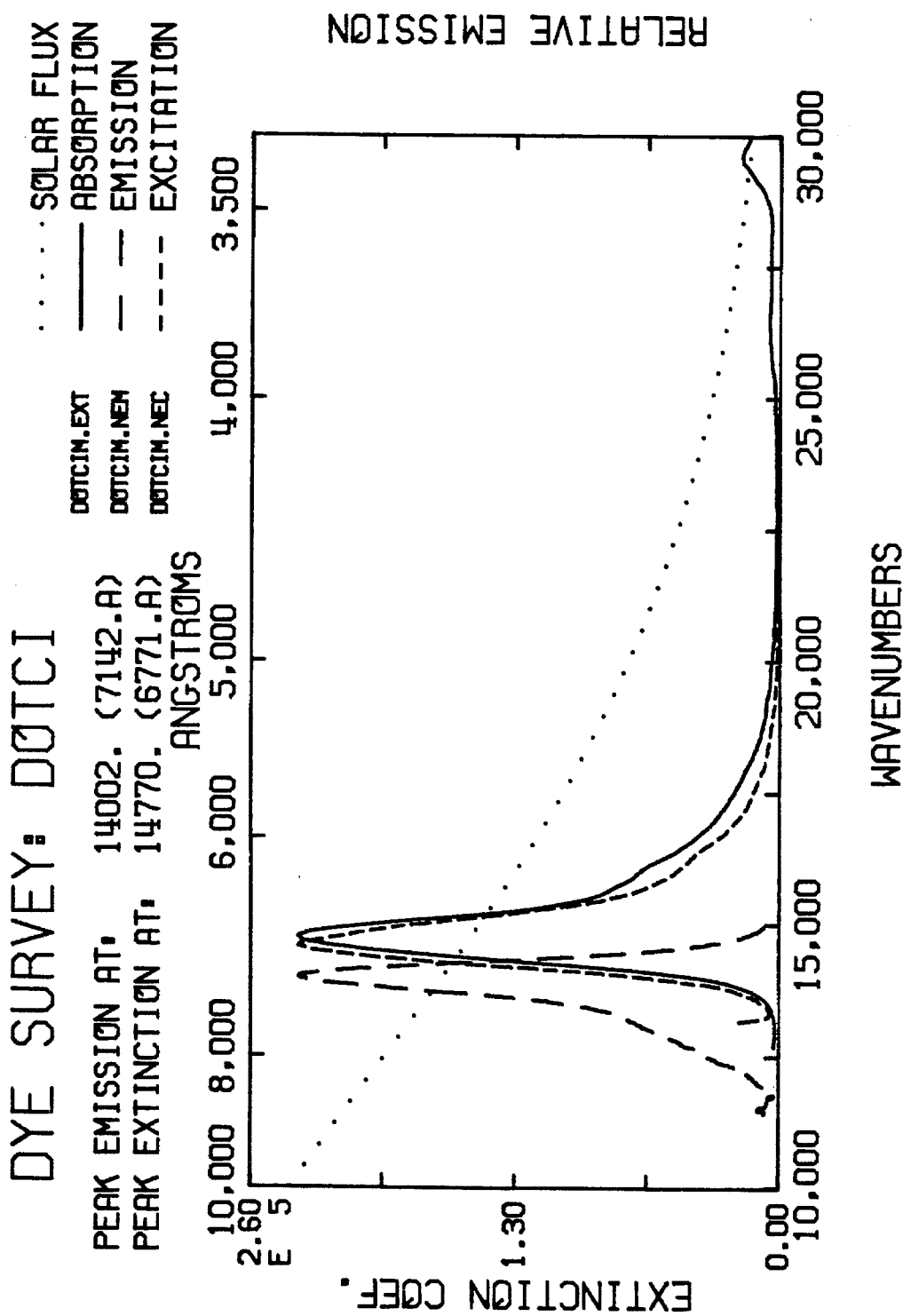
DYE SURVEY: DOTCI
PEAK EMISSION AT: 14002. (7142.A)
PEAK EXTINCTION AT: 14770. (6771.A)
DOTCIM.EXT
DOTCIM.NEN
DOTCIM.NEC
.....SOLAR FLUX
ABSORPTION
EMISSION
EXCITATION
ANGSTROMS
10,000 8,000 6,000 5,000 4,000 3,500
30,000 25,000 20,000 15,000 10,000
WAVENUMBERS
EXTINCTION COEF.
2.60 E 5
1.30
0.00
RELATIVE EMISSION

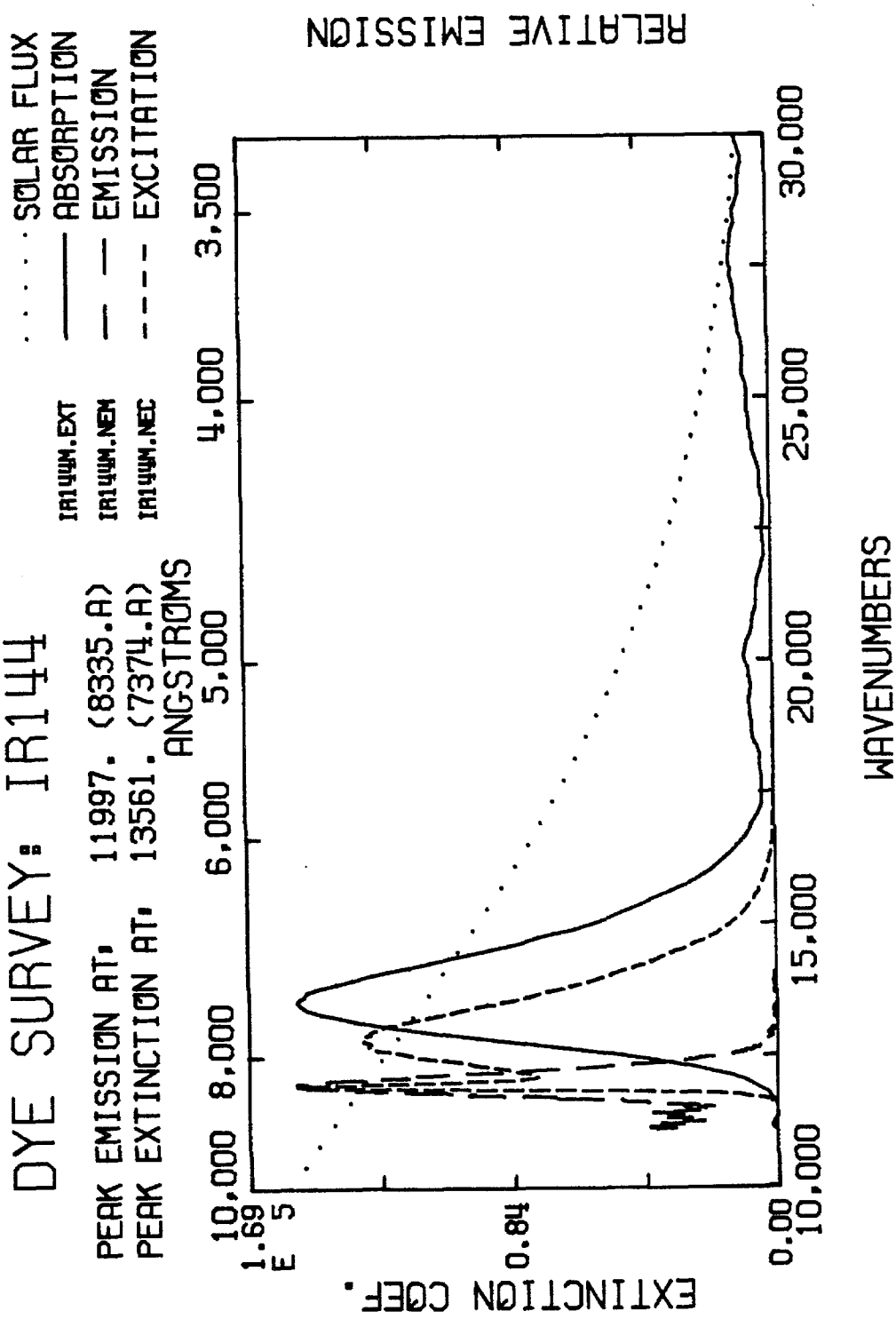
DYE SURVEY: IR144
PEAK EMISSION AT: 11997. (8335.A)
PEAK EXTINCTION AT: 13561. (7374.A)
IR144M.EXT
IR144M.MEM
IR144M.MEC
SOLAR FLUX
ABSORPTION
EMISSION
EXCITATION
RELATIVE EMISSION
EXTINCTION COEF.
1.69 E 5
0.84
0.00
10,000 8,000 6,000 5,000 4,000 3,500
ANGSTROMS
10,000 15,000 20,000 25,000 30,000
WAVENUMBERS

Figure 26. Three emission spectra of methanol dye solutions resulting from 4,500 Å excitation. The top spectrum is from a micromolar oxazine-720 solution, and the lower spectra are micromolar and hundred micromolar concentrations, respectively, of coumarin-540, rhodamine-640, and oxzaine-720.

EMISSION SPECTRA SHOWING ENERGY TRANSFER
IN MULTIPLE DYE METHANOL SOLUTIONS.
22,220 WAVENUMBER (4500 Å) EXCITATION

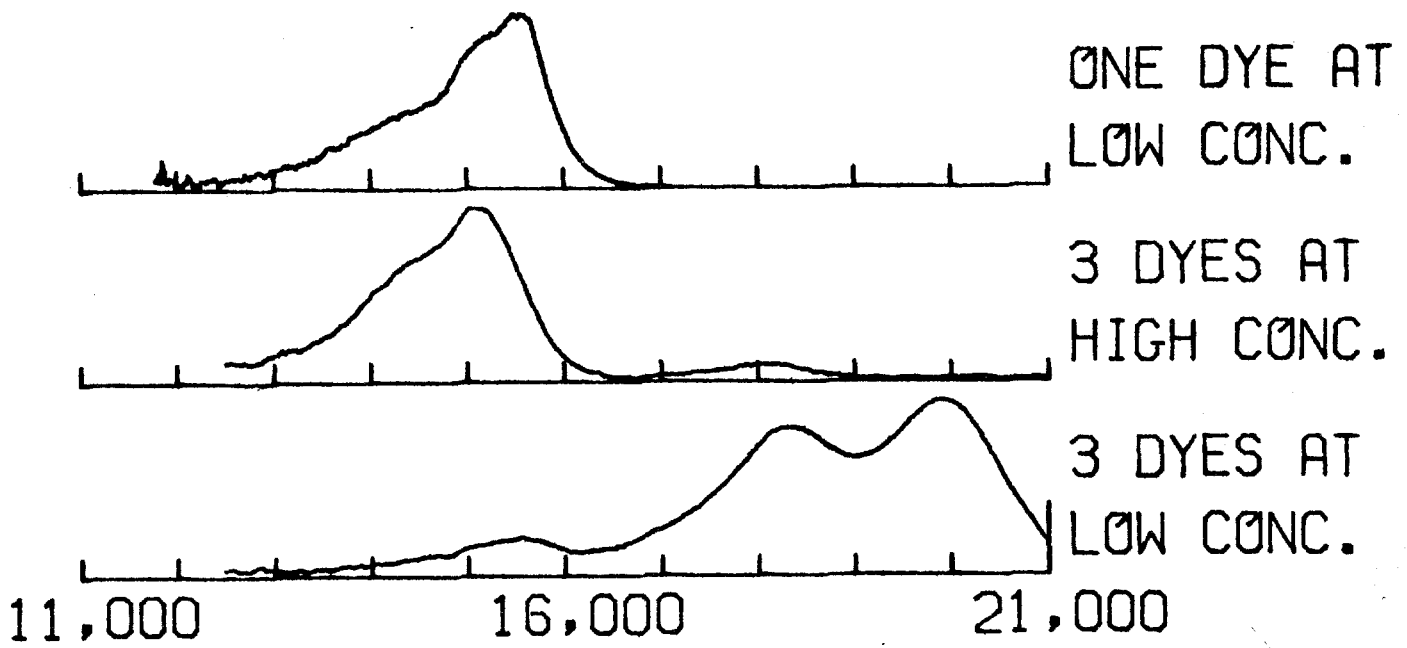

Figure 27. Three excitation spectra of methanol dye solutions with emission detection at 6,400Å. The three spectra correspond to the same solutions used in Figure 26.

EXCITATION SPECTRA SHOWING ENERGY TRANSFER
IN MULTIPLE DYE METHANOL SOLUTIONS
15,630 WAVENUMBER (6400 Å) DETECTION

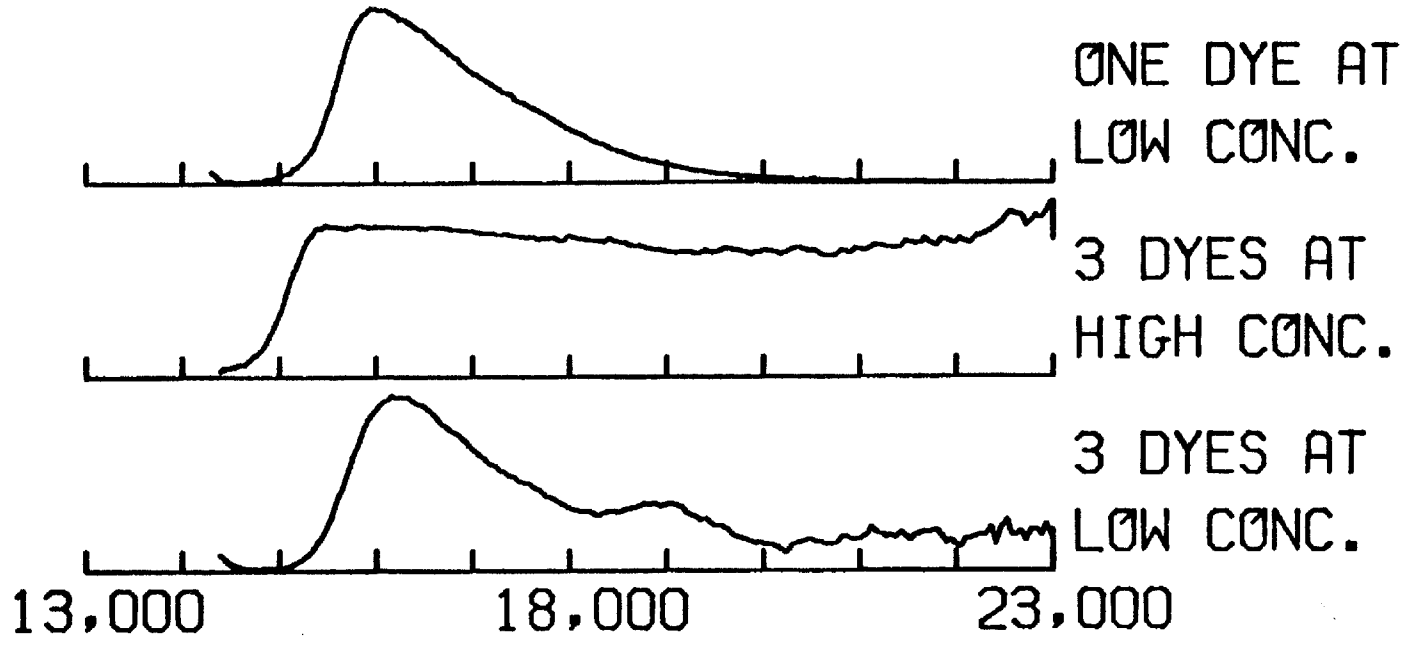

coefficients, are summarized in Table 1.

Measurements were also made on the spectral characteristics of multiple dye solutions. Dyes could not be combined indiscriminately, possibly due to agglomeration phenomenon between some dyes which quenched their emission when they were in solution together. For example, our oxazine-720 and oxazine-750 solutions showed quenching of their emission when they were in solution with rhodamine-610 or with rhodamine-590. Agglomeration has previously been observed to quench the emission of xanthene dyes (Joshi and Pant, 1976, and Kajiwara, Chambers, and Kearns, 1973). An example of a successful multiple dye combination is sulforhodamine-640, rhodamine-590, and coumarin-540. Figures 26 and 27 show emission and excitation spectra, respectively, for an oxazine-720 methanol solution, a dilute (micromolar) oxazine-720/rhodamine-640/coumarin-540 methanol solution, and of a concentrated (hundred micromolar) methanol solution of the same three dyes. The emission spectra of the multiple dye solution at low concentrations is dominated by rhodamine and coumarin emission, while the oxazine dominates the emission at higher concentrations. If we detect the emission of oxazine, as shown in Figure 27, as a function of excitation energy, the low concentration multiple dye solution is dominated by the pure oxazine absorption peak, while the high concentration multiple dye solution gives a nearly constant response across the visible spectrum.

Quantum Efficiency of Luminescence

We did not measure the quantum efficiency of luminescence for any of the dyes. The usual nontriviality of measuring quantum

efficiencies would have been further complicated by requiring an accurately calibrated system response from 4,000Å to 8,000Å (see Demas and Crosby, 1971). We have instead used literature values for the measured quantum efficiencies. These are given with the appropriate references in Table 1.

II. PHOTOBLEACHING MEASUREMENTS

Organic laser dyes have the good attributes of high quantum efficiency of luminescence, well separated absorption and emission spectra, and a wide selection of possible spectral positions. They have the bad characteristic that their performance deteriorates due to exposure to light. More specifically, the total luminescence from a dye-containing sample under solar exposure will decrease with time. The time required for the emission to drop to 50% of its initial value can vary from minutes to years. The precise rate of decline varies with the particular dye, the surrounding matrix or solvent material, impurities in the surrounding material, the spectral character of the incident light, the intensity of the light, and on the temperature of the sample. Other variables may also be important.

Studies in the Literature

Studies have been published on dye photodegradation rates in a variety of systems. Two groups at Bell Labs have measured xanthene dye photodegradation quantum efficiences in liquid (Shank and Ippen, 1971) and in plastics (Kaminow, Stulz, Chandross, and Pryde, 1972). Similar studies were done by Beer and Weber in Germany (Beer and Weber, 1972). In all cases the excitation source for CW irradiation

was the 5,145Å line from an argon ion laser. Sample temperatures were near room temperature. Photodegradation was determined by a decrease in the peak absorption of the solution, not by change in the emission. The results of these measurements are summarized in Table 2.

The optical density has also been seen to decay due to thermal excitation in darkness. Dyes dissolved in glycerin were found to be relatively stable for temperatures below 100° C (Weber, 1976). Rhodamine-590 was found to be more sensitive to thermal degradation in PMMA matrixes (Higuchi and Muto, 1981). The decay rate in PMMA increases sharply from about 10^{-7}/sec at 65° C to a plateau of about 8×10^{-7}/sec for temperatures from 70° C to 85° C. The sudden increase in the decay rate was postulated to be related to the glass transition temperature for the plastic. The decay rate for rhodamine-590 in PMMA at 65° C corresponds to roughly a year at 9 hours per day of exposures.

There is some concurrence in the literature that the dominant degradation mechanism is related to triplet formation in the dyes. ESR studies led Yamashita and Kashiwagi to propose two laser-induced photochemical reactions (Yamashita and Kashiwagi, 1976). Highly excited molecules in the triplet state can transfer sufficient energy to the surrounding solvent to rupture a C—H bond in the solvent molecule, and the resulting radical combines with the dye. Alternatively, intersystem crossing from the first singlet to the lowest triplet state can result in a different radical formation which depends on the particular structure of the dye. Weber (Weber, 1973) found that degradation

Table 2. Literature values for the quantum efficiency of photobleaching of laser dyes. In all cases the excitation source was the 5,145Å line from an argon ion laser. The number of photons absorbed was determined by the attenuation of the laser. The number of molecules which had been bleached was assumed to be given by the change in peak optical density. (These should be compared to our results for solar bleaching on page 207).

Table 2.

Literature Values for Photobleaching Quantum Efficiencies.

(5, 145Å excitation)

Dye	Solvent	$\frac{\text{Molecules}}{\text{Photon}}$	Reference
Rhodamine-590	H_2O+Triton X-100	8×10^{-6}	(a)
	H_2O+Triton X-100	7×10^{-6}	(c)
	methanol	5×10^{-7}	(a)
	PMMA	$0.4 - 2 \times 10^{-6}$	(b)
Rhodamine-610	methanol	17×10^{-6}	(c)
Cresyl Violet	methanol	9×10^{-6}	(c)
Fluorescein	ethanol	4×10^{-6}	(a)
Rhodamine-S	ethanol	1.7×10^{-6}	(a)

(a) Shank and Ippen, 1971.

(b) Kaminow, Stulz, Chandross, and Pryde, 1972.

(c) Beer and Weber, 1972.

rates in a variety of solutions were reduced by the addition of a triplet quencher such as oxygen.

PMMA itself has proved very stable under solar exposure. A plate has been observed to retain 80-90% of its optical clarity across the visible spectrum after 17 years of exposure on a test frame in Albuquerque (Rainhart and Schimmel, 1975, and Fox, Isaacs, and Stokes, 1963).

Degradation Measurements

We made preliminary measurements of the degradation rates of dyes in a variety of hosts to determine the viability of various dye-host combinations as LSC prototypes.

Absolute absorption measurements are much simpler than absolute emission intensity measurements. In general, we would measure change in the peak absorption across the thickness of a plate and assume that a decrease in this peak absorption was related to the fraction of the dye molecules that had chemically reacted. It is likely that the emission intensity might not be directly related to the absorption. Increased scattering in the plate and degradation products both might contribute to the absorption, causing the remaining dye concentration to be over-estimated. To test the correlation between absorption and emission degradation, we made the following measurements on a 3 mm thick PMMA plate containing 140 micromolar coumarin-540 and 97 micromolar rhodamine-590. A portion of the unexposed plate was exposed to Michigan sunlight filtered by a plate glass window for a total of about 1,000 hours of direct sunlight. We measured the

emission of this exposed plate by illuminating the sample with a dispersed tungsten lamp. The spectral distribution of the tungsten lamp closely approximated that of a 3000° K black body. A silicon cell was brought into optical contact with the edge using ethylene glycol as an index matching fluid. The output short circuit current of the cell was measured with an HP-3466A digital multimeter. The emission of the plate exposed behind plate glass had dropped about 30% compare to a similar sample that had been stored in the dark. The peak optical density of the rhodamine had dropped from 2.7 to 2.2 during exposure, or a drop of about 20%, while the coumarin peak had been reduced from 2.3 to 1.7, or a drop of about 30%. A section of the same unexposed plate was exposed to direct sunlight for 243 total hours. This resulted in an emission decrease of about 30%, and in a decrease in the peak optical density of the coumarin of about 20%. We find, therefore, that there is rough parity between change in the absorption spectrum and change in the emission from the edge of a plate. If the rates are not equal, the emission will degrade somewhat faster.

Simulated solar exposure tests were made on an LSC plate containing about 100 micromolar concentrations of rhodamine-590 and coumarin-540. Samples of this material 0.3 × 1 × 3 cm in size were cut from the plate. Optical absorption spectra were measured, and the optical density of the spectral peaks of rhodamine-590 and coumarin-540 at 5,300Å and 4,600Å, respectively, were noted for the unexposed material. The samples were then placed in a QUV accelerated weathering tester, and were subjected to a test cycle consisting of 8 hours of exposure to UV light from a bank of four S-40 UV

fluorescent lamps at a temperature of 60° C followed by four hours of darkness at 50° C and 100% relative humidity. This cycle was repeated for a total of 2,400 hours. The samples were removed from the QUV at approximately 200 hour intervals at which times their optical absorption spectra were measured. Figure 28 a plot of the peak optical density for both dyes as a function of total test hours. The decay times from the slopes of these plots are about 1,000 and 10,000 hours for rhodamine and coumarin, respectively. The QUV apparatus has a peak spectral intensity at 3,130Å, with an intensity of 1.8 microwatt per Angstrom per square centimeter at that wavelength. Acceleration factors of 8-25 hours of environmental exposure per hour of QUV test time have been suggested (Grossman, 1977).

Solar Exposure of PMMA Samples

The first sample tested was a 76 micromolar rhodamine-590 PMMA plate 3 mm thick. Acetic acid was added to the monomeric solution prior to polymerization to increase the solubility of the dye. A two-week continuous exposure (336 total hours) caused a decrease in the peak optical density from 4.0 to 2.8, as measured on a Cary-14 Spectrophotometer. We estimate from the change in absorption that the bleaching rate was about 10^{-6} molecules per photon. This estimate is obtained by calculating the fraction of an AMO spectrum (assumed to be a 5,800° K black body) which would have been absorbed by the initial concentration of rhodamine-590. This yields an approximate number of photons absorbed by the sample per unit area. The number of dye molecules which have photochemically reacted is assumed to be given by the decrease in peak optical density. This calculated

Figure 28. Dye deterioration in a QUV test chamber. Two LSC samples consisting of rhodamine-590 or coumarin-540 in PMMA were exposed for 2,400 hours to simulated solar exposure. (One hour exposure in this apparatus is considered roughly equivalent to eight hours of sunlight for paint samples.) The decay times for the two samples were about 1,000 and 10,000 QUV hours, respectively.

DYE DETERIORATION IN A QUV TEST CHAMBER.

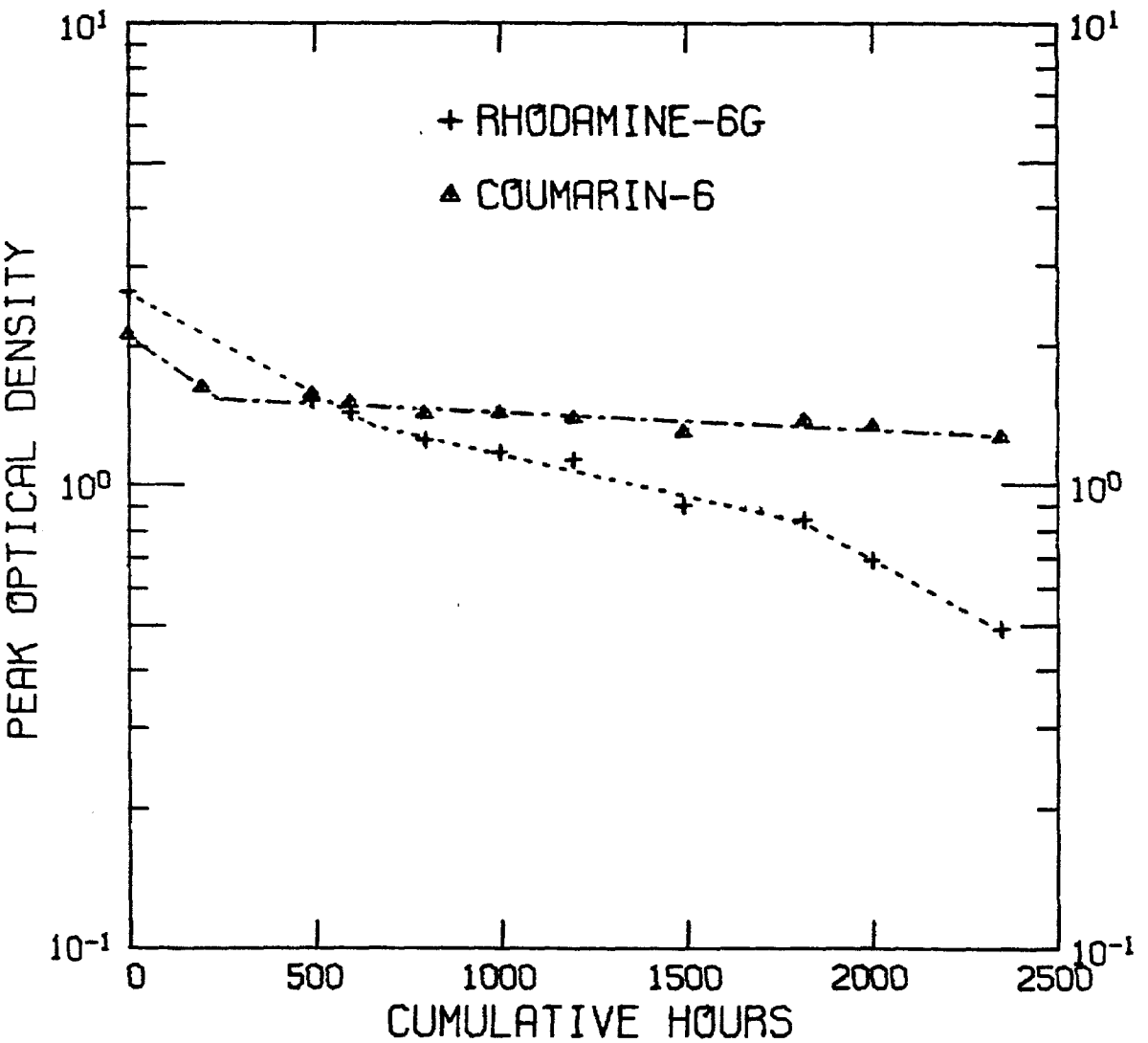

degradation rate is roughly equivalent to that measured by argon ion irradiation.

A PMMA plate containing 210 micromolar coumarin-540, 81 micromolar rhodamine-590, and 22 micromolar sulforhodamine-640 was exposed to direct insolation for 243 continuous hours. The total emission from the plate decreased 50%, as measured using the above technique. The peak optical density of the three dyes decreased 52%, 50%, and 51%, respectively. This sample showed particularly good correlation between decline in emission and absorption. Additional samples of this plate were exposed over the same period to determine the spectral dependence of the degradation rate. Three samples were protected by either an eighth-inch thick soda-lime glass cover, a Schott GG400 UV cut-off filter, or by OD-2 neutral density filters. All samples were sealed against the outside atmosphere with polyvinyl-chloride electrical tape. Figure 29 shows a plot of the absorption spectra of the three exposed samples described, plus the unprotected exposed sample and the control or dark sample. Little change was observed in the sample protected by neutral density filters. No other spectral dependences are obvious from the data. Note that degradation in the absorption peak is usually accompanied by a slight increase in the near UV absorption, which might be related to bleaching products.

The 3 mm think PMMA plate containing rhodamine-590 was examined for changes in collection efficiency due to solar exposure. A silicon cell was mounted against a polished edge of the unexposed plate, and the short circuit current from the cell was measured with an HP-3466A DMM. A focussed spot excitation from a 3,000°K

Figure 29. Solar bleaching of a multiple dye LSC plate. These are the absorption spectra for a PMMA plate containing 210, 81, and 22 micromolar concentrations of coumarin-540, rhodamine-590, and sulforhodamine-640, respectively. The five spectra correspond to an unexposed control plus 243 continuous hours of exposure through either optical density (2) filters, 400 nm cut-off filters, soda-lime glass, or no filtering.

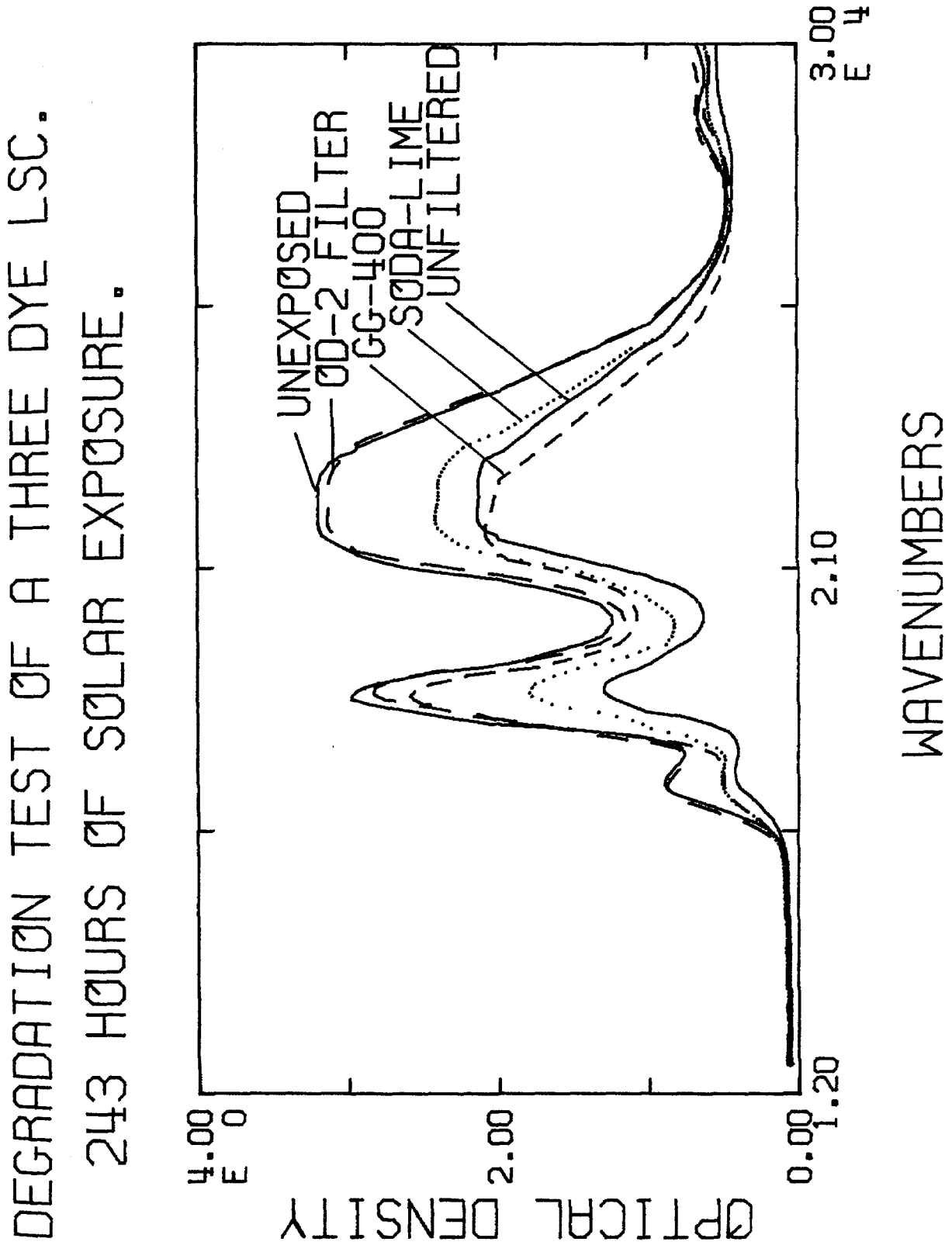
DEGRADATION TEST OF A THREE DYE LSC.
243 HOURS OF SOLAR EXPOSURE.
UNEXPOSED
OD-2 FILTER
GG-400
SODA-LIME
UNFILTERED
OPTICAL DENSITY
4.00
E 0
2.00
0.00
1.20
2.10
3.00
E 4
WAVENUMBERS

tungsten lamp was scanned from the center of the plate towards the cell, and the short circuit current was recorded as a function of the excitation-cell distance. This procedure was repeated for the plate which had been exposed for 336 total hours. The results of these measurements are given in Figure 30. The output from the exposed plate was actually greater than the output from the unexposed plate for small excitation-to-cell distances. At longer distances the unexposed plate had a higher collection efficiency.

We made single dye plates containing coumarin-460, 500, and 540, rhodamine-590 and 610, and oxazine-725 in PMMA. After about 250 hours of continuous exposure, the emission had dropped 13% for the coumarin-540, which was the best case, and had dropped 66% for the oxazine-725, which was the worst case, with the other dyes following in between these two limits. If the emission is assumed to decrease in a roughly exponential manner, these correspond to half-lives ranging from 300 to 3,000 hours (12 to 120 days).

Methanol solutions of the dyes coumarin-500, 535, and 540, rhodamine-590 and 640, sulforhodamine-640, cresyl violet-670, LD-700, and oxazine-720 were prepared in soda-lime glass vials 2.5 cm in diameter. Oxygen was removed from the samples by bubbling nitrogen gas through the solutions for an hour in a nitrogen atmosphere. The screw-on caps were sealed with RTV silicon rubber sealant. The optical density of the samples were measured every few days without disturbing the seals. Figure 31 shows the measured peak optical densities of the solutions as a function of total exposure time, which included hours of darkness. The maximum exposure time was 432 hours,

Figure 30. Emission vs distance for a plate before and after exposure. A spot excitation was scanned towards an edge-mounted cell, and the resulting short circuit current was measured as a function of distance between the spot and the cell.

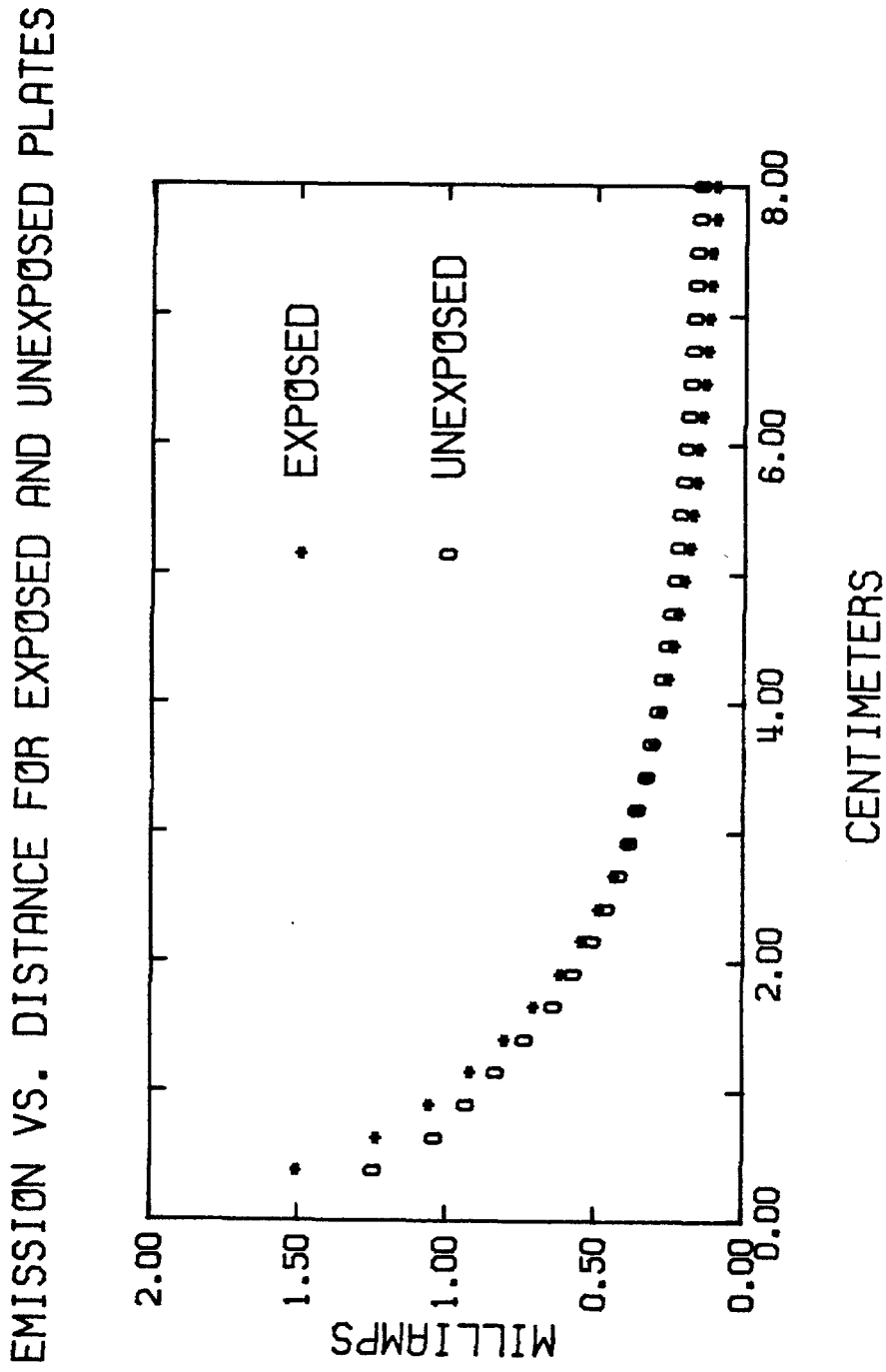
EMISSION VS. DISTANCE FOR EXPOSED AND UNEXPOSED PLATES
EXPOSED
UNEXPOSED
MILLIAMPS
2.00
1.50
1.00
0.50
0.00
0.00
2.00
4.00
6.00
8.00
CENTIMETERS

Figure 31. Peak optical densities of methanol dye solutions under continuous solar exposure. 2. 5 cm i. d. soda-lime glass bottles were filled with solutions of oxazine-720 perchlorate, LD-700 perchlorate, cresyl violet-670 perchlorate, rhodamine-590 perchlorate, coumarin-540, coumarin-535, and coumarin-500. The screw-on caps were sealed with RTV. Absorption spectra were taken without disturbing the seals.

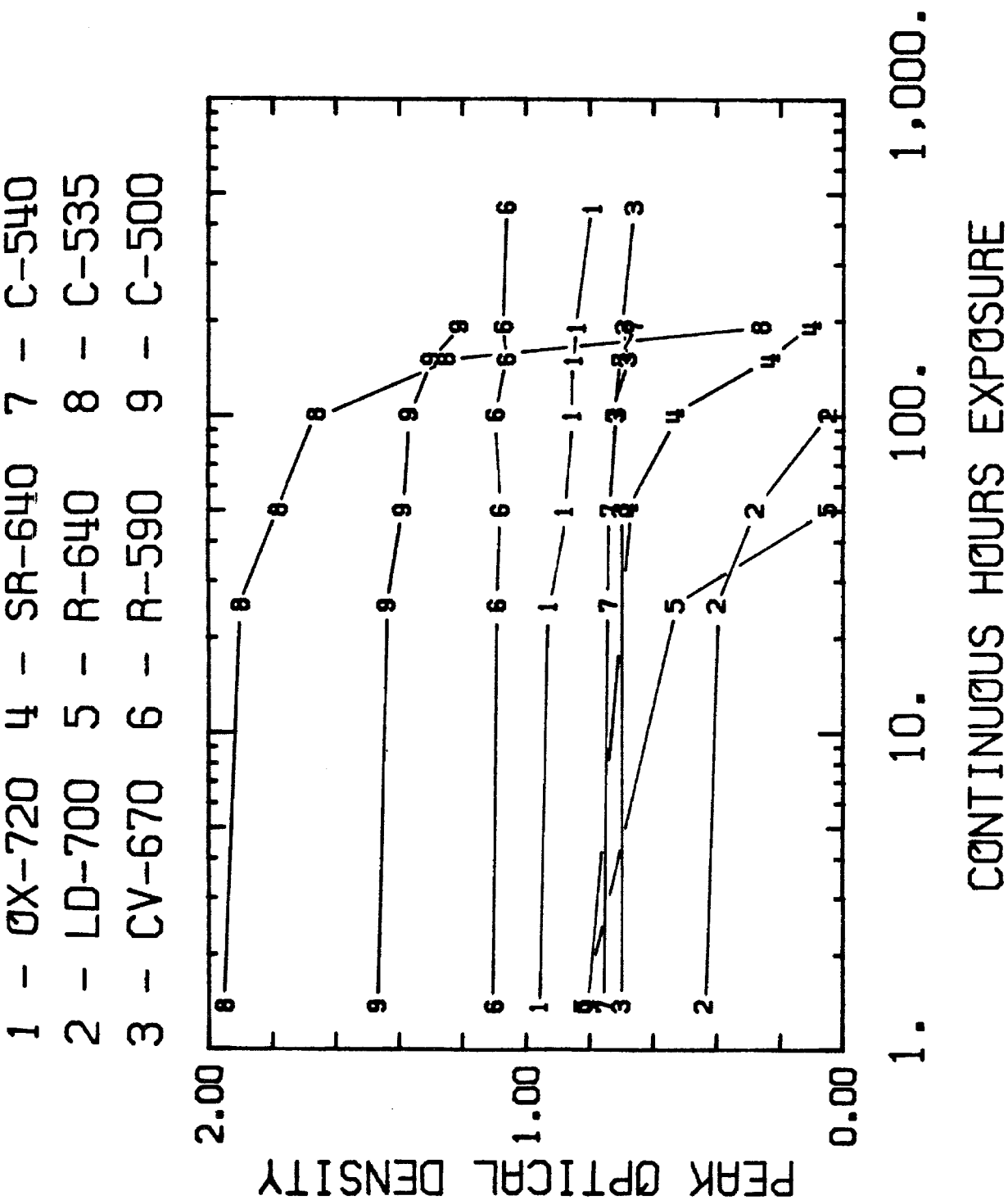
1 - ØX-720 4 - SR-640 7 - C-540
2 - LD-700 5 - R-640 8 - C-535
3 - CV-670 6 - R-590 9 - C-500
PEAK ØPTICAL DENSITY
2.00
1.00
0.00
1.
10.
100.
1,000.
CØNTINUØUS HØURS EXPØSURE

(18 days). This was insufficient time to obtain accurate decay rates for the longer lifetime dyes. Using an exponential as a rough approximation to the time dependence of the optical density, the lifetime for the solutions ranged from 50 hours for rhodamine-640 to about 10,000 hours (one year) for rhodamine-590. Among the relatively stable dyes were coumarin-540 (3,000 hours), oxazine-720 (2,000 hours), and cresyl violet (7,000 hours).

We measured photodegradation rates for five of the most stable dyes in a degassed environment. Methanol solutions of coumarin-540, rhodamine-590, sulforhodamine-640, cresyl violet-670, and oxazine-750 were placed in quartz cuvettes having the outer dimensions 1.3 × 1.3 × 6 cm. The concentrations of the solutions were adjusted so that the peak optical density across the cuvettes were between 0.5 and 1.0. These samples were degassed by six freeze-pump-thaw cycles on a vacuum minifold, and then flame sealed. The resulting lifetimes were 3.3, 10.0, 36.0, 0.3, and 1.0 direct sunlight hours, respectively. Figures 32 through 36 show the absorption spectra of these samples as a function of time.

DCM degradation rates were measured in methanol, dimethylformamide, dimethylsulfoxide, and chloroform solutions. Solutions were prepared with accurate DCM concentrations and were placed in soda-lime glass bottles. The solvents were not degassed. Caps were sealed on using RTV sealant. The samples were exposed for 210 hours (9 days) including hours of darkness. Figures 37 and 38 show before and after absorption spectra for DCM in methanol and

Figures 32 - 36. Solar exposure of degassed methanol dye solutions in quartz cuvettes. Absorption spectra are presented which were made after intervals of exposure to sunlight. The hours of exposure, and the resulting peak optical densities are listed on each plot.

SOLAR EXPOSURE OF C-540. QUARTZ CUVETTE WITH VACUUM DEGASSED METHANOL.

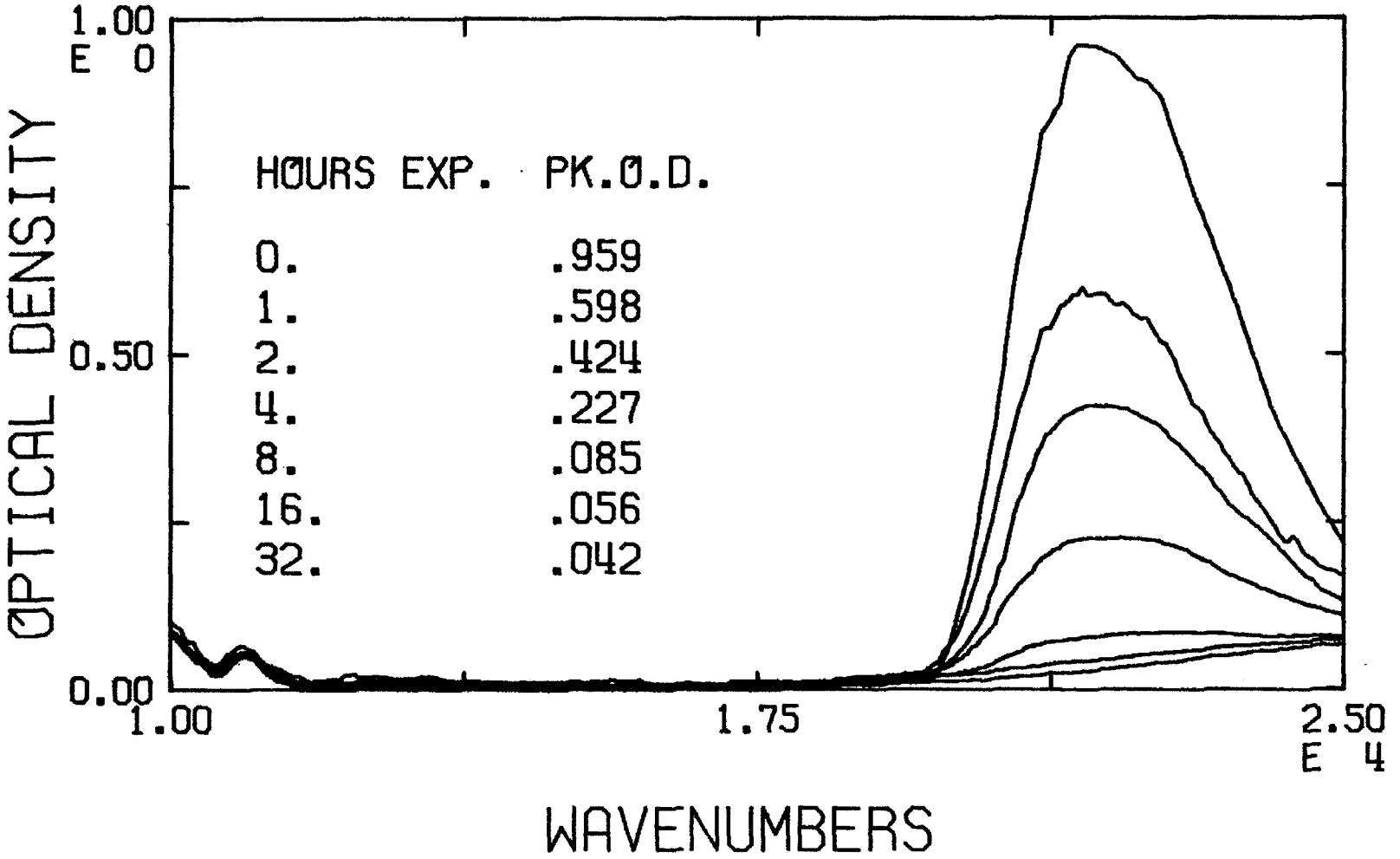

SOLAR EXPOSURE OF R-590. QUARTZ CUVETTE WITH VACUUM DEGASSED METHANOL.

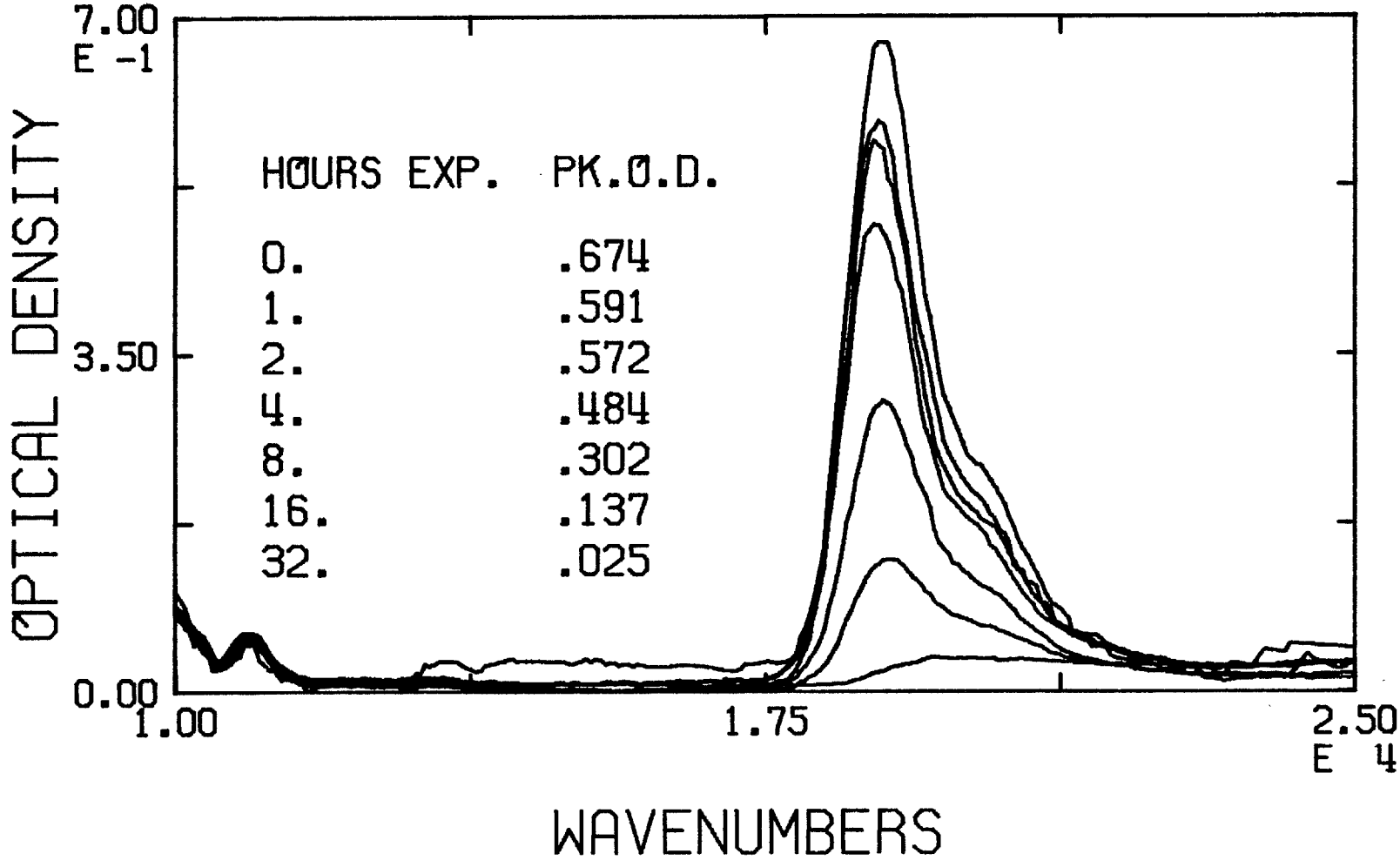

SOLAR EXPOSURE OF SR-640. QUARTZ CUVETTE WITH VACUUM DEGASSED METHANOL.

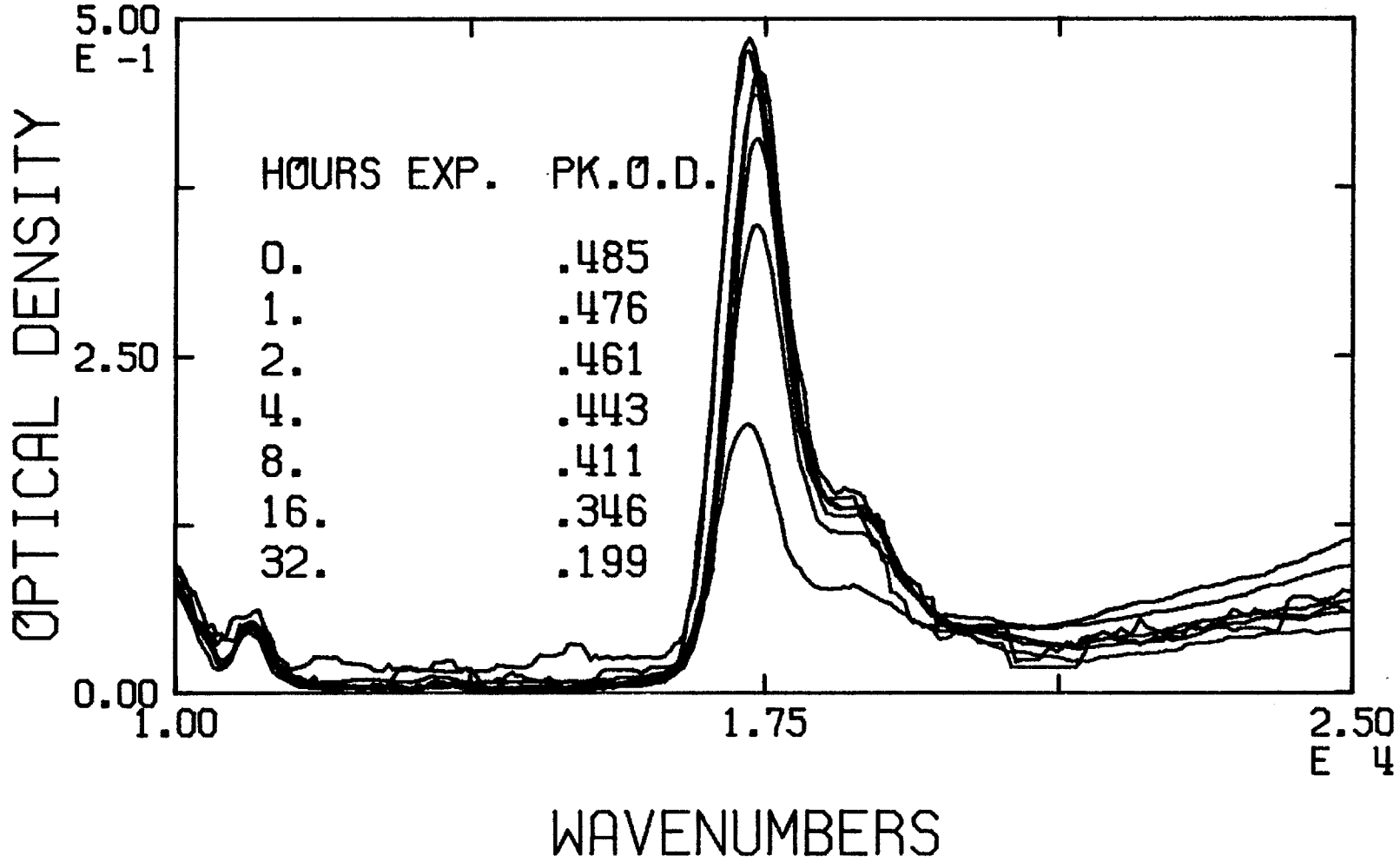

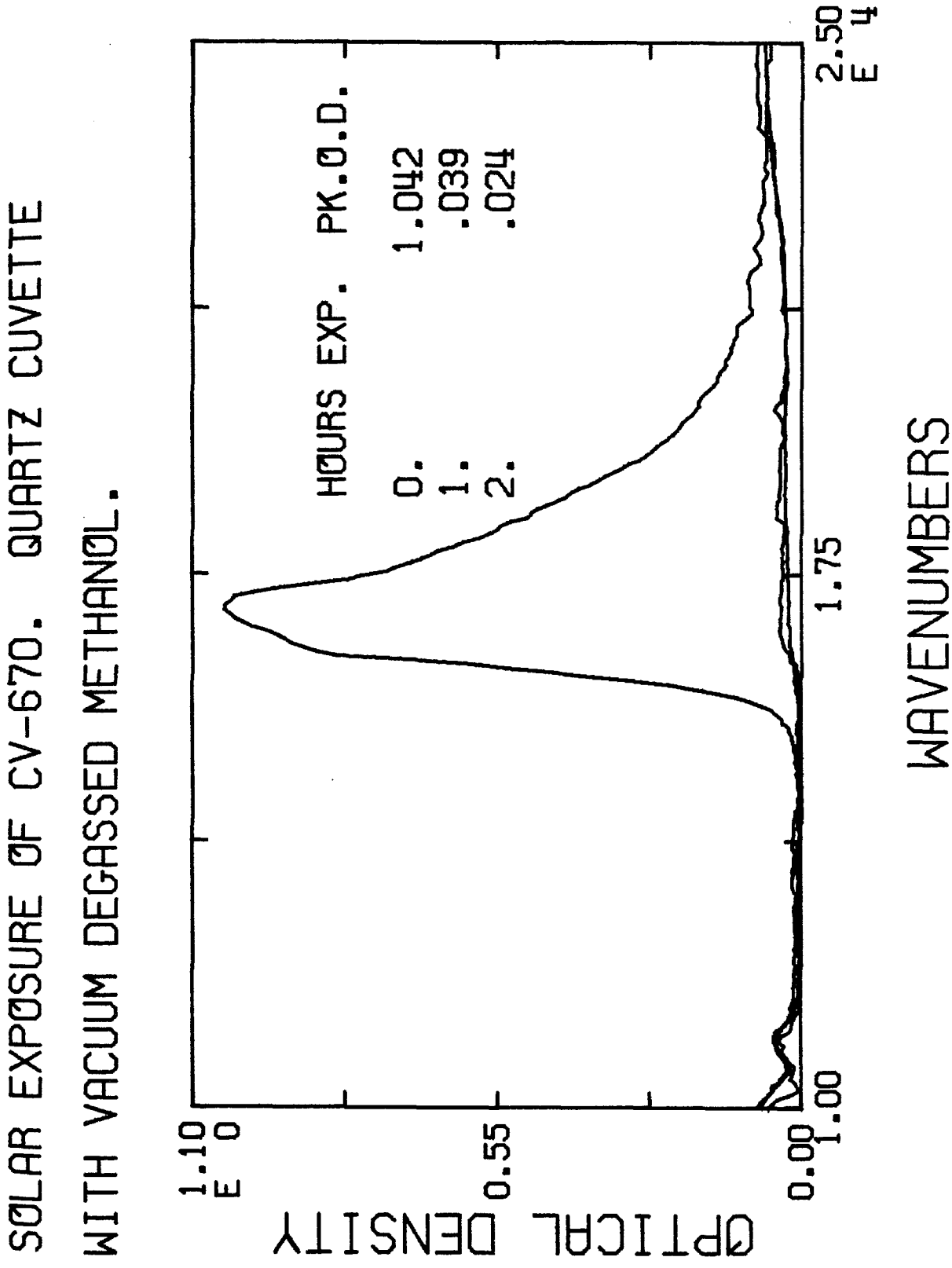
SOLAR EXPOSURE OF CV-670. QUARTZ CUVETTE
WITH VACUUM DEGASSED METHANOL.
HOURS EXP. PK.O.D.
0. 1.042
1. .039
2. .024
OPTICAL DENSITY
1.10
E 0
0.55
0.00
1.00
1.75
2.50
E 4
WAVENUMBERS

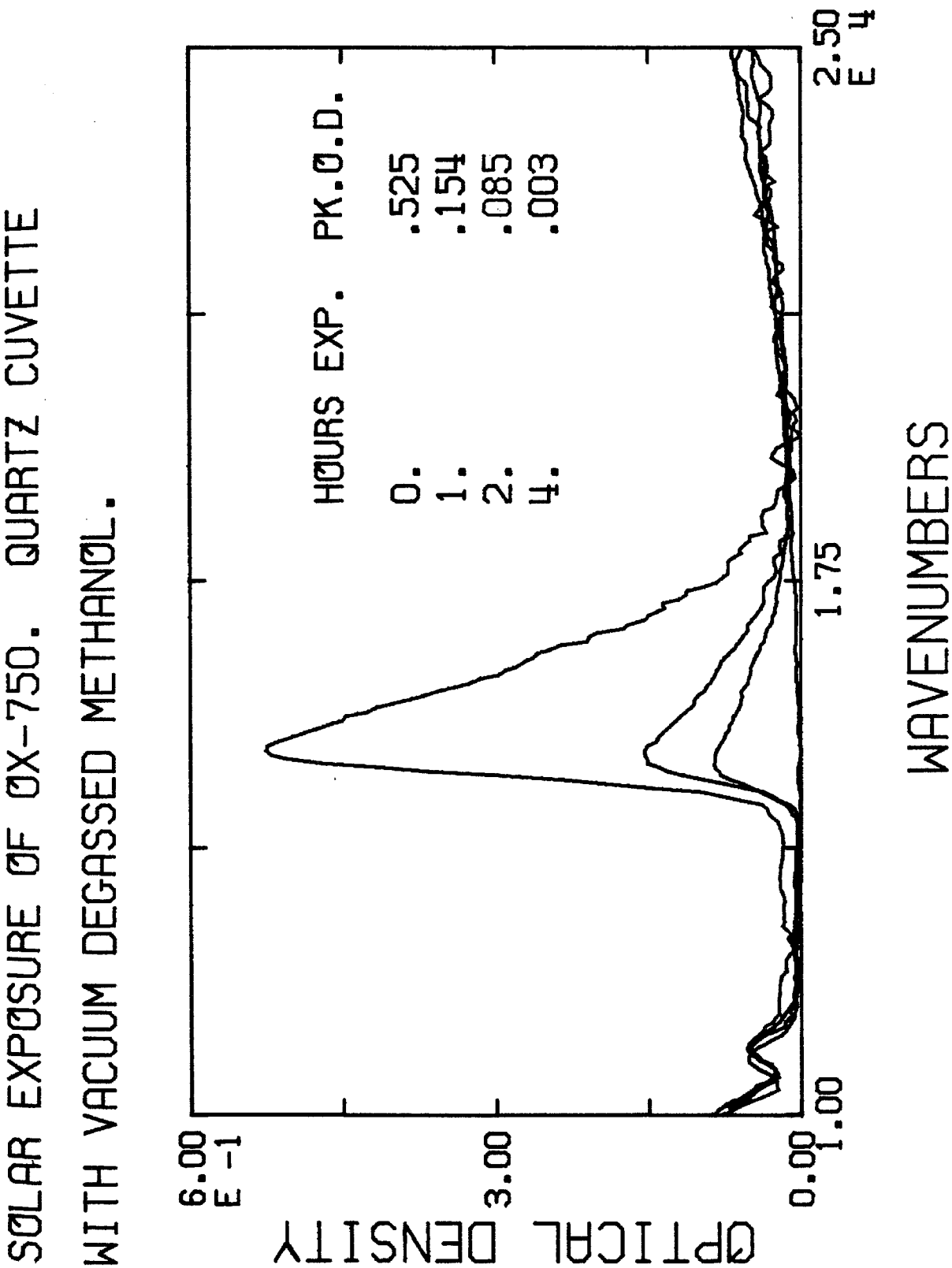
SOLAR EXPOSURE OF OX-750. QUARTZ CUVETTE
WITH VACUUM DEGASSED METHANOL.
HOURS EXP. PK.O.D.
0. .525
1. .154
2. .085
4. .003
OPTICAL DENSITY
6.00
E -1
3.00
0.00
1.00
1.75
2.50
E 4
WAVENUMBERS

Figures 37 and 38. Solar exposure of DCM. Absorption spectra of DCM in methanol (Figure 37) and dimethylformamide (Figure 38) are presented before and after 210 hours of continuous solar exposure in soda-lime glass bottles.

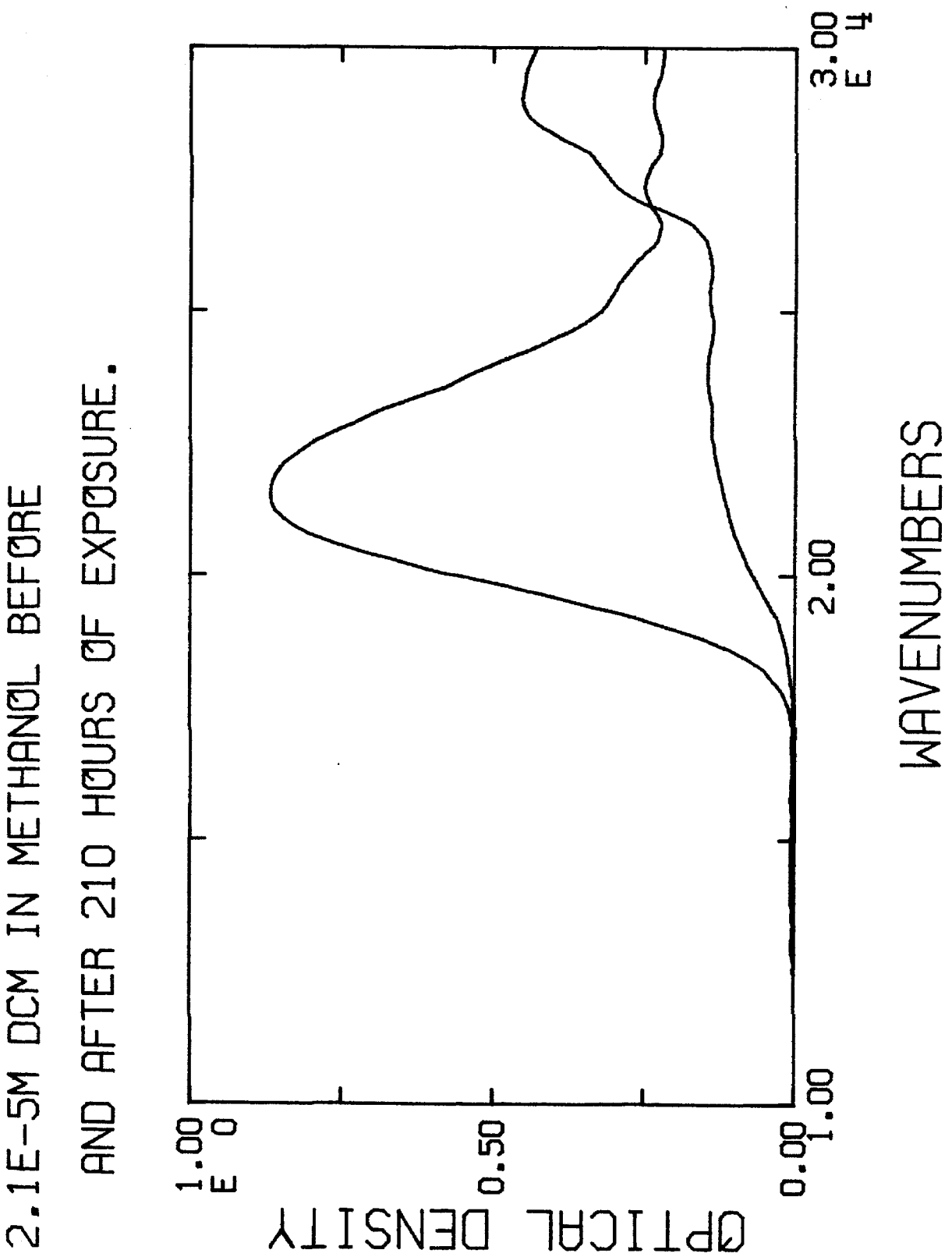
2.1E-5M DCM IN METHANOL BEFORE
AND AFTER 210 HOURS OF EXPOSURE.
OPTICAL DENSITY
1.00
E 0
0.50
0.00
1.00
2.00
3.00
E 4
WAVENUMBERS

2.01E-5M DCM IN DIMETHYLFORMAMIDE BEFORE AND AFTER 210 HOURS OF EXPOSURE.

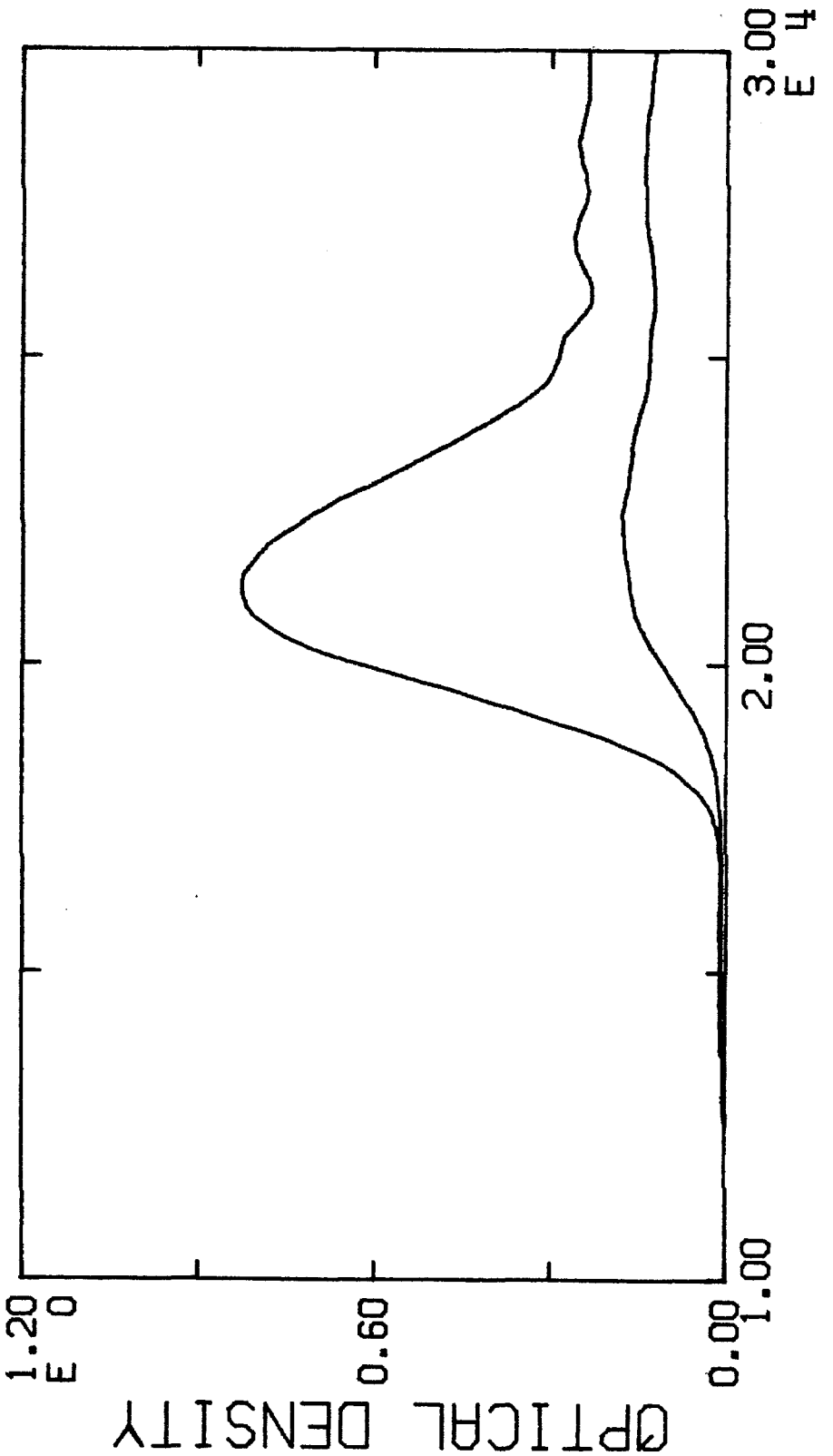

dimethylformamide. In all cases the dye lifetime was substantially less than 210 hours.

III. SELF-ABSORPTION IN RHODAMINE-575

Emission and absorption spectra from luminescent materials will typically have some overlap, such that there is a finite probability of re-absorbing or self-absorbing the emission from a luminescing specie. In particular this probability of self-absorption in an LSC will increase as the pathlength traveled by the emission in the plate increases. Such an effect limits the size of an effective LSC plate. We were, therefore, interested in a detailed study of the self-absorption effect, at least for one particular luminescing system.

Rhodamine-575 was chosen to be studied for two reasons. It is a typical xanthene organic laser dye, which is a large class of efficient and commonly used luminescing dyes (Kuhn, 1959). Its molecular structure is shown in Figure 39, and is almost identical to that of rhodamine-590. The first reason rhodamine-575 was chosen was, therefore, that we hoped results from this dye would be gnerally true at least for the xanthene dyes. The second reason was that we wished to pump the dye in the extreme low energy tail of its absorption band using our rhodamine-590 dye lasers. This indicated the choice of rhodamine-575 in the xanthene family.

Rod Emission

We measured the changes in the intensity and spatial characteristics of rhodamine-575 emission by scanning the position of a small excitation spot with respect to the sample, and then observing the

Figure 39. Structure of rhodamine-575.

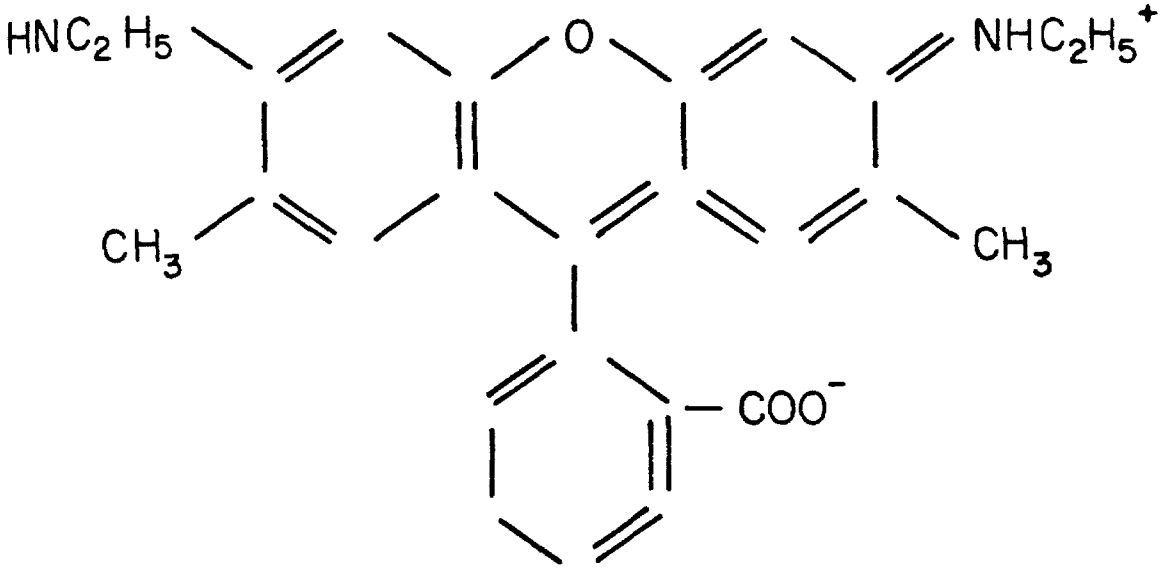

Structure of Rhodamine-575

resulting emission from a fixed point on the sample. Figure 40 depicts the apparatus used. The 22,940 cm^{-1} (4,359 Å) line from a 200 watt Oriel 6137 high pressure mercury lamp was filtered by a Bausch and Lomb 33-86-25 monochromator, modulated by a PAR-BZ-1 chopper, and focused by a ×40 microscope objective onto one end of a one meter section of Math Associates OC-1200 glass optical fiber bundle. Since we were interested in the change of intensity as well as the spectral shape of the emission as a function of the pathlength through the sample, it was important that the position of the excitation source at the sample be adjustable without any variation in the intensity. Small changes in the curvature of an optical fiber cause little change in its transmission, so that the free end of the fiber was used as the mobile excitation. The free end was mounted on a micrometer stage that would track parallel to the rod-shaped sample of LSC material, as shown in Figure 40. Three different types of samples were tested: methanol solutions, cast PMMA, and diffused PMMA. Samples were mounted inside 7 mm o.d. (5 mm i.d.) borosilicate glass tubes to maintain a uniform contact between the excitation fiber and the sample. The end of the tube adjacent to the detecting monochromator was sealed with a 1 cm glass plug. The detection system was a 0.25 meter Jarrell Ash spectrometer, a Hamamatsu 928 PMT, and a PAR HR-8 lock-in amplifier. The detection monochromator was scanned and the output of the lock-in amplifier was sampled by the PDP 11-03/2, as described in Section I.

The results from one such measurement are shown in Figure 41. In this case the borosilicate glass tube was filled with a 92 micromolar

Figure 40. Apparatus for measuring the intensity and spectral shifts of sample emission as a function of sample pathlength. The 4,359 Å line from a mercury lamp was monochromated, chopped, and focused onto the end of an optical fiber. The position of the opposite end of the fiber was scanned by a micrometer stage along a rod-shaped LSC sample. The output was detected by a scanning monochromator.

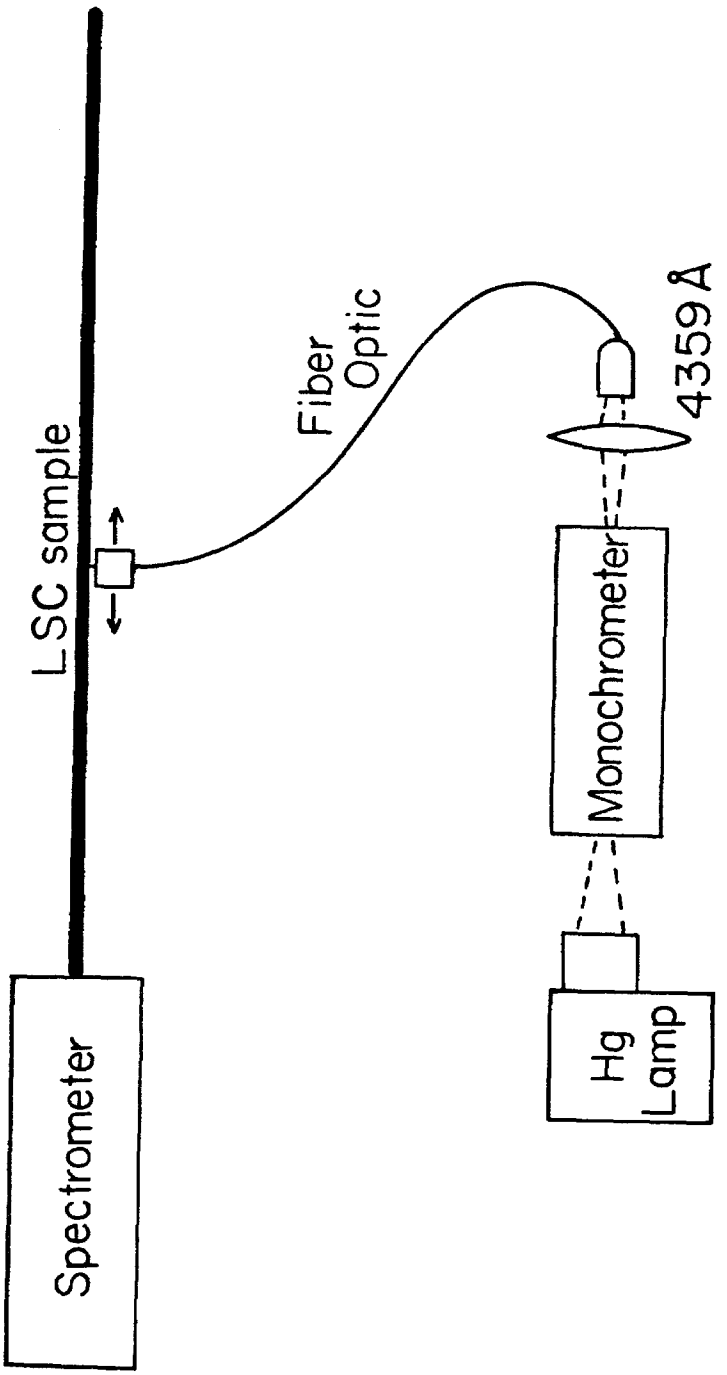
LSC sample
Fiber Optic
4359 Å
Monochrometer
Hg Lamp
Spectrometer

Figure 41. Emission spectra from a 92 micromolar methanol solution of rhodamine-575. The sample pathlengths, in order of most to least intense, were 0.3, 1.0, 3.0, 10.0, and 30.0 cm.

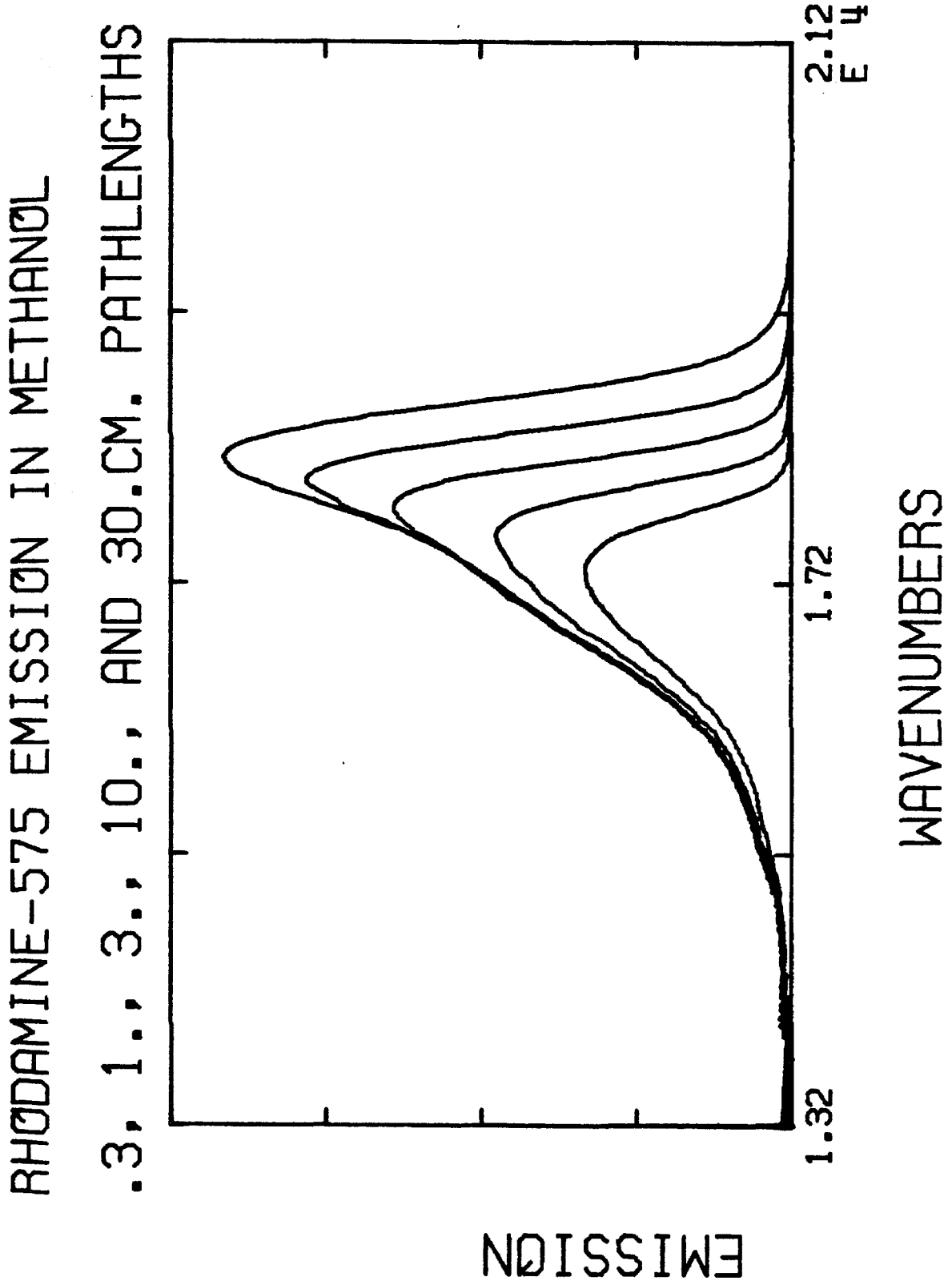
RHODAMINE-575 EMISSION IN METHANOL
.3, 1., 3., 10., AND 30.CM. PATHLENGTHS
EMISSION
1.32
1.72
2.12
E 4
WAVENUMBERS

solution of rhodamine-575 in methanol. Spectra were taken for the following distances between the fiber excitation and the glass plug seal at the end of the tube: 0.3, 1.0, 3.0, 10.0, and 30.0 cm. System response corrections were made to compensate for the detection monochromator and PMT, as described in Section I. Apart from this correction, the amplitudes of each spectrum correspond to the actual intensities emerging from the end of the sample rod. The predominant observed effect was that the higher energy portion of the emission band erodes away with greater pathlength through the rod, and that the change in emission intensity varies roughly as the inverse of the logarithm of the pathlength. Similar results were obtained from the PMMA samples. Figure 42 shows a similar set of spectra for a cast PMMA rod.

Spectral Homogeneity

We attempted to measure the spectral homogeneity of the absorption and emission bands for rhodamine-575 in different host materials. Luminescence spectra were taken using the apparatus shown in Figure 43. A spectra Physics 160 argon ion laser was used directly as the exciting source, or instead served as a pump for a Spectra Physics 375A dye laser. The dye laser operated with an ethylene glycol solution of rhodamine-590. When we excited the sample at an energy considerably below its peak absorption, it was important that very little spontaneous emission of a higher energy than the principal lasing wavelength be present in the sample excitation beam. The dye laser was, therefore, followed by several sharp cut filters, a dispersive prism, and a slit aperature. Neutral density filters were used to adjust the

Figure 42. Emission spectra from rhodamine-575 cast in PMMA. The dye concentration in the rod was approximately 20 micromolar. The emission pathlengths, in order of most to least intense, were 0.16, 0.4, 1.0, 4.0, and 10.0 cm.

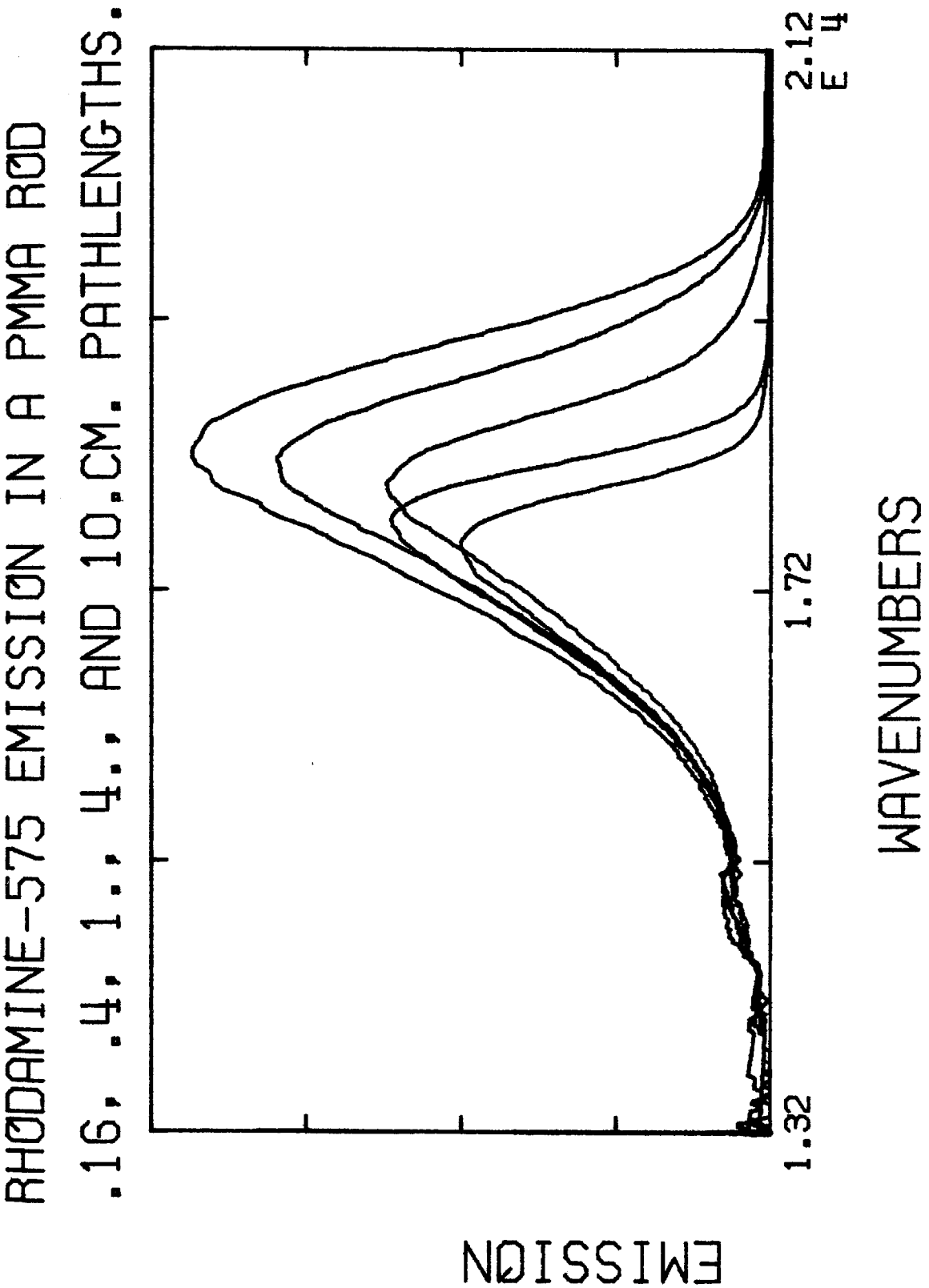
RHODAMINE-575 EMISSION IN A PMMA ROD
.16, .4, 1., 4., AND 10.CM. PATHLENGTHS.
EMISSION
1.32
1.72
2.12
E 4
WAVENUMBERS

Figure 43. Apparatus for measuring luminescence of liquid, cast plastic, and diffused plastic samples at different temperatures and excitation energies.

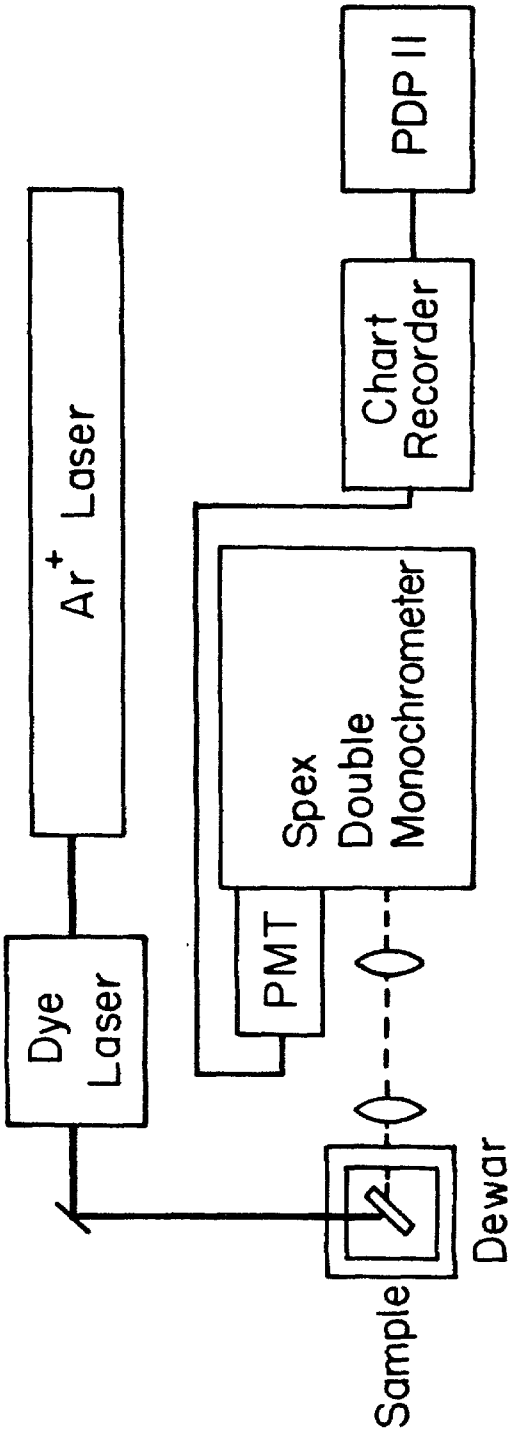
PDP 11
Chart Recorder
Ar+ Laser
Spex Double Monochrometer
Dye Laser
PMT
Dewar
Sample

input power to the sample. The samples were held in a glass dewar with windows positioned for both the excitation beam and for the resulting right angle emission. The luminescence spectra were taken both at room temperature and with the samples immersed in liquid nitrogen. Since the excitation was not chopped, stray room light had to be eliminated. The luminescence resulting from the laser excitation was collected by a Spex 1419A Sample Illuminator, and was then analyzed by a Spex 14018 double monochromator which utilized 2,400 grooves/mm holographic gratings. (The sample illuminator was a collection optics stage originally designed for Raman Spectroscopy. It contained the dispersive prism, slit, sample translation stage, and matched f-number optics for the spectromator.) A polarizing filter in the collection optics was used to suppress scattered laser light, followed by a depolarizing prism to compenstate for the polarization response of the gratings. The spectrally resolved output was measured by a Hamamatsu 955 PMT followed by a Spex DPC-2 photon counter. The final chart recorder output was digitized and stored by the PDP 11-03/2. System response correction was done by digitizing the measured spectrum of a calibrated tungsten lamp, as described in Section I.

The liquid sample studied in this manner was 18 micromolar rhodamine-575 in methanol. This was mounted in a 1.3 mm o.d. capillary tube, oriented so as to minimize the pathlength of the output emission. When the methanol was cooled to liquid nitrogen temperatures it formed a fractured glass. The cast plastic sample was a

20 × 25 mm PMMA rod containing an effective concentration of 14 micromolar rhodamine-575. The diffused sample was a 1.6 mm diameter rod of Rhomm and Hass plexiglass that had been soaked for 4 hours in a 100 micromolar solution of rhodamine-575 in a mixture of 0.91 methanol and 0.09 dichloromethane by volume.

The results from the liquid sample are shown in Figure 44. The 200 cm^{-1} wide notches in the spectra are due to a shutter which blocked the PMT as the spectrometer was scanning across the laser frequency. The lower three spectra correspond to room temperature emission for laser excitations at 16,509, 17,164, and 20,492 cm^{-1}, respectively. The peak of the emission for the lowest energy excitation is at the same frequency as that of the highest energy excitation, despite the fact that some of the emitted photons were blue-shift (shifted to higher energy) as much as 1,700 cm^{-1} up from the excitation frequency. This anti-Stokes shift energy is greater than 8 kT for room temperature spectra, (kT = 0.026 ev = 208.5 cm^{-1} for T = 300 K). Introducing sharp-cut filters into the excitation beam centered intensity in proportion to the reduction in the excitation intensity, but caused no shift in the observed spectral shape. We concluded that these emission spectra did not include emission due to stray light excitation of higher energy. The upper plot shows emission spectra at 77° K due to excitations at 16,877, 17,163, and 20,493 cm^{-1}. The luminescence spectrum produced by the highest energy excitation is a slightly narrower version of the room temperature spectrum. The lower energy excitation at low temperature produced negligible emission at higher energies, which agrees with the previous result that the

Figure 44. Emission spectra for rhodamine-575. The lower three plots show room temperature emission in methanol at three different excitation energies. The upper plots are similar spectra taken at 77°K.

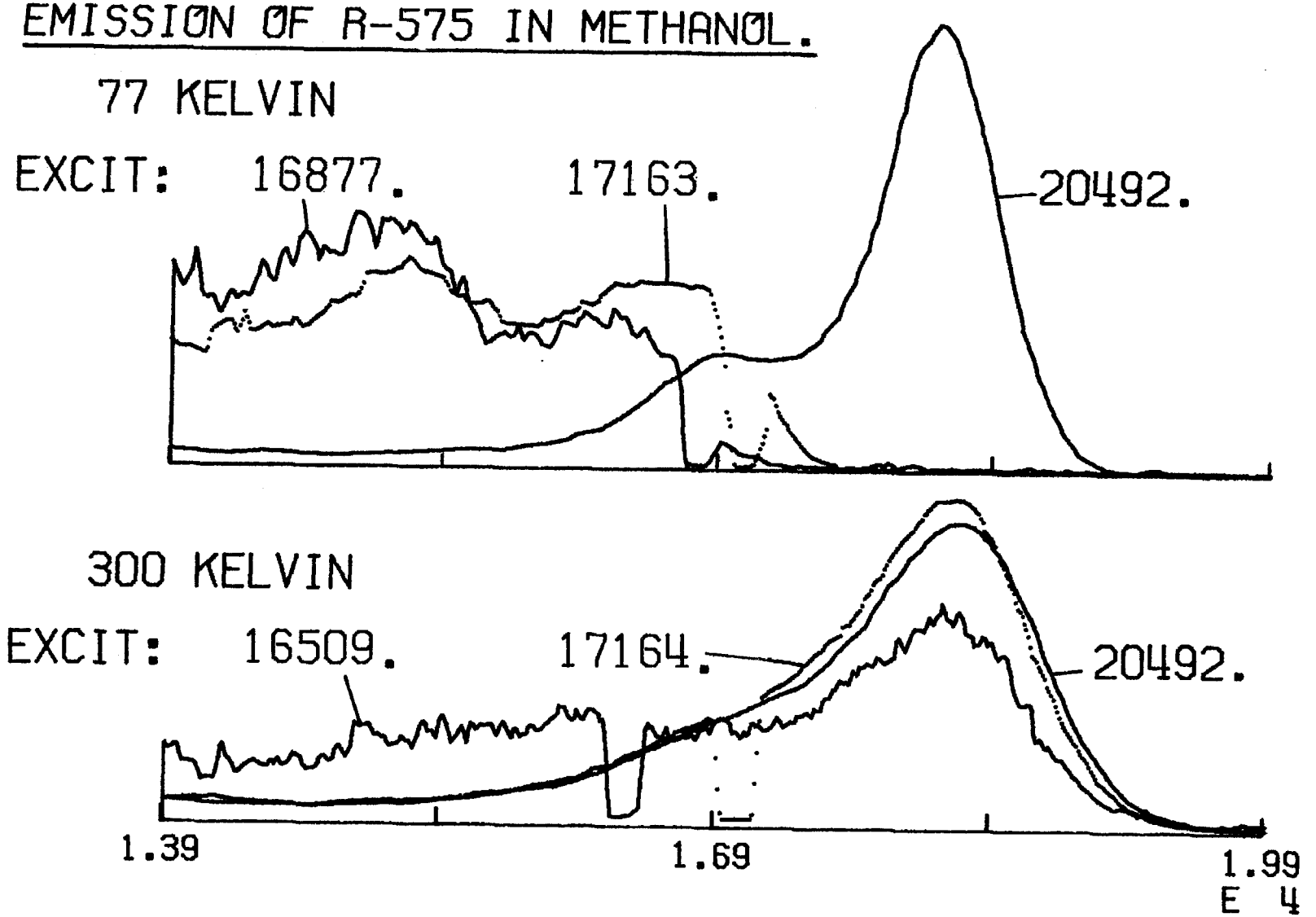
EMISSION OF R-575 IN METHANOL.
77 KELVIN
EXCIT: 16877.
17163.
20492.
300 KELVIN
EXCIT: 16509.
17164.
20492.
1.39
1.69
1.99
E 4
WAVENUMBERS

emission at room temperature from low energy excitation was due to anti-Stokes shifting of the excitation. Similar large anti-Stokes shifts have been observed in vapor phase dye spectra (Pappalardo and Ahmed, 1972).

Figure 45 gives corresponding results for rhodamine-575 cast in PMMA. The lower plot shows the room temperature luminescence spectra normalized to unit area. These spectra differ from the methanol solutions in that the emissions produced by low energy excitations at 16,273 and 17,060 cm^{-1} were greatly skewed towards the red, whereas the higher energy excitations at 19,436 and 20,492 cm^{-1} produce emission with the same general shape and position as the methanol room temperature emission. The upper plot shows the low temperature emission due to excitations at 17,423, 19,436, and 20,492 cm^{-1}. As in the liquid samples, the anti-Stokes shifted emission was suppressed at 77°K, however in this case the emission shape varied greatly with the energy of the excitation.

The diffused plastic sample showed anti-Stokes emission intermediate between that of the cast plastic and liquid solution. Figure 46 shows the room temperature emission of a PMMA sample soaked in a methanol solution of rhodamine-575. The excitation positions were 16,116, 17,449, 19,436, and 20,492 cm^{-1}. The emission spectra have been normalized to unit area. While there is some variation in the peak position with excitation energy, we found that the spectra was dominated by large anti-Stokes shifts for low excitation energies, as was the case for the methanol solutions.

Figure 45. Emission of rhodamine-575. The lower three plots represent emission in cast PMMA at room temperature for three different excitation energies. The upper plots are similar spectra taken at liquid nitrogen temperatures. All spectra are normalized to unit area.

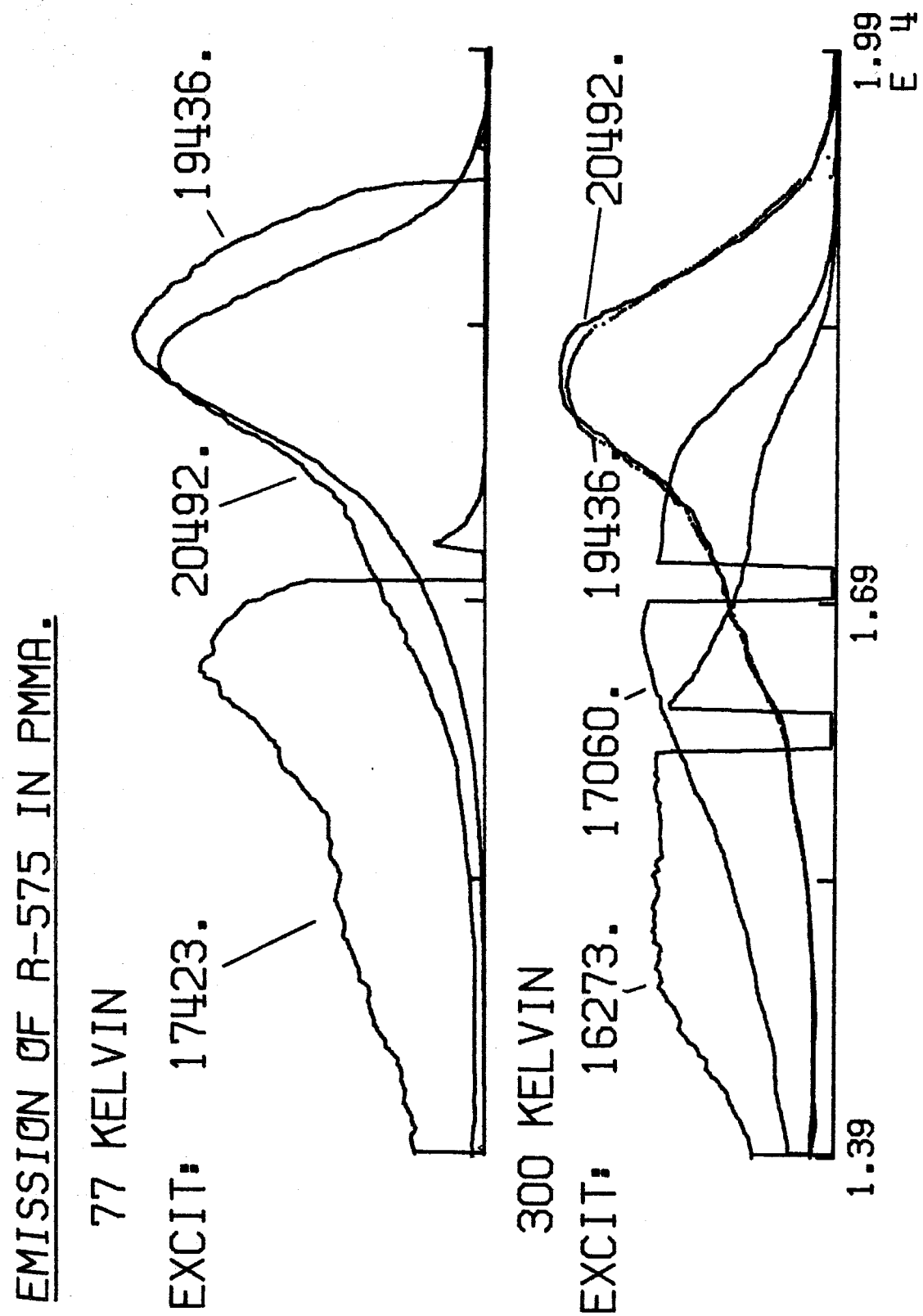
EMISSION OF R-575 IN PMMA.
77 KELVIN
EXCIT: 17423.
20492.
19436.
300 KELVIN
EXCIT: 16273.
17060.
19436
20492.
1.39
1.69
1.99
E 4
WAVENUMBERS

Figure 46. Emission of rhodamine-575 in diffused PMMA at room temperature. The four normalized spectra correspond to four different excitation energies.

EMISSION OF R-575 IN PMMA.

SURFACE DIFFUSED DYE

300 KELVIN

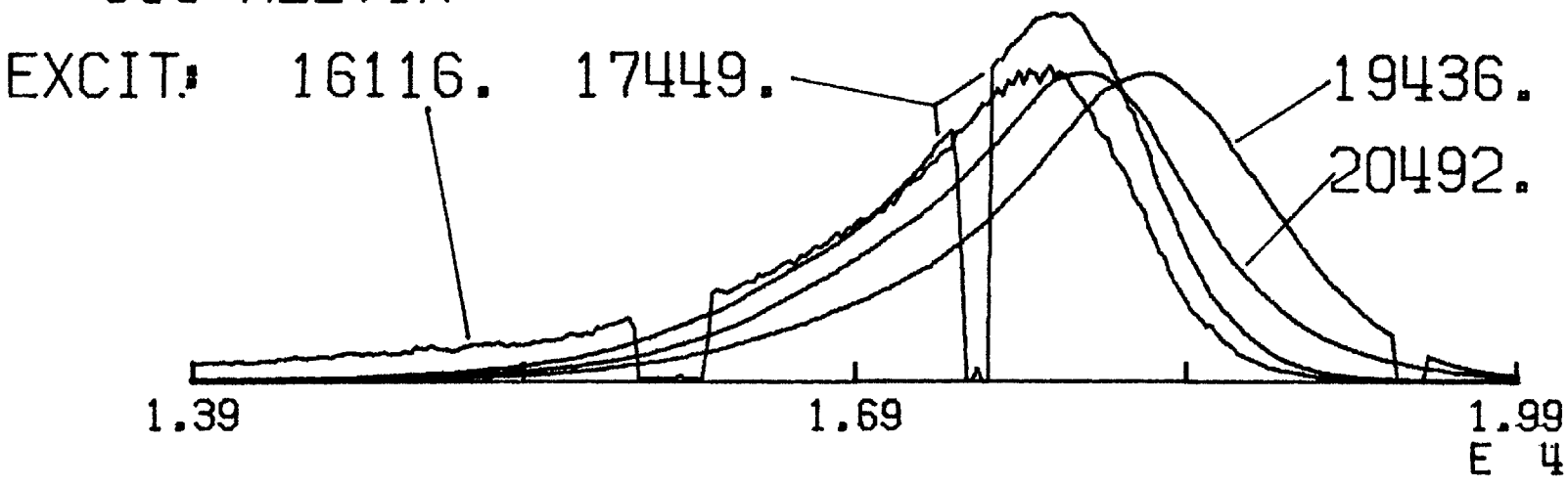

WAVENUMBERS

Preliminary measurements were made of the emission spectra of rhodamine-575 in cast PMMA at liquid helium temperatures. There was no pronounced change in spectral shape between the liquid nitrogen and liquid helium spectra.

Polarization Measurements

We suspected that self-absorption rates could be measured rather simply by observing the relative polarization intensities of emission from a sample excited by polarized light. Light from a tungsten lamp was monochromated at 20,200 cm^{-1}, chopped, and passed through an adjustable polarizer (Polaroid HN38). This light was focused onto an ethylene glycol solution of rhodamine-575. The concentration was varied during the course of the experiment by changing the dye solution. The resulting emission perpendicular to the axis of the excitation was passed through a second adjustable polarizer, and the intensity at 17,860 cm^{-1} was measured with a second monochromator, a PMT, and a lock-in amplifier. The lamp, monochromators, PMT, and lock-in have been described in Section I. The polarizers were controlled by the PDP 11-03/2, which also digitized and stored the output of the lock-in.

Dye solutions were used in the place of cast plates for two reasons. The first was that dyes in solution show far greater spectral homogeneity, which allowed for more tractable modeling of the self-absorption process. The second reason was that the use of solutions facilitated changing the dye concentrations in the sample. Ethylene glycol was chosen because it has a viscosity of about 20 centipoises at room temperature, and should produce rotational diffusion times

for the dye molecule which are long enough that emission from a polarized excitation would also be partially polarized, assuming that the absorption and emission dipoles are aligned. If this is the case, then emission polarized in the $\hat{Z}$ direction should be more intense than emission polarized in the $\hat{X}$ direction for a $\hat{Z}$ polarized excitation (see Figure 47). $\hat{Y}$-polarized excitation should produce equal intensities for both polarizations of emission.

We varied the dye concentration of the sample and measured the intensity of the $\hat{Z}$- and $\hat{X}$-polarized emission at each concentration. The sample dye concentration was varied from 0.2 micromolar to 100 micromolar by factors of 2.0. The pathlength in the sample traversed by the emission en route to the detection monochromator was 0.7 cm. The observed intensities were corrected for background and for the polarization response of the system.

Figure 48 shows the variation between the $\hat{Z}$- and $\hat{X}$-polarized emissions for $\hat{Z}$-polarized excitation as a function of concentration. The plotted value is the polarization anisotropy, which is the emission intensity of the $\hat{Z}$- minus the $\hat{X}$-polarized intensities, both divided by the sum of the $\hat{Z}$- plus two times the $\hat{X}$-polarized emission intensities. For very low concentrations, the anisotropy plateaus at about 0.18, or equivalently, the ratio of the parallel to the perpendicular emission is about 1.65. As the concentration increases, the apparent polarization of the emission decreases. The error bars reflect variations of repetitive measurements at a single concentration. These errors could probably be substantially reduced by the use of a more intense excitation source.

Figure 47. Principal directions for polarization anisotropy measurements. Emission is detected perpendicularly to the excitation axis. The excitation and emission both have vertically and horizontally polarized components. If the excitation is vertically polarized, emission is parallel if it is vertically polarized and perpendicular if it is horizontally polarized.

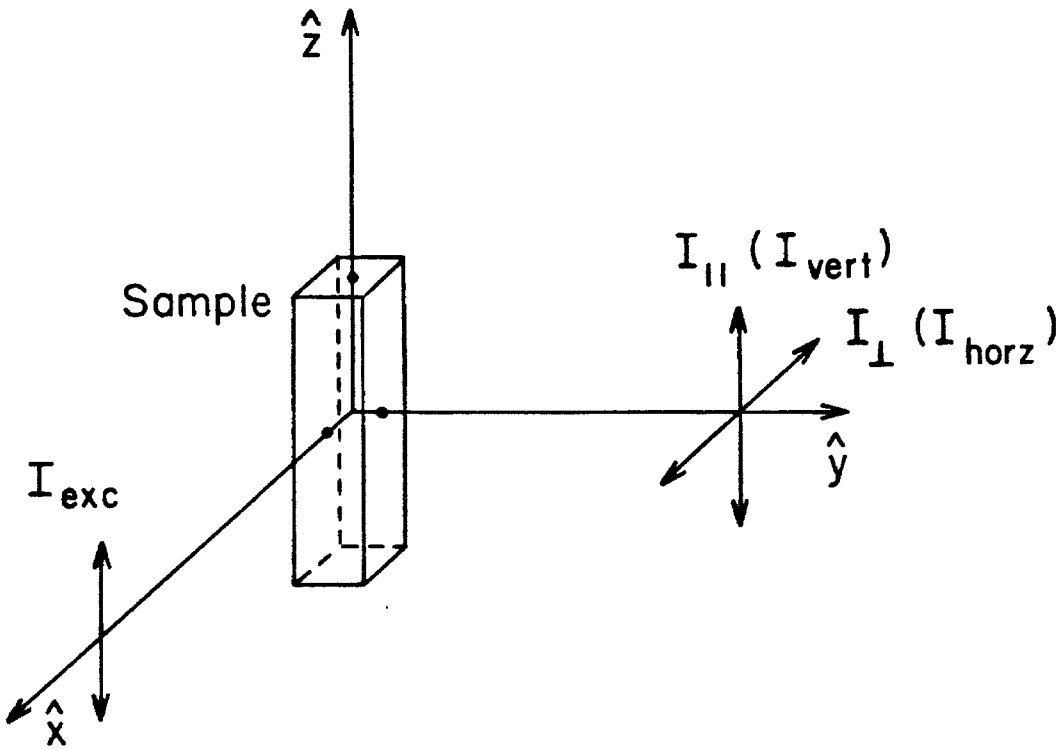
$\hat{z}$
Sample
$I_{\parallel}$ (I_{vert})
$I_{\perp}$ (I_{horz})
$\hat{y}$
I_{exc}
$\hat{x}$

Figure 48. Polarization anisotropy vs. sample concentration for rhodamine-575 in ethylene glycol. The reduced polarization anisotropy is the difference between the parallel and perpendicular intensities divided by the sum of the parallel and twice the perpendicular intensities. The solid line serves only to connect the data points.

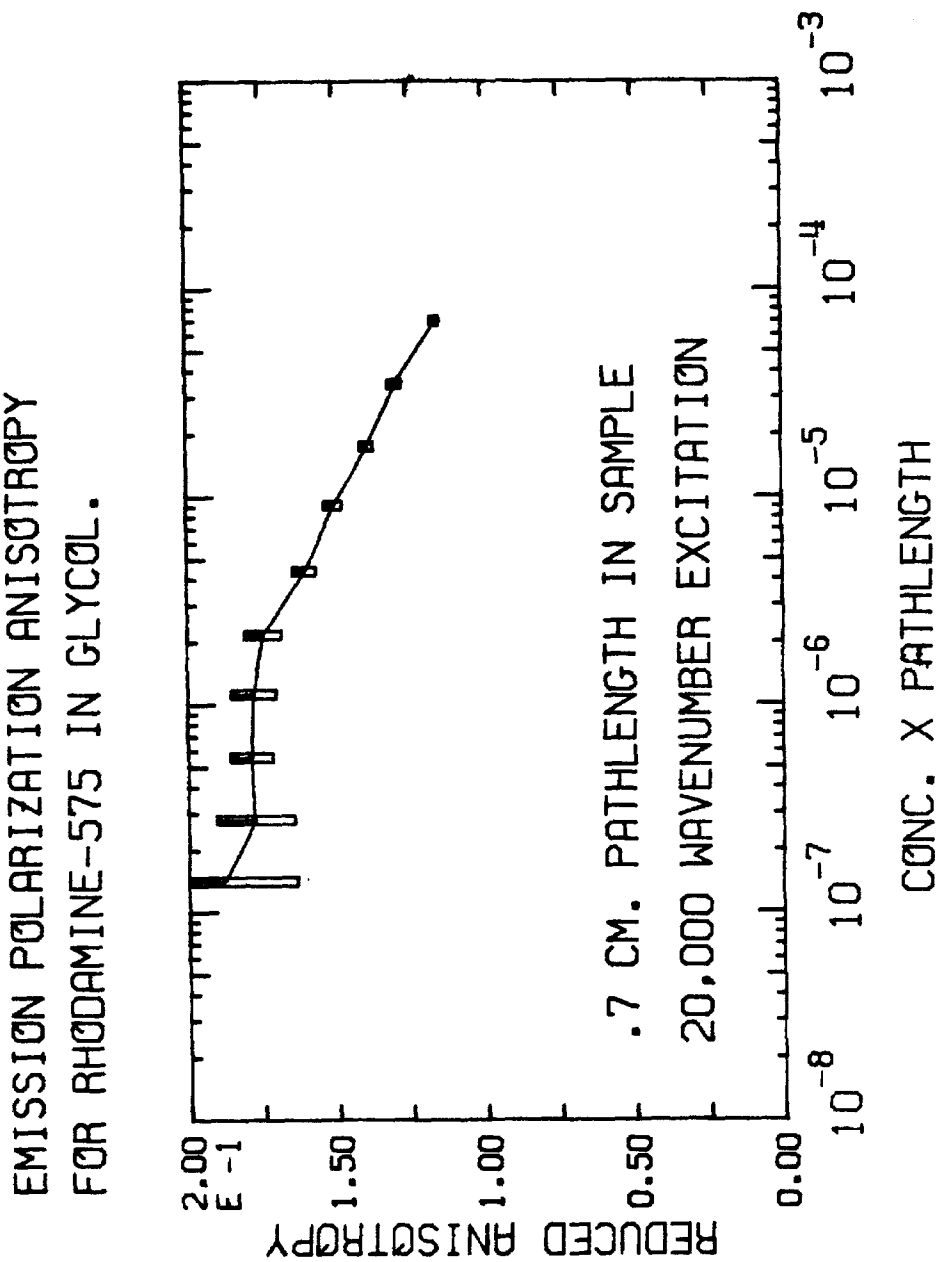
EMISSION POLARIZATION ANISOTROPY
FOR RHODAMINE-575 IN GLYCOL.
REDUCED ANISOTROPY
2.00
E -1
1.50
1.00
0.50
0.00
10^-8
10^-7
10^-6
10^-5
10^-4
10^-3
.7 CM. PATHLENGTH IN SAMPLE
20,000 WAVENUMBER EXCITATION
CONC. X PATHLENGTH

Transient Emission Measurements

We measured the time evolution of the emission intensity resulting from very short pulse excitation of dyes in a variety of hosts. Time-resolved luminescence measurements were performed with a mode-locked argon ion laser (Spectra Physics model 171/342) and a photon counting apparatus. The experimental apparatus was expertly planned and assembled by David Millar and Raymond Robbins (Robbins, Millar, and Zewail). Samples were illuminated with vertically polarized 19,436 cm^{-1} light pulses at a repetition rate of about 100 khz, with a typical pulse half-width of less than 200 picoseconds. Emission from the sample was monitored by a Philips XP2020Q photomultiplier. Cut-off filters at 5,000 Å and 5,700 Å were placed between the sample and the PMT to reduce scattered laser light, plus an analyzing polarizer to sample different emission polarization intensities. The system response, measured by laser light scattered from a dilute coffee creamer solution sample, is shown in the upper plot in Figure 49 and usually had a response time of less than 250 picoseconds.

The first type of measurement we made was to find the total lifetime of the dye as a function of concentration. In this case the dye emission was filtered by a polarizer at 54.7 degrees from the laser's original vertical polarization so as to average between the emission of the parallel and perpendicular polarization components. The lower plot in Figure 49 shows typical transient emission data for a 4.6 micromolar solution of rhodamine-575 in methanol. The dye was contained in a 1.0 × 0.5 cm (i.d.) cuvette so that, on average, the

Figure 49. System response and transient lifetime measurement. The upper plots show a typical histogram of the system response to a 5,145Å pulse from a mode-locked argon ion laser, with a duration of less than 200 picoseconds, scattered off of a dilute coffee creamer solution. The width and asymmetry of the response was predominantly due to the PMT. The lower plot shows the observed emission of a 4.6 micromolar rhodamine-575 solution, superimposed on a best fit exponential convolution of the system response. The exponential fit gives a lifetime of 4.1 nanoseconds.

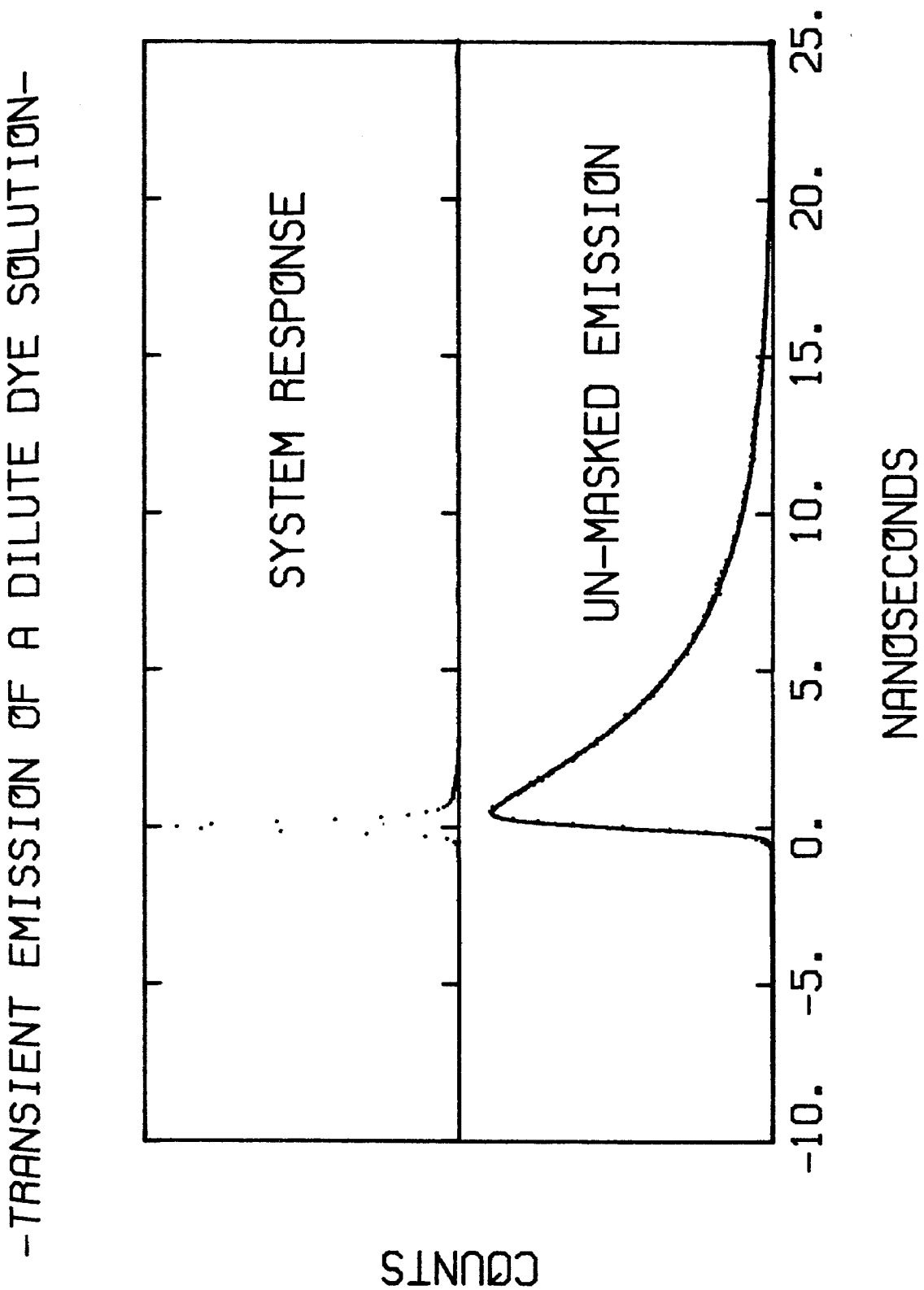
-TRANSIENT EMISSION OF A DILUTE DYE SOLUTION-
SYSTEM RESPONSE
UN-MASKED EMISSION
COUNTS
-10.
-5.
0.
5.
10.
15.
20.
25.
NANOSECONDS

emission passed through 0. 5 cm of sample before arriving at the collection optics. The extinction coefficient for rhodamine-575 at the lasing wavelength was about 90,000 moles per cm per liter, so that, even at this low concentration, about 40% of the laser excitation was absorbed by the sample. Superimposed on the raw data in Figure 49 is a least squares fit of a single exponential including a convolution of the system response given in the upper plot. The best exponential fit gave an observed lifetime of 4. 13 nanoseconds at this concentration. Similar measurements have been made on rhodamine-590, rhodamine-610 and Kiton red-620 (Hammond, 1979). The measurement technique used was incompatible with our need for measuring high rates of self-absorption in arbitrary geometries. In general, lifetimes also increase with decreasing temperature (Theiss and Weber, 1974).

We measured excitation lifetimes for a sequence of dye concentrations from 0. 2 to 100 micromolar for rhodamine-575 in both methanol and ethylene glycol. As in the polarization measurements, we opted for solution samples because of both the ease of changing concentrations and because of the better spectral homogeneity of the dye in solution as opposed to the dye in PMMA.

Figure 50 shows the fitted lifetimes as a function of concentration in methanol. The highest concentration used was a factor of ten below the critical concentration, as defined by the Förster model. (The critical concentration for transfer from rhodamine-575 to itself in methanol is 4.6×10^{-3} M). At low concentrations the lifetime of rhodamine-575 approached an asymptotic value of 3. 7 nanoseconds, while at high concentrations it increased to three times its low

Figure 50. Measured lifetime of rhodamine-575 in methanol as a function of concentration. (The solid curve serves only to connect the data points.)

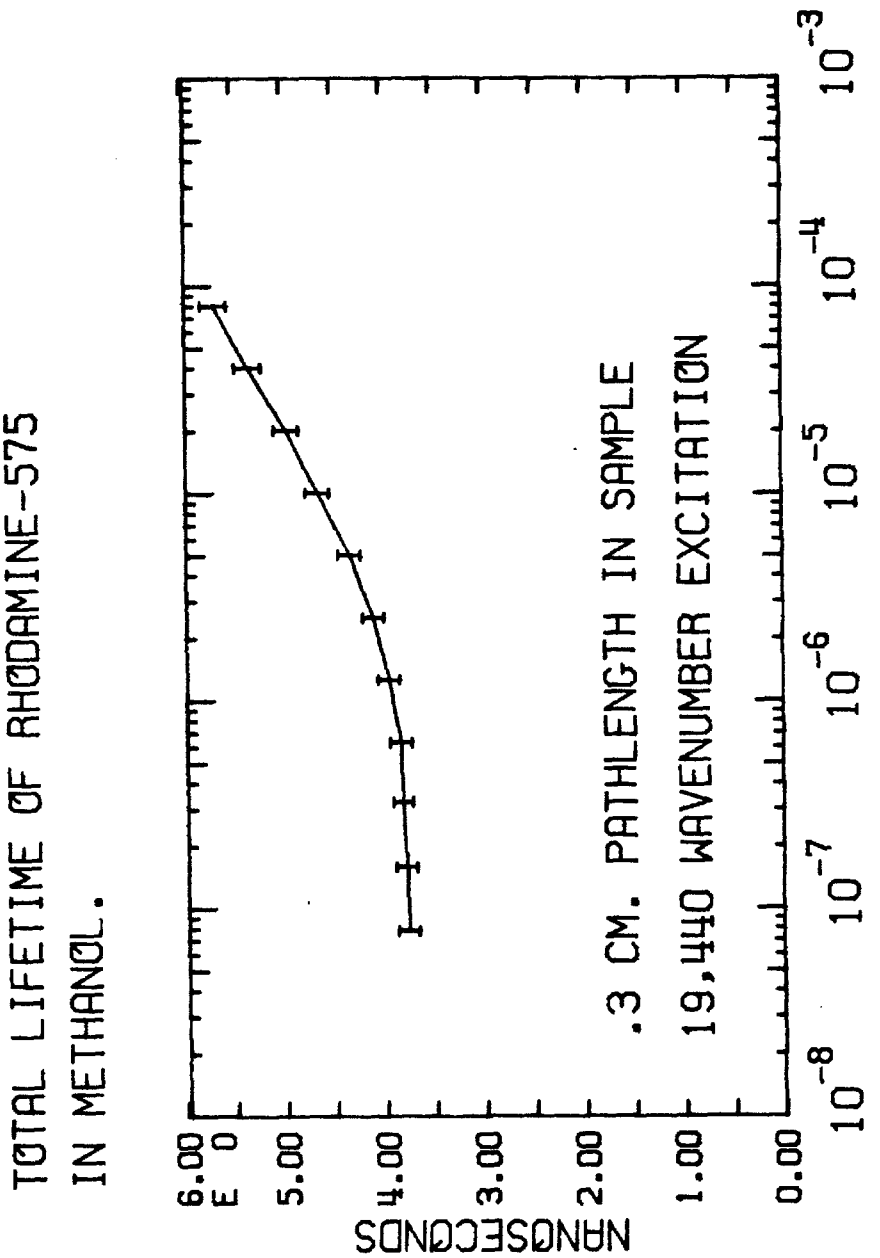
TOTAL LIFETIME OF RHODAMINE-575
IN METHANOL.
NANOSECONDS
6.00
5.00
4.00
3.00
2.00
1.00
0.00
.3 CM. PATHLENGTH IN SAMPLE
19,440 WAVENUMBER EXCITATION
10^{-8}
10^{-7}
10^{-6}
10^{-5}
10^{-4}
10^{-3}
CONC. X PATHLENGTH

concentration value. The errors bars in Figure 50 indicate the uncertainty of the lifetime in the numerical fitting of the data. As in the previous case, the emission was filtered with a polarizer 54.7 degrees from the vertical to sample equally the vertical and horizontal (parallel and perpendicular) polarization components. Care was taken not to mask any portion of the emission of the dye from illuminating the PMT.

Others have suggested that variations in excitation lifetime might be due to molecular re-orientation times (Shapiro and Winn, 1980). To help determine the mechanism for lifetime lengthening of the dye with increasing concentration, we performed a measurement of the emission intensity as a function of time, except that in this case part of the sample cuvette was blocked so that dye in a portion of the cuvette could not directly illuminate the detector. Figure 51 shows a schematic of the sample geometry with respect to the exciting laser and the output emission. The sample used in this case was rhodamine-575 in methanol at 460 micromolar. At this concentration 99% of the excitation was absorbed in the first 0.05 cm of the sample. We were not interested in measuring the emission resulting directly from this excitation, but in the emission that followed the self-absorption of this first emission. The mask shown in Figure 51 achieved this condition. The transient emission spectrum resulting from this configuration is shown in the upper plot in Figure 52. When the mask was removed, we obtained the lower plot in Figure 52. The solid curves superimposed on these two spectra are fitted theoretical functions, and will be described in the fourth chapter. It was evident

Figure 51. Position of the first generation mask. The 5,145Å laser line is 99% absorbed in the first 0.05 cm of the 460 micromolar rhodamine-575 methanol solution. Blocking just the left portion of the cell, as shown, prevents emission due to the initial excitation from being detected directly.

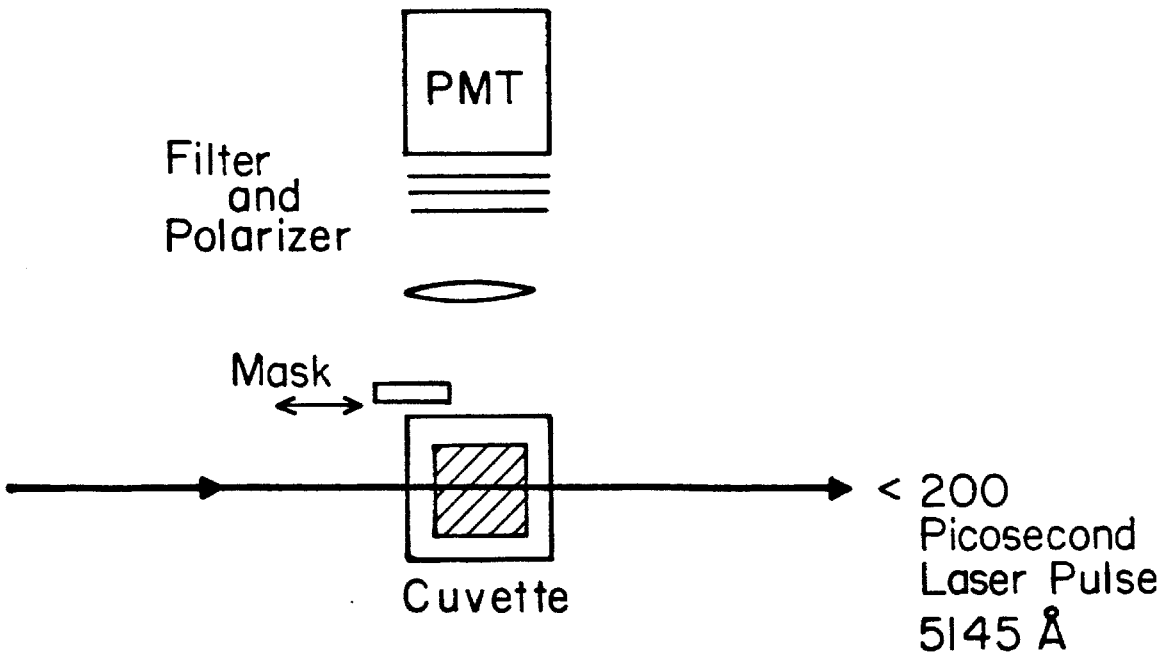
PMT
Filter
and
Polarizer
Mask
Cuvette
< 200
Picosecond
Laser Pulse
5145 Å

Figure 52. Unmasked and masked transient emission spectra. The upper plot shows the transient emission histogram from a 460 micromolar rhodamine-575 methanol solution for the case where a mask is placed between the region excited by the laser and the detector. The lower plot is the same measurement with the mask removed.

-TRANSIENT EMISSION OF CONCENTRATED DYE SOLUTIONS-

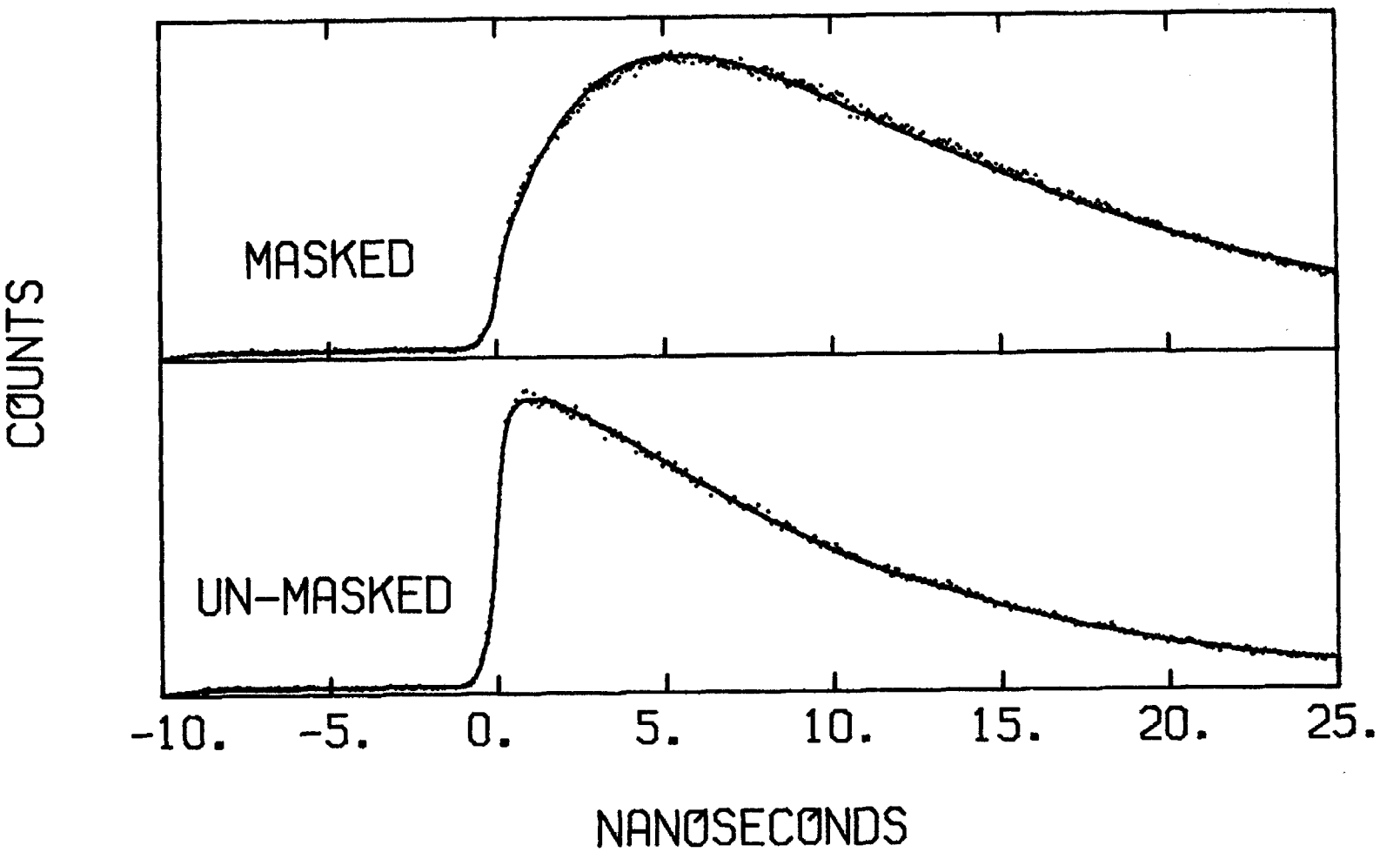

that there were significant distortions of the single exponential decay when the initially excited portion of the sample was masked.

IV. PROTOTYPE TESTING

LSC research has a bottom line in the sense that the primary goal is to build devices which are useful for converting sunlight into other forms of energy. We believe that the best characterization of an LSC plate is to measure its flux gain with a particular type of cell. The flux gain, G_{flux}, is defined to be the factor by which the power output of a cell increases when it is attached to the LSC plate, as opposed to facing the sun directly. A second important parameter to report is the geometric gain of a plate, which is the ratio of the area of the LSC which is exposed to the sun (the LSC face) to the area covered by solar cells (the LSC edge). The geometric gain, G_{geom}, can be measured with a ruler. These two numbers will dictate the initial cost of the device as well as its efficiency. For example, if the AM1 efficiency of the cell is known, η_{cell}, then the efficiency of the cell-LSC combination, η_{LSC}, is the cell efficiency times the flux gain divided by the geometric gain, $\eta_{LSC} = \eta_{cell} \cdot G_{flux}/G_{geom}$.

Table 3 lists the performance parameters for a variety of devices tested by ourselves and others. The measured performance of an LSC depends on the temperature, the angular distribution of the incident light, the spectral content of the light, and probably other factors. Unfortunately, the testing procedure varies for the different prototypes, so we will try and describe the circumstances for each of the tests.

Table 3. Prototype performances. Devices B and D were made and tested by Owens Illinois. The rest were made and tested here. The geometrical gain is defined to be the ratio of the area of the plate exposed to the sun divided by the area of the edge which absorbs light. The flux gain is the factor by which the output power of a solar cell is increased when it is mounted on a plate. The collector efficiency is the assumed AM1 cell efficiency times the flux gain divided by the geometrical gain, and corresponds to the electrical power out per solar power input.

Table 3.

Device	No. Dyes	Matrix	Geometrical Gain	Flux Gain	Assumed Cell Eff.	Collector Eff.
A	2	PMMA	23	2.1	18%	1.9%
B		thin film	11	1.3	21%	2.5%
C	3	ethylene glycol	36	3.8	18%	1.9%
D	3	thin film	11	1.7	21%	3.2%
E	1	PMMA	68	5.1	18%	1.3%
F	1	PMMA/DMSO	92	4.4	18%	0.9%

Devices B and D in Table 3 were built and tested by Owens-Illinois. The dyes were contained in thin plastic films attached to the surface of clear acrylic substrates. Measurements were made under actual insolation (presumably direct sunlight), with the plate edges roughened and blackened where cells were not mounted. These plates have achieved the highest efficiencies, but their small geometric gains make them somewhat ineffective as concentrators. For example, cells mounted on device D had only a 70% increase in output over similar cells which faced the sun directly.

Device C was constructed by gluing two 110 × 110 × 0.3 cm plexiglass plates on opposing sides of 0.08 cm thick plexiglass spacers. The assembly was mounted on a mirror backing. The resulting gap between the plates was filled with an ethylene glycol solution containing 57, 94, and 51 micromolar solutions of coumarin-540, rhodamine-590, and rhodamine-640, respectively. The edges of the sandwich assembly were made light absorbing with black electrician's tape except for the portion coupled to the cell. The flux gain was measured under actual insolation by first measuring the short circuit current on a standard cell under direct insolation, and then measuring the short circuit current for the same cell coupled to the plate, using ethylene glycol as an index matching fluid. We calculate that this dye combination will absorb about 30% of a 5,800°K black body spectrum in a two pass geometry. The collector efficiency given in Table 3 is the cell AM1 efficiency times the flux gain divided by the geometric gain.

Device E was a 120 × 100 × 0.4 cm PMMA plate containing 220 micromolar DCM. The edges were taped as before except where the

cells were mounted. The measurements were made using two cells with AM1 efficiencies matched to within 5%, and both with an active area of 0.4 × 2 cm. One cell was mounted co-planar to the LSC face as a reference, and the other was contacted with the LSC edge using ethylene glycol as an index matching fluid. The tests were made using a xenon flashlamp AMO simulator at JPL. The flux gain was determined to be the ratio of the peak power of the LSC-mounted cell to the reference cell, corrected for flash to flash variations. We calculate that this plate should absorb 30% of a 5,800° K spectrum. The collector efficiency was determined in the same manner as for device C.

The performance of device E is less than would be expected from the DCM CODE of 240 in methanol. The reason is clear from the absorption and emission spectra of DCM in PMMA, shown in Figure 12. The overlap is much greater in PMMA than in methanol, so that the CODE of DCM in PMMA is only 20. A similar effect had been observed for other dyes in plastics by Sah (Sah and Baur, 1980), who found that much of the original Stokes shift could be restored by adding solvent to the monomer prior to polymerization. On the basis of this suggestion, we made a PMMA plate containing 4.5 × 10 M DCM and 3% dimethylsulfoxide by volume. The device geometry and testing procedure was the same as for device E. The performance of this plate is listed as device F. The DMSO did not appreciably restore the solution Stokes shift, and caused significant loss of plate quality.

V. SUMMARY

1. The low concentration absorption, emission, and excitation spectra in methanol for 18 organic laser dyes were catalogued.

2. Photobleaching rates for a variety of plastic and solution samples were measured under actual insolation. Degradation was measured both by emission and absorption decay; the two rates were found to be similar. Degradation rates increased with time. Sample lifetimes varied between hours and years.

3. Emission spectra as a function of self-absorption pathlength were taken of rhodamine-575 in solution, in diffused PMMA, and in case PMMA.

4. Emission spectra of rhodamine-575 in methanol, in diffused PMMA, and in cast PMMA were taken as a function of temperature and excitation energy. The peak position of the emission was independent of temperature and excitation energy for the methanol and diffused PMMA samples, and varied considerably in cast PMMA.

5. The component polarization intensities of the emission of rhodamine-575 resulting from plane polarized excitation was measured as a function of concentration for a fixed self-absorption pathlength. The emission became increasingly unpolarized with increasing concentration.

6. The total lifetime of rhodamine-575 in solution was measured as a function of concentration for a fixed self-absorption pathlength using very short pulse excitation. The measured lifetime increased with increasing concentration. The transient emission spectra showed

an anomolously slow build up time if the initially excited portion of the cell was masked.

7. Performance measurements were made on a variety of prototype devices. Our highest gain collector had a flux gain of 5.1 and an estimated overall efficiency of 1.3%. Our highest efficiency collector was a liquid cell with a flux gain of 3.8 and an estimated overall efficiency of 1.9%.

CHAPTER 3

I. SINGLE DYE MODEL FOR THE PERFORMANCE OF AN LSC

There are many design variables in an LSC. Which dye should be used and at what concentration? How large should the plate be? What type of solar cell should be mounted on the plate? We wished to find a reasonably accurate model that would take the measured characteristics of the components, including, for example, the absorption spectrum of a particular dye, and from this would predict the light output and electrical efficiency of an LSC using that dye. What follows is such a model. Its strength is that it appears to be fairly accurate when correlated to actual prototypes. Its weakness is that it is too complicated to allow rapid assessment of a variety of possible systems.

Photon Flow Diagram

We can trace the flow of excitations in an LSC with the aid of the flow chart in Figure 53. Above all is the sun. Part of its incident flux will be initially lost due to reflection from the LSC surface, and part is lost because its wavelength does not correspond to the absorption band of the dye used. What is left is the absorbed solar flux in the dye ensemble, denoted by S. There is a net rate of excitation, J, of the dye ensemble, which in steady state must correspond to the rate of de-excitation. The photon output of the dye ensemble is the quantum efficiency of luminescence, η, times J. This luminescence is geometrically divided into the fraction $JP\eta$ which is emitted within any of the critical escape cones, and the fraction $J(1-P)\eta$ which is trapped. Light emitted into the critical cones has an average probability $\bar{r}$ that self-absorption will take place before the light can escape

Figure 53. Photon flow diagram for a single dye LSC. Light from the sun is partially reflected, partially absorbed by the dye ensemble, and partially transmitted through the LSC plate. Emission is geometrically divided between the critical escape cone and light trapped by total internal reflection. Light can be re-cycled into the dye ensemble by self-absorption. Collected light is converted to electricity by a photovoltaic cell (PVC).

Photon Flow Diagram for a Single Dye LSC

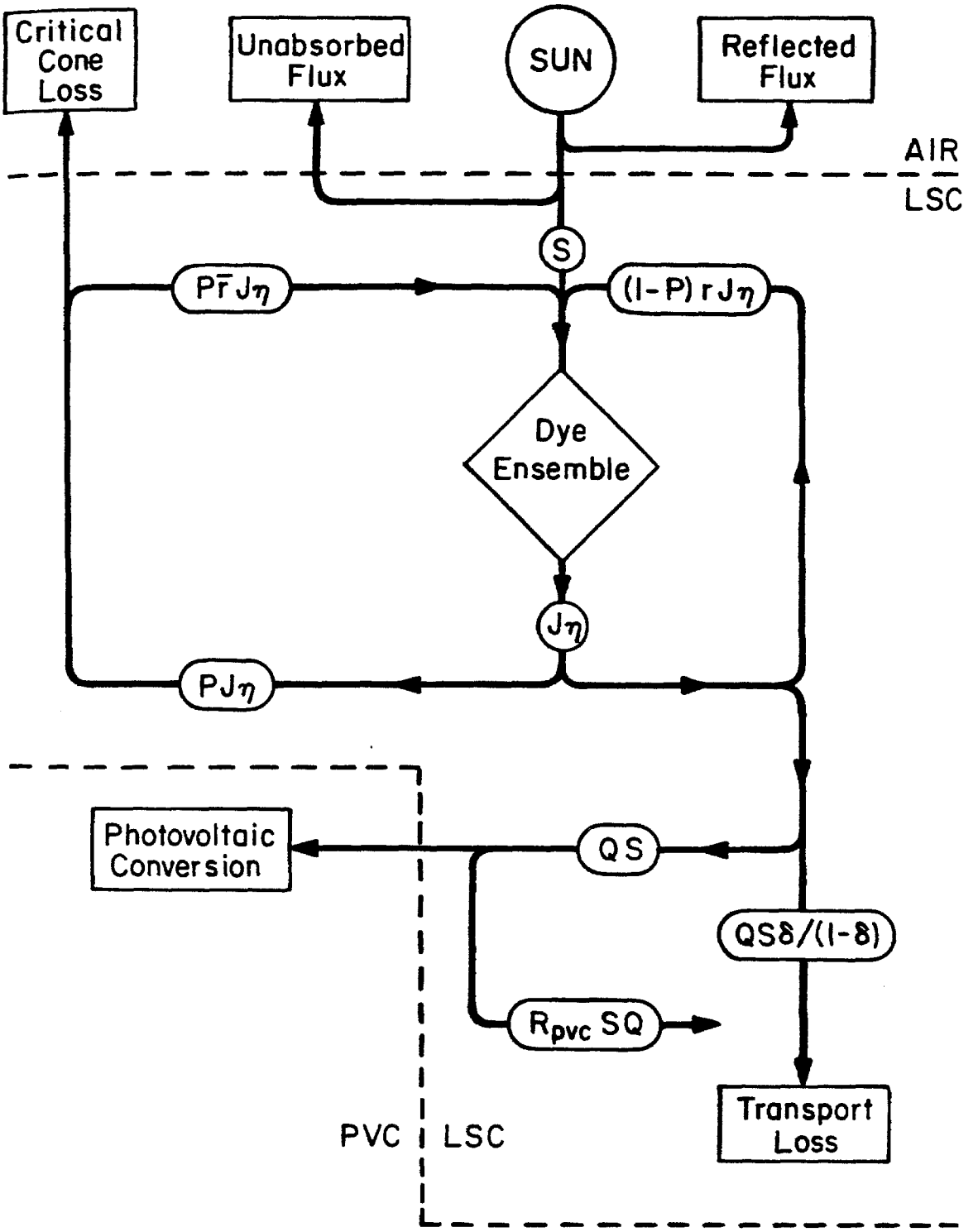

out of the LSC, so that there is a feedback loop of magnitude $\bar{r}\,JP\eta$ of emissions into the critical cones that are recovered as excitations in the dye ensemble.

A similar feedback loop occurs for self-absorption of trapped light. In this case the probability that a trapped photon will be self-absorbed before it reaches the LSC-cell interface is r. An additional lumped parameter δ describes the fraction of the trapped luminescence which is lost due to matrix absorption or imperfect reflections. A hardy fraction, Q, of the originally absorbed solar photons, arrives at the LSC-cell interface where a reflection can take place of magnitude QR_{cell}. In this analysis we will assume that such reflected flux is lost.

Solar Absorption - S

The solar spectrum is a variable quantity. We usually use a 5,800°K black body spectrum in our calculations. A comparison of a measured solar spectrum (Boer, 1977) and a 5,800°K black body spectrum is given in Figure 54. The solar flux per wavenumber will be denoted by $I(\bar{\nu})$, and the total flux by I, where

$$I = \int_0^\infty I(\bar{\nu})\, d\bar{\nu} \qquad (1)$$

Clearly this could be extended to include angular variations in spectrum and intensity, such as would be expected in a mixture of direct and diffuse insolation.

A fraction of this incident light will be reflected at the surface.

Figure 54. Comparison of an AM1 solar spectrum and a 5,800°K black body spectrum.

THE SOLAR SPECTRUM.

TOTAL INCIDENT LIGHT DURING A
COOL SUMMER DAY IN DELAWARE.

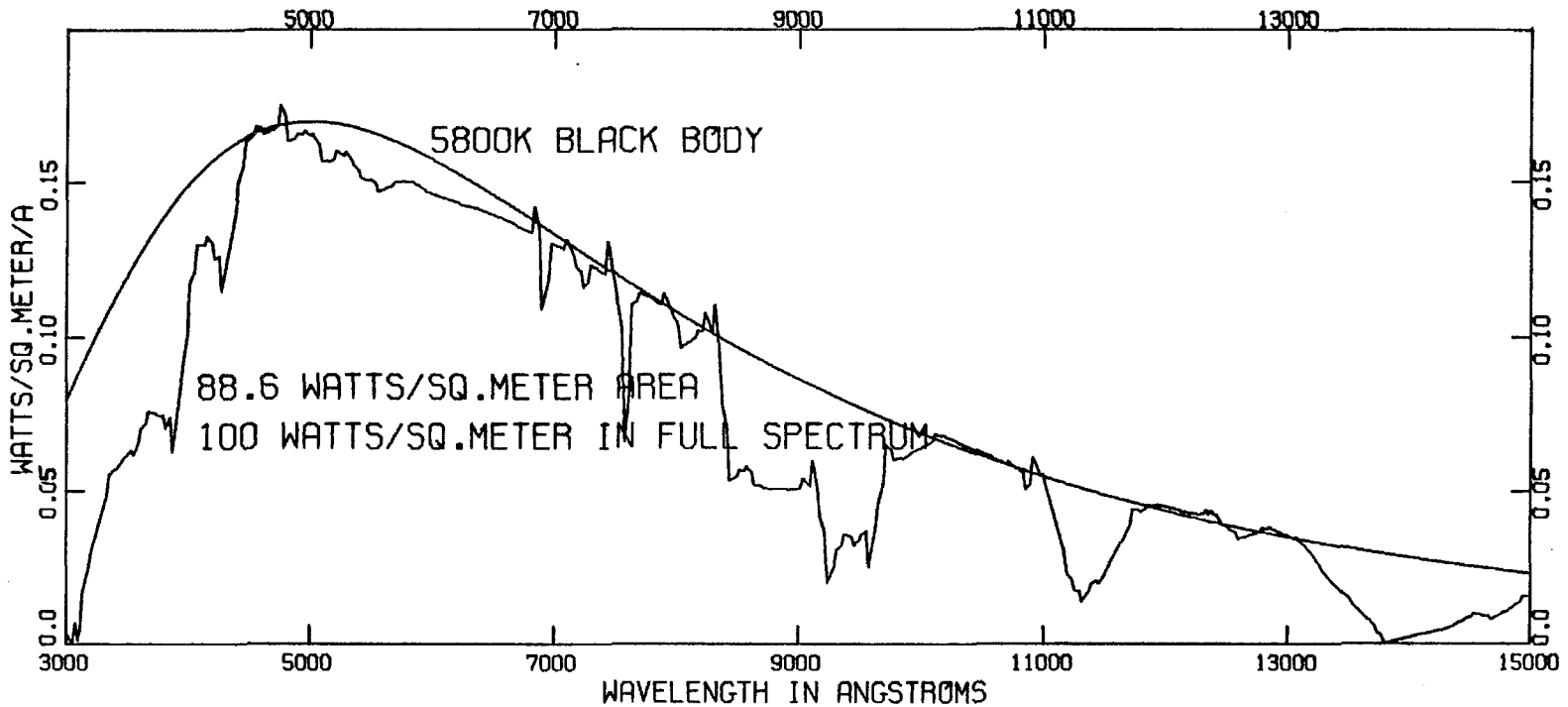

The reflection coefficient R can be computed by the Fresnel equation for an uncoated LSC (Born and Wolf, 1975), or by similar relations for LSCs with index-matching coatings (Hovel, 1975). (The reflection coefficient for vertical incidence on an uncoated plate with an index of refraction n is $(n-1)^2 / (n+1)^2$.)

Passing the air-LSC interface, the light will be partially absorbed by both the dye molecules and by the matrix material. The absorption pathlength for light incident on the plate with an angle θ is

$$\ell_s = \frac{D}{\sqrt{1 - \sin^2(\theta)/n^2}} \quad . \tag{2}$$

where D is the thickness of the plate. The length is twice that expression if a backing mirror is used. If the matrix material has an absorption coefficient $a(\bar{\nu})$, such that the attenuation of light of wavenumber ν over a distance ℓ_s is given by $10^{-\ell_s a(\bar{\nu})}$, then the light absorbed by the plate in photons per square meter per second is

$$S = \int_0^\infty I(\bar{\nu})\,(1 - R(\bar{\nu}))\,[1 - 10^{-\ell_s(C \cdot \epsilon(\bar{\nu}) + a(\bar{\nu}))}] \cdot \frac{C \cdot \epsilon(\bar{\nu})}{a(\bar{\nu}) + C \cdot \epsilon(\bar{\nu})} \tag{3}$$

for vertical incidence (Batchelder, Zewail, and Cole, 1979). $\epsilon(\bar{\nu})$ and C are the molar extinction coefficient and the dye concentration,

respectively.

The index of refraction of the usual matrix material is quite low (typically about 1. 5) so that reflection losses tend to also be low. As the angle of incidence increases, the apparent area of the plate decreases as the cosine of the angle of incidence. As the angle increases, the reflection coefficient also increases, however this is usually more than offset by the increased absorption pathlength for oblique angles of incidence light in the plate. As a result the angle of incidence dependence of an LSC is very nearly that of an idealized black body absorber, as shown in Figure 55.

Quantum Efficiency of Luminescence - η

We have calculated the number of excitations per second per square meter of the dye ensemble due to the sunlight, which is the S just calculated. The quantum efficiency of luminescence is the probability η that these excitations will be emitted as photons. There is an assumption that only excitations which excite the molecules into one of the electronic excited state manifolds are included both in S and in measurements of η.

Escape Probability - P

Luminescence incident on the LSC faces at an angle greater than the critical angle will be totally internally reflected. (The critical angle in this case is given by $\theta_c = \sin^{-1}(1/n)$, where n is the index of refraction of the plate.) The critical cone originates at the point of luminescence and forms a critical angle everywhere it intersects a surface. If the luminescence is isotropic and the LSC is planar, the

Figure 55. Dependence of absorbed flux on angle of incidence. The lowest curve indicates the flux absorbed by a millimolar rhodamine-590 plate 3 mm thick. This is very similar to the simple cosine law of a black body absorber with a reduced total absorption, as shown in the middle curve.

ABSORBED SOLAR ENERGY VS. ANGLE OF INCIDENCE.

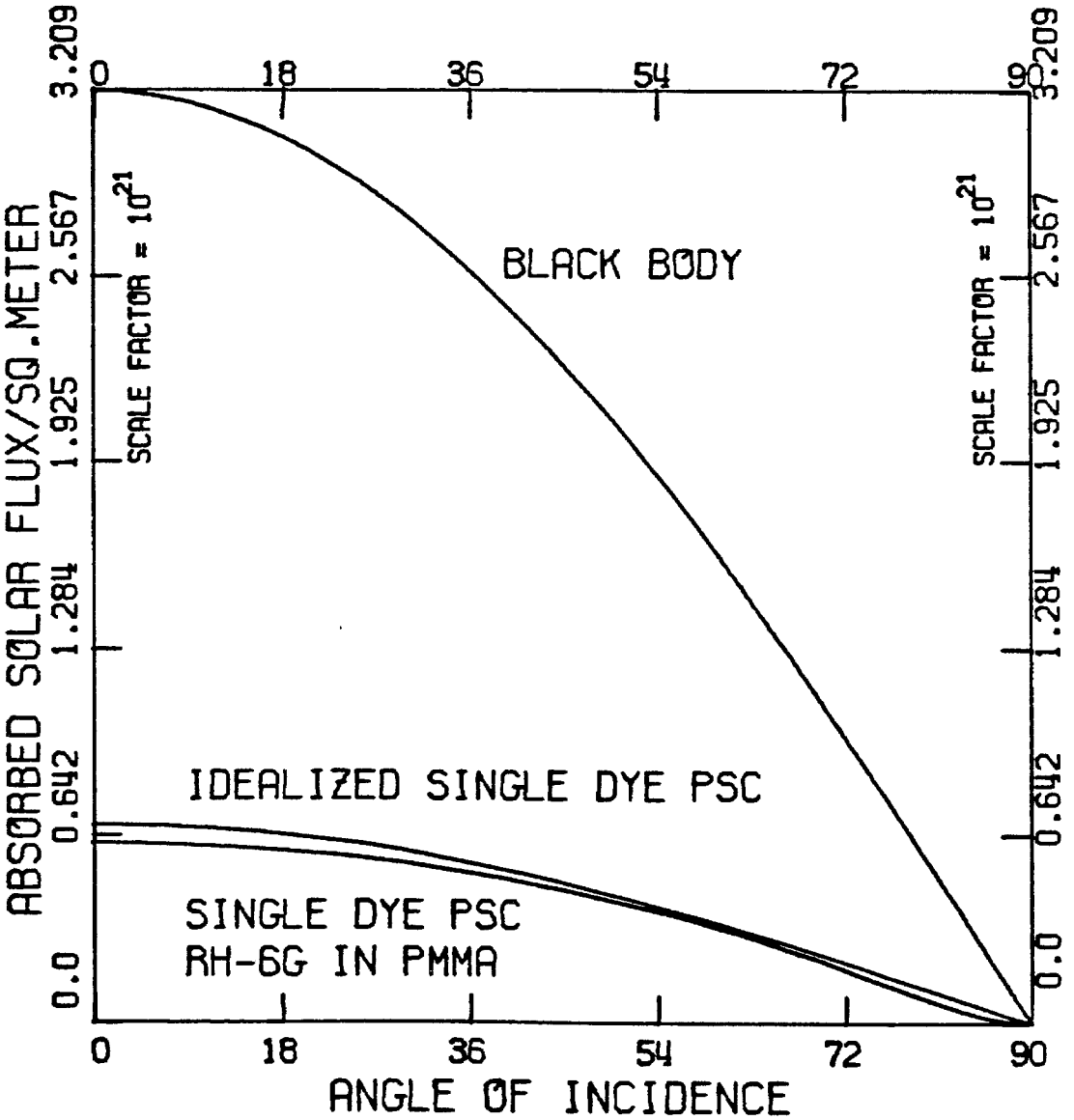

probability P that luminescence will escape out of the critical cones is the sum of the solid angles of the upper and lower critical cones divided by the total solid angle of emission

$$P = \frac{\int_0^{\theta_c} \sin(\theta)\, d\theta + \int_{\pi-\theta_c}^{\pi} \sin(\theta)\, d\theta}{\int_0^{\pi} \sin(\theta)\, d\theta}$$

$$= 1 - \cos(\theta_c) = 1 - \sqrt{1 - 1/n^2} \qquad (4)$$

There is an approximation in the above definition of P that the dye molecules show no angular dependence on their absorption and emission. Actually, to a good approximation, dye molecules typically appear as electric dipoles, usually with the absorption dipole collinear with the emission dipole. This decreases the calculate amount of light trapped, because the incident sunlight will be mostly absorbed by dipoles which are oriented in the plane of the LSC, and these dipoles have a greater chance of emitting into the critical cones. Specifically, the emission angular dependence, $I(\theta_e, \theta_x)$, of the emission intensity in an LSC plate as a function of the excitation angle of incidence, θ_x, is

$$I(\theta_e, \theta_x) = \langle [\hat{E}(\theta_x) \cdot \hat{\mu}(\theta_{ma})]^2 [\hat{\mu}(\theta_{me}) \cdot \hat{E}(\theta_e)]^2 \rangle \qquad (5)$$

where the brackets denote an average overall dipole orientations θ_{ma} and θ_{me}. Figure 56 shows the coordinate system and angle definitions for this calculation. $\hat{E}$ is a unit vector in the direction of the electric fields of the light. $\hat{\mu}(\theta_{ma})$ and $\hat{\mu}(\theta_{me})$ are unit vectors in the directions of the absorption and emission dipoles, respectively. The angular dependence of the emission intensity in the plate is therefore

$$I(\theta'_x, \theta_e) = \frac{1}{4\pi} \int_0^{2\pi} d\phi_{ma} \int_0^{\pi} d\theta_{ma} \sin(\theta_{ma})$$

$$\cdot \left(\sin(\theta'_x) \cos(\theta_{ma}) + \cos(\theta'_x) \sin(\theta_{ma}) \cos(\phi'_x - \phi_{ma})\right)^2$$

$$\cdot \left[1 - (\cos(\theta_{ma}) \cos(\theta_e) + \sin(\theta_{ma}) \sin(\theta_c)\right.$$

$$\left. \cdot \cos(\phi_{ma} - \phi_e))^2\right]$$

$$I(\theta'_x, \theta_e) = 4 - \cos^2(\theta'_x) - 2\cos^2(\theta_e) + 3\cos^2(\theta'_x)\cos^2(\theta_e)$$

$$\sin(\theta'_x) = \frac{1}{n} \sin(\theta_x). \tag{6}$$

For a planar geometry, the escape probability is again computed by dividing the solid angle of the escape cone, this time times the intensity as a function of angle, by the solid angle of emission weighted by the same intensity:

Figure 56. Coordinate system for the critical cone escape calculation. The probability of escape out of a planar LSC with an index of refraction n is actually greater than $1 - (1 - 1/n^2)^{1/2}$ due to the dipole character of the absorption and luminescence. We assume sunlight enters at some polar angle θ_s, is absorbed by a dipole with orientation (θ_a, θ_e), and is emitted by a dipole with the same orientation in a direction (θ_e, ϕ_e).

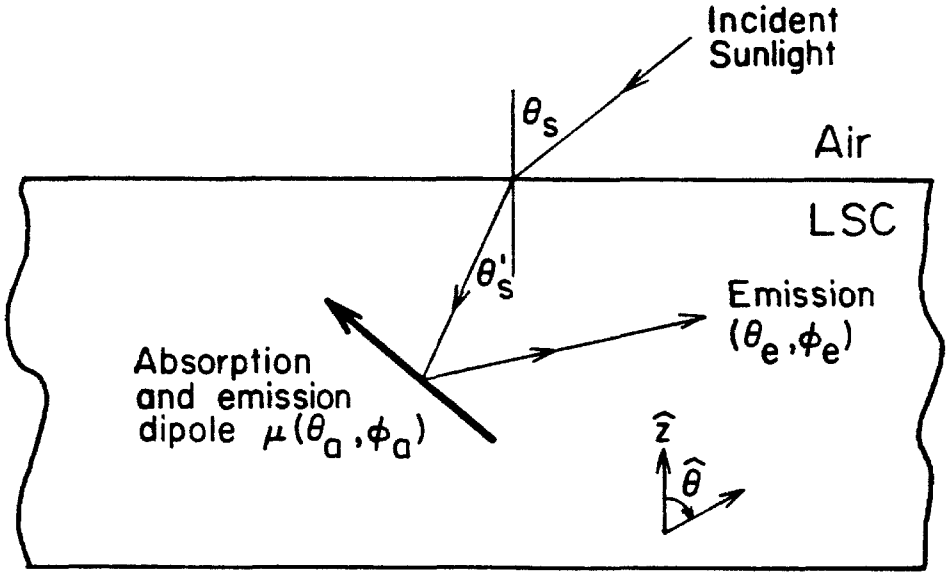

Coordinate System for Critical Cone Escape Calculation.

$$P(\theta_x') = \frac{\int_0^{\theta_c} \sin(\theta_e)\, I(\theta_e, \theta_x')\, d\theta_e}{\int_0^{\pi/2} \sin(\theta_e)\, I(\theta_e, \theta_x')\, d\theta_e}$$

$$= 1 - (1 - 1/n^2)^{1/2} \left(1 - \frac{3\cos^2(\theta_x') - 2}{10n^2}\right) . \qquad (7)$$

We finish by correcting the excitation angle in the plate for the solar angle of incidence by Snell's law:

$$P(\theta_x) = 1 - (1 - 1/n^2)^{1/2} \left(1 - \frac{1}{10n^2} + \frac{3\sin^2(\theta_x)}{10n^4}\right) \qquad (8)$$

This gives an escape probability of 0.29 for vertical incident light on an OSC with an index of 1.49, as opposed to 0.26 for the same calculation ignoring the dipole nature of the dyes.

Self-Absorption Probabilities - r and $\bar{r}$

We define the average probability that luminescence outside of the critical cones will be self-absorbed to be r. Similarly, $\bar{r}$ can be experimentally measured in a variety of ways. We will presently compute r indirectly via the collection probability Q. We will approximate $\bar{r}$ by a Beer-Lambert absorption probability across the thickness of the plate averaged over all wavenumbers:

$$\bar{r} = \int_0^\infty d\bar{\nu}\ f(\bar{\nu})\ [1 - 10^{-T \cdot C \cdot \epsilon(\bar{\nu})}] \qquad (9)$$

This is a crude approximation to a proper spatial average. We justify it in this case because it will become evident that the probability of self-absorption in the critical cones must be very small for an LSC to be efficient. This will be discussed in more detail in the next chapter as the characteristic length approximation.

Collection Probability - Q

We define Q to be the fraction of the original excitations S that arrive at the edge-mounted solar cells. If we ignore self-absorption and matrix absorption, this will be the quantum efficiency of emission times the trapping probability (one minus the escape probability P). Such luminescence is directly due to solar excitation; we will refer to it as first generation emission. The first generation collection probability in this approximation is, therefore, $Q^{(1)} = \eta(1 - P)$. Let us now include self-absorption. First generation emission can be self-absorbed, leading to second generation emission. In general, ith generation emission is self-absorbed to produce $(i+1)$th generation emission. The total collection efficiency is, therefore, the sum of the collection efficiencies for each generation:

$$Q = Q^{(1)} + Q^{(2)} + Q^{(3)} + \ldots$$

The photon flow diagram in Figure 53 shows that if we ignore transport

losses in the form of matrix absorption, scattering centers, and incomplete internal reflection due to surface roughness, we see that the fraction of the first generation emission that reaches the LSC-cell interface is $(1 - r)(1 - P)$, and that which is self-absorbed for the first time is $[\bar{r}\,P + r(1 - P)]$. This process repeats itself in a geometric series so that the total transmitted fraction Q can be expressed in terms of r, $\bar{r}$, η and P:

$$\begin{aligned} Q &= (1 - r)(1 - P)\eta \\ &\quad + (1 - r)(1 - P)\eta \cdot \eta\,[F\,P + r(1 - P)] \\ &\quad + (1 - r)(1 - P)\eta \cdot \eta^2\,[\bar{r}\,P + r(1 - P)]^2 \\ &\quad + \ldots \end{aligned}$$

$$Q = \frac{\eta(1 - r)(1 - P)}{1 - \eta\,[\bar{r}\,P + r(1 - P)]} \qquad (10)$$

We can also calculate Q from the spectroscopic and geometric parameters for a particular plate. This calculation is tractable for a particular geometry called the planar solar concentrator, or PSC, which is an infinite ribbon of width L bearing cells on both edges of the ribbon. We will only calculate the collection of first generation emission in this geometry, $Q_{PSC}^{(1)}$. This is obtained by integrating the probability of arrival for all paths from a given volume element, over all volume elements across the width, L, of the PSC, and over all

wavenumbers of the emission weighted by the normalized luminescence spectrum of the dye $f(\bar{\nu})$.

$$Q_{PSC}^{(1)} = \frac{\eta}{2\pi L} \int_0^{\infty} d\bar{\nu}\, f(\bar{\nu}) \int_0^{L} dy \int_0^{\pi} d\phi \int_{\theta_c}^{\pi/2} \sin(\theta)\, d\theta$$

$$\cdot \left[10^{-(L-y)(a(\bar{\nu})+C\cdot\epsilon(\bar{\nu}))/\sin(\theta)\sin(\phi)}\right.$$

$$\left. + \; 10^{-(L+y)(a(\bar{\nu})+C\cdot\epsilon(\bar{\nu}))/\sin(\theta)\sin(\phi)}\right] \qquad (11)$$

$\epsilon(\bar{\nu})$ is the extinction coefficient of the dye, C is the dye concentration, and $a(\bar{\nu})$ is the matrix absorption. The integral over y can be done analytically giving

$$Q_{PSC}^{(1)} = \frac{\eta}{\pi} \int_0^{\infty} d\bar{\nu}\, f(\bar{\nu}) \int_{\theta_c}^{\pi/2} \sin(\theta)\, d\theta \cdot \int_0^{\pi/2} d\phi\, \frac{\sin(\theta)\sin(\phi)}{L\cdot(\epsilon(\bar{\nu})\cdot C + a(\bar{\nu}))}$$

$$\cdot \left\{1 - 10^{-2L(\epsilon(\bar{\nu})\cdot C + a(\bar{\nu}))/\sin(\theta)\sin(\phi)}\right\} \qquad (12)$$

So how do we compute the collection probability of higher order generations? One way is to keep track of where in the plate that self-absorption takes place, and thereby keep a strict accounting of the excitation population of each generation. We will do this in the next chapter. Here we will utilize the experimental observation that, at

least in some matrix materials, the emission spectrum is independent of the energy of the excitation (the spectrum is predominantly inhomogeneously broadened). This means that there is no memory of the exciting energy. If we make the approximation that the excitation concentration in the plate is spatially isotropic, then we can assume that the fraction of each generation that is collected is $Q^{(1)}$.

We defined r and $\bar{r}$ so that $Q^{(1)} = \eta(1 - r)(1 - P)$. We have also derived $Q^{(1)}_{PSC}$ in terms of the spectroscopic components for a particular ribbon geometry plate. Therefore, we can solve for r in terms of $Q^{(1)}$. Inserting this into the definition of the total collection probability Q gives

$$Q = \frac{Q^{(1)}}{1 + Q^{(1)} - \eta(1 - P(1 - \bar{r}))} \quad . \tag{13}$$

The remaining lumped parameter is $\bar{r}$, the self-absorption probability for luminescence in the critical cone. We will use the approximation from Eq. (9) for this term, which is a simple Beers-Lambert law absorption probability over a pathlength of one-half the plate thickness.

Cell Response - R_{cell}, η_{cell}

A fraction R_{cell} of the collected light is reflected at the LSC-cell interface. Despite the improved index matching between the LSC and the cell with respect to the air-to-cell matching, the reflection at this interface is greater for light emerging from an LSC due to the high average angle of incidence of the light.

We can compute the angular distribution of light emerging from a PSC geometry device in the following way. There are four steps in computing the angular dependent intensity $I(\theta, \bar{\nu})$. The first is to unfold the geometry by the method of images to straighten the zigzag optical paths formed by the multiple reflections off of the LSC faces. Figure 57a shows the usual trapped photon propagating towards an edge-mounted cell. In Figure 57b we show the same photon propagating in the unfolded version, with the result that the optical path has been straightened and the point of emission has been moved from point a to point b. The second step is to divide the unfolded geometry into a number of finite elements such that each element subtends a constant solid angle and normal thickness with respect to the point of absorption on the cell. This simplifies the integration by insuring that each element contributes the same initial flux in the direction of the cell. The third step is to find the limits of integration in the polar coordinates of the point on the cell dictated by the position of these finite elements in the unfolded geometry. Finally, we integrate over the contribution from every element multiplied by the Beers-Lambert attenuation $10^{-r(a(\bar{\nu})+C\cdot\epsilon(\bar{\nu}))}$, where r is the radial distance to the cell.

Figures 58, 59, and 60 show how this technique is applied to a PSC geometry LSC. The unfolded PSC geometry is a symmetric wedge of width $2L$ and maximum height $4L\cot(\theta_c)$. The next step is to divide this unfolded geometry into a series of ribbons parallel to the cell of thickness dy. These are then divided into circular sections of width

Figure 57a. A typical photon trajectory for emission from a point (a) in a planar LSC.

Figure 57b. This trajectory can be unfolded by the method of images to form a straight line from a point (b).

Figure 58. Unfolded geometry of an LSC. An LSC unfolds to form a symmetrical wedge. Any trapped light trajectory in the original geometry will have a straight line equivalent in the unfolded geometry.

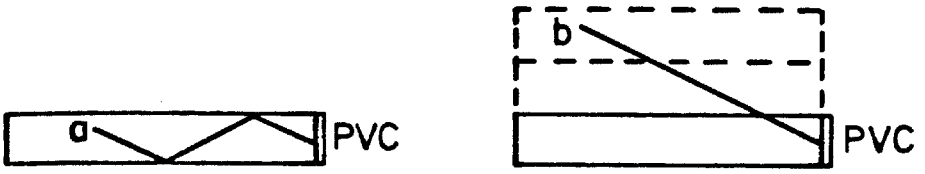
a
PVC
b
PVC

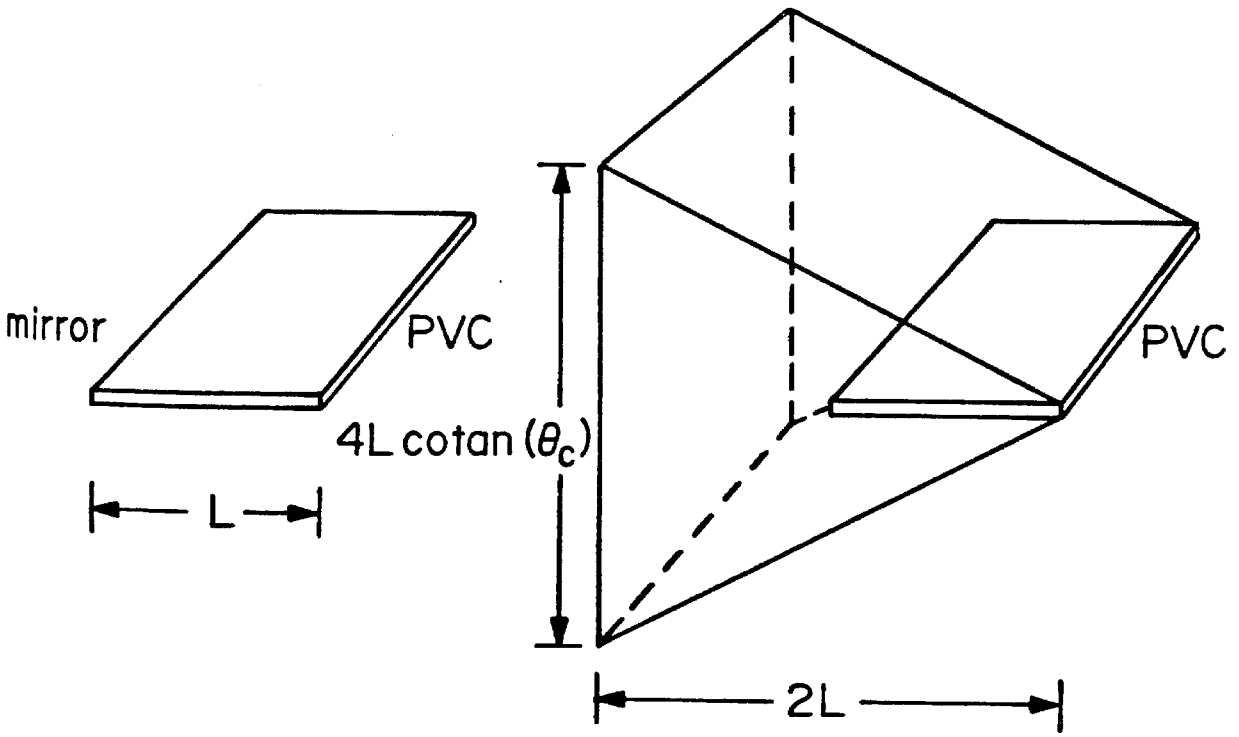
mirror
PVC
4L cotan (θ_c)
L
PVC
2L

Figure 59. The symmetric wedge divided into finite elements. The wedge is separated into plates of thickness dy, each plate being parallel to the cells (PVC's). Each ring is broken into concentric rings, and each ring into subsections.

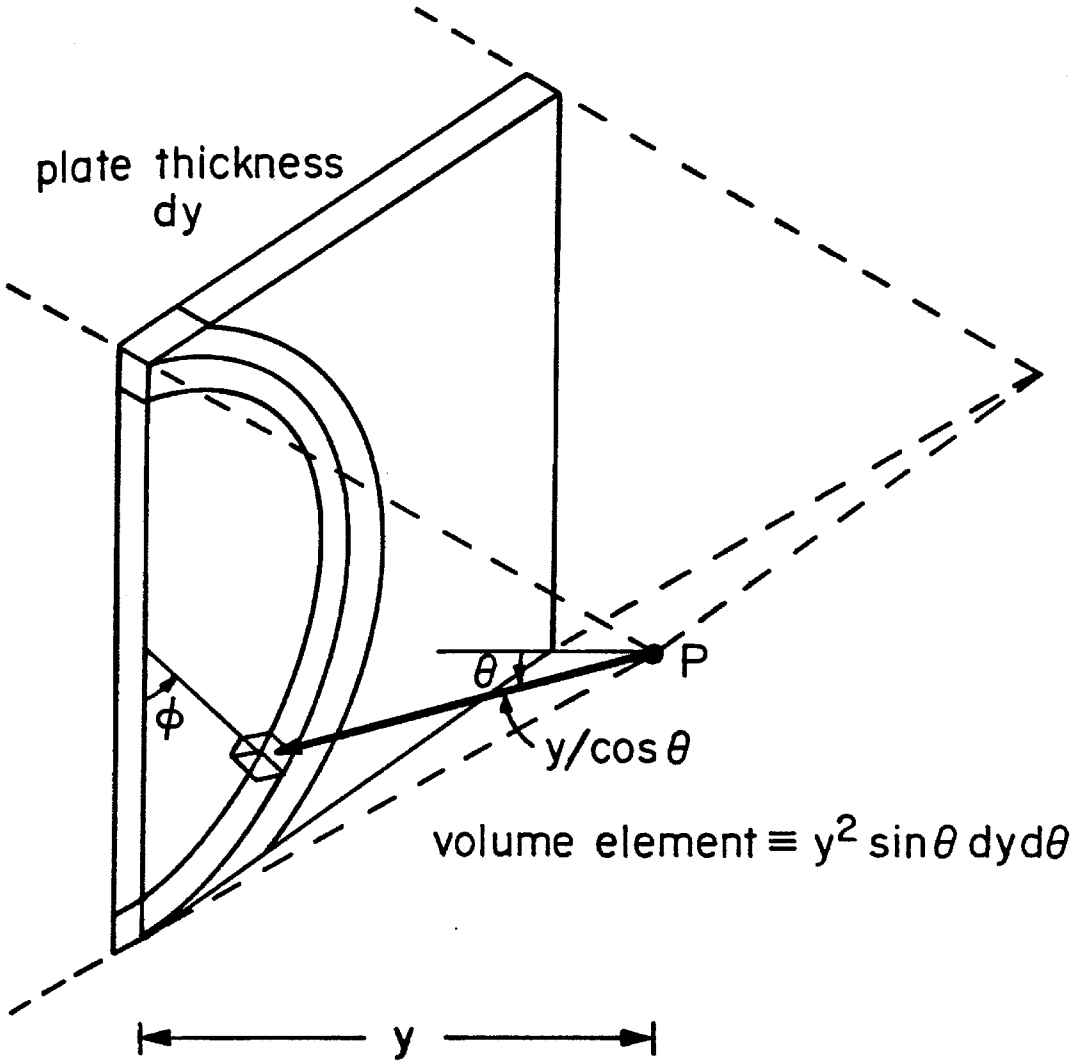
plate thickness
dy
θ
P
ϕ
y/cos θ
volume element ≡ y² sin θ dy dθ dϕ/cos²θ
y

Figure 60. Polar coordinate system in the frame of the solar cells (PVC's). The dotted semicircles represent sections of the half-sphere where there can be no incident light (because it has been lost out of the critical cones). For $\theta < \pi/2 - \theta_c$, there are no restrictions on the allowed values of ϕ. For larger values of θ, ϕ is restricted from the dotted semicircles.

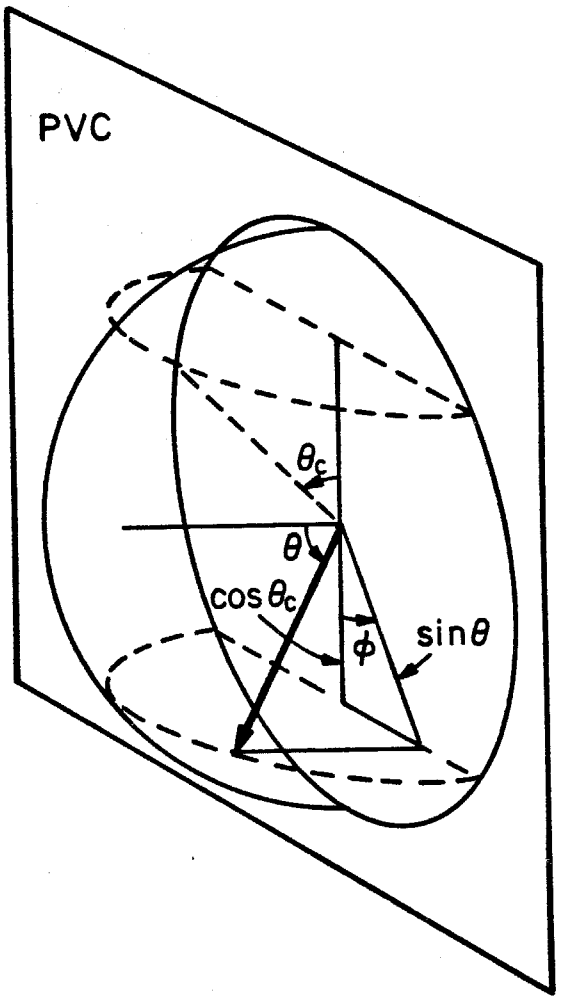
PVC
θ_c
θ
$\cos\theta_c$
ϕ
$\sin\theta$

y $d\theta/\cos(\theta)$, where θ is the polar angle from the point of absorption on the cell. Such a finite element is pictured in Figure 59 and satisfies the criteria of constant initial emission into a constant solid angle from the absorber over all the finite elements. The third step is to find the limits of θ and ϕ in the polar system about the absorption point on the cell. By inspection of Figure 60, $0 \leq \phi \leq 2\pi$ for $0 \leq \theta \leq \pi/2 - \theta_c$, and ϕ runs between $\cos^{-1}[\frac{\cos(\theta_c)}{\sin(\theta)}]$ and $\pi - \cos^{-1}[\frac{\cos(\theta_c)}{\sin(\theta)}]$ and similarly between $\pi + \cos^{-1}[\frac{\cos(\theta_c)}{\sin(\theta)}]$ and $2\pi - \cos^{-1}[\frac{\cos(\theta_c)}{\sin(\theta)}]$ for $\pi/2 - \theta_c \leq \theta \leq \pi/2$. The integral form for $I(\theta, \bar{\nu})$ simplifies to

$$I(\theta, \bar{\nu}) = \int_0^{2L} dy \sin(\theta) \cdot A \cdot 10^{-y(a(\bar{\nu}) + C \cdot \epsilon(\bar{\nu}))/\cos(\theta)}$$

$$A = \begin{cases} 1 & 0 \leq \theta \leq \pi/2 - \theta_c \\ 1 - 2/\pi \cos^{-1}[\frac{\cos(\theta_c)}{\sin(\theta)}] & \pi/2 - \theta_c \leq \theta \leq \pi/2 \end{cases} \quad (14)$$

Figure 61 shows the result of calculating $I(\theta, \bar{\nu})$ for matrix optical densities of 0. 0, 0. 01, and 0. 15 as measured across the width of the PSC. The peak in the curves occurs at 47 degrees for PMMA matrix material, which is the compliment of the critical angle. It is striking to note that if the matrix material is nonabsorbing, there is a substantial amount of light arriving at the cells at a completely glancing angle

Figure 61. Angular dependence of LSC light output. The intensity peaks at the compliment of the critical angle. The geometry used was an infinite ribbon with an index of 1.49. The matrix absorption optical densities are measured across the width of the LSC.

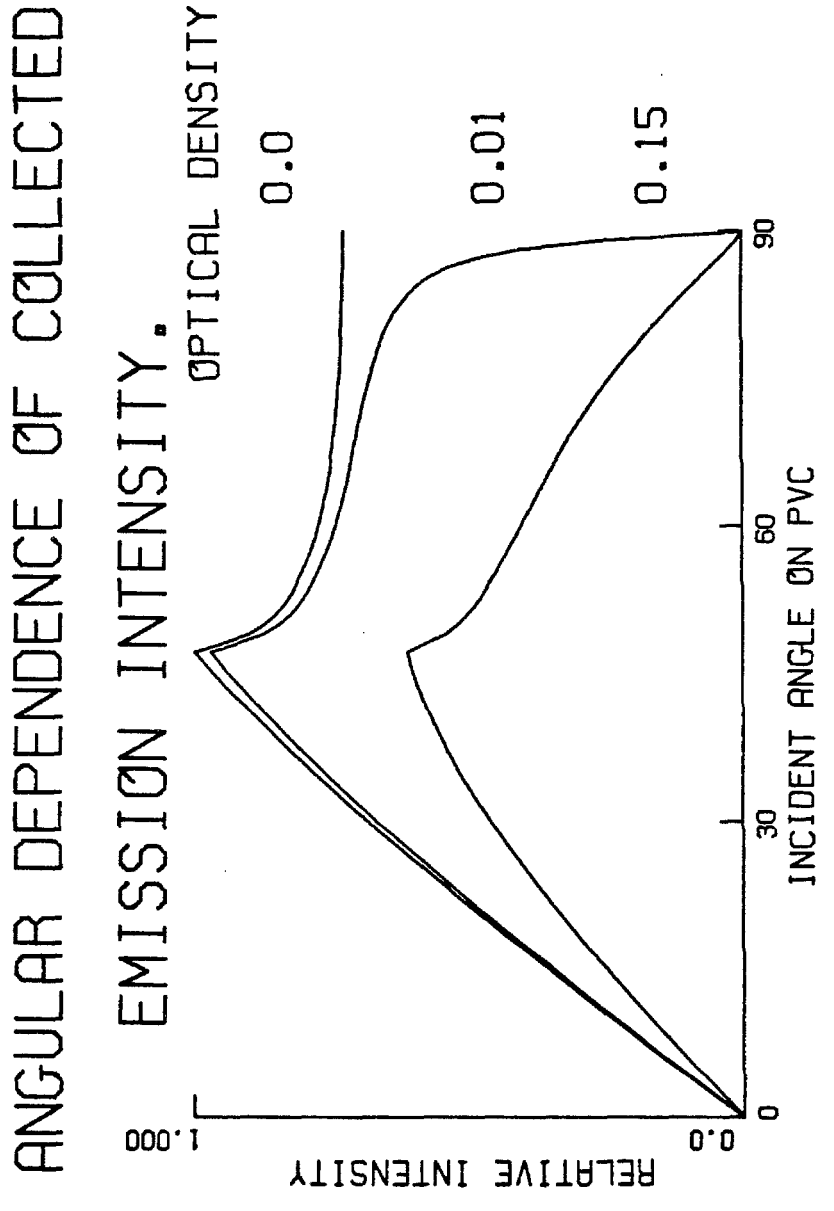
ANGULAR DEPENDENCE OF COLLECTED
EMISSION INTENSITY.
OPTICAL DENSITY
0.0
0.01
0.15
1.000
0.0
RELATIVE INTENSITY
0
30
60
90
INCIDENT ANGLE ON PVC

of incidence. This effect is peculiar to the infinite geometry of the PSC, and is a strong point against using such a geometry in a prototype device.

The reflection coefficient R_{cell} can now be calculated. If $I(\theta, \bar{\nu})$ is the angular dependence off the output light, the reflection coefficient will be the appropriate Fresnel reflection coefficient $R(\theta, \bar{\nu})$ weighted over wavenumbers and angles of incidence:

$$R_{cell} = \int_0^{\pi/2} \sin(\theta)\, d\theta \int_0^{\infty} d\bar{\nu}\, f(\bar{\nu})\, I(\theta, \bar{\nu})\, R(\theta, \bar{\nu}) \qquad (15)$$

The cells used in prototype testing typically had single layer SiO antireflection coating, which has an index of 1.9. We will assume that the reflection loss for the cell facing the sun directly is negligible.

We use the approximation that the quantum efficiency of the solar cell was independent of the energy of the exciting light for typical dye emission. The primary justification for this approximation is that the spectral response of the silicon cells we used was reasonably flat over the range of 5,000Å to 8,000Å (1.4 to 2.7eV) (Hovel, 1975). We also made the approximation that there were no variations in cell efficiency due to the intensity of the LSC output. This is reasonable because of the empirical fact that the LSCs typically only produce flux gains on the order of two. Therefore, if the cell converts the solar spectrum with a particular Air Mass One (AM1) efficiency η_{cell}, then the light transmitted into the cell from the plate is converted with the same total energy efficiency.

System Performance - η_{LSC}, G_{flux}

The fraction of the useful sunlight absorbed by the plate is $S/\bar{I}$. Q of that fraction is delivered to the LSC-cell interface. The geometric gain G_{geom} is the area of the LSC exposed to sunlight divided by the area of cell (or absorber) mounted on the edge of the plate. The intensity of the light arriving at the solar cell is, therefore, $G_{geom} \cdot S \cdot Q. \ (1 - R_{cell})$ is transmitted into the cell. The flux gain G_{flux}, or the ratio of the power from a cell mounted on the plate to that from a cell facing the sun directly, is

$$G_{flux} = Q \cdot S/I \cdot G_{geom} \cdot (1 - R_{cell}). \qquad (16)$$

The efficiency of an LSC-cell combination, η_{LSC}, is the electrical power out divided by the solar power in. The AM1 efficiency of the cell is the electrical power out divided by the solar power in. To obtain the efficiency for the combination we multiply η_{cell} by the fraction of the useful solar flux that is transmitted into the cell:

$$\eta_{LSC} = \eta_{cell} \cdot G_{flux}/G_{geom} = \eta_{cell} \cdot S/I \cdot (1 - R_{cell}) \cdot Q \qquad (17)$$

This completes the LSC performance model. A sample calculation using this model is given in Chapter 5.

II. MULTIPLE DYE SYSTEMS

Including a variety of dye types in an LSC, whether homogeneously mixed in the plate material or separated into thin films, will allow a broader band of the solar spectrum to be absorbed than in a single dye system. This does not necessarily lead to a more efficient device. (The highest light output LSC plate to date contains only one dye, DCM.) We will now examine features of multiple dye LSCs.

Photon Flow Diagram

The task at hand is to develope a formalism for attacking the multiple dye LSC problem, which we will do in a parallel manner to the technique used in the single dye case. Again a flow chart, shown in Figure 62, will organize the interaction of the various processes. What is shown is a single step in a sequence that is repeated to form the photon cascade; dye i is some intermediate dye which can absorb the luminescence from other dyes higher in the cascade as well as transferring the excitation to dyes further down the cascade. The dyes are ordered such that dye 1 has the highest energy luminescence spectrum and dye N, the final dye, has the lowest. Light from the sun is partially reflected at the air-LSC interface. Of the light that is transmitted, part will be unabsorbed by any dye, the part S_i will be absorbed by dye i, and the rest will be absorbed by other dyes in the in the cascade. Excitations of dye i-1 are transferred radiatively to dye i with a probability $r(i-1,i)$, or nonradiatively with a probability $d(i-1,i)$. The nonradiative channel is typically dipole-dipole transfer, depicted by a double line. Similarly, excitations on dye i

Figure 62. Flow chart for energy channels in a multiple dye LSC. This diagram is essentially the same as the single dye case in Figure 53. Two principal changes are the additional absorption of sunlight by other dyes, and both radiative and nonradiative transfer of excitations between dyes.

Energy Flow Diagram for a Multiple Dye LSC

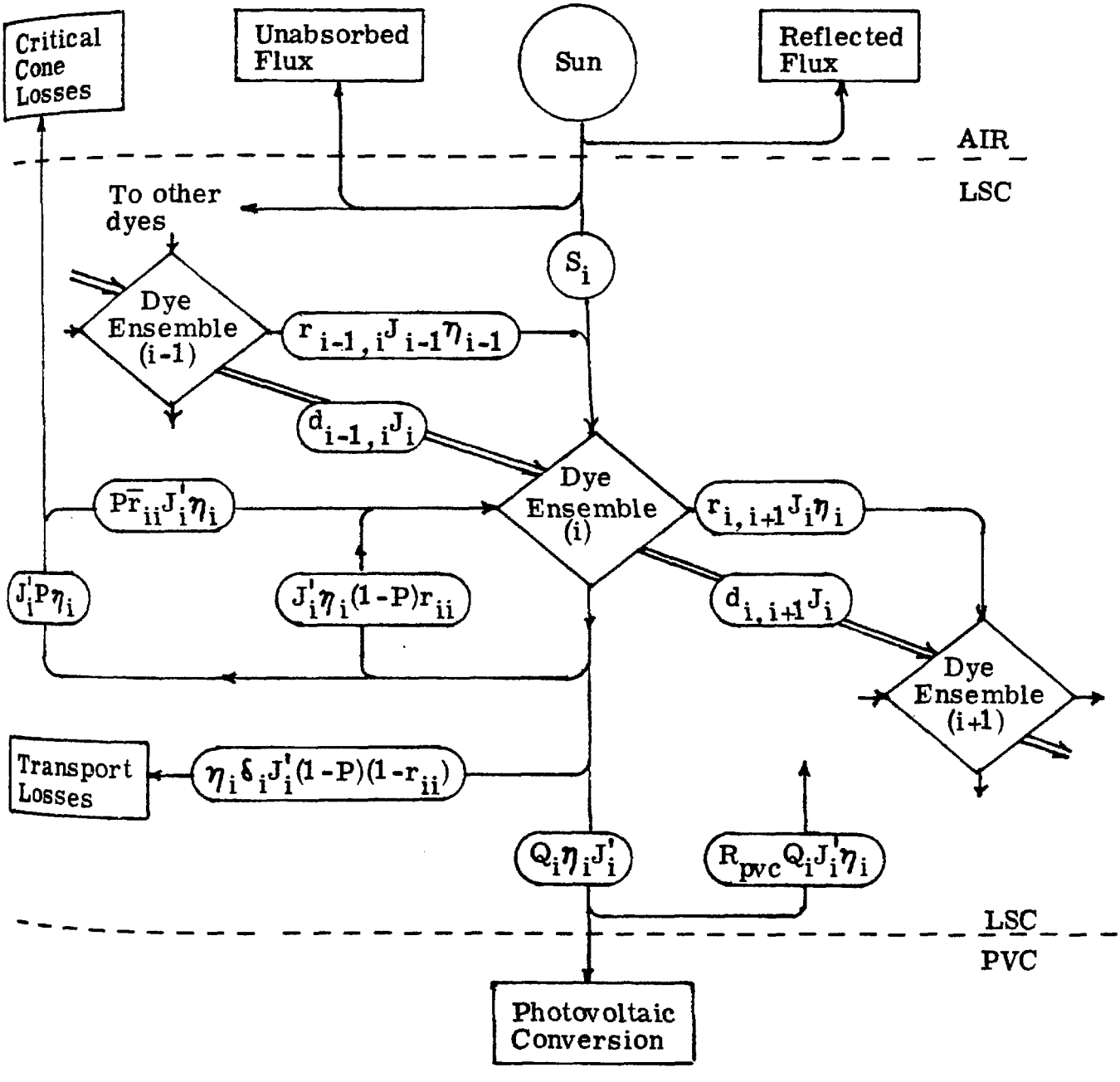

can be transferred radiatively or nonradiatively to dye $i+1$ (or to other dyes, such as itself). Excitations which are not transferred to other dyes follow a similar flow as in the single dye case; in fact, the emission of the last dye in a multiple dye LSC is treated identically to emission in a single dye LSC. Emission in the critical cone is reabsorbed with a probability $\sum_i \bar{r}(i,j)$ or is lost out of the critical cone. Emission outside of the critical cone is self-absorbed with a probability $\sum_i r(i,j)$, or is lost during transport with a probability $\delta(i)$, or is reflected at the LSC-cell interface, or if all else fails it is absorbed and converted into electricity in the cells.

Solar Absorption - S_i

Continuing the same approach as in the single dye system, each dye has its own molar extinction coefficient $\epsilon_i(\bar{\nu})$ and concentration C_i, which combine to give an absorption coefficient

$$a_T(\bar{\nu}) = \sum_i C_i \epsilon_i(\bar{\nu}) \tag{18}$$

$a(\bar{\nu})$ is the matrix absorption coefficient. Apart from the abundance of subscripts, the solar absorption is computed as in the single dye case:

$$S_i = \int_0^\infty I(\bar{\nu})\, d\bar{\nu}\, (1 - R(\bar{\nu}))\, [1 - 10^{-\ell_s (a_T(\bar{\nu}) + a(\bar{\nu}))}]\, \frac{C_i \cdot \epsilon_i(\bar{\nu})}{a_T(\bar{\nu}) + a(\bar{\nu})} \tag{19}$$

Direct Transfer Coefficient - d(i, j)

If dye i is in an excited singlet state (assuming that the ground state is a singlet state), and nearby there is a different dye j whose energy levels for absorption are resonant with the excitation energy on dye i, then there is a finite probability that the excitation will be transferred nonradiatively from dye i to dye j. In this case the dye i is termed the donor, and dye j is the acceptor, and the average probability that the event will occur is d(i, j) the probability of direct transfer. This would appear to be a very promising mode of operation for an LSC. If all transfer of excitation had to be done radiatively, there would be critical cone and quantum efficiency losses at every stage in the photon cascade.

The predominant form of nonradiative or direct transfer in systems where a dye is dispersed in a solid matrix is dipole-dipole transfer. If the dye molecules are suspended in a fluid vehicle, or if dipole radiation is not an allowed transition for one of the molecules, then electron exchange and higher order transfer interactions must be considered, respectively. There is an effective critical distance for dipole-dipole nonradiative transfer specifically in the limit of random orientation and high viscosity (Förster, 1959):

$$R_0^6\ (i,j) = \frac{9000\ \ell n(10) \cdot K^2 \cdot \eta_i}{128 \cdot \pi^5 \cdot n^4\ N_{a\nu}} \int_0^\infty f_i(\bar{\nu})\ \epsilon_j(\bar{\nu})\ \frac{d\bar{\nu}}{\bar{\nu}^4} \qquad (20)$$

i refers to the donor type and j to the acceptor. $f_i(\bar{\nu})$ is the

normalized emission spectrum of the donor dye, and $\epsilon_j(\bar{\nu})$ is the extinction coefficient of the acceptor. η_i is the quantum efficiency of luminescence of the donor, and K is an orientation factor relating the two dipole moments. K^2 is 2/3 if the orientation is completely random. n is the index of fraction of the plate, and $N_{a\nu}$ is Avagadro's number.

This critical transfer distance $R_0(i,j)$ defines a critical molar concentration $C_0(i,j)$ of dye j with respect to transfer from dye i such that the average spacing of the donor and acceptor in random distribution is equal to $R_0(i,j)$:

$$C_0(i,j) = \frac{3000}{2 \cdot \pi^{3/2} \cdot N_{a\nu} \cdot R_0^3(i,j)} \tag{21}$$

There will be competition between a variety of acceptors, so that we need a way to compare the associated transfer rates between different pairs of donors and acceptors. Still assuming that dipole-dipole non-radiative transfer is the predominant mechanism, we define Γ_i to be the total critical concentration fraction for direct transfer out of dye i:

$$\Gamma_i = \sum_{j \neq i} \frac{C_j}{C_0(i,j)} \tag{22}$$

where the sum is overall possible species of acceptors j. The quantum efficiency of such tranfer has been shown by Förster to be (Birks, 1970):

$$\psi_i = \sqrt{\pi}\, \Gamma_i \exp(\Gamma_i^2)\,[1 - \mathrm{erf}(\Gamma_i)] \tag{23}$$

The dependence of the nonradiative transfer quantum efficiency on the ratio of the actual acceptor concentration to the critical concentration is illustrated in Figure 63.

Finally, we can define the probability of direct transfer from donor i to acceptor j as the product of the total probability ψ_i that Förster transfer out of the donor will occur times the fraction of the acceptors of dye j weighted by the critical concentrations:

$$d(i,j) = \frac{\psi_i \cdot C_j}{\Gamma_i C_0(i,j)} \tag{24}$$

It has been hypothesized that the direct transfer rate will have a strong temperature dependence (Katraro, Ron, and Speiser, 1977).

Quantum Efficiency of Luminescence - η_i

The existence of direct transfer channels reduces the quantum efficiency of luminescence of the participating dyes. If the quantum efficiency of direct transfer out of dye i is ψ_i, and the quantum efficiency of luminescence of an isolated sample of dye i is $n_0(i)$, then the quantum efficiency of luminescence in the presence of direct transfer will be

$$\eta_i = \eta_0(i)(1-\psi_i) \tag{25}$$

Figure 63. Nonradiative transfer efficiency vs acceptor concentration in the Förster model. This shows the standard relationship between the acceptor concentration (divided by the calculated critical acceptor concentration) and the quantum efficiency for transfer described in 3. II.

NON-RADIATIVE TRANSFER EFFICIENCY VS. ACCEPTOR CONCENTRATION IN THE FÖRSTER MODEL.

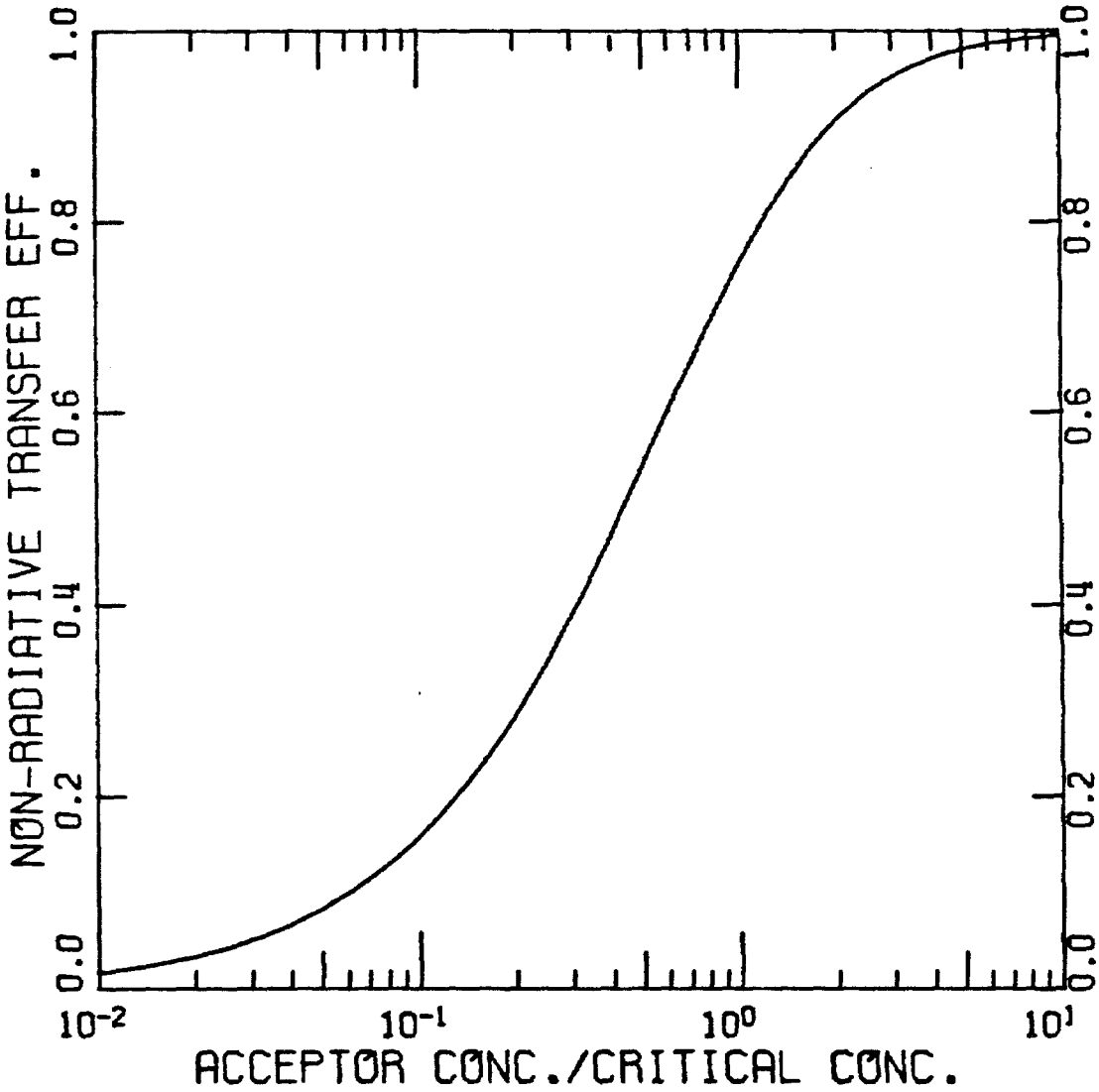

Radiative Transfer Coefficients - $r(i,j)$, $\bar{r}(i,j)$

The most tractable method for computing the reabsorption probabilities is to use the characteristic pathlength approximation developed in the next chapter. In this approximation the probability for emission from dye i outside of the critical cone to be absorbed by dye j is

$$r(i,j) = \int_0^\infty f_i(\bar{\nu})\, d\bar{\nu}\, \frac{C_j \epsilon_j(\bar{\nu})}{a_T(\bar{\nu}) + a(\bar{\nu})} \left[1 - 10^{-\ell_c (a_T(\bar{\nu}) + a(\bar{\nu}))}\right] \qquad (26)$$

where ℓ_c is the characteristic length of the device. Similarly the probability for absorption inside the critical cone is the same expression as Eq. (26) except the thickness T is substituted for ℓ_c.

Collection Probability - Q

A well chosen cascade will have stronly overlapping absorption and emission bands. The effect of this on Q is that only emission from the final dye will be able to propagate freely in the plate, the rest will be absorbed by other dyes in the cascade. In steady state the number of excitations in dye one, J_1, is

$$J_1 = S_1 + J_1 \left[\eta_1(\bar{r}(1,1)\, P + r(1,1)(1-P)) - \sum_{i>1}^{N} (d(1,i) + \eta_1(\bar{r}(1,i)\, P + r(1,i)(1-P)))\right] \qquad (27)$$

Similarly the number of excitations in the second dye is

$$J_2 = S_2 + J_1(\eta_1(\bar{r}(1,2)\ P + r(1,2)\ (1-P) + d(1,2))$$

$$+ J_2[\eta_2\ \bar{r}(2,2)\ P + r(2,2)(1-P))$$

$$- \sum_{i>2}^{N} (d(2,i) + \eta_2(\bar{r}(2,i)\ P + r(2,i)\ (1-P)))] \qquad (28)$$

and so on for each dye. The final collection efficiency Q is the single dye collection efficiency for emission from the final (Nth) dye times the fraction of the initial solar excitations that are transferred to the final dye:

$$Q = \frac{\eta_N\ (1 - r(N,N))\ (1-P)}{1 - \eta_{NN}\ (\bar{r}(N,N)\ P + r(N,N)\ (1-P))}$$

$$\cdot \frac{S_N + \sum_{i\epsilon 1}^{N-1} J_i\ (d(i,N) + \eta_i\ (\bar{r}(i,N)\ P + r(i,N)\ (1-P)))}{I} \qquad (29)$$

The LSC efficiency and flux gain are then calculated in an identical manner as for the single dye case.

III. SUMMARY

1. A flow diagram for the energy flow channels in an LSC is developed. Lumped parameters are assigned to the various channels.

2. A geneological model is proposed. Self-absorption creates emission from higher order generations. Performance

characteristics are obtained by a weighted sum over all generations.

3. An analytical form for calculating performance is developed for an infinite ribbon geometry. The lumped parameters are then derived in terms of this calculation.

4. We define the two important performance parameters for an LSC. These are the flux gain, G_{flux}, or the increase in the power output of an edge mounted cell over that of the same cell directed at the sun, and the collector efficiency, η_{LSC}, or the electrical power out per solar power incident on the plate.

5. The single dye plate performance calculation is contained for a multiple dye plate. The important new effects are an increase in the initially absorbed sunlight and nonradiative transfer between different dyes.

CHAPTER 4

I. INTRODUCTION

This chapter pays special attention to self-absorption, or more specifically to a dye ensemble's reabsorbtion of its emission. First we develop the limiting case of highly self-absorbing system, which is a scattering plate with no Stokes' shift. Next we derive a Green's function formalism for an analytical solution in the special case of an LSC rod. A formalism is developed to analyze the self-absorption rates as measured by transient emission and polarization experiments. A simplified self-absorption model is presented which assumes a characteristic pathlength for self-absorption to occur which is determined by the size of the LSC. Finally, a new engineering parameter, the critical optical density of a particular dye (CODE), is proposed as a rapid way of designing an LSC.

II. THE SCATTERING PLATE

It is instructive to calculate the collection efficiency of a purely scattering plate. Consider the Planar Solar Concentrator (PSC) geometry of LSC made from a ribbon of clear material having a thickness T and a width W. We hypothesize that there is a plane of isotropic scattering centers located a distance T/2 from either exposed surface, such that light impinging upon this scattering plane is isotropically scattered with a scattering efficiency η_{SCAT}. Cells are mounted on both edges as shown in Figure 64. The fraction of an isotropically scattered light flux incident on the scattering plane a distance x away from one edge, and that is intercepted by that edge is:

Figure 64. Collection from a scattering plate. Suppose an infinite ribbon of clear LSC material has cells mounted on both edges and has a plane of isotropic scattering centers midway between the faces of the ribbon. The fraction of the incident light which is collected with the scattering plane ig given as a function of the ratio of the width to the thickness of the ribbon.

IMITATION OF LUMINESCENCE COLLECTION BY SIMPLE SCATTERING IN A CLEAR INFINITE RIBBON. LIGHT SCATTERED TWICE IS IGNORED.

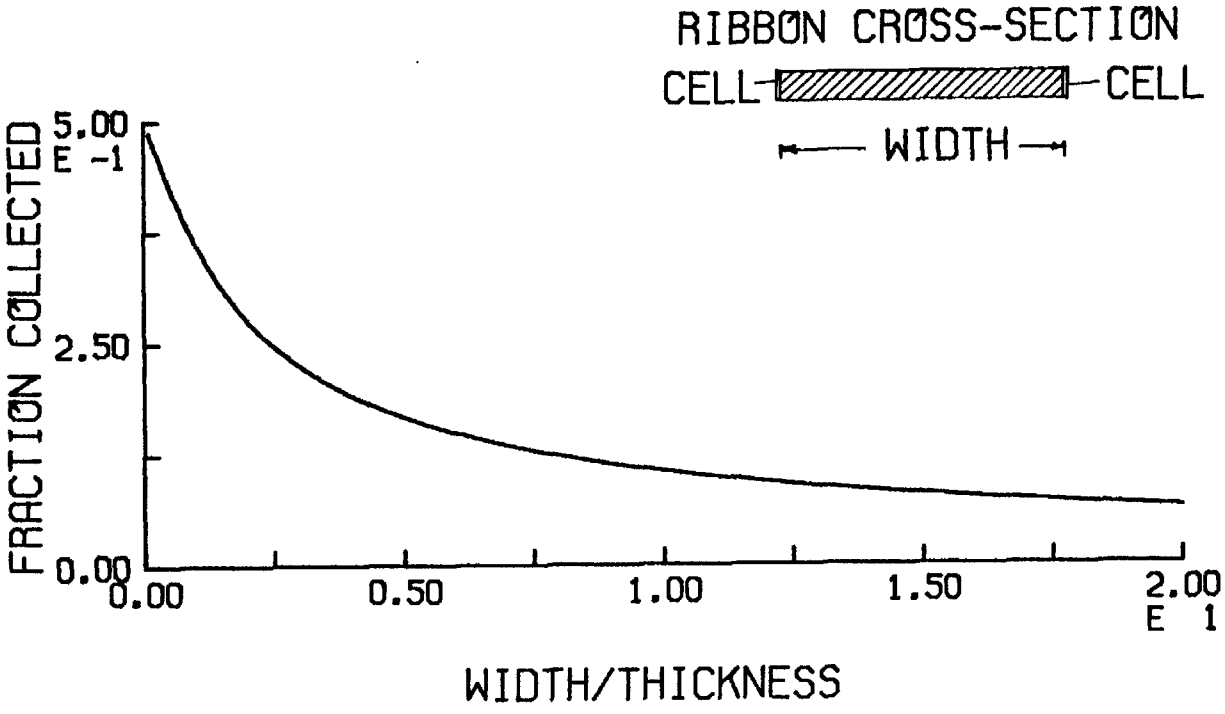

$$F(x) = \frac{1}{4\pi} \int_{-\pi/2}^{\pi/2} d\phi \int_{a_-}^{a_+} \sin(\theta)\, d\theta$$

$$= \frac{T}{2\pi x} \int_{-\pi/2}^{\pi/2} d\phi \; \frac{\cos(\phi)}{\sqrt{1+(T\cos(\phi)/x)^2}}$$

$$= \frac{1}{\pi} \tan^{-1}\left(\frac{T}{x}\right) \qquad (30)$$

where $a_\pm = \pi/2 \pm \tan^{-1}(T\cos(\phi)/x)$. We have allowed only light trajectories which do not intercept the scattering plane.

If the scattering plate has solar cells mounted on both edges, the fraction of the scattered incident light which is collected without intercepting the scattering plane a second time is:

$$Q_S^{(1)} = \frac{2}{W}\eta_{SCAT} \int_0^W dx\, F(x)$$

$$= \frac{2T}{\pi W}\eta_{SCAT}\left[\frac{W}{T}\tan^{-1}\left(\frac{T}{W}\right) + \frac{1}{2}\ell n\left(1+\left(\frac{W}{T}\right)^2\right)\right] \qquad (31)$$

where η_{SCAT} is the scattering efficiency of the scattering plane.

We note that if the scattered light does not escape out of the critical cones, and if it is not collected by the solar cells, then it must intercept the scattering plane again. Assuming that the spatial distribution of this scattered light is uniform in the plane, we find

that the higher generation collection efficiences are

$$Q_S^{(2)} = (1-P)(\eta_{SCAT} - Q_S^{(1)}) \cdot Q_S^{(1)}$$

$$Q_S^{(3)} = (1-P)^2 (\eta_{SCAT} - Q_S^{(1)})^2 \cdot Q_S^{(1)}$$

.

.

.

Therefore, the total probability of the solar cells collecting the scattered incident light is:

$$Q_S = \sum_i Q_S^{(i)}$$

$$= \frac{Q_S^{(1)}}{1-(1-P)(\eta_{SCAT} - Q_S^{(1)})} \qquad (32)$$

If we ignore intensity effects on the efficiency of the edge mounted cells, and also ignore reflection losses at the scattering plate-cell interface, then if η_{cell} is the AM1 efficiency of the cell under direct insolation then the efficiency of the scattering plate-cell combination is

$$\eta_{SCAT\ collector} = \eta_{cell} \cdot Q_S \qquad (33)$$

$Q_S^{(1)}$ is plotted as a function of the width to thickness ratio in Figure 64.

III. SELF-ABSORPTION IN A SEMI-INFINITE ROD

Consider a semi-infinite rod of LSC material having a diameter d, and containing luminescing centers at a concentration of C moles per liter, with an extinction coefficient $\epsilon(\bar{\nu})$ and a normalized luminescence spectrum $f(\bar{\nu})$. $a(\bar{\nu})$ is the matrix absorption. P is the probability of escape out of the rod, $P = 1/n$ where n is the index of refraction of the matrix material. The differential of the transmission probability through a distance x of this material at a wavenumber $\bar{\nu}$ with respect to x is

$$\frac{\partial}{\partial x} T(x, \bar{\nu}) = \ell n(10) \cdot C \cdot \epsilon(\bar{\nu}) \cdot 10^{-x(a(\bar{\nu}) + C \cdot \epsilon(\bar{\nu}))} \qquad (34)$$

We have assumed that $a(\bar{\nu})$ is small. The rod is a three-dimensional system, which requires that we average over all possible paths. Suppose a molecule located on the symmetry axis of the rod emits a photon whose path makes an angle θ with respect to the symmetry axis. (We will assume that all emission from a particular disk element occurs at the center of the disk. This is a reasonable approximation for emission pathlengths which are longer than the diameter of the rod.) If the emission occurs at a point y from the end of the rod, and we are interested in the absorption probability per unit length at a distance x from the end of the rod, then the length of a trajectory will be $a/\cos(\theta)$, where $a = |x - y|$. Similarly the incremental distance da is increased by a factor of $1/\cos(\theta)$. The probability of absorption per unit length becomes

$$\Lambda(x, y, \bar{\nu}) = \int_0^{B'} \frac{\sin(\theta)}{\cos(\theta)} \, d\theta \, \ell n(10) \, C \, \epsilon(\bar{\nu}) \, 10^{-|x-y|(a(\bar{\nu})+C\cdot\epsilon(\bar{\nu}))/\cos(\theta)}$$

$$B' = \begin{cases} \pi/2 - \theta_c & \text{for} \quad |x-y| > \frac{d}{2} \tan(\theta_c) \\ \tan^{-1}\left(\frac{d}{2|x-y|}\right) & \text{for} \quad |x-y| < \frac{d}{2} \tan(\theta_c) \end{cases} \qquad (35)$$

The upper limit of integration depends on the distance $|x-y|$. If, for example, $|x-y| < \frac{d}{2} \tan(\theta_c)$, light from y with a polar angle greater than $\pi/2 - \theta_c$ can reach x, even though it would not be trapped by total internal reflection. Now let

$$z = |x-y| \cdot (a(\bar{\nu}) + C \cdot \epsilon(\bar{\nu}))/\cos(\theta)$$

$$\frac{dz}{z} = \tan(\theta) \, d\theta \qquad (36)$$

Substituting in Eq. (35) gives

$$\Lambda(x, y, \bar{\nu}) = \int_A^B dz \, \frac{10^{-z}}{z} \, \ell n(10) \cdot C \cdot \epsilon(\bar{\nu})$$

$$A = |x - y| \cdot (a(\bar{\nu}) + C \cdot \epsilon(\bar{\nu}))$$

$$B = \begin{cases} |x - y| \cdot (a(\bar{\nu}) + C \cdot \epsilon(\bar{\nu}))/\sin(\theta) & \text{for } |x - y| > \frac{d}{2} \tan(\theta_c) \\ \sqrt{\frac{d^2}{4} + (x - y)^2} \; (a(\bar{\nu}) + C \cdot \epsilon(\bar{\nu})) & \text{for } |x - y| < \frac{d}{2} \tan(\theta_c) \end{cases}$$

(37)

We perform a weighted average over the luminescence spectrum to arrive at the probability $\Lambda(x, y)$ that emission originating at a position x will be absorbed at a position y:

$$\Lambda(x, y) = \int_0^\infty d\bar{\nu} \; f(\bar{\nu}) \, \Lambda(x, y, \bar{\nu}) \tag{38}$$

Next we define $\Xi^{(i)}(x)$ to be the spatial distribution of the ith generation of excitations along the rod. For example, if the rod is initially excited by a focused light source at a position x, then $\Xi^{(1)}(x)$ is approximately a delta function at x:

$$\Xi^{(1)}(x) = \delta(x) \, I_0$$

Excitations directly due to absorption of the externally incident light are the first generation excitations. Second generation excitations

arise from the self-absorption of the first generation emissions. For example,

$$\Xi^{(2)}(x) = \eta \int_0^\infty dy\, \Lambda(x, y)\, \Xi^{(1)}(y)$$

and in general

$$\Xi^{(i)}(x) = \eta \int_0^\infty dy\, \Lambda(x, y)\, \Xi^{(i-1)}(y) \tag{39}$$

where η is the quantum efficiency of luminescence. The luminescence spectrum observed at the end of the rod ($x = 0$) is the sum of the intensities due to all of the different generations of excitations in each element attenuated by the appropriate absorption coefficient for propagation through the rod:

$$Q(\bar{\nu}) = \int_0^{\pi/2 - \theta_c} d\theta\, \tan(\theta) \int_0^\infty dx \int_0^\infty d\bar{\nu}\, f(\bar{\nu}) \cdot \eta$$

$$\cdot \left[10^{-x(a(\bar{\nu}) + C \cdot \epsilon(\bar{\nu}))/\cos(\theta)}\right] \sum_{i=1}^{\infty} \Xi^{(i)}(x) \tag{40}$$

In the limiting case that the Stokes' shift is large, the probability for reabsorbing the emission is approximately zero everywhere, so that $\Lambda(x, y) = 0$. Therefore, $\Xi^{(i)}(x) = 0$ for $i > 1$, and only the first generation emission is collected.

IV. SELF-ABSORPTION AND EMISSION POLARIZATION

Suppose we excite an LSC with vertically polarized light and detect either the vertically or horizontally polarized emission intensities emitted in a horizontal direction, as shown in Figure 47. If the orientation of the absorption dipole moments of the luminescing centers is initially isotropic, then the probability that any center will absorb an excitation as a function of its absorption dipole orientation is proportional to the square of the cosine of the angle between the absorption moment and the electric field. Using a more concise notation (Gordon, 1966 and Tao, 1969), if $\hat{E}_i$ is a unit vector in the direction of the electric field of the polarized excitation, and $\hat{\mu}_a$ is the absorption dipole moment, then the angular dependence of the excitation probability is given by $[\hat{E}_i \cdot \hat{\mu}_a]^2$. If we assume that the emission dipole moment $\hat{\mu}_e$ is parallel to the absorption dipole, and that the orientation of these moments is fixed on the time scale of the total lifetime of the excitation, then the intensity of the emitted light polarized in the direction $\hat{E}_f$ is given by (apart from a constant factor):

$$I = \langle [\hat{E}_i \cdot \hat{\mu}_a]^2 [\hat{\mu}_e \cdot \hat{E}_f]^2 \rangle \tag{41}$$

The brackets denote an average over all orientations. The emission intensity polarized parallel to the excitation is, therefore, given by

$$I_{\parallel} = \langle [\hat{E}_i \cdot \hat{\mu}_a]^2 [\hat{\mu}_e \cdot \hat{E}_i]^2 \rangle$$

$$= \frac{1}{4\pi} \int_0^{2\pi} d\phi \int_0^{\pi} d\theta \sin(\theta) \cos^4(\theta)$$

$$= \frac{1}{5} \tag{42}$$

Similarly the emission intensity polarized in a direction perpendicular to the excitation is

$$I_\perp = \frac{1}{2} \langle [\hat{E}_i \cdot \hat{\mu}_a]^2 [\hat{\mu}_e \times \hat{E}_i]^2 \rangle$$

$$= \frac{1}{8\pi} \int_0^{2\pi} d\phi \int_0^{\pi} d\theta \sin^2(\theta) \cos^2(\theta)$$

$$= \frac{1}{15} \tag{43}$$

The reduced anisotropy measures the degree of polarization of the emission. It is defined to be

$$RA = \frac{I_\parallel - I_\perp}{I_\parallel + 2I_\perp} \tag{44}$$

The initial excitation has no perpendicular (horizontal) component, so that its reduced anisotropy is one. From the intensities just calculated, we see that the parallel polarized emission have three times the intensity of the perpendicular component, which gives $RA^{(1)} = 0.4$ for

for the first generation emission. If the orientation of the luminescing dipole is different from that of the absorption dipole, or if the molecule rotates in space between the time of absorption and emission, then in general the reduced anisotropy decreases by a factor e:

$$RA = \frac{2}{5} \cdot e$$

$$0 \leq e \leq 1 \tag{45}$$

Emission from an LSC due to polarized excitation displaying a characteristic anisotropy of 2e/5 can, therefore, be identified as emission from the first generation of excitations. We will now compute the reduced anisotropy of higher order emissions. In the radiation field limit (where the average distance between reabsorptions is $\gg 5,000\text{Å}$) the angular distribution of the emission from a dipole is also proportional to the square of the projection of the emitting dipole moment on the emitted electric field. Thus the second generation parallel and perpendicular emission intensities are

$$I_{\parallel}^{(2)} = \langle [\hat{E}_i \cdot \hat{\mu}_{a1}]^2 [\hat{\mu}_{e1} \cdot \hat{E}]^2 [\hat{E} \cdot \hat{\mu}_{a2}]^2 [\hat{\mu}_{e2} \cdot \hat{E}_f]^2 \rangle \tag{46}$$

$$I_{\perp}^{(2)} = \frac{1}{2} \langle [\hat{E}_i \cdot \hat{\mu}_{a1}]^2 [\hat{\mu}_{e1} \cdot \hat{E}]^2 [\hat{E} \cdot \hat{\mu}_{a2}]^2 [\hat{\mu}_{e2} \times \hat{E}_f]^2 \rangle \tag{47}$$

We use the identity that the cosine of the angle ψ between two vectors with orientations (θ, ϕ) and (θ', ϕ') is $\cos(\psi) = \cos(\theta)\cos(\theta') +$

$\sin(\theta)\,\sin(\theta')\,\cos(\phi-\phi')$.

In the far field limit, the parallel and perpendicular second generation intensities are

$$I_{\parallel}^{(2)} = \frac{1}{(4\pi)^3}\int_0^{2\pi} d\phi_1 \int_0^{\pi} d\theta_1 \sin(\theta_1) \int_0^{2\pi} d\phi \int_0^{\pi} d\theta \sin(\theta) \int_0^{2\pi} d\phi_2$$

$$\cdot \int_0^{\pi} d\theta_2 \sin(\theta_2)$$

$$\cdot \cos^2(\theta_1) \cdot [\cos(\theta)\cos(\theta_1) + \sin(\theta)\sin(\theta_1)\cos(\phi-\phi_1)]^2$$

$$\cdot \cos^2(\theta_2) \cdot [\cos(\theta)\cos(\theta_2) + \sin(\theta)\sin(\theta_2)\cos(\phi-\phi_2)]^2$$

$$= \frac{47}{15^3} \tag{48}$$

$$I_{\perp}^{(2)} = \frac{1}{2(4\pi)^3}\int_0^{2\pi} d\phi_1 \int_0^{\pi} d\theta_1 \sin(\theta_1) \int_0^{2\pi} d\phi \int_0^{\pi} d\theta \sin(\theta) \int_0^{2\pi} d\phi_2$$

$$\cdot \int_0^{\pi} d\theta_2 \sin(\theta_2)$$

$$\cdot \cos^2(\theta_1) \cdot [\cos(\theta)\cos(\theta_1) + \sin(\theta)\sin(\theta_1)\cos(\phi-\phi_1)]^2$$

$$\cdot (1-\cos^2(\theta_2))\,[\cos(\theta)\cos(\theta_2) + \sin(\theta)\sin(\theta_2)\cos(\phi-\phi_2)]^2$$

$$= \frac{39}{15^3} \tag{49}$$

We have assumed that the absorption and emission dipoles are both parallel and fixed in space on a time scale of the excitation lifetime. Thus the second generation reduced isotropy is

$$RA^{(2)} = \frac{I_{\parallel}^{(2)} - I_{\perp}^{(2)}}{I_{\parallel}^{(2)} + 2I_{\perp}^{(2)}} = \left(\frac{2}{5}\right)^3 \tag{50}$$

We have calculated the third generation result to be $(2/5)^5$. We believe that the ith generation reduced anisotropy is given by

$$RA^{(i)} = \left(\frac{2}{5}\right)^{2i-1} \tag{51}$$

The first generation reduced anisotropy is less than or equal to 0.4. The maximum for the second generation is 0.064, and for the third is 0.01024. Thus it is reasonable to ignore the contributions from higher order generations to the polarization anisotropy.

Suppose that we measure the reduced anisotropy of the emission from an LSC due to a polarized excitation. The measured value will be the weighted average of the reduced anisotropy of each generation times the fraction of the emission which is comprised of that generation:

$$RA_{exp} = \sum_{i=1}^{\infty} RA^{(i)} Q^{(i)}/Q \tag{52}$$

In the limit of very low concentrations, there is no self-absorption, so that $Q^{(1)} = Q$ and $RA_{exp} = 2e/5$. For higher concentrations we use the technique of averaging over each generation:

$$RA_{exp} = [\frac{2e}{5}\eta(1-r)(1-P)$$

$$+ (\frac{2e}{5})^3 \eta^2 (1-r)(1-P)(\bar{r}P + r(1-P))$$

$$+ (\frac{2e}{5})^5 \eta^3 (1-r)(1-P)(\bar{r}P + r(1-P))^2$$

$$+ \ldots]/Q$$

$$= \frac{2e}{5} \cdot \frac{1 - \eta(\bar{r}P + r(1-P))}{1 - (\frac{2e}{5})^2 \eta (\bar{r}P + r(1-P))} \qquad (53)$$

If the excitation is near enough to the edge of the plate such that the probability of self-absorption inside and outside of the critical cones is about the same, $(r = \bar{r})$, then

$$RA_{exp} = \frac{2e}{5} \cdot \frac{(1-\eta r)}{1 - (\frac{2e}{5})^2 \eta r} \simeq \frac{2e}{5}(1-\eta r) \qquad (54)$$

Similar simplifications arise if the measurement is arrange so that P is zero.

V. SELF-ABSORPTION AND TRANSIENT EMISSION

The rates of self-absorption both inside and outside of the critical cones can be calculated directly from measured transient emission spectra. Suppose at some time $t = 0$ we have placed n_0 excitations in a dye ensemble with a light pulse whose duration is very short compared to the total lifetime of the excitations. The rate of change of this population with time will be proportional to the population by the usual kinetic equation

$$\frac{\partial n^{(1)}(t)}{\partial t} = -\frac{n^{(1)}(t)}{\tau}$$

$$n^{(1)}(0) = n_0 \tag{55}$$

where τ is the total lifetime. We assume that there is no transit time dispersion due to emission from different parts of the sample, or in other words, that the lifetime is long compared to the transit time for the light in the sample. Since typical fluorescent dyes have lifetimes on the order of nanoseconds, this restricts the applicability of this technique to devices about a foot across or smaller. If r is the probability that the emission is self-absorbed outside of the critical cones, and $\bar{r}$ is the probability of self-absorption within the critical cones, P is the probability of trapping in the critical cones, and η

is the quantum efficiency of luminescence, then the kinetic equation for the number of second generation excitations as a function of time, $n^{(2)}(t)$, resulting from first generation emissions is

$$\frac{\partial}{\partial t} n^{(2)}(t) = - \frac{n^{(2)}(t)}{\tau} + \eta\, n^{(1)}(t) \left(\bar{r}\, P + r(1 - P)\right) / \tau \qquad (56)$$

We will assume that the probability of self-absorption is independent of the number of emissions previously experienced by the excitation. This is equivalent to assuming the limit of a predominantly homogeneously broadened ensemble at temperatures sufficiently high to allow anti-Stokes shifting of emission which is large compared to the emission linewidth. The third generation excitations are therefore

$$\frac{\partial}{\partial t} n^{(3)}(t) = - \frac{n^{(3)}(t)}{\tau} + \eta\, n^{(2)}(t) \left(\bar{r}\, P + r(1 - P)\right) / \tau \qquad (57)$$

These form a system of equations with the solutions

$$n^{(1)}(t) = n_0\, e^{-t/\tau}$$

$$n^{(2)}(t) = n_0 \frac{t}{\tau}\, \eta\, \left(\bar{r}\, P + r(1 - P)\right)\, e^{-t/\tau}$$

$$\vdots$$

$$n^{(i)}(t) = n_0 \left[\frac{t}{\tau}\, \eta\, \left(\bar{r}\, P + r(1 - P)\right)\right]^{i-1}\, e^{-t/\tau} / (i - 1)\,! \qquad (58)$$

Summing the various generations gives the number of excitations in the ensemble as a function of time:

$$N(t) = \sum_{i=1}^{\infty} n^{(i)}(t)$$

$$= n_0 \exp\left(-\frac{t}{\tau}\left(1 - \eta\left(\bar{r}\,P + r(1-P)\right)\right)\right) \qquad (59)$$

Thus self-absorbed emission will have an apparent lifetime which is lengthened by a factor $1/[1 - \eta(\bar{r}\,P + r(1-P))]$. This factor is equal to one if $r = \bar{r} = 0$. Measurements of the experimental transient emission decay can, therefore, give τ, $\tau/(1 - r\eta)$, and $\tau/[1 - (\bar{r}\,P + r(1-P))]$ for the three cases of an extremely dilute sample, edge emission due to an excitation near to the edge, and from general illumination of the plate, respectively.

If each generation of excitations is distributed throughout the sample in such a way that the average probability of emission from each generation reaching the detector is the same, then the transient emission spectrum should have the simple exponential behavior of Eq. (59). It is quite possible, however, to configure the exciting source and sample in such a way that first generation emission has a very different probability of reaching the detector. For example, if the exciting laser pulse is at an energy corresponding to the absorption maximum for the emitting center, then nearly all of the laser light will be absorbed in typically less than the first few millimeters of the sample. A mask can then be placed between this excited region and

the detector, such that the excited region of the sample can illuminate the rest of the sample without illuminating the detector (see Figure 51). Assuming that none of the first generation emission illuminates the detector due to scatter in the rest of the sample, and that $r = \bar{r}$, we find that the measured transient spectrum should be proportional to the usual total decay of the population minus the first generation emission:

$$n_{mask}(t) = n(t) - n^{(1)}(t) = n_0 [e^{-t(1 - r\eta)/\tau} - e^{-t/\tau}] \qquad (60)$$

If the probability of self-absorption is high enough, a significant fraction of the first generation emission can be reabsorbed in the masked region. In this case, some fraction of the higher order generations will have to be subtracted. Because of the sensitivity to scattering and inadvertent masking of higher order generations, this technique is inferior to the simple lifetime measurements for determining self-absorption probabilities.

VI. CHARACTERISTIC LENGTH APPROXIMATION

While the technique developed in Section II is useful for obtaining spectral information about the emission from an LSC rod, a simpler calculation appears to be a reasonably good approximation for calculating self-absorption probabilities. In the simplest one-dimensional case, the probability that self-absorption will occur is found by the Beers-Lambert law:

$$r = \int_0^\infty d\bar{\nu}\, f(\bar{\nu}) \left[1 - 10^{-xC\epsilon(\bar{\nu})}\right] \tag{61}$$

r is the probability that emission with the normalized spectral distribution $f(\bar{\nu})$ will be self-absorbed by the luminescing centers having an extinction coefficient $\epsilon(\bar{\nu})$ and a concentration C over a pathlength x. The approximation that we will make in this section is that the probability of self-absorption for emission in an LSC plate is given by this equation, where x is the characteristic length of the plate. This characteristic length is basically a weighted average of the trajectory lengths traversed by light in the plate.

We have not saved any labor by analytically computing the weighted average of the trajectory lengths to arrive at a characteristic pathlength. What we will show instead is, for a small class of device geometries and dye concentrations, that the properly averaged characteristic length corresponds to a characteristic dimension of an LSC plate. For example, the characteristic length of a square LSC is the length of the side. The characteristic length for self-absorption in the critical cone is the thickness of the LSC plate. In general we justify this approximation by showing that the self-absorption probability has roughly a logarithmic dependence on the pathlength (see Fig. 69), so that precision in identifying the proper pathlength is not crucial. However, it is useful to explicitly calculate the weighted average pathlength traveled by light collected in an LSC, and to compare this result to that predicted by the characteristic length approximation.

We use the collection efficiency formalism of Eq. (12) to compute the first generation collection efficiency, $Q^{(1)}_{PSC}$, for an infinite ribbon geometry (PSC) LSC. This is probably a worst case analysis, since the infinite ribbon geometry can have extremely long pathlengths at low dye concentrations. We assume that the width of the ribbon was variable, that the thickness was one centimeter, that the index of refraction was 1. 5, and that cells were mounted on both edges of the ribbon. Since $Q^{(1)} = \eta(1 - r)(1 - P)$, computing $Q^{(1)}$ using Eq. (12) gave the self-absorption probability r. Using Eq. (61), we found the average pathlength of the collected light in the plate that would result in the computed r. Figure 65 shows the results of this calculation, where we have calculated the average pathlength as a function of the plate width for four different concentrations of the dye rhodamine-575. The assumed quantum efficiency was 0. 9. The dashed line indicates the characteristic length approximation result, which is that the average pathlength is assumed to be the width of the plate. At low concentrations and PSC widths, the average is less than the width. The cross-over point occurs when the width times the concentration divided by the thickness equals about 0. 1 for this dye. Thus the characteristic length approximation would give the correct result for a plate with a geometric gain of 100 and a concentration of 5×10^{-4} molar, which is typical for an optimized device.

VII. CRITICAL OPTICAL DENSITY (CODE)

The preceding calculation of self-absorption probabilities and average pathlengths traveled by light in the plate make clear that the

Figure 65. Average pathlength of collected emission vs width of an LSC. We have calculated the average distance traversed by emission in a plate, which is collected at the edge, for four different concentrations of rhodamine-575. The plate was assumed to be 1 cm thick, so that 10^{-5} M corresponds to a peak optical density of one through the plate. The dashed line indicates the characteristic length approximation.

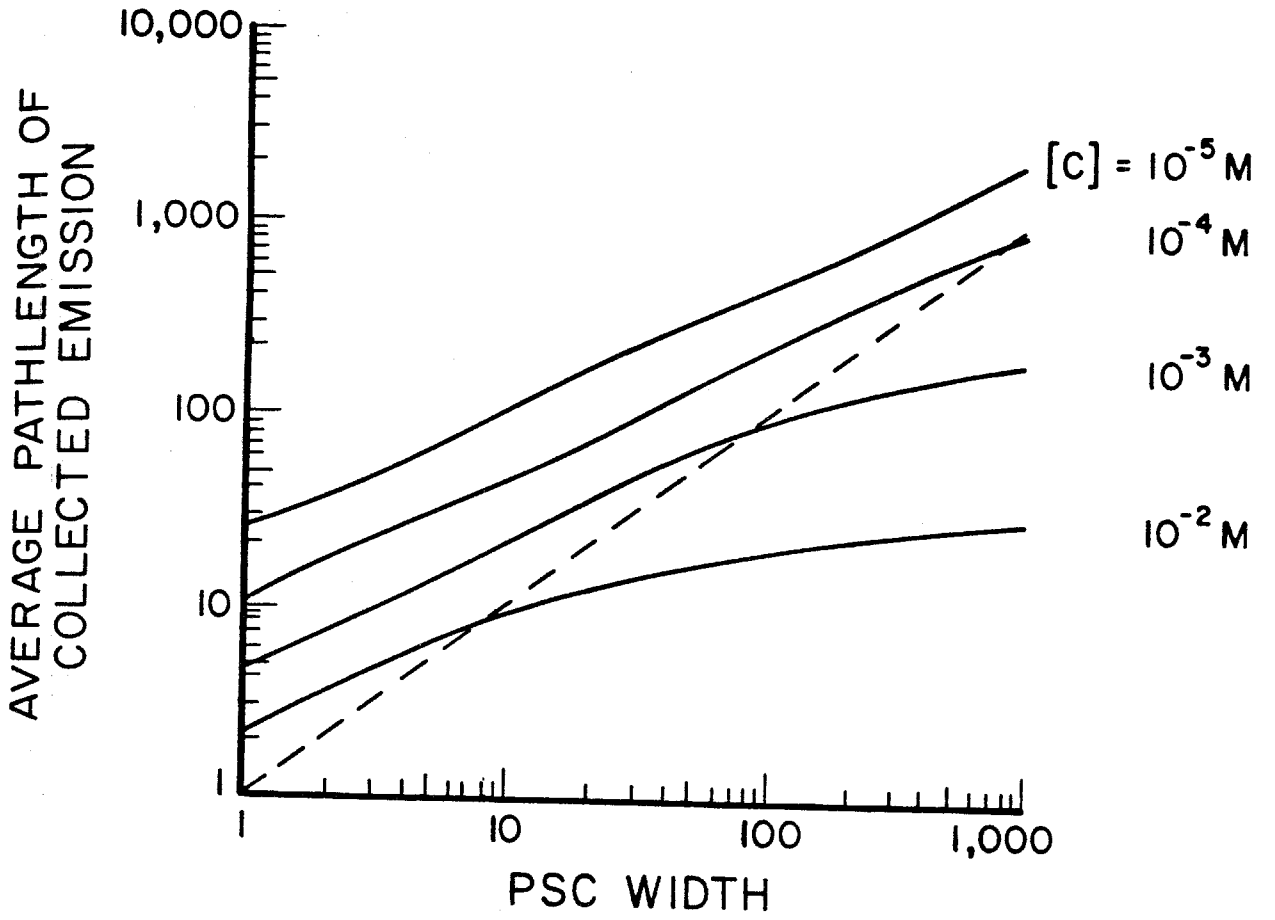
AVERAGE PATHLENGTH OF COLLECTED EMISSION
10,000
1,000
100
10
1
1
10
100
1,000
PSC WIDTH
[C] = 10^-5 M
10^-4 M
10^-3 M
10^-2 M

performance of an LSC varies in a rather complicated way with a host of parameters such as the size, the types of dyes used, and the concentration of those dyes. From an engineering standpoint, we do not desire to know the performance of a plate for all possible conditions; there is only a relatively narrow class of size and efficiency which is interesting to look at. We are, therefore, interested in finding a single scalar parameter which will predict LSC performance for a particular dye in this restricted class with relative ease.

We define a new self-absorption parameter, the critical optical density (CODE), to be the peak optical density of a sample containing a luminescing species, such that the emission from the species has a fifty percent chance of being self-absorbed while traversing the sample. Mathematically, if a luminescing species has a normalized luminescence spectrum $f(\bar{\nu})$, a molar concentration c, and an extinction coefficient $\epsilon(\bar{\nu})$ with a maximum value of $\epsilon(\bar{\nu}_{max})$, and this species is contained in a sample with an optical length L, then the critical optical density is

$$\text{CODE} \equiv L \cdot C \cdot \epsilon(\bar{\nu}_{max}) \tag{62}$$

where the concentration and pathlength have been adjusted so that

$$\frac{1}{2} = \int_0^\infty f(\bar{\nu})\, d\bar{\nu}\; 10^{-L\,C\,\epsilon(\bar{\nu})} \; . \tag{63}$$

The critical optical density is the radiative analog to the Förster

critical concentration (see 3. II.). It is useful because it prescribes the efficiency of an LSC as a function of the size or geometric gain. In Figure 66 we have plotted the collection efficiency of an arbitrary LSC plate as a function of self-absorption probability, using Eq. (10). The index of refraction is assumed to be 1. 49. The solid lines refer to the case where there is no self-absorption in the critical cones, and the dotted lines are an opposite limit where the self-absorption rates are equal inside and outside of the critical cones. The vertical line originating at $r = 0.5$ intersects the curves at the CODE operating point (by definition). For example, a typical LSC plate will have an index of refraction of 1. 5, or an escape probability of 0. 26, a quantum efficiency of 0. 9, and negligible self-absorption in the critical cone. If the self-absorption probability is 0. 5, we find from Figure 65 that the collection efficiency of the plate is also about 0. 5. To obtain reasonably good absorption of sunlight, or of emission from other dyes, the peak optical density of the final dye must be at least one across the thickness of the LSC. In this case, the critical optical density will be the number of plate thicknesses which the emission can traverse before fifty percent is self-absorbed. Since the geometric gain of a plate is roughly the width of a plate divided by its thickness, the critical optical density is roughly the maximum geometric gain of a plate, using the particular luminescing center as a single or final dye in a cascade, which produces a collection efficiency of 50%.

Calculating the performance of an LSC using this procedure is simple. We initially restrict the geometric gain of the plate to be equal to the measured CODE of the dye used (or of the final dye used

Figure 66. Collection efficiency vs self-absorption probability. We have calculated the collection efficiency of an arbitrary LSC, assuming $P = 0.26$. The solid lines are for self-absorption in the critical cones being set to zero, and the dotted lines being set equal to the self-absorption probability outside of the critical cones. The vertical line at $r = 0.5$ indicates the collection efficiency at the critical optical density (CODE).

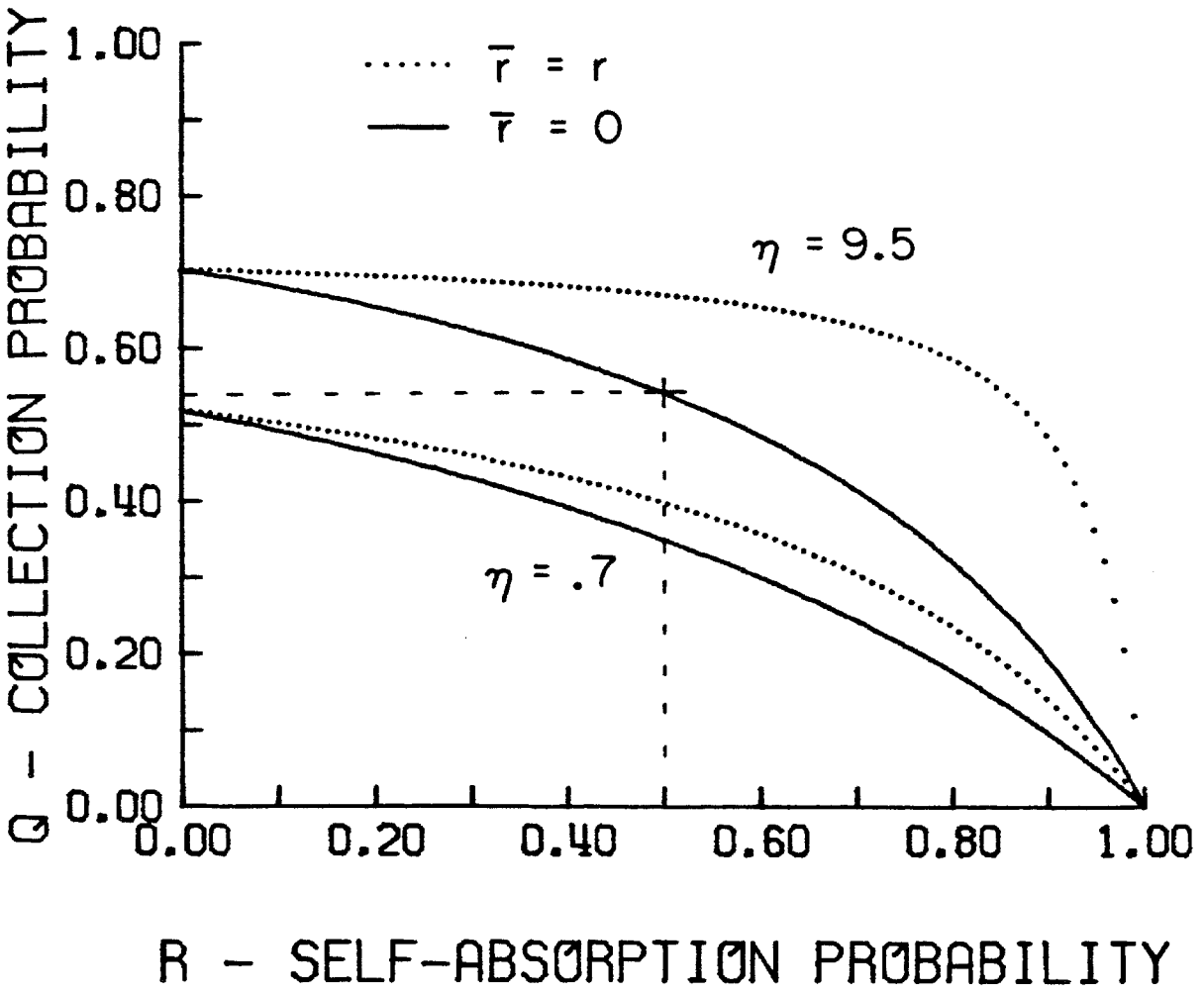
Q - COLLECTION PROBABILITY
1.00
0.80
0.60
0.40
0.20
0.00
0.00
0.20
0.40
0.60
0.80
1.00
$\bar{r} = r$
$\bar{r} = 0$
$\eta = 9.5$
$\eta = .7$
R - SELF-ABSORPTION PROBABILITY

in a multiple dye plate). We also require that the concentration of this dye is such that the peak optical density across the thickness of the plate is one. Under these conditions we have just shown that the collection efficiency will be

$$Q = \eta / 2 \tag{64}$$

where n is the quantum efficiency of luminescence. We then need to know the fraction of the solar flux which is absorbed by the dye. This is shown in 3.I to be S/I. S/I is typically about 15% per dye for the very narrow band dyes such as rhodamine-590, and 30% for broad band dyes such as DCM. The total collector efficiency is given in the usual way to be

$$\eta_{LSC} = \eta_{cell} \cdot S/I \cdot \eta/2 \tag{65}$$

where η_{cell} is the AM1 efficiency of the cells used. The flux gain is

$$G_{flux} = G_{geom} \cdot S/I \cdot \eta/2 \tag{66}$$

VIII. SUMMARY

1. We derive the performance of a plate containing an isotropically scattering plane as a limiting case of a self-absorbing system.

2. We model the intensity and spectral dependence of self-absorbed emission in the quasi-one-dimensional case of a rod of LSC material.

3. The polarization component intensities of emission resulting from polarized excitation are related to self-absorption probabilities. Emission from higher order generations is shown to be negligibly polarized.

4. Changes in the measured total lifetime in transient emission experiments is related to self-absorption probabilities. The masking of first generation emission is shown to produce a transient emission spectrum which is the difference of two exponentials.

5. We show that in a regime typical of actual devices the average trajectory length traveled by emission in the plate is on the order of the dimensions of the plate. This leads to a simple characteristic length approximation for the self-absorption probability.

6. We assign a critical optical density (CODE) to each dye. The CODE is the peak extinction coefficient times some pathlength and concentration such that the probability of self-absorption is 50%. We also show that the CODE is the geometric gain of a plate containing the dye at a peak concentration such that the peak optical density through the thickness of the plate is one, so that the collection efficiency of the plate is 50% times the quantum efficiency of luminescence.

CHAPTER 5

I. ANALYSIS OF EXPERIMENTAL RESULTS

In this chapter we will analyze the data described in Chapter 2 using the techniques developed in Chapters 3 and 4. Degradation rates for a variety of dyes and vehicles are tabulated. Focusing on the particular dye rhodamine-575, we find that the spectra are predominantly inhomogeneously broadened only in the cast PMMA samples. We compared measured self-absorbed emission spectra with theoretical models. The self-absorption probability of rhodamine-575 in solution is measured using three independent techniques. The full analytical model from Chapter 2 is applied to the single dye rhodamine-575 system. Finally, the critical optical densities of all of the dyes surveyed are tabulated.

Dye Degradation Rates

Table 4 is a compilation of observed degradation rates for dyes measured by ourselves and others. The error bars on measurements made here are large due to uncertainties in the amount of light absorbed by the sample. The average number of molecules degraded per absorbed solar photon was computed by computing S for the samples under an AM0 spectrum at 1,000 watts per square meter for eight hours per 24 hours of total exposure. The absorption spectrum used was the initial dye spectrum before exposure. This overestimates the flux absorbed, since the absorption coefficient decreases with exposure. We estimate that the resulting calculated number of photons absorbed is accurate to within an order of magnitude. The change in the number of dye molecules in the sample was assumed to

Table 4. Measured quantum efficiencies for photodegradation due to solar exposure. The number of photons absorbed by the sample was estimated to be the fraction of a 5,800°K black body spectrum absorbed by the sample's initial absorption spectrum times 0.017 photon moles per square centimeter per hour times the number of hours of effective full sunlight absorbed by the sample at 50% degradation. The number of molecules reacted was assumed to be given by the change in peak optical density. We estimate that this technique of calculation is only accurate to within an order of magnitude.

Table 4.

Quantum Efficiencies for Photodegradation due to Solar Exposure.

Dye	Solvent	Molecules bleached † / Absorbed photon
Coumarin-500	methanol	3×10^{-6}
Coumarin-535	methanol	4×10^{-6}
Coumarin-540	methanol	6×10^{-7}
	methanol in quartz	2×10^{-5}
	PMMA	2×10^{-6}
DCM	methanol	2×10^{-6}
Rhodamine-590	methanol	2×10^{-7}
	methanol in quartz	3×10^{-6}
	PMMA	1×10^{-6}
	PMMA with acetic acid	1×10^{-5}
Rhodamine-640	methanol	5×10^{-6}
Sulforhodamine-640	methanol	1×10^{-6}
	methanol in quartz	6×10^{-7}
Cresyl Violet	methanol	2×10^{-7}
Oxazine-720	methanol	1×10^{-7}
Oxazine-750	methanol in quartz	1×10^{-5}

† The accuracy is estimated to be within an order of magnitude.

be proportional to the change in the peak optical density of the sample.

In general we found no dyes which are stable against photodegradation in PMMA plates for periods longer than a year. Dyes in methanol solutions showed somewhat better stability when exposed in sode-lime glass bottles. Dyes in degassed methanol in quartz cuvettes degraded substantially in several hours. Our results for quantum efficiencies for photodegradation are consistent with the results of others. Under optimal circumstances the quantum efficiences for photodegradation for typical efficient organic laser dyes are on the order of 10^{-6}.

Dye stability will have to be improved about two orders of magnitude to obtain acceptable stability levels. This can be seen in the following way. In order to minimize self-absorption, we can require that a typical plate will have a peak optical density of one. If we assume that a typical peak extinction coefficient for a dye is 50,000 liters per mole centimeter, then there will be about 10^{20} molecules per square meter. (This argument will also pertain to the final dye in a multiple dye plate.) If the dye absorbs 30% of the useful visible solar spectrum, in 20 years the plate will have absorbed 10^{28} photons per square meter. Acceptable performance, therefore, required that the quantum efficiency of photodegradation be at most 10^{-8}.

Spectral Homogeneity

In some host materials, the absorption and emission spectra of all of the dye molecules in a sample appear to be approximately the same. In such a case the dye ensemble is said to be spectrally homogeneous. For example, in Figure 44 the maximum of the emission

spectrum for rhodamine-575 in methanol at room temperature is independent of the excitation energy, even for excitations which are 2,000 wavenumbers lower in energy than the emission peak. This 'blue-shifted' emission disappears when the sample is cooled to liquid nitrogen temperatures, so that this extra energy in the emission must come from thermal energy in the molecule or from the surrounding material. If the same dye is infused into a PMMA plate, essentially the same results are produced, as shown in Figure 46. We, therefore, conclude that, for these two host materials, the absorption and emission spectra are predominantly homogeneously broadened. By contrast, dyes which were dissolved in methyl methacrylate monomer and then polymerized displayed characteristics of inhomogeneous broadening. As shown in Figure 45, the emission spectrum depends on the precise energy of the excitation. It was thus possible to select portions of the dye ensemble which displayed significantly different spectral characteristics than the ensemble average.

We have seen that dye molecules in a host material at room temperature are able to emit light several thousand wavenumbers greater in energy then that of the initial excitation. This is not surprising, since these molecules typically have a large number of internal degrees of freedom. At liquid nitrogen temperatures, KT is reduced by a factor of four, which apparently is sufficient to decrease the available energy in the molecule or in the surrounding bath sufficiently so that these large blue-shifted emissions do not appear. This temperature sensitivity would imply that even larger blue-shifts of emission would be possible in plates at the elevated temperatures of roof-mounted

collectors.

Self-Absorbed Emission Spectrum

Figure 67 shows the analytic results for the collection efficiency $Q(\overline{\nu})$ as a function of wavenumber for a semi-infinite rod. The absorption and emission spectra used were numerically generated spectra similar in form to those of rhodamine-575. The pathlengths, rod diameter, and dye concentrations are the same as for the experimental data shown in Figure 41. The scattering coefficient used in this calculation is 0.0035 cm^{-1}. The absorption spectrum is the sum of two gaussians with peak positions of 19,500 and 20,300 cm^{-1}, peak widths of 840 and 680 cm^{-1}, and peak heights of 94,000 and 27,000 liters per mole centimeter, respectively. The emission spectrum was the same sum of two gaussians reflected about 19,000 cm^{-1} and normalized to unity. The shift in spectral position with increasing self-absorption is accompanied by a decrease in collected intensity, in good agreement with the experimental data in Figure 41. Figure 68 shows a similar calculation, except that the Stokes shift between the absorption and the emission spectrum has been increased from 1,000 to 2,500 cm^{-1} (to lower their overlap). While the nonzero scattering losses cause an overall decrease in the intensity with increasing pathlength, the emission spectrum is seen not to shift appreciably.

Self-Absorption Probability Measurements

We have shown results on three different measurements of the effects of self-absorption in rhodamine-575: spectral overlap, emission depolarization, and lifetime broadening. We are interested in determining the consistency of these different measurements in

Figures 67 and 68. Analytic result for emission spectra as a function of sample pathlength. Experimental absorption and emission spectra were each fitted as the sum of two gaussians. These are used with the model from 4. III to imitate the experiment shown in Figure 41. The Stokes shift used in Figure 67 is $1,000\,cm^{-1}$.

The calculation was repeated in Figure 69, except that the Stokes shift was increased to $2,500\ cm^{-1}$.

ANALYTIC ABSORPTION AND FLUORESCENCE SPECTRA.
EMISSION SPECTRA WITH VARIABLE PATHLENGTH IN SAMPLE.

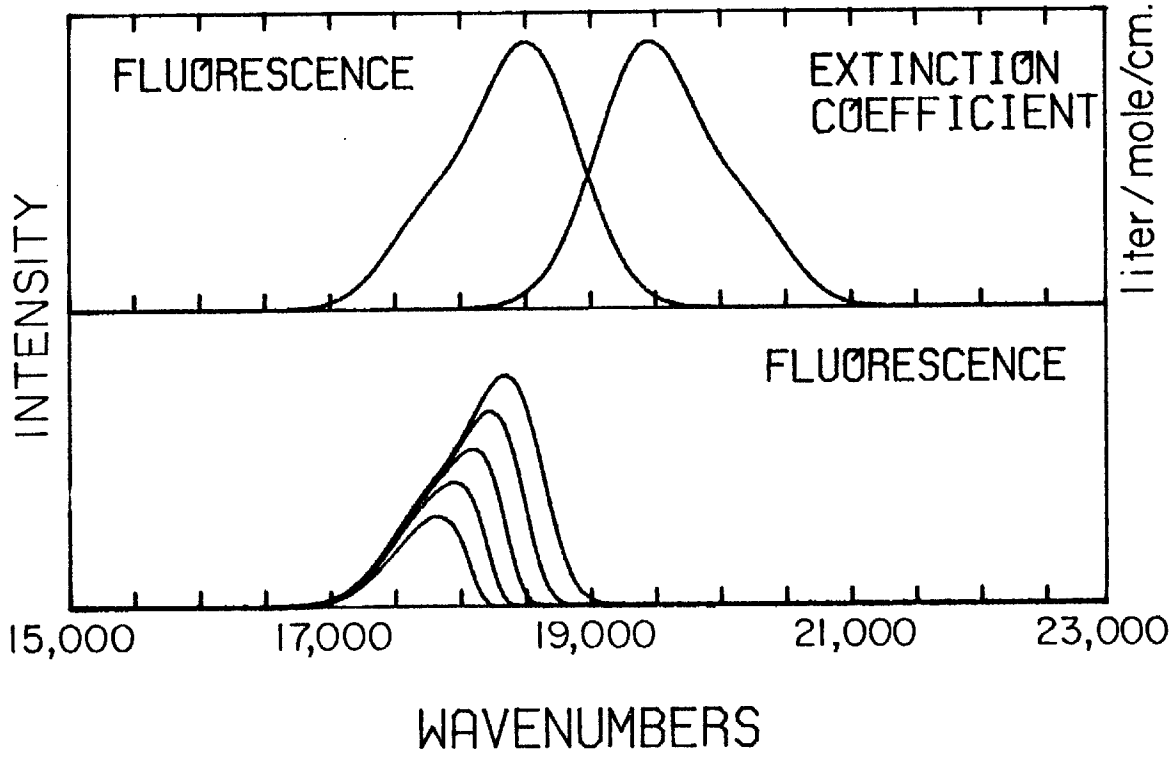

ANALYTIC ABSORPTION AND FLUORESCENCE SPECTRA.
EMISSION SPECTRA WITH VARIABLE PATHLENGTH IN SAMPLE

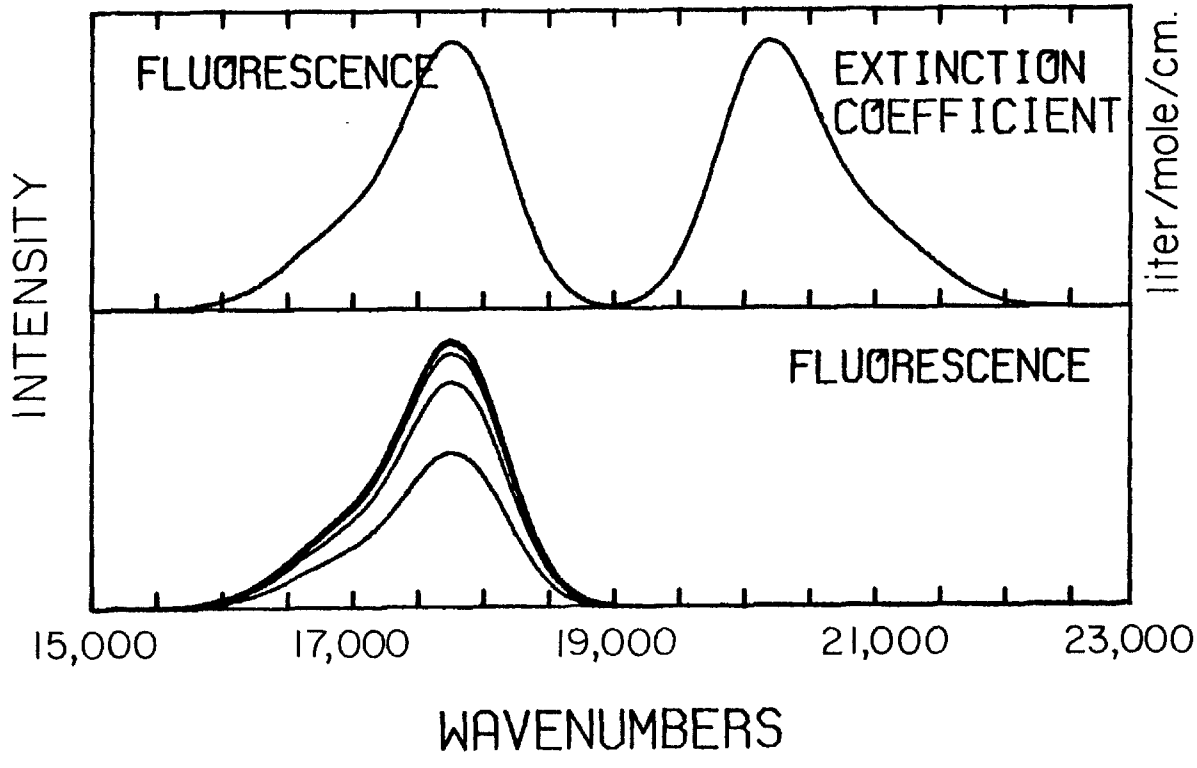

determining the actual self-absorption rates.

For a square cuvette sample geometry, the probability of self-absorption in the critical cones is about the same as the probability of self-absorption outside of the critical cones. This self-absorption probability, r, can be calculated in three different ways. We will assume that the characteristic length approximation of Eq. (61) applies for the spectral overlap calculation, with the length determined by the pathlength through the sample from the excitation source to the detector. This is actually the weakest approximation in all of the three techniques, and will lead to discrepancies at very low and high self-absorption rates. We will use Eq. (54) to find $r \cdot \eta$ from the reduced anisotropy measurements. If RA_{max} is the maximum reduced anisotropy (2e/5) measured at low concentrations and short pathlengths, then the product of the self-absorption probability and the quantum efficiency, $r \cdot \eta$, from Eq. (54) is

$$r\eta = 1 - \frac{RA_{exp}}{RA_{max}} \tag{67}$$

Similarly, from Eq. (59), if τ_{min} was the shortest total lifetime measured at low concentrations and short pathlengths, the same result should be given by the relation

$$r\eta = 1 - \frac{\tau_{min}}{\tau_{exp}} \tag{68}$$

where τ_{exp} is the measured lifetime. If we apply the preceding two relations to the measured transient emission and steady state depolarization measurements on rhodamine-575, we obtain the results shown in Figure 69. We have plotted the calculated product of the quantum efficiency time the concentration of the sample through which the emission had to travel. The solid line is the result from the characteristic length approximation. (This is actually just the self-absorption probability, and not the product of the self-absorption with the quantum efficiency.) There is very good agreement between the lifetime lengthening and the emission depolarization measurements. The measured value of $RA_{max} = 0.18$ for rhodamine-575 in glycol is consistent with a rotational diffusion time of several nanoseconds, which is the rate observed for similar dyes in glycol (Von Jena and Lessing, 1979). We conclude that there is good accord between the three different measurement techniques.

Optimal Efficiency

We believe we know all of the characteristics of rhodamine-575 which determine the efficiency of a single dye LSC. As a test, we will calculate the optimal efficiency of an LSC containing rhodamine-575 as a function of the size and concentration. We use the PSC geometry formalism from Eq. (12) to compute the first generation collection efficiency. The self-absorption rate in the critical cones is computed using the characteristic length approximation. These are combined using Eq. (13) to give the total collection efficiency, with the approximations of no reflection losses and only homogeneous spectral broadening. We will assume edge mounted silicon cells having 18% AM1

Figure 69. Self-absorption probabilities for rhodamine-575. This shows a juxtaposition of predicted self-absorption probabilities for three measurement methods: spectral overlap convolution (solid), emission depolarization (boxes), and transient lifetime (bars). The second two techniques are plotted assuming the quantum efficiency of luminescence is one.

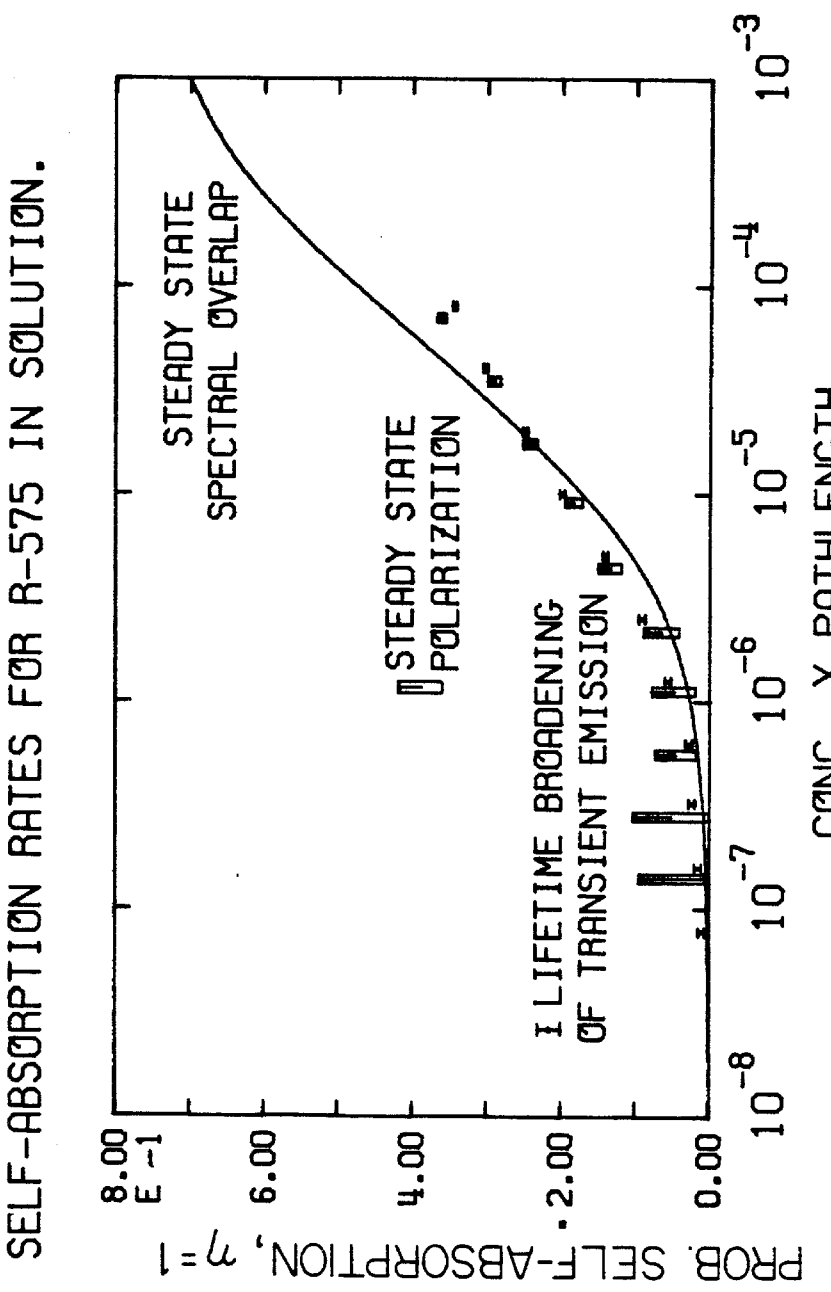
SELF-ABSORPTION RATES FOR R-575 IN SOLUTION.
PROB. SELF-ABSORPTION, $\eta = 1$
8.00 E -1
6.00
4.00
2.00
0.00
10^{-8}
10^{-7}
10^{-6}
10^{-5}
10^{-4}
10^{-3}
CONC. X PATHLENGTH
STEADY STATE SPECTRAL OVERLAP
STEADY STATE POLARIZATION
LIFETIME BROADENING OF TRANSIENT EMISSION

efficiency are coupled to a plate with an index of refraction of 1.49. The quantum efficiency of the dye is assumed to be 0.9. The result of the calculation is given in Figure 70. For the sake of comparison, the system efficiency of a scattering plate (4.II) with an identical geometry is included. The single dye plate outperforms the scattering plate for geometric gains greater than 10. From Table 1, we find that the CODE of rhodamine-575 is about 20. Thus, for a plate with a geometric gain of 20, we expect a collection efficiency of about $0.9 \cdot 0.5$, and that about 30% of the solar flux to which the cell would be sensitive would be absorbed by the plate. The estimate for the efficiency for such a plate from a CODE calculation is, therefore, 2.4%. The plate concentration for the code calculation is 10^{-5} M. The optimized plate actually has 100 times this dye concentration for a gain of 20, giving an efficiency of 4%.

CODES of the Dyes

Table 1 gives the critical optical densities for the organic laser dyes tested. The error bars are due principally to uncertainty in the measurement of the absorption tails. Typical values for the critical optical densities are about 20. Such dyes, therefore, produce collection efficiencies of less than 50% if incorporated in plates with geometric gains greater than 20 due to self-absorption effects. Several dyes have critical concentrations around 80. These tend to be the U. V. and blue absorbing coumarin dyes. While they have much improved CODEs, their high energy absorption bands are not effective in absorbing sunlight. DCM (4-dicyanomethylene-2-methyl-6-p-dimethylaminostyryl-4H-pyran) is by far the most promising dye

Figure 70. Efficiency of a single dye LSC. We assume that rhodamine-575 is the only dye in a 1 cm thick infinite ribbon (PSC) geometry LSC. We have calculated the optimal dye concentration using a binary search routine. The coarseness of the concentration plot reflects time restraints on the search. The efficiency was calculated using the full PSC calculation described in Chapter 3. An average matrix optical density of 4×10^{-3} per centimeter was assumed. 18% efficiency AM1 Si cells were assumed to be mounted on both edges of the ribbon.

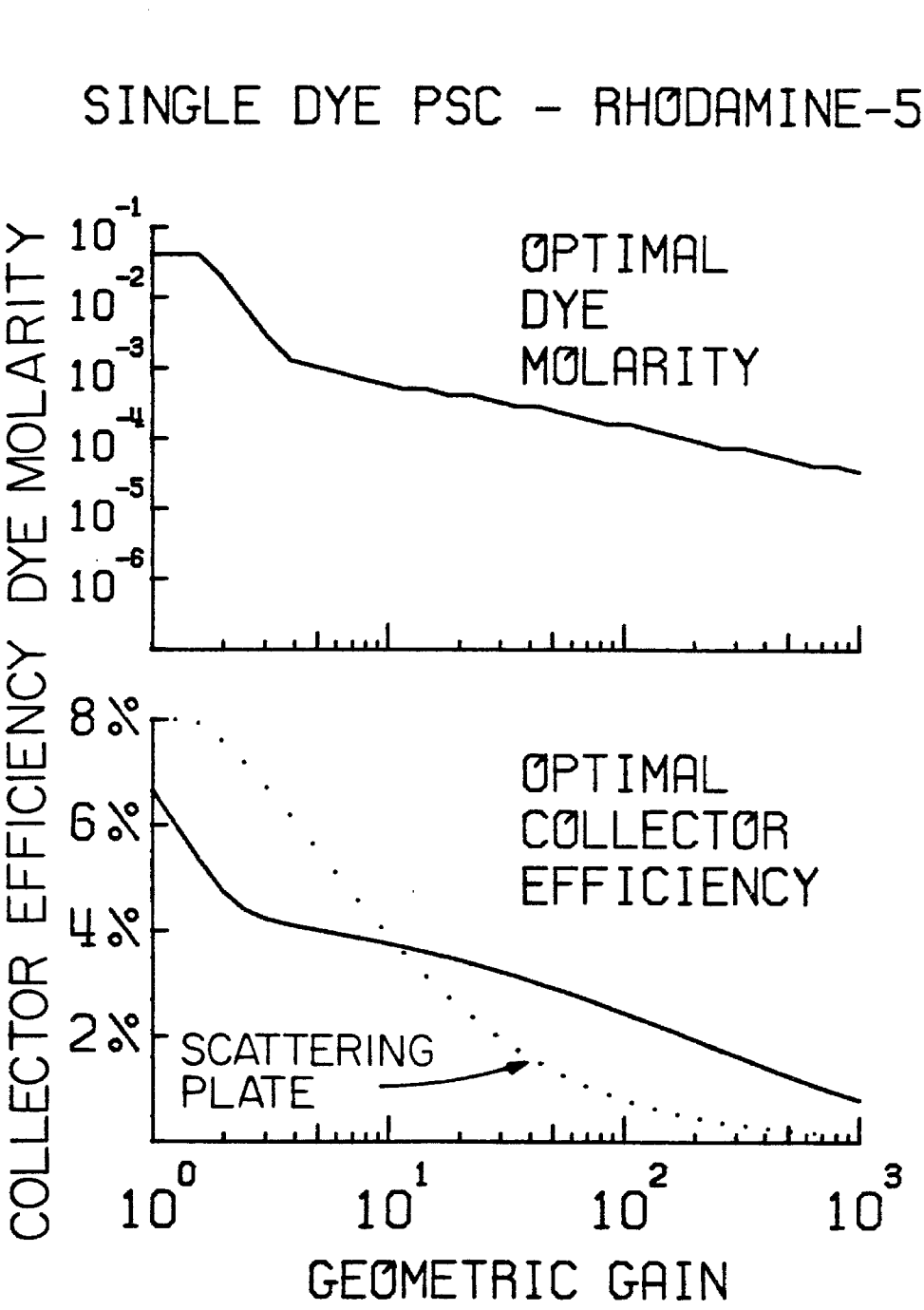
SINGLE DYE PSC - RHODAMINE-575
COLLECTOR EFFICIENCY
DYE MOLARITY
10^{-1}
10^{-2}
10^{-3}
10^{-4}
10^{-5}
10^{-6}
OPTIMAL
DYE
MOLARITY
8%
6%
4%
2%
OPTIMAL
COLLECTOR
EFFICIENCY
SCATTERING
PLATE
10^{0}
10^{1}
10^{2}
10^{3}
GEOMETRIC GAIN

found to date. It has a moderately blue absorption, which allows for 30% absorption of an AM0 spectrum, as well as a CODE of 250. The performance of DCM is considerably reduced when it is case directly in PMMA, which is probably due to the decreased Stokes shift. The methanol performance can be partly restored by adding solvent to the monomer prior to polymerization.

II. SUMMARY

1. The best case quantum efficiency for photodegradation was found to be on the order of 10^{-6} molecules per absorbed photon, in agreement with literature values. Rates on the order of 10^{-8} are required for a twenty year useful life.

2. Rhodamine-575 in cast PMMA was found to be predominantly inhomogeneously broadened, while the same dye in methanol and in diffused PMMA showed spectral homogeneity. At room temperature the dye could emit at energies over $2,000\,cm^{-1}$ (0.25 ev) greater than the exciting energy.

3. Good agreement was obtained between experimentally measured self-absorbed emission spectra and numerically modeled self-absorption for the LSC rod geometry.

4. The self-absorption probability for rhodamine-575 as a function of concentration and pathlength was computed from the characteristic pathlength approximation (spectral information) from emission polarization measurements, and from transient emission measurements. Good agreement was obtained between the three techniques, with very good agreement between the second two techniques.

5. We calculated the efficiency of a rhodamine-575 plate as a function of size and optimized concentration. The results are in general agreement with prototype measurements.

6. Critical optical densities (CODEs) were calculated for the dyes surveyed. The CODEs for methanol solutions are tabulated in Table 1. Casting the dyes in PMMA can reduce the Stokes shift, which reduces the CODE. The Stokes shift in PMMA can be increased by adding solvent such as DMSO to the monomer prior to polymerization.

CHAPTER 6

I. INTRODUCTION

Winston derived (Winston, 1974) the maximum gain for a mirror concentrator using geometric optics arguments. Rabl later found (Rabl, 1976) the same results from the second law of thermodynamics. The basic result is that an optimal concentrator on the earth can reproduce the original brightness at the surface of the sun. Since the geometric dispersion experienced by sunlight in traveling to the earth is a factor of $\sin^2(\theta_s)$, where θ_s is the half-angle of the solar disk (0.267 degrees) the maximum gain is, therefore, the inverse of that dispersion, or $1/\sin^2(0.267) = 46,050$. This is also an application of the brightness theorem from geometric optics (Born and Wolf, 1975).

It is tempting to try to develop similar relationships for the performance of an LSC. Since the energy of the incident light is not preserved in an LSC, the above result must be generalized appropriately. We will first give the results of a detailed balance calculation which gives the intensity of the plate output as a function of size, ignoring self-absorption effects. We then repeat the result due to Yablonovitch which generalizes the brightness theorem from geometric optics to include nonconservative systems. This approach incorporates self-absorption effects. The Yablonovitch result is applied to the spectra of all of the dyes surveyed, and the resulting prediction of the maximum concentration attainable is compared with the results of the CODE calculation. Finally, we incorporate these results in a simple model of the optimal efficiency of a self-absorbing LSC.

II. DETAILED BALANCE CALCULATION

Consider an LSC as shown in Figure 1. A ribbon of thickness D and width L is mirrored on one edge, and has a black body absorber cavity mounted on the other edge. The geometric gain of the ribbon is L/D. We define a thermodynamic gain of the plate to be the fourth power of the ratio of the black body absorber energy to the sun's temperature, divided by $\sin^2(\theta_c)$:

$$G_{therm} = \left(\frac{T_a}{T_s}\right)^4 \sin^{-2}(\theta_s) \tag{69}$$

This is equivalent to the concentration factor for the device. The energy radiated and absorbed by the black body cavity in equilibrium is proportional to the fourth power of its temperature. If the temperature of the absorber is equal to the sun's temperature, then Eq. (69) reduces to Winston's result. We will assume spectral properties for the LSC ribbon to calculate the equilibrium temperature of the absorber. This temperature then determines the maximum concentration possible by such a ribbon.

The energy input into the system is from the absorption of sunlight. The total solar energy per unit length of the ribbon is assumed to be

$$I_s = \sigma T_s^4 \sin^2(\theta_s) \cdot L \tag{70}$$

where σ is the Stephan Boltzman constant ($5.67 \cdot 10^{-8}$ joule meter^{-2} second^{-1} K^{-4}). The spectral intensity of the sunlight per unit length is

$$I_s(\bar{\nu})\, d\bar{\nu} = I_s \cdot 15 \left(\frac{hc}{\pi K T_s}\right)^4 \frac{\bar{\nu}^3\, d\bar{\nu}}{e^{hc\bar{\nu}/KT_s} - 1} \tag{71}$$

(Landau and Lifshitz, 1977). We approximate the absorption spectrum as being zero everywhere except between $\bar{\nu}_1$ and $\bar{\nu}_2$, where the absorption across the thickness of the plate is assumed to be 100%. The emission is assumed to be monochromatic at $\bar{\nu}_0$. The energy which is absorbed, luminesced, and trapped by our idealized LSC is, therefore

$$E_{in} = \eta(1 - P) \int_{\bar{\nu}_1}^{\bar{\nu}_2} d\bar{\nu}\; I_s(\bar{\nu})\, \frac{\bar{\nu}_0}{\bar{\nu}} \tag{72}$$

where P is the critical cone loss and n is the quantum efficiency of luminescence. If $\bar{\nu}_0 < \bar{\nu}_1 < \bar{\nu}_2$, there is no self-absorption.

We include three mechanisms by which energy can leave the system. The spectral distribution of the light emerging from the cavity per unit length is

$$I_a(\bar{\nu})\, d\bar{\nu} = I_a \cdot 15 \left(\frac{hc}{n\pi K T_a}\right)^4 \frac{\bar{\nu}^3\, d\bar{\nu}}{e^{hc\bar{\nu}/nKT_a} - 1} \tag{73}$$

where the total emerging intensity per unit length is

$$I_a = \sigma T_a^4 n^2 D \tag{74}$$

n is the index of refraction of the ribbon. A fraction of this emission, GF, is immediately lost out of the critical cones:

$$GF = \frac{2}{\pi} \int_{\pi/2-\theta_c}^{\theta_c} d\theta \cos(\theta) \sin(\theta) \cos^{-1} \left[\frac{\cos(\theta_c)}{\sin(\theta)}\right] \tag{75}$$

The fraction which is then lost to matrix absorption is $\delta(1 - GF)$. Finally, there is energy lost through absorption by the dye. This has two components: the fraction of the absorbed emission which is radiated out of the critical cone, and the fraction of the photon's energy which is lost in the Stokes shift. The total energy lost out of the system is given by

$$E_{out} = I_a [GF + \delta(1 - GF)] + (1 - \delta)(1 - GF) \int_{\bar{\nu}_1}^{\bar{\nu}_2} I_a(\bar{\nu})\, d\bar{\nu}$$

$$- (1 - P)(1 - GF)(1 - \delta)\, \eta \int_{\bar{\nu}_1}^{\bar{\nu}_2} I_a(\bar{\nu})\, d\bar{\nu}\, \frac{\bar{\nu}_0}{\bar{\nu}} \tag{76}$$

We find the temperature of the absorber by numerically equating the energy in and out of the system. We have shown in Figure 71 the results from performing the above calculation for an LSC absorbing in

Figure 71. Thermodynamic gain of an idealized LSC. We compute the gain of an LSC (Planar Solar Collector geometry, PSC) by substituting a black body cavity for the edge mounted cells, and then computing the temperature of the cavity by a detailed balance calculation. The straight diagonal line indicates the operation of concentrators using geometric optics such as mirrors and lenses.

THERMODYNAMIC GAIN OF AN IDEALIZED LSC.

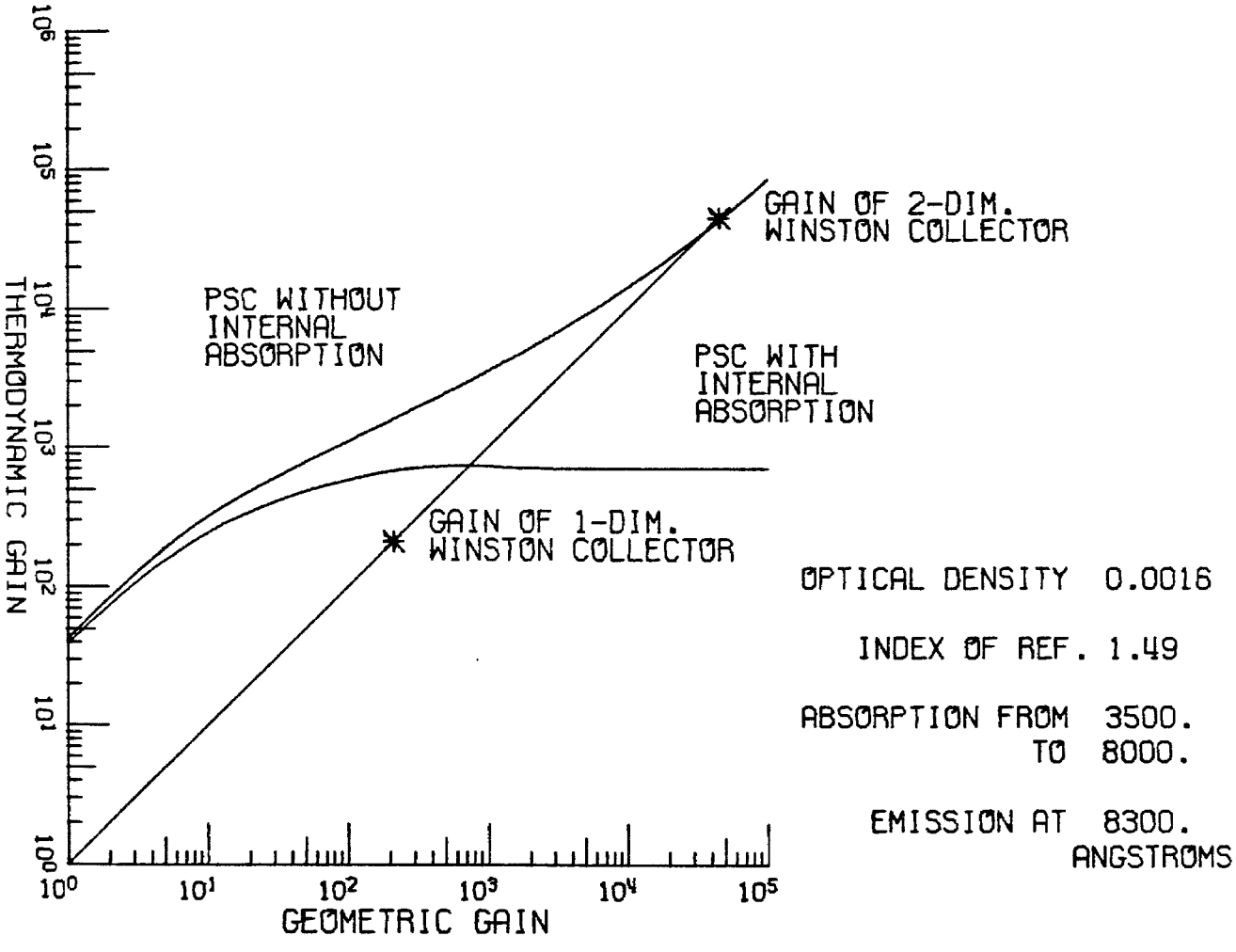

the region from 3,500Å to 8,000Å, emitting at 8,300Å, and for geometric gains ranging from 1 to 10^5. The two upper curved lines show the thermodynamic gain (or energy density gain) for the cases of no matrix absorption (upper curve) and for a matrix absorption corresponding to an optical density of 0.0016 across the LSC thickness. The straight diagonal line represents all nonlossy geometric optics collectors, because in such collectors the thermodynamic gain can be equal to the geometric gain. The stars indicate the operating points of the one-dimensional (trough) and two-dimensional Winston collectors.

Under the conditions of the model there is a considerable buildup of energy in the plate-cavity system. For example, an LSC with no gain at all ($G_{geom} = 1$) would cause the cavity to rise to a temperature of 1,000°K. A similar black body facing the sun directly only would rise to about 400°K. While the technique can be elaborated to include effects such as self-absorption in more realistic dye spectra, the results in their present form are overly optimistic in the predicted light output.

III. GENERALIZED BRIGHTNESS THEOREM OF YABLONOVITCH

A more generalized approach to a thermodynamic limit to the performance of an LSC would be to consider the incident sunlight and the light trapped in the plate as two systems of photon gasses in equilibrium. This system was first studied by Kennard (Kennard, 1918), and by Ross (Ross, 1961). Recently Yablonovitch (Yablonovich, 1980) has applied these results to the LSC. The simplest result from his paper is the most useful, and that is a generalization of the

brightness theorem of optics to inelastic processes (optical elements which change the energy of the light).

We will follow closely the derivation of 'a generalized brightness theorem' for optical systems, including inelastic processes given by Yablonovitch. According to statistical mechanics, the entropy change associated with the loss of a photon from the incident solar Bose field is

$$\Delta S_1 = -K \ell n\left(1 + \frac{8\pi \bar{\nu}_1^2}{B_1}\right) \tag{77}$$

where n is the index of refraction of the LSC plate, $\bar{\nu}$, is the wavenumber of the light, and B_1 is the brightness of the incident field in photons per unit area, per wavenumber, per unit time, and per 4π solid angle. The entropy increase in the concentrated field due to the fluorescent emission of one photon is

$$\Delta S_2 = K \ell n\left(1 + \frac{8\pi \bar{\nu}_2^2}{B_2}\right) + \frac{hc\,(\bar{\nu}_1 - \bar{\nu}_2)}{nT} \tag{78}$$

where the additional term is due to the thermal dissipation of the Stokes shift at an ambient temperature T. By the second law of thermodynamics, $\Delta S_1 + \Delta S_2 \geq 0$, therefore

$$K \ell n\left(1 + \frac{8\pi \bar{\nu}_1^2 K^2}{B_1}\right) / \ell n\left(1 + \frac{8\pi \bar{\nu}_2^2 n}{B_2}\right) \leq \frac{hc\,(\bar{\nu}_1 - \bar{\nu}_2)}{nT} \tag{79}$$

or the achievable concentration ratio or flux gain is

$$G_{flux} = \frac{B_2}{B_1} \leq \frac{\bar{\nu}_2^2}{\bar{\nu}_1^2} \exp\left(\frac{hc(\bar{\nu}_1 - \bar{\nu}_2)}{nKT}\right) \qquad (80)$$

If $\bar{\nu}_1 = \bar{\nu}_2$, this reduces to the brightness theorem from optics. This limit as stated sets a rough upper bound for the possible gain of an LSC, in that the details of the spectral structure are not incorporated. As a first approximation, we will assume that most emission occurs at the peak of the emission spectrum and similarly most of the absorption occurs at the peak of the absorption spectrum. Table 5 is obtained by plugging known values of the spectra maxima for the dyes surveyed into Eq. (81). The CODE calculation results are included in Table 5 for comparison.

The reasonable correspondence between the spectrally derived CODE and the thermodynamically derived maximum gain is somewhat fortuitous. Eq. (80) can be employed in a less approximate manner by utilizing it for relating the achievable gain for emission at $\bar{\nu}_1$ due to absorption at $\bar{\nu}_2$. We assume that the incident solar flux has a flat spectral response, and that the concentration of a dye in an LSC plate will be adjusted such that the peak optical density through the thickness of the plate is one. The maximum light concentration for the dye will, therefore, be the weighted average of this wavenumber dependent gain times the normalized emission spectrum:

Table 5. Maximum light concentration for selected organic laser dyes. The second column gives the Stokes shift in electron volts between the peaks of the absorption and emission spectra. The third column gives the critical distance for dipole-dipole transfer from a dye molecule to another similar dye molecule, as defined by Eq. 20. The fourth column contains the critical optical densities for methanol solutions. The fifth column contains the maximum light concentration as defined by the Yablonovitch relation in Eq. 80, where $\overline{\nu}_1$ and $\overline{\nu}_2$ are the wavenumber positions of the peak extinction and emission spectra values, respectively. Finally the last column is obtained using Eq. 81, which performs an average of Eq. 80 over both the absorption and emission spectra.

Table 5.

Dye	Stokes shift e. v.	R_o, Å	CODE	$C_{Yabl.}$	$G_{Yabl.}$
Coumarin-480	0. 53	25. 3	113.	2.1×10^{9}	3.6×10^{17}
Coumarin-500	0. 63	26. 4	25. 7	1.3×10^{11}	1.2×10^{18}
Coumarin-535	0. 31	33. 0	31. 3	3.7×10^{5}	3.5×10^{17}
Coumarin-540	0. 25	33. 7	82. 7	2.2×10^{4}	5.6×10^{13}
DCM	0. 67	24. 2	244.	5.4×10^{11}	4.6×10^{13}
Rhodamine-560	0. 12	43. 8	17. 0	162.	6.7×10^{14}
Rhodamine-575	0. 117	46. 1	34. 2	113.	3.3×10^{11}
Rhodamine-590	0. 104	48. 7	25. 3	69.	2.1×10^{10}
Rhodamine-610	0. 101	49. 4	36. 3	58.	1.1×10^{11}
Kiton red-620	0. 086	52. 4	15. 8	32.	9.2×10^{10}
Rhodamine-640	0. 096	53. 1	16. 6	48.	1.1×10^{11}
Sulforhodamine-640	0. 08	54. 7	17. 0	25.	1.3×10^{11}
Cresyl violet-670	0. 094	50. 2	16. 8	44.	1.2×10^{8}
Oxazine-720	0. 07	54. 4	16. 9	16.	8.7×10^{7}
Oxazine-750	0. 079	55. 5	24. 5	24.	4.6×10^{7}
DODCI	0. 073	65. 1	11. 0	19.	3.1×10^{7}
DOTCI	0. 089	69. 8	7. 5	36.	2.1×10^{5}
IR-144	0. 18	61. 9	15. 7	1417.	1.5×10^{4}

$$G_{flux} = \int_0^\infty f(\bar{\nu}_2)\, d\bar{\nu}_2 \int_0^\infty d\bar{\nu}_1 \,(1 - 10^{-\epsilon(\bar{\nu}_1)\cdot C\cdot x})$$

$$\cdot \frac{\bar{\nu}_2^2}{\bar{\nu}_1^2} \exp\left(\frac{hc}{KT}(\bar{\nu}_1 - \bar{\nu}_2)\right) \Big/ \int_0^\infty (1 - 10^{-\epsilon(\bar{\nu}_1)\cdot C\cdot x})\, d\bar{\nu}_1$$

$$= \int_0^\infty f(\bar{\nu}_2)\, \bar{\nu}_2^2 \exp\left(-\frac{hc}{KT}\bar{\nu}_2\right) d\bar{\nu}_2$$

$$\cdot \frac{\int_0^\infty [1 - 10^{-\epsilon(\bar{\nu}_1)\cdot C\cdot x}] \exp\left(\frac{hc}{KT}\bar{\nu}_1\right) \frac{d\bar{\nu}_1}{\bar{\nu}_1^2}}{\int_0^\infty [1 - 10^{-\epsilon(\bar{\nu}_1)\cdot C\cdot x}]\, d\bar{\nu}_1} \qquad (81)$$

Results for this calculation are also tabulated in Table 5.

The success of the Yablonovitch result lies in the choice of the emission and absorption maxima as the wavenumber values used in the calculation. When the entire fluorescence spectrum is included instead of just the peak position, unphysically large light gains are predicted.

An obvious result from Table 5 is that the dye with the largest Stokes shift, DCM in methanol, also has the highest possible light concentration potential. This is experimentally verified in that a DCM plate presently holds the record for the brightest light output of any LSC. The Stokes shift for this dye is 5,760 wavenumbers or 0.67 ev (1 ev = 8,654.7 cm^{-1}), as shown in Table 5.

IV. OPTIMAL EFFICIENCY MODEL

We have seen that an LSC can achieve higher light concentrations as the Stokes shift between the absorption and emission spectrum is increased. Self-absorption ceases to limit the flux gain for a dye like DCM, whose Stokes shift corresponds to about 0.7 ev (peak absorption to peak emission). In general, as the Stokes shift becomes larger than 0.7 ev, the efficiency of the plate will decline for two reasons. The first is that less of the solar flux is utilized, the second is that progressively lower voltage output cells must be used to convert the output light. We can extend the usual treatment of the optimal efficiency of a solar cell (Wolf, 1960) in a simple manner to include the effect of the Stokes shift in an LSC on the overall efficiency of the collector.

Consider the 5,800 °K black body spectrum in Figure 72. We assume that the dye in an LSC absorbs all of the solar flux from the peak of its absorption out to higher energies. We assume that there is some gap between this absorption cutoff and the absorption edge of the cell. The energy per unit area incident on the LSC is

$$E_{in} = A \cdot \int_0^\infty hc\ \bar{\nu}^3\, d\bar{\nu}\ (e^{hc\bar{\nu}/KT_S} - 1)^{-1}$$

$$= A \cdot \frac{\pi^4}{15} \frac{(KT_S)^4}{(hc)^3} \qquad (82)$$

A is a constant that scales the incident solar intensity. Let the output

Figure 72. Simple model of LSC efficiency. The envelope function is the flux distribution from a 5800° K black body. The shaded region is the flux above E_{abs} which is absorbed by the LSC. E_{cell} is the absorption cutoff of the cell.

SOLAR SPECTRUM.

POSITION OF ABSORP.EDGE AND CELL OUTPUT ENERGY.

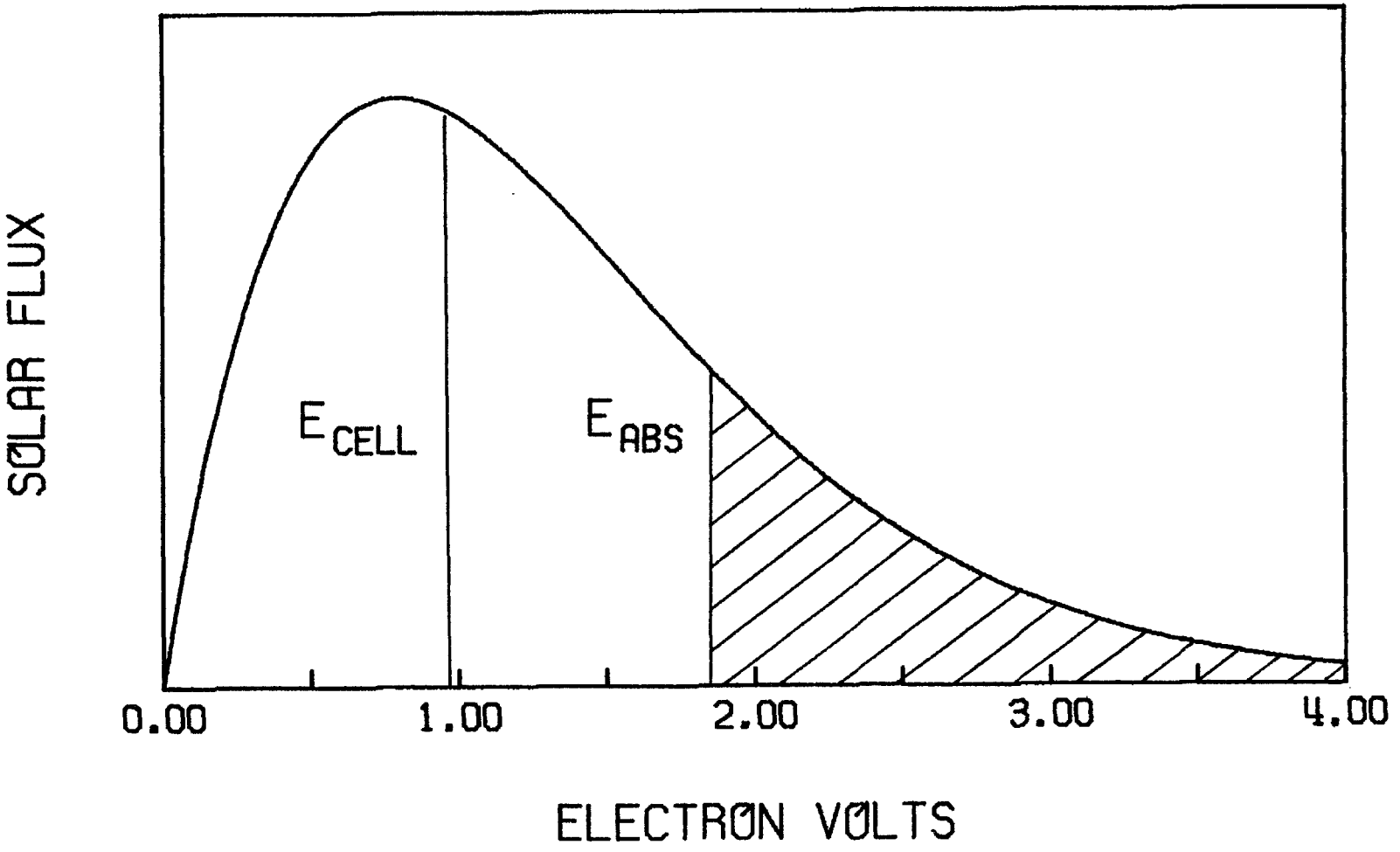

energy of the cell be E_{out}. The energy output of the LSC mounted cells is maximally

$$E_{LSC} = A \cdot (1 - P) \cdot E_{out} \cdot \int_{E_{ab}/hc}^{\infty} d\bar{\nu}\ \bar{\nu}^2\ (e^{hc\bar{\nu}/KT_s} - 1)^{-1} \qquad (83)$$

where (1 - P) is the fraction trapped in the critical cone. We assume that there is sufficient Stokes shift such that the only dominant loss mechanism is light escaping out of the critical cones. Combining Eqs. (82) and (83) gives an optimal efficiency for an LSC:

$$\eta_{LSC} = \frac{E_{LSC}}{E_{in}} = (1 - P)\frac{15}{\pi^4}\ \frac{E_{out}}{KT_s}\ \int_{E_{ab}/KT_s}^{\infty} dx\, x^2\, (e^x - 1)^{-1} \qquad (84)$$

Silicon cells are the obvious candidates for the edge-mounted cells. Their typical output voltage is about 0. 5 ev, with an absorption edge at about 1. 0 ev. If we assume a Stokes shift of 0. 7 ev is required for eliminating self-absorption losses, then the absorption edge of the dye should be at 1. 6 ev. We assume 70% critical cone trapping. Under these assumptions we find that the maximum efficiency of an LSC is 8. 3%. Figure 73 shows the efficiency of LSC plates utilizing silicon cells or gallium arsenide cells as a function of the difference between the absorption cutoff of the dye and the bandgap of the semiconductor. Clearly this calculation gives an upper limit on the efficiency, since we have ignored numerous loss mechanisms such as matrix absorption,

Figure 73. Collector efficiency vs Stokes shift. We assume the sun is a 5800° K black body, and that the LSC plate absorbs all light above a cutoff energy E_{ABS}. We assume all the light is emitted just above the band gap energy, E_{cell}, so that the Stokes shift is $E_{ABS} - E_{cell}$. We also assume the output from the cells is 0.5 ev below the band gap energy. The two cases plotted are for Ga As (upper) and Si (lower). The dotted line indicates the operating point using a dye with a Stokes shift similar to that of DCM.

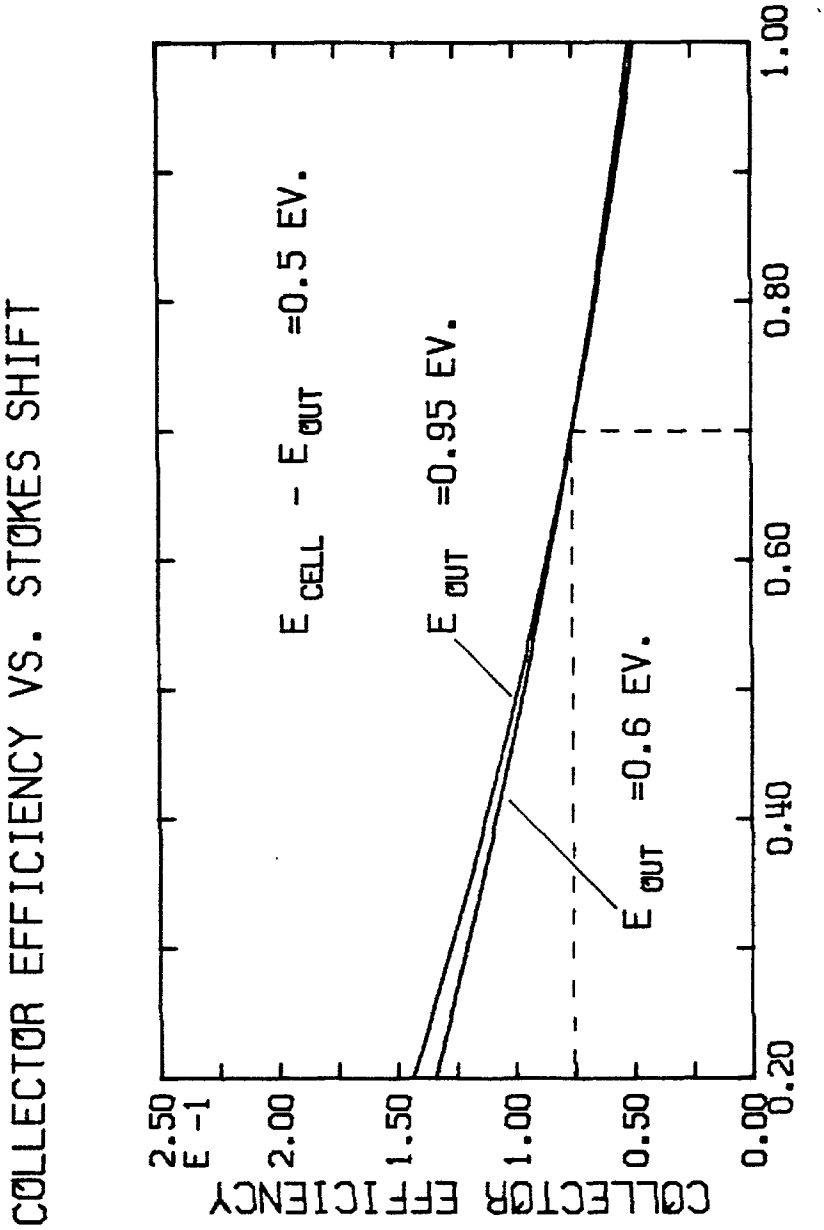
COLLECTOR EFFICIENCY VS. STOKES SHIFT
COLLECTOR EFFICIENCY
E -1
2.50
2.00
1.50
1.00
0.50
0.00
0.20
0.40
0.60
0.80
1.00
E ABS - E CELL IN E.V.
E CELL - E OUT =0.5 EV.
E OUT =0.95 EV.
E OUT =0.6 EV.

emission at lower energies than the absorption edge of the cell, and incomplete absorption of sunlight in the absorption band of the plate. The computed efficiency also benefits from the use of a 5,800° K black body spectrum. If we repeat the calculation using a measured solar spectrum, we find the efficiency is 9.3% for an absorption cut-off at 1.6 ev and an output voltage of 0.5 v.

V. SUMMARY

1. We developed a detailed balance calculation for the light output from an LSC. The edge mounted cell is replaced by a black body absorber, and the temperature of this absorber is computed at equilibrium from a balance of the energy absorbed and emitted by the black body.

2. We compute Yablonovitch's prediction for the light concentrating ability of dyes as a function of the absorption and emission energies, and the temperature of the surrounding material. This model gives reasonable results for dyes with Stokes shifts of less than 0.2 ev in the simple approximation that all light is absorbed at the peak of the absorption spectrum and all light is emitted at the peak of the emission spectrum.

3. A very simple model for the ultimate efficiency of an LSC including self-absorption effects is presented. We use the empirical measurement that dyes with CODEs over 100 have Stokes shifts of 0.7 ev or more. This model predicts that plates with geometric gains greater than 100 will have a maximum efficiency of 9%.

CHAPTER 7

I. INTRODUCTION

In this chapter we will briefly summarize the status of the LSC technology and offer our opinions as to what the subsequent steps should be in its development.

Prototype Performance

The most efficient LSC reported to date was a thin film multiple dye plate made by Owens-Illinois. Its measured efficiency was 3.2%. However, the plate area was so small compared to its thickness that even a purely scattering plate (one which contained scattering centers instead of luminescing centers) could produce at least this efficiency if it were made with the same geometry. This is, therefore, not representative of an LSC which is performing appreciable light concentration.

The most efficient device made to date which outperforms a scattering collector was a liquid LSC made by ourselves. Its efficiency was 1.9%, and its flux gain (the increase in output power from a cell when it is attached to the plate) was 3.8. We made the highest flux gain device, which was a PMMA containing DCM. It was 1.3% efficient with a flux gain of 5.1. This is a high concentration factor for a device with nearly the same absorption dependence on the angle of incidence of the input light as a black body absorber.

We have experimentally verified that the most important factor limiting performance, especially flux gain, is self-abosrption. For example, the LSC with the highest flux gain contains the dye with the highest Stokes shift of all the dyes we have measured. (We also found

that the Stokes shift is nearly halved when DCM is cast in PMMA, as compared to DMSO solutions).

How well can LSCs be expected to perform? A numerical model incorporating the methanol spectra of a standard xanthene dye predicts that 4% efficiency with a flux gain of 20 should be achievable. A CODE calculation based on the DMSO spectra of the dye DCM predicts that 3% efficiency and a flux gain of 40 should be possible. If we assume that a 0.7 ev Stokes shift is required for high flux gains, then an upper limit of about 9% efficiency results from a simple thermodynamic model.

Stability

We found lifetimes on the order of a month for dye photodegradation in PMMA plates. Dyes in solution typically did better, with methanol samples having lifetimes between several hours and several years.

Our measurements are in reasonable agreement with published quantum efficiencies for photodegradation. Typical optimal values for such quantum efficiencies are 10^{-6} molecules per absorbed photon, which corresponds to device lifetimes of about two months. We presently do not know to what extent the maximum stability can be improved. Twenty year device lifetimes probably require quantum efficiencies for photodegradation of less than 10^{-8}.

Future Development

Two areas of research emerge as the next logical step in LSC development. These are to examine the liquid LSC in more detail, and to undertake the synthetic chemistry of dye optimization.

We feel that the homogeneous spectra and large Stokes shifts characteristic of dyes in solution are highly desirable. Either the liquid cell design, or some matrix-solvent combination, should supercede the cast plastic design. The efficiency and gain should improve due to the higher Stokes shift. (The highest efficiency high gain plate was a liquid cell containing dyes with only moderate Stokes shifts.) In addition, the photodegradation problem is diminished due to both more chemically inactive surroundings and by the ability to replenish the dye.

None of the dyes available to us were satisfactory for use in an LSC. The closest approximation to the perfect dye is DCM. The principal problem with DCM is that both its emission and absorption are about 2,000 wavenumbers too high in energy. A difficult but important task would be to try and synthesize new dyes with the right spectra, a high quantum efficiency of luminescence, and good stability.

APPENDIX I

ECONOMICS OF LSC APPLICATIONS

Research into LSCs is motivated by the need to increase the affordability of solar power. Given our present understanding of the technology, it is reasonable to perform at least a preliminary assessment of the LSCs economic viability. We do not have the data or the expertise to rigorously model the manufacturing costs on a large scale. Our aim is to discover whether the LSC is conspicuously promising in comparison to other photovoltaic designs, and so we require a result which is accurate to within roughly a factor of two. We will use results of an LSC manufacturing analysis by Owens-Illinois (Rapp et al, 1980) to estimate the module cost. We will compare the price and performance of an LSC system with two other potential conversion techniques: high efficiency silicon cells with mirror concentrators, and thin film silicon cells.

The cost of 3 mm thick plexiglass plate from Du Pont is about $8.70 per square meter assuming very high volume manufacturing. Approximately one-half gram of high purity dye is needed per square meter. We will assume that the price of dye will drop a factor of 10 from the present average cost of about $20.00 per gram because of high volume production, so that dye will cost $1.00 per square meter. A tempered glass cover is required to prevent surface abrasion and for UV protection. Owens estimates this should cost $4.30 per square meter. A 2 mm nontempered glass backing is probably also required, for $2.70. Either aluminum foil or a mirrored surface on the backing plate is probably required, at a cost of $.50 per square meter. We will assume a geometric gain of 50. Nonencapsulated 18% AM1 silicon

cells at $500 per square meter will cost $10.00. Owens estimates assembly and packaging costs at $7.00 per square meter. The cost of a square meter LSC module at the factory is summarized as follows:

3 mm plexiglass plate	$ 8.70
0.5 grams dye	$ 1.00
3 mm tempered cover glass	$ 4.30
2 mm backing glass	$ 2.70
mirroring	$ .50
18% AM1 silicon cells	$10.00
assembly and packing	$ 7.00
	$34.20

The upper limit on the efficiency of the module is 9%. Practically speaking, we feel efficiencies of 3% are readily attainable by properly casting DCM or one of its derivatives in PMMA in the presence of DMSO. We assume that the peak solar power is 1,000 watts per square meter. Therefore, the cost per peak watt of the LSC modual is $.43 and $1.14 for 9% and 3% efficient modules, respectively.

For comparison, we will use Hovel's estimates (Hovel, 1978) for the price and efficiency of a system using silicon cells and mirror concentrators. We will assume that encapsulated 20% AM1 efficiency silicon cells cost $1,250 per square meter, and that trough collectors will produce geometric gains of 30 with 80% efficiency. The cell cost is $41.70 per square meter, and the concentrator cost is estimated to be $60.00 per square meter. The total price per square meter is $101.70. The efficiency of the combination is about 16%, giving $.64 per peak watt. Estimates on the performance of thin film

silicon cells suggest that AM1 efficiencies of 10% and costs per peak watt of $. 50 are reasonable (Hovel, 1975).

The key performance parameters of the three systems is summarized in Table A1. It is interesting to compare the noncell costs of

Table AI. Comparison of photovoltaic converters.

	LSC	Silicon Thin Film	Silicon with Mirror Concentrator
Efficiency	9% - 3%	10%	16%
Cost per peak watt	$. 43 - $1. 14	$. 50	$. 64

the LSC module and the mirror concentrator. The cost of the LSC module without the cells is $24. 20, and the cost of the mirrors alone is $60. The fractional loss in output introduced by the LSC is between 0. 17 and 0. 44 (for 3% and 9% system efficiencies, respectively), against 0. 80 for the mirror collector. The LSC is 2. 4 times cheaper than the mirrors, and the mirror is between 1. 8 and 4. 7 times more efficient.

The baseline for performance for utility power generation is apparently set by coal technology. For photovoltaic power to be competitive, the converters themselves should cost between $. 10 and $. 40 per peak watt, and should have an overall efficiency of at least 10% to offset noncell costs (Robinson, 1979). We can readily conclude that LSCs will not be competitive with coal because they cannot achieve the required efficiency.

We can conclude that LSCs do not compare favorably with mirror or lens concentrators due to the LSC's power efficiency. The inefficiency of the LSC overcomes its cost advantage for practical devices. There is an exception to this rule, however. Mirrors and lenses are in general unable to concentrate diffuse light, whereas an LSC can. Applications that require concentration of diffuse sources will benefit from the use of LSCs. A good example of such an application is scintillation counting, where LSC-like devices are presently being utilized very effectively. However, the ability to concentrate diffuse light is probably not a significant advantage for photovoltaic power generation, since regions that receive predominantly indirect sunlight usually also receive less total sunlight than would be desirable for power generation.

Summary

1. We estimate the cost of a square meter LSC module to be $34.20 based on a manufacturing analysis by Owens-Illinois. We estimate the efficiency of a practical device to be 3%, and the maximum efficiency to be 9%. Assuming the peak solar power is 1,000 watts per square meter, the cost per peak watt is between $.43 and $1.14 for 9% and 3% efficient devices, respectively.

2. The low efficiency of LSCs prevent them from being competitive with coal for utility power generation.

3. Conventional concentrators such as mirrors appear to be preferable to LSCs due to their higher efficiency, despite their higher cost. The exception is for applications requiring concentration of

diffuse or indirect light. In such applications an LSC can outperform conventional concentrators.

APPENDIX II

MOLECULAR ABSORPTION AND LUMINESCENCE

We have considered organic laser dyes throughout the text as though they were very small black boxes that absorb and emit light in well characterized ways. In this appendix we will elaborate on the operation of these dye molecules in a schematic fashion. Our purpose is not to derive spectral characteristics from molecular parameters. Instead we are interested in defining and motivating the existence of terms like the Stokes shift and the extinction coefficient.

Absorption and emission by an organic dye molecule is a quantum mechanical many body problem. If we consider the atoms of the molecule as masses interconnected by springs, and ignore the effect of the surrounding material, there are in general 3N-6 independent internal modes of oscillation (3N-5 for a linear molecule) where N is the number of atoms (Tinkham, 1964). A typical molecule will have on the order of 30 atoms, or 100 normal vibrational modes. We will try to get some understanding for this system by examining a particular optically active mode (one with a high electrical polarizability in an optical frequency). There is a generalized interatomic spacing coordinate associated with this mode (corresponding to the interatomic spacing in a diatomic molecule, for example). There is a coulombic repulsion between the nuclei which dominates at very small distances. Since the molecule is stable, there must also be an attraction which dominates at longer distances. Combining these two effects gives a potential surface for the energy in the system as a function of this generalized coordinate. If the electron cloud is in some excited state, the form of the attractive interaction can change, so that in general

there is a different potential surface for each electronic state. Two such potential surfaces are shown in Figure A1. The equilibrium positions are not necessarily the same. The lowest energy electronic state or ground state usually has all the electron spins combined pairwise, forming a singlet state. The lowest energy excited state can be a triplet state, or one with unpaired electron spins, due to a more strongly bonding character of this configuration.

The restoring force near the equilibrium position can be expanded as a simple harmonic quantum mechanical oscillator. Near the minimum of the electron surface are quantized vibrational levels corresponding to simple harmonic oscillator-like wave functions. As in the case of the simple harmonic oscillator, the system is most probably at the equilibrium position for low vibrational states, and is most probably as far away as possible from the equilibrium position for the higher vibrational states. The system is further complicated by a sequence of rotational modes (in the gas or liquid phase) or librational modes (in the solid phase) which are superimposed on each vibrational state.

So far we have been cavalier about separating the electronic motion from the nuclear motion. The outer shell electrons that participate in optical processes and chemical bonding have oscillation frequencies on the order of 10^{16} per second, while the nuclear vibrations occur on the order of 10^{13} per second. Thus it is reasonable to assume that the nuclei experience some average force due to the electrons, but that they are not sensitive to the particular position of the electrons.

Figure AI. Energy level diagram for absorption and emission. The ordinate is in increasing internal energy, and the abscissa is the coordinate corresponding to the optically active mode. (In a diatomic molecule, this would correspond to the interatomic distance.) The two curves are the ground and first excited electronic surfaces. (a), (b), (c), and (d) correspond to absorption, relaxation, emission, and final relaxation (Karplus and Porter, 1970).

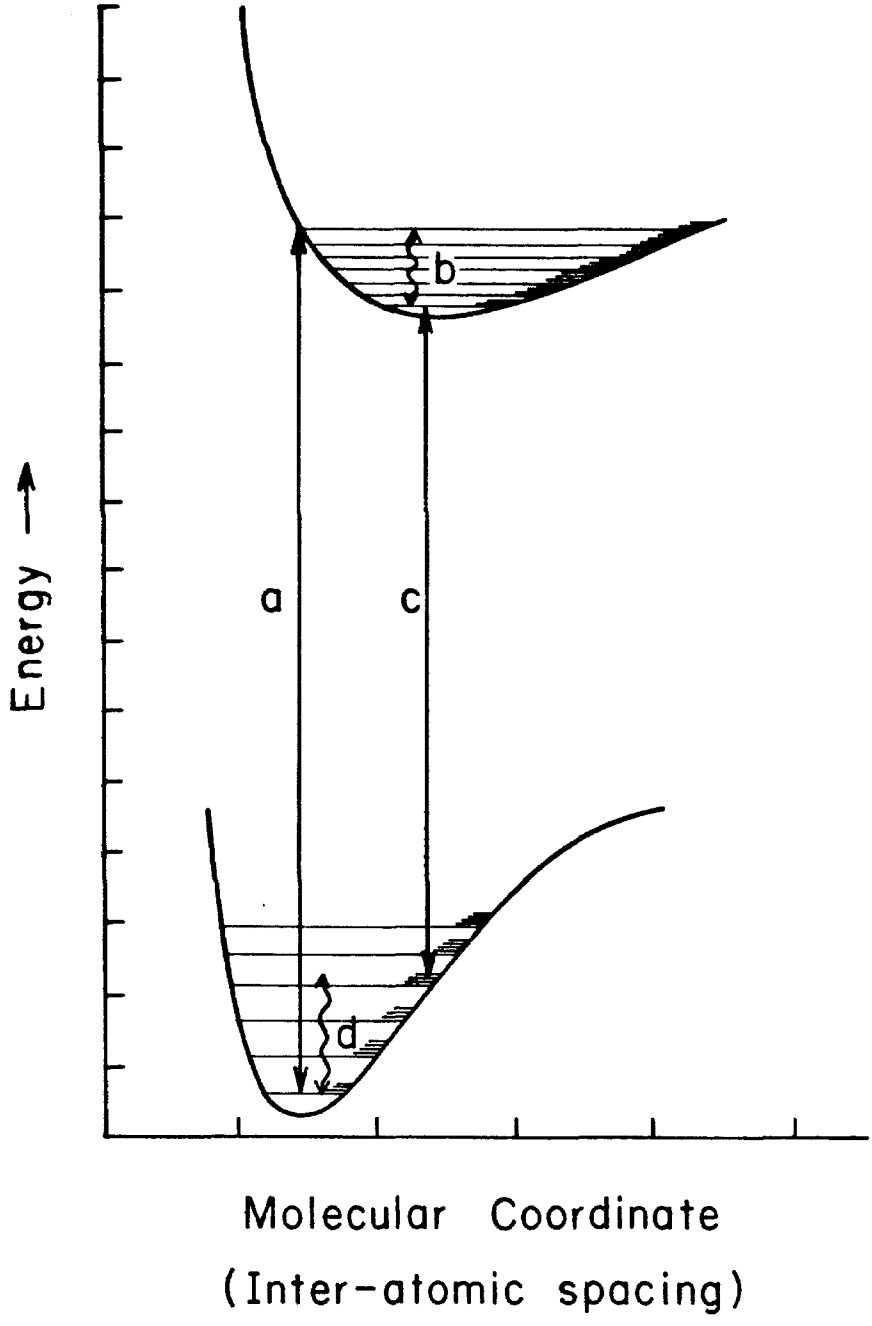
Energy
a
b
c
d
Molecular Coordinate
(Inter-atomic spacing)

This assumption is formalized in the Born-Oppenheimer approximation, which is that the electron wave functions can be calculated assuming that the nuclear positions are fixed.

Suppose we subject this mode to an oscillating electric field. The transition probability per unit time might be calculated using the approach of Fermi's Golden Rule No. 2 (Schiff, 1968). This requires knowledge of the dipole coupling between initial and final states separated by an energy equal to $hc\bar{\nu}$, as well as the density of states near the final state. There are two reasons why the mode is most easily excited by energies corresponding to higher level vibrational states in the excited electronic state. The first is that the density of vibrational and librational states increases with higher energy. The second is that the nuclear positions are effectively stationary over the time required to undergo the transition. This means that transitions are vertical in Figure A1. This second approximation is known as the Frank-Condon principle. Since the equilibrium positions are usually not the same, a vertical transition from the equilibrium position of the ground state will terminate at a vibrationally excited state on the excited electronic surface.

The mode we have just excited is coupled to many others around it, both in the molecule and in the surrounding material. Excess vibrational energy can be coupled out of this mode, bringing it into thermal equilibrium in the excited electronic state. This relaxation process takes place very quickly (on the order of 10^{-12} seconds). At this point there will be some probability per unit time that the mode will spontaneously emit (Yariv, 1975). The rate and energy of the

emission is determined by the same sorts of considerations as for absorption. The final state after emission will most likely be an excited vibrational state in the electronic ground state. Again vibrational relaxation will occur. The whole process of excitation, relaxation, emission, and final relaxation is depicted by processes (a), (b), (c), and (d) in Figure AI. The differences between the energy of (a) and (c) is the Stokes shift of the emission with respect to the excitation energy. The lifetime for singlet fluorescence is typically about a nanosecond in these molecules, and the lifetime for triplet phosphorescence is about a millisecond. The combination of both singlet and triplet emission is termed luminescence.

Throughout the text we used the extinction coefficient to represent the absorption characteristics of a molecule. The extinction coefficient can be related in a simple way to the absorption cross section in cm^{-2}:

$$\sigma(\bar{\nu}) = \frac{\ell n(10) \cdot 1000 \cdot \epsilon(\bar{\nu})}{C \cdot N_{a\nu}} \qquad (A.1)$$

Similarly, the extinction coefficient is related to the imaginary part of the atomic electronic susceptibility (Yariv, 1975). The electronic displacement vector is defined to be $\bar{D} = (\epsilon + \epsilon_0 \chi(\bar{\nu}))\,\bar{E}$, where ϵ_0 is the electric permeability of vacuum, ϵ is the dielectric constant far from the absorption (so that the index of refraction is $n = \sqrt{\epsilon/\epsilon_0}$), and $\chi(\bar{\nu})$ is the susceptibility. If we rewrite $\chi(\bar{\nu}) = \chi'(\bar{\nu}) - i\chi''(\bar{\nu})$,

then the extinction coefficient can be written in terms of $\chi''(\bar{\nu})$:

$$\epsilon(\bar{\nu}) = \frac{\pi C \bar{\nu} \chi''(\bar{\nu})}{n^2 \ell n(10) \cdot C} \qquad (A.2)$$

Other possible modes of de-excitation from the excited electronic state are possible apart from radiation. Let τ be the lifetime of the excited state, τ_r be the radiative lifetime, and τ_{nr} be the nonradiative lifetime:

$$1/\tau = 1/\tau_r + 1/\tau_{nr} \qquad (A.3)$$

We can define the quantum efficiency of luminescence, η, to be

$$\eta = \tau/\tau_r \qquad (A.4)$$

In other words, η is the fraction of the excitations that will produce emissions.

APPENDIX III

TOTAL INTERNAL REFLECTION AND WAVEGUIDES

We normally assume that light arriving at the LSC-air interface is very far away from its point of emission compared to the wavelength of the light. The problem can, therefore, be simplified to the case of a plane wave incident on a plane boundary. Let the incident, reflected, and transmitted electric fields be $E_0 \exp(i \bar{K} \cdot \bar{x} - i\omega t)$, $E_0' \exp(i\bar{K}' \cdot \bar{x} - i\omega t)$, and $E_0'' \exp(i\bar{K}'' \cdot \bar{x} - i\omega t)$, respectively (Jackson, 1975). Let the boundary between a material with index n and a material with index n' occur at the $z = 0$ plane. If the phase of the wave is constant everywhere on the boundary, then $(\bar{K} \cdot \bar{x}) = (\bar{K}' \cdot \bar{x}) = (\bar{K}'' \cdot \bar{x})$ for $z = 0$. This relation tells us that the three wave vectors are co-planar, and that the index times the sine of the angle of incidence (or exit) is a constant (Snell's law). If the index of one of the materials is 1, then we have that the criteria for total internal flection is that $\sin(\theta) \geq 1/n$, because θ would be imaginary for the transmitted wave. There is a nonpropagating evanescent wave outside of the trapped material in this case which decays exponentially.

There is an interesting case which perhaps should receive more attention. What happens if the incident light cannot be considered a plane wave? Specifically, suppose the LSC is a thin dielectric slab, whose thickness is on the order of the wavelength of light. In this case the photons no longer propagate as a series of straight lines between reflections. Instead the slab acts like a waveguide, and will support TE and TM modes in certain wavelength regimes (Yariv, 1975). Only TE_0 and TM_0 modes can propagate if the thickness is less than about a third of a wavelength. (The slab begins to act like the usual LSC

plate for thicknesses greater than about three wavelengths.) There are two prominent disadvantages with this geometry. The layer would have to have a dye concentration on the order of 1 molar, or in other words be solid dye. This would probably lead to severe emission quenching. The second problem is that devices with geometric gains of 100 would only have a characteristic largest dimension of about 10 microns.

APPENDIX IV

BLACK BODY RADIATION

In Chapter 6 we use several results on the properties of a photon gas in thermal equilibrium. These can be derived in the following manner (Yariv, 1975). The allowed electromagnetic radiation modes depend in general on the geometry of the cavity which contains them. However, if the cavity size is large compared to the wavelength of the radiation, then we can assume a cubic cavity with a volume L^3. This imposes the boundary condition that the fields be periodic in L. For example, the allowed wavenumbers in the x direction will be $k_x = 2\pi m/L$, for some interger m. Each mode, therefore, has a volume $(2\pi/L)^3$. The number of modes between 0 and k is the volume of a sphere of radius k, times the number of modes per unit volume, times 2 (for the two possible polarization directions): $N_m(\bar{\nu}) = 4\pi k^3/3 \cdot (L/2\pi)^3 \cdot 2 = k^3 L^3/3\pi^2$. Since $k = 2\pi\bar{\nu}$, $N_m(\bar{\nu}) = 8\pi\bar{\nu}^3 L^3/3$. The density of states is the number of modes per wavenumber per unit volume:

$$\delta(\bar{\nu}) = \frac{1}{L^3} \cdot \frac{\partial N_m(\bar{\nu})}{\partial \bar{\nu}}$$

$$= 8\pi \bar{\nu}^2 \qquad \text{(A. 5)}$$

The average number of photons in any mode is given by the Bose distribution $\bar{n}(\bar{\nu}) = [\exp(hc\bar{\nu}/nkT) - 1]$. n is the index of refraction of the medium. The total number of photons, $N(\bar{\nu})$, and the energy in the cavity, $E(\bar{\nu})$, is given by

$$N(\bar{\nu})\,d\bar{\nu} = L^3 \rho(\bar{\nu})\,\bar{n}(\bar{\nu})\,d\bar{\nu} = \frac{8\pi\,\bar{\nu}^2 L^3 d\bar{\nu}}{e^{h\bar{\nu}c/nkT}-1} \qquad (A.6)$$

$$E(\bar{\nu})\,d\bar{\nu} = N(\bar{\nu})\,d\bar{\nu} \cdot \frac{hc\bar{\nu}}{n} \qquad (A.7)$$

The energy emitted into a 2π solid angle by a surface of area A at a temperature T is given by integrating $E(\bar{\nu})$ over all wavenumbers and multiplying by $c/4nL^3$ (Landau and Lifshitz, 1977):

$$E = \frac{A \cdot C}{4nL^3} \int_0^\infty E(\bar{\nu})\,d\bar{\nu}$$

$$= A n^2 T^4 \frac{2\pi^5 k^4}{15 c^2 h^3}$$

$$= A n^2 T^4 \sigma \qquad (A.8)$$

σ is the Stefan-Boltzmann constant, which is most easily remembered as 5.67×10^{-8} watts per square meter per K^4. This is used in Eqs. (70) and (74). The brightness of the emission, in photons per wavenumber per second per unit area per solid angle, is given by $N(\bar{\nu})/L^3$ (Planck, 1959):

$$B(\bar{\nu}) = \frac{8\pi\,\bar{\nu}^2}{e^{hc\bar{\nu}/nKT} - 1} \tag{A.9}$$

This can be rewritten as

$$\frac{hc\bar{\nu}}{nT} = K\,\ell n\left[1 + \frac{8\pi\bar{\nu}^2}{B}\right] \tag{A.10}$$

In general, the energy in a thermodynamic system is related to the other variables by (Goodstein, 1975)

$$\delta E = T\delta S - P\delta V + \mu\delta N \tag{A.11}$$

$\mu = 0$ for an ideal gas. The entropy change resulting from removing a photon of wavenumber $\bar{\nu}$ from a photon gas with brightness B is

$$\frac{\Delta S}{\Delta N} = -\frac{1}{T}\frac{\Delta E}{\Delta N} = -K\,\ell n\left[1 + \frac{8\pi\bar{\nu}^2}{B}\right] \tag{A.12}$$

This result is used in Eq. (77).

APPENDIX V

SOLAR CELLS FOR USE WITH LSCs

In the text we have treated the edge-mounted solar cells as devices which convert light above some absorption cutoff energy with a constant energy efficiency. This efficiency is taken to be characterized by the measured AM1 efficiency of the cell. We ignore the effect of the spectral position of the LSC light output (as long as it is above this cutoff energy), the intensity and the angular distribution of the light, as well as parameters such as the cell temperature. In other words we have treated the LSC as a lens-like system with low enough light concentration so as not to heat the cell (and lower its efficiency) or substantially increase the incident flux (and increase its efficiency). These approximations require some additional justification.

Measured spectral responses for both p on n silicon cells and $Ga_{1-x}Al_xAs$ - GaAs cells are typically flat within ± 10% from 6,000Å to 9,000Å (1.5 to 2.25 ev) (Hovel, 1975). Since this is the most probable spectral band for the light output from an LSC, it is a good approximation to ignore the effect of the output wavelength on the cell response. The LSC plates are, in general, more sensitive to the blue end of the spectrum than either type of cell. We have assumed that the resulting increase in the conversion efficiency was ignorable due to both the relatively low flux at these high energies, and to the low conversion efficiency produced by a low voltage output from a high energy photon.

Increasing the concentration of the light incident on the cell increases the open circuit voltage, and, therefore, can increase the efficiency. The open circuit voltage is given by

$$V_{oc} = \frac{A_0 KT}{q} \ell n \left[\frac{I_{sc}}{I_0} + 1 \right] \qquad (A.13)$$

T is the junction temperature, K is Boltzmann's constant, q is the electronic charge, I_{sc} is the short circuit current, and A_0 and I_0 are device parameters. I_0 is the dark or reverse saturation current. A typical value of I_0 for a room temperature silicon cell is a microampere per square centimeter. If the short circuit current is increased by increasing the light on the cell the open circuit voltage increases logarithmically. A typical value for the short circuit current from a silicon cell under one sun is about 30 milliamps. Therefore, a cell mounted on an LSC with a flux gain of 10 might be expected to have an increased open circuit voltage by about 20%.

The increased concentration usually also brings about an increase in the cell temperature. The cell temperature on the highest efficiency LSC claimed to date was reported to be 60°C (Friedman, 1980). Thermally generated carriers cause a strong increase in the dark current with temperature, which in turn lowers the output voltage. Thus the higher temperature of an LSC-mounted cell can cause a decrease in the cell efficiency which usually more than compensates for the increase in efficiency due to light concentration. The IR absorption of PMMA is problematic in this regard because the plate itself can get hotter when exposed to the sun than a cell separate from an LSC. Thermal contact between the plate and the cell can, in this case, lower the cell's

performance.

We originally expected GaAs cells to perform better than silicon cells when mounted on LSCs. This is because there are no dyes to our knowledge that will efficiently absorb and emit in the far red, so as to take advantage of silicon's smaller band gap. However, we measured 60% higher flux gains for a silicon cell than for a gallium arsenide cell when interfaced with the fluid LSC. It should be emphasized that this was one measurement made with one particular cell. Owens-Illinois also reported better performance with silicon cells than with gallium arsenide. It is possible that silicon cells might perform better with LSCs than GaAs cells will. One reason might be that the silicon cells can be etched to have a rougher surface. This is done to improve light transmission into the cell. The gallium arsenide cells may not have been treated in a similar way.

APPENDIX VI

THE BRIGHTNESS THEOREM

Born and Wolf derive the following inequality for the brightness B_1 in energy per area per 4π steradians produced by light from a source with brightness B_0 passing through an arbitrary optical apparatus:

$$B_1 \leq \left(\frac{n_1}{n_0}\right)^2 B_0 \qquad \text{(A. 14)}$$

n_0 and n_1 are the indices of refraction at the source and detector, respectively. This result is obtained by ray tracing techniques.

We note that the same result can be obtained for nonimaging optics for the special case of black body radiators using the second law of thermodynamics. Suppose a spherical black body radiator at a temperature T_0 is radiating in a medium with index n_0. Using Eq. (A. 8), we find that the brightness of the sphere is $B_0 = n_0^2 T_0^4 \sigma$. Let this sphere communicate with a second sphere with a temperature T_1 in a medium with an index n_1. The brightness of this second sphere will be $B_1 = n_1^2 T_1^4 \sigma$. By the second law of thermodynamics, at equilibrium we have that $T_1 \leq T_2$, or that $B_1 \leq \left(\frac{n_1}{n_0}\right)^2 B_0$.

REFERENCES

Acrilex Incorporated, 8 Hope Street, Jersey City, New Jersey, 07307.

Baczynski, A., Marszalek, T., Walerys, H., and Zietek, B., Acta Phys. Polo. ,A44, No. 6, 805-812 (1973).

Batchelder, J. S., Zewail, A. H., and Cole, T., Appl. Optics, 18, No. 18, 3090-3110 (1979).

Batchelder, J. S., and Zewail, A. H., United States Patent 4, 227, 939.

Baur, G., and Greubel, W., Appl. Phys. Lett., 31, No. 1, 4-6 (1977).

Beer, D., and Weber, J., Opt. Comm., 5, No. 4, 307-309 (1972).

Birks, J. B., Photophysics of Aromatic Molecules, (Wiley Interscience, New York, 1970) p. 571.

Bloembergen, N., Nonlinear Optics, (W. A. Benjamin, Massachusetts, 1965).

Boer, K. W., Solar Energy, 19, 525-538 (1977).

Born, M., and Wolf, E., Principles of Optics, (Pergamon Press, New York, 1975).

Demas, J. N., and Crosby, G. A., J. Phys. Chem., 75, No. 8, 991-1024 (1971).

Drake, J. M., Morse, R. I., Steppl, R. N., and Young, D., Chem. Phys. Lett., 35, No. 2, 181-188 (1975).

Drexhage, K. H., "Structure and Properties of Laser Dyes," ed. F. P. Schafer, Topics in Applied Physics I, Dye Lasers (Springer-Verlag, New York, 1977) p. 144.

Exciton Chemical Company, P. O. Box 3204, Overlook Station, Dayton, Ohio, 45431.

Förster, T., Disc. of the Faraday Soc., 27, 7-17 (1959).

Fox, R. B., Isaacs, L. G., and Stokes, S., J. Polym. Sci. A, 1, 1079-1086 (1963).

Friedman, P. S., LSC Contract Report, Owens-Illinois SERI Contract XS-9-8216-1, 1980.

Garwin, R. L., Rev. Sci. Inst., 31, 1010-1011 (1960).

Goetzberger, A., Appl. Phys., 16, 399-404 (1978).

Goetzberger, A., and Greubel, W., Appl. Phys., 14, 123-139 (1977).

Goetzburger, A., and Schirmer, O., Appl. Phys., 19, 53-58 (1979).

Goodstein, D. L., States of Matter, (Prentice Hall, New Jersey, 1975) p. 25.

Gordon, R. G., J. Chem. Phys., 45, No. 5, 1643-1648 (1966).

Grossman, G., J. Coating Tech., 49, 45 (1977A).

Hammond, P. R., J. Chem. Phys., 70, No. 8, 3884-3894 (1979).

Hammond, P. R., Optics Comm., 29, No. 3, 331 (1979).

Higuchi, F., and Muto, J., Phys. Lett., 81A, No. 1, 95-96 (1981).

Hovel, H. J., Solar Cells, Semiconductors and Semimetals, (Academic Press, New York, 1975) Vol. 11.

Hovel, H. J., IBM J. Res. Develop., 22, No. 2, 112-121 (1978).

Ippen, E. P., Shank, C. V., and Dienes, A., J. Quant. Elect., April, 178-179 (1971).

Jackson, J. D., Classical Electrodynamics, (J. Wiley and Sons, New York, 1975).

Joshi, N. B., and Pant, D. D., J. Lum n., 14, 1-8 (1976).

Kajiwara, T., Chambers, R. W., and Kearns, D. R., Chem. Phys. Lett., 22, No. 1, 37-40 (1973).

Kaminow, I. P., Stulz, L. W., Chandross, E. A., and Pryde, C. A. Appl. Opt., 11, No. 7, 1563-1567 (1972).

Karplus M., and Porter, R. N., Atoms and Molecules, (W. A. Benjamin, Menlo Park, California, 1970) p. 450.

Karstens, T., and Kobs, K., J. Phys. Chem., 84, No. 14, 1871-1872 (1980).

Katraro, R., Ron, A., and Speiser, S., Chem. Phys. Lett., 52, No. 1 16-19 (1977).

Keil, G., J. Appl. Phys. 40, No. 9, 3544-3547 (1969).

Kennard, E. H., Phys. Rev., 11, No. 1, 29-38 (1918).

Knof, J., Theiss, F. J., and Weber, J., Opt. Comm., 17, No. 3, 264-266 (1976).

Kuhn, H., Progress in the Chemistry of Organic Natural Products, ed. D. L. Zechmeister (Springer-Verlag, Wien, 1959) Vol. 16, p. 411.

Landau, L. D., and Lifshitz, E. M., Statistics Physics, (Pergamon Press, New York, 1977) p. 166.

Lempicki, A., Andrews, A., McCollum, B., Nettel, S. J., and Solomon, E. I., Phys. Rev. Lett., 44, D-3 (1980).

Lerner, R. M., private communication, 1979.

Levitt, J. A., and Weber, W. H., Appl. Optics, 16, No. 10, 2684-2689 (1977).

Lytle, J. D., Wilkerson, G. W., and Jaramillo, J. G., Appl. Optics, 18, 1842-1844 (1979).

Magde, D., Brannon, J. H., Cremers, T. L., and Olmsted III, J., J. Phys. Chem., 83, No. 6, 696-699 (1979).

Mandal, K., Pearson, T., and Demas, J., Anal. Chem., 52, 2184-2189 (1980).

Offenhartz, P., and Micheels, R., SERI Contract Report XS-9-8041-13, 1980.

Pappalardo, R., and Ahmed, S., J. Chem. Phys. 56, No. 10, 5135-5143 (1972).

Planck, M., The Theory of Heat Radiation, (Dover Publications, New York, 1959) p. 176.

Q-Panel Company, 15610 Industrial Parkway, Cleveland, Ohio, 44135.

Rabl, A., Solar Energy, 18, 93-111 (1976).

Rainhart, L. G., and Schimmel, W. P., Jr., Solar Energy, 17, 259-264 (1975).

Rapp, C. F., Boling, N. L., Thomas, I. M., Opdycke, G. L., Fechter, R. B., Chrysochoos, J., and Friedman, 'Determination of the Technical and Economic Feasibility of Luminescent Solar Concentrators, Final Report of Owens-Illinois, Sandia 77-7005, 1980.

Reynolds, G. A., and Drexhage, K. H., Optics Comm., 13, No. 3 222-225 (1975).

Robbins, R., Millar, D., and Zewail, A., J. Chem. Phys., to be published.

Robinson, A. L., Science, 203, 629 (1979).

Ross, R. T., J. Chem. Phys. 46, No. 12, 4590-4593 (1961).

Sah, R. E., and Baur, G., Appl. Phys., 23, 369-372 (1980).

Schiff, L. I., Quantum Mechanics, (McGraw-Hill, New York, 1968) p. 285.

Shapiro, S. L., and Winn, K. R., Chem. Phys. Lett., 71, No. 3, 440-444 (1980).

Shurcliff, W. A., and Jones, R. C., J. Opt. Soc. Amer., 39, No. 11, 912-916 (1949).

Shurcliff, W. A., J. Opt. Soc. Amer., 41, No. 3, 209 (1951).

Swartz, B. A., Cole, T., and Zewail, A. H., Optics Lett., 1, No. 2, 73-75 (1977).

Tao, T., Biopolymers, 8, 609-632 (1969).

Theiss, F. J., and Weber, J., Optics Comm., 12, No. 4, 368-369 (1974).

Tinkham, M., Group Theory and Quantum Mechanics, (McGraw-Hill, New York, 1964) p. 239.

Von Jena, A., and Lessing, H. E., Chem. Phys., 40, 245-256 (1979).

Weber, J., Opt. Comm., 7, No. 4, 420-422 (1973).

Weber, J., Phys. Lett., 57A, No. 5, 465-466 (1976).

Weber, W. H., and Lambe, J., Appl. Optics, 15, No. 10, 2299-2300 (1976).

Weiss, E., and Speiser, S., Chem. Phys. Lett., 40, No. 2, 220-221 (1976).

Winston, R., Solar Energy, 16, 89-95 (1974).

Wolf, M., Proc. IEEE, 48, 1246-1263 (1960).

Yablonovitch, E., J. Opt. Soc. Amer., 70, No. 11, 1362-1363 (1980).

Yamashita, M., and Kashiwagi, H., IEEE J. Quant. Elect., QE-12, No. 2, 90-95 (1976).

Yariv, A., Quantum Electronics, (J. Wiley and Sons, New York, 1975).